An FHWA Special Study: Post-Tensioning Tendon Grout Chloride Thresholds

PUBLICATION NO. FHWA-HRT-14-039

MAY 2014

U.S. Department of Transportation
Federal Highway Administration

Research, Development, and Technology
Turner-Fairbank Highway Research Center
6300 Georgetown Pike
McLean, VA 22101-2296

FOREWORD

Elevated levels of chloride were recently discovered in a commercially available pre-bagged grout product made for post-tensioned (PT) tendons. These chloride values exceed the current limits set by all of the domestic and international regulatory committees. However, there is limited information reported in the literature pertaining to actual chloride threshold of seven-wire PT strands. For this reason, the Federal Highway Administration sponsored a 6-month accelerated corrosion testing program to determine chloride threshold(s) of PT strands exposed to chloride-contaminated grout. The findings of this study should be useful to bridge owners who may be responsible for similarly affected PT bridges.

This report presents two chloride threshold values determined for the PT strands that are fully encased in the commercially available grout described above. The first threshold is 0.4 percent chloride concentration by weight of cement, which is the lowest amount to initiate corrosion of strands. At this threshold, the testing program demonstrated that rust spots can form, and a small number of pits start to form beneath some of the rust spots. The second chloride threshold is 0.8 percent chloride by weight of cement in association with corrosion propagation. At this threshold, the testing program demonstrated that corrosion starts to intensify in terms of number of pits and pit depth; therefore, this threshold is considered to be critical. Once chloride concentration exceeds the critical threshold, significant corrosion damage can be anticipated, and the long-term structural integrity of the PT bridges may be compromised. If PT tendons contain carbonated grout, segregated grout, duct cracks, grout voids filled with water with or without chloride ions, or free sulfate ions in contact with the strands, corrosion might start below the proposed threshold values.

Jorge E. Pagán-Ortiz
Director, Office of Infrastructure
Research and Development

TECHNICAL REPORT DOCUMENTATION PAGE

1. Report No. FHWA-HRT-14-039	2. Government Accession No.	3. Recipient's Catalog No.
4. Title and Subtitle An FHWA Special Study: Post-Tensioning Tendon Grout Chloride Thresholds		5. Report Date May 2014 6. Performing Organization Code
7. Author(s) Seung-Kyoung Lee and James Zielske		8. Performing Organization Report No.
9. Performing Organization Name and Address Center for Advanced Infrastructure and Transportation Rutgers University, The State University of New Jersey 100 Brett Road Piscataway, NJ 08854-8058		10. Work Unit No. 11. Contract or Grant No. DTFH61-08-C-00005
12. Sponsoring Agency Name and Address Office of Infrastructure Research and Development Federal Highway Administration 6300 Georgetown Pike McLean, VA 22101-2296		13. Type of Report and Period Covered Final Report January 2012–September 2013 14. Sponsoring Agency Code

15. Supplementary Notes
The Contracting Officer's Technical Representatives (COTRs) were Y.P. Virmani and Hamid Ghasemi, HRDI-60.

16. Abstract

Elevated levels of chloride were recently discovered in a commercially available pre-bagged grout product made for post-tensioned (PT) tendons. Chloride concentrations were reported to be as high as 5.27 percent by weight of cement. These numbers exceed the current limits set by all of the domestic and international regulatory committees. For example, the chloride limits for prestressed concrete imposed by American Concrete Institute committees are either 0.06 percent water-soluble chloride by weight of cement or 0.08 percent acid-soluble chloride by weight of cement. *Chloride threshold* is defined as a minimum chloride concentration needed to induce corrosion. However, there is limited information reported in the literature pertaining to actual chloride threshold of seven-wire PT strands. For this reason, the Federal Highway Administration sponsored a 6-month accelerated corrosion testing program to determine chloride threshold(s) of PT strands exposed to chloride-contaminated grout.

Based on the test results obtained through the 6-month accelerated corrosion testing program and subsequent autopsy of the specimens, two chloride threshold values were determined for the PT strands fully encased in normal grout. The first threshold is 0.4 percent chloride concentration by weight of cement, which is the lowest amount needed to initiate corrosion of strands. At this threshold, rust spots can be formed, and a small number of pits start to form beneath some of the rust spots. The second critical chloride threshold is found in association with corrosion propagation. At this threshold, corrosion starts to intensify in terms of the number of pits and pit depth. Test data and autopsy results obtained in this study indicated that 0.8 percent chloride by weight of cement is the critical threshold. Once chloride concentration exceeds the critical threshold, significant corrosion damage can occur rapidly, and structural integrity of the PT bridges may be compromised in the near future. The actual deterioration rate will be influenced by many factors. These threshold values are applicable to normal grout condition only. They may not be adequate in other conditions such as carbonated grout, segregated grout, duct cracks, grout voids filled with water with or without chloride ions, or free sulfate ions in contact with the strands. In these circumstances, corrosion should start below the proposed threshold values.

17. Key Words	18. Distribution Statement
Chloride threshold, Chloride, Corrosion initiation, Corrosion propagation, Seven-wire strand, Post-tensioning, Grout, Autopsy, Accelerated corrosion testing, Sulfate ions, Void	No restrictions. This document is available to the public through the National Technical Information Service, Springfield, VA 22161.

19. Security Classif. (of this report)	20. Security Classif. (of this page)	21. No of Pages	22. Price
Unclassified	Unclassified	196	

Form DOT F 1700.7 (8-72) Reproduction of completed pages authorized

SI* (MODERN METRIC) CONVERSION FACTORS

APPROXIMATE CONVERSIONS TO SI UNITS

Symbol	When You Know	Multiply By	To Find	Symbol
		LENGTH		
in	inches	25.4	millimeters	mm
ft	feet	0.305	meters	m
yd	yards	0.914	meters	m
mi	miles	1.61	kilometers	km
		AREA		
in^2	square inches	645.2	square millimeters	mm^2
ft^2	square feet	0.093	square meters	m^2
yd^2	square yard	0.836	square meters	m^2
ac	acres	0.405	hectares	ha
mi^2	square miles	2.59	square kilometers	km^2
		VOLUME		
fl oz	fluid ounces	29.57	milliliters	mL
gal	gallons	3.785	liters	L
ft^3	cubic feet	0.028	cubic meters	m^3
yd^3	cubic yards	0.765	cubic meters	m^3
	NOTE: volumes greater than 1000 L shall be shown in m^3			
		MASS		
oz	ounces	28.35	grams	g
lb	pounds	0.454	kilograms	kg
T	short tons (2000 lb)	0.907	megagrams (or "metric ton")	Mg (or "t")
		TEMPERATURE (exact degrees)		
°F	Fahrenheit	5 (F-32)/9 or (F-32)/1.8	Celsius	°C
		ILLUMINATION		
fc	foot-candles	10.76	lux	lx
fl	foot-Lamberts	3.426	$candela/m^2$	cd/m^2
		FORCE and PRESSURE or STRESS		
lbf	poundforce	4.45	newtons	N
lbf/in^2	poundforce per square inch	6.89	kilopascals	kPa

APPROXIMATE CONVERSIONS FROM SI UNITS

Symbol	When You Know	Multiply By	To Find	Symbol
		LENGTH		
mm	millimeters	0.039	inches	in
m	meters	3.28	feet	ft
m	meters	1.09	yards	yd
km	kilometers	0.621	miles	mi
		AREA		
mm^2	square millimeters	0.0016	square inches	in^2
m^2	square meters	10.764	square feet	ft^2
m^2	square meters	1.195	square yards	yd^2
ha	hectares	2.47	acres	ac
km^2	square kilometers	0.386	square miles	mi^2
		VOLUME		
mL	milliliters	0.034	fluid ounces	fl oz
L	liters	0.264	gallons	gal
m^3	cubic meters	35.314	cubic feet	ft^3
m^3	cubic meters	1.307	cubic yards	yd^3
		MASS		
g	grams	0.035	ounces	oz
kg	kilograms	2.202	pounds	lb
Mg (or "t")	megagrams (or "metric ton")	1.103	short tons (2000 lb)	T
		TEMPERATURE (exact degrees)		
°C	Celsius	1.8C+32	Fahrenheit	°F
		ILLUMINATION		
lx	lux	0.0929	foot-candles	fc
cd/m^2	$candela/m^2$	0.2919	foot-Lamberts	fl
		FORCE and PRESSURE or STRESS		
N	newtons	0.225	poundforce	lbf
kPa	kilopascals	0.145	poundforce per square inch	lbf/in^2

*SI is the symbol for the International System of Units. Appropriate rounding should be made to comply with Section 4 of ASTM E380.
(Revised March 2003)

TABLE OF CONTENTS

LIST OF FIGURES

LIST OF TABLES

CHAPTER 1. INTRODUCTION

The number of prestressed concrete bridge structures utilizing high-strength seven-wire strands has steadily increased since the 1970s. The prestressing strands can be used in pre-tensioned and post-tensioned (PT) structures. The latter utilizes plastic or metal ducts that are initially empty tubes that allow for a bundle of the seven-wire strands to be fed through after the ducts are embedded in the concrete. The strands are fixed at both end anchorage points by a wedge plate and steel wedges that grip each strand. Ultimately, they are pulled to a pre-determined level of stress using a specialized hydraulic jack. The assembly of the prestressed seven-wire strands and the duct is called a PT tendon. In this report, a prestressed seven-wire strand will be simply referred to as a "PT strand." Figure 1 shows schematic of a typical PT tendon system.[1]

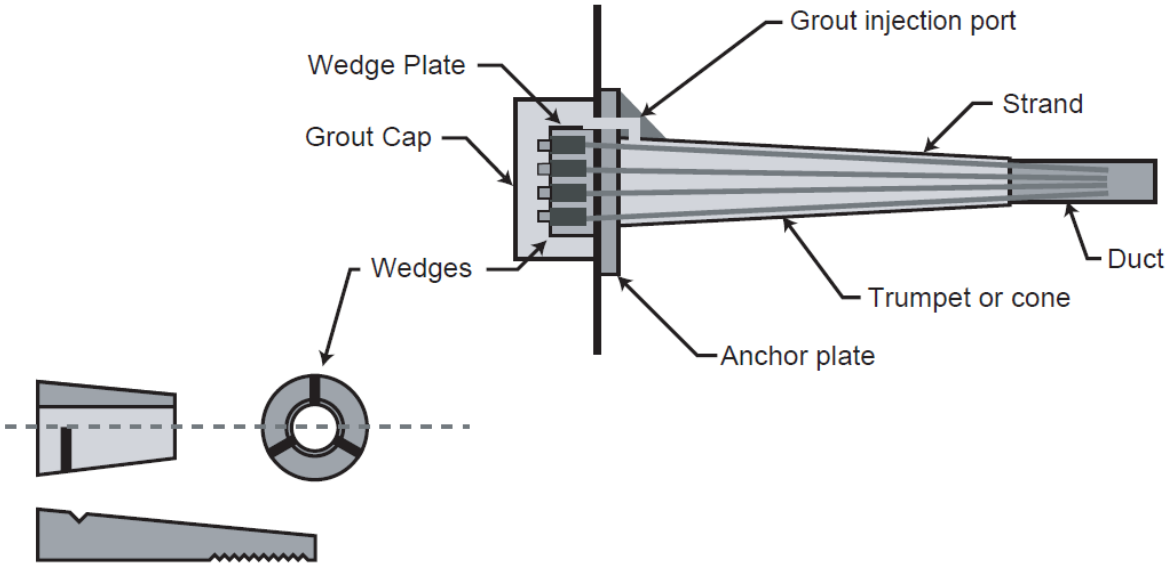

Figure 1. Illustration. Typical PT anchorage hardware for strand tendons.[1]

The PT tendon is divided into two types: (1) unbonded tendons typically filled with grease or wax and (2) bonded tendons filled with cementitious material called grout. For bonded PT tendons and cables, the grout functions as the last layer of corrosion protection for the highly stressed PT strands by providing a high pH environment to form a protective oxide film on the strand surface and acting as a physical barrier to water and oxygen. Corrosion of strands initiates when the protective oxide film is compromised due to chloride attack or carbonation of the surrounding grout upon exposure to water and air. Once corrosion initiates, corrosion propagates at a certain rate controlled by many factors such as oxygen availability, moisture content, electrical resistance, grout pH, and chloride concentration.

The literature review for this study has shown that among several causes in earlier tendon corrosion failures, any one or a combination of some of the following deficiencies can trigger active corrosion with presence of moisture and oxygen: voids, micro-cracks, sedimentation leading to variable water-cement ratio, bleed water, and contamination with chloride or sulfate ions.[2,3] Uneven grout cover ranging from very thick to virtually no cover within a typical duct system can also result in corrosion in the thin and no cover sections where PT strands in a tendon

have a greater chance of getting exposed to water and oxygen if the tendon fails to maintain its water/air tightness. Some examples caused by this type of corrosion in the field tendons are provided in appendix A. The prestressing strand is less tolerant to corrosive environments than ordinary reinforcing steel because of its much higher load-bearing requirement per unit area. While some tendon corrosion problems were observed in the grout defects filled with water and oxygen, various amounts of chloride ions were found in other incidents. A couple of investigative reports claimed that sulfate ions could be responsible for tendon corrosion as well.[2,4] In particular, a laboratory study conducted by the Florida Department of Transportation (FDOT) demonstrated that aggressive nature of free sulfate ions can result in intensive corrosion.[4] Excessive free sulfate ions found in segregated grout were also a suspect of corrosion failure of some tendon specimens employed in the present study. Recognizing the importance of having high-quality grout in the PT system concrete bridges and cable stayed bridges, commercially available pre-packaged grouts were introduced to the construction market to minimize quality variations that may occur in the construction sites. In addition, enhanced grout installation guidelines and training certification programs were developed. These changes have been beneficial and improved the quality of in-place grouts.

A recent discovery of grout with elevated levels of chloride used in a PT concrete straddle cap located in Corpus Christi, TX, led to a full investigation to better understand the extent of the potential corrosion problem that may be caused by the use of chloride-contaminated grout.[5] The grout in question was a commercially available pre-packaged product. According to an investigative report, the reported chloride concentration was as high as 5.27 percent (52,700 ppm) by weight of cement, and the chloride concentration in the retained bags was as high as 0.5 percent by weight of cement.[5,6] Figure 2 shows a 4-month-old segregated grout in question, and table 1 shows its corresponding chloride concentration data. Label A indicates normally hardened grout, and label B indicates defective grout that contained numerous air voids.

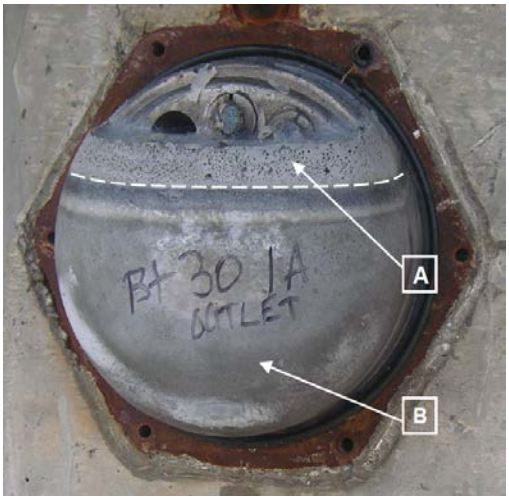

Figure 2. Photo. Chloride-contaminated grout in the straddle caps for Carbon Plant Road bridge.[5]

Table 1. Chemical analysis results.[5]

Sample	Instrument	Chloride Percent by Weight*	ppm
Tendon 1A inlet "A"	Scanning electron microscope (SEM)/ energy dispersive spectroscopy (EDS)	N/A	N/A
	X-ray fluorescence	5.27	52,700
	Ion chromatography	2.13	21,330
Tendon 1A, outlet "B"	SEM/EDS	0.54	5,400
Tendon 1B, inlet "B"	SEM/EDS	0.41	4,100
Tendon 2B, inlet "A"	SEM/EDS	0.57	5,700
Tendon 2B, inlet "B"	SEM/EDS	0.22	2,200

*Chloride percent by weight reported using SEM/EDS is for total chlorides.
N/A = Not available.

It is apparent that the confirmed chloride concentrations exceeded the past and current limits set by all of the domestic and international regulatory committees such as American Concrete Institute (ACI) 201, 318, 222R, and British Code CP 110. Because the existing limits are based on either weight percent of cement or weight percent of grout, a conversion between the two units has to be made with certain assumptions regarding the fraction of cement in a given weight or volume of a grout sample. According to the current chloride limit by ACI committees, maximum water-soluble chloride content by weight of cement of 0.06 percent (600 ppm) is allowed for the prestressed concrete. The specified limit for the acid-soluble by weight of cement is 0.08 percent (800 ppm). (See references 7–10.) The former indicates chloride ions currently available for corrosion, while the latter indicates total amount of chloride ions potentially available for future corrosion. The Virginia Department of Transportation (VDOT) also limits total (acid-soluble) chloride ions by weight of cementitious material to a maximum 0.08 percent (800 ppm), whereas FDOT Standard Specification Section 934 limits chloride content to a maximum of 0.40 lb/yd^3.[11] As noted in the ACI 222R-01 committee report, other international codes have different specified chloride limits for pre-hydrated grouts despite lack of rationale for the established values.[10] The same report also introduces a dimensionless ratio of $[Cl^-]/[OH^-]$, which can be used as a chloride threshold in relation to corrosion initiation of reinforcing steel. More information can be found in the literature review report.[3]

Dr. David Whiting stated in his article, *Origins of Chloride Limits for Reinforced Concrete,* that:

> "… "limits" refers to the amounts of chloride which are permitted in fresh concrete by code authorities. This is not necessarily equal to the so-called "threshold" limit for corrosion, which is the actual amount of chloride needed to initiate corrosion under a given set of conditions. The former term "limits" is thus an artificial criterion set by man; the "threshold" is set by nature. Thus, while the "limits" must be set, the "threshold" must be investigated."(pg. 3)[12]

This statement points out that even though the code specifications have built in a factor of safety, the allowable chloride limits are not adequate to predict corrosion behavior of the PT concrete

bridges subjected to corrosive environments. Corrosion process of the PT strands and cables consists of two steps: (1) corrosion initiation and (2) corrosion propagation. Corrosion initiates when a protective oxide film is compromised due to chloride attack or carbonation (lowing pH) of the surrounding grout. An FDOT study demonstrated that corrosion can initiate on the unstressed strands exposed to fresh water mixed with a chloride concentration of 500 ppm in a simulated corrosion study.[13] Once corrosion begins, the corrosion propagation stage follows a kinetic process in the given condition. The rate of corrosion is influenced by many factors including electrical resistance, temperature, and dissolved oxygen. In addition, a limited laboratory experiment performed at the Federal Highway Administration's (FHWA) Turner-Fairbank Highway Research Center for the internal San Francisco-Oakland Bay Bridge tendon corrosion study suggested that the corrosion rate of the prestressing wires may be related to chloride concentration, pH, and stress level. Therefore, it is imperative to take into account stress level, concentration of actual chloride in the grout, and pH at the strand/grout interface to determine a single chloride threshold or a range of chloride threshold values for any PT tendons and cables.

CHAPTER 2. OBJECTIVE AND SCOPE OF WORK

The objective of this study was to determine chloride threshold values of PT strands exposed to chloride-contaminated grout. For this, a comprehensive investigation has been conducted over 12 months to complete the following two tasks:

- **Task 1**: Literature review on chloride threshold for prestressed strands.
- **Task 2**: Accelerated corrosion testing to determine chloride threshold values to initiate corrosion and critical threshold values for recognizable corrosion-induced damage. This task had three subtasks employing three types of specimens as follows:
    - **Task 2.1**: Single-wire specimens.
    - **Task 2.2**: Single-strand specimens.
    - **Task 2.3**: Multi-strand specimens.

Based on the study findings, additional work was performed to present current corrosion risk assessment and estimate overall long-term safety of the PT strands exposed to the chloride-contaminated grout.

TASK 1: LITERATURE REVIEW ON CHLORIDE THRESHOLD FOR PRESTRESSING STRANDS

A thorough literature review was conducted as far back as the 1950s to disseminate historical chloride limit data applicable to the prestressed strand. Also, the PT tendon corrosion failure reports were gathered and analyzed to extract pertinent information for this study. The complete literature review report was published as an FHWA summary report.[3]

TASK 2: ACCELERATED LABORATORY CORROSION TESTING

Accelerated laboratory corrosion testing was performed to determine chloride threshold values for the prestressed strands through investigating interacting effects among multiple parameters including chloride concentration, presence of voids, stress level, temperature, relative humidity (RH), and pH using new 0.6-inch, 270-ksi low-relaxation grade strands. The strands employed in this research study were handled in the same way as delivered without additional cleaning and installed in the actual bridges. After they were delivered to the laboratory, they were stored in a clean and dry condition to prevent atmospheric corrosion.

CHAPTER 3. EXPERIMENTAL PROCEDURE

MATERIALS

The 0.6-inch, 270-ksi low-relaxation grade PT strand was used in this study. Great care was taken not to contaminate the surface of the strands during the handling and storage. More than 50 center (i.e., king) wires were extracted from 5-ft-long PT strands by untwisting and removing the outer six wires. These king wires were used for the electrochemical testing of task 2.1, which called for electrochemical testing of instantaneous corrosion rate and corrosion potential of king wires exposed to different aqueous test solutions having 10 chloride concentrations and 2 pH values. The sodium chloride weight in a test solution was equivalent to the chloride concentration in a grout mix expressed in terms of weight percent of cement that was calculated based on the cement content of 33.3 lb per grout bag (50 lb) and 12.5 lb of distilled water for each bag. The following calculations exemplify a chloride concentration equivalent to 1.0 percent chloride by weight of cement:

- 1.0 percent of chloride by weight of cement required where 33.3 lb × 0.01 lb = 0.33 lb of chloride ions for a 50-lb bag.
- Since 60.7 percent of sodium chloride is chloride, 1.0 percent of chloride by weight of cement required is 0.33 lb ÷ 0.607 = 0.55 lb of sodium chloride for a 50-lb bag.
- The fraction of sodium chloride for one unit weight of mixing water is 0.55 lb ÷12.5 lb = 0.044.
- Hence, 1.6 oz (0.044 × 35.27 oz (i.e., 1,000 g) = 1.6 oz) of sodium chloride should be added to 0.26-gal of a test solution containing chloride ions equivalent to 1.0 percent chloride by weight of cement.

Table 2 lists 10 required amounts of sodium chloride in the 0.26-gal test solutions.

Table 2. Sodium chloride contents for task 2.1 test solutions.

Chloride Concentration by Weight of Cement (percent)	Weight of Sodium Chloride in 0.26-gal Water (oz)
0.00	0.000
0.04	0.063
0.08	0.123
0.20	0.308
0.40	0.616
0.60	0.924
0.80	1.232
1.00	1.540
2.00	3.077
3.00	7.693

Table 3 lists the chemical compositions for making solutions with a pH of 9.0 and 13.6, respectively, in the 0.26-gal test solutions.[14] These solutions were prepared to simulate carbonated grout and concrete (pH 9.0) and high alkaline environment like uncarbonated grout and concrete (pH 13.6). These represent typical pH values observed in the field.

Table 3. Chemical compositions for task 2.1 test solutions.

Solution with pH 9.0		Solution with pH 13.6		
Sodium Carbonate	**Sodium Bicarbonate**	**Calcium Hydroxide**	**Sodium Hydroxide**	**Potassium Hydroxide**
0.147 oz	0.875 oz	0.070 oz	0.291 oz	0.816 oz

A total of 64 50-lb grout bags were acquired from a local distributor of the same manufacturer that produced the grout containing the elevated chloride. It is claimed to be a non-shrink, non-bleed, high flow, sand-free, cementitious grout. Upon receiving them, three bags were randomly selected for trial mixes to cast 10 4-by-8-inch cylinders for determining background chloride and confirming that the calculated weights of sodium chloride were correct to produce the target chloride concentrations. For this, seven chloride concentration mixes and three chloride-free mixes were cast. Table 4 provides final sodium chloride weights needed to produce the target chloride concentrations in the full batches based on the following:

- The weight of cement contained in a 50-lb grout bag is 33.3 lb.
- The weight of mixing water is 12.5 lb per manufacturer's recommendation.
- Six bags of grout were mixed for specimen fabrication.

Table 4. Sodium chloride weights for tasks 2.2 and 2.3 specimen grout mixes.

Chloride Concentration by Weight of Cement (percent)	Weight of Chloride Ions Required for One 50-lb Grout Bag (lb)	Weight of Chloride Ions Required for Six 50-lb Grout Bags (lb)	Weight of Sodium Chloride Required for Six-Bag Grout Mix (lb)*	Weight of Water Required for Six-Bag Grout Mix (lb)**	Total Weight of Six-Bag Grout Mix (lb)***
0.00	0.00	0.00	0.00	75.00	375.00
0.08	0.03	0.16	0.26	75.00	375.30
0.20	0.07	0.40	0.66	75.00	375.70
0.40	0.13	0.80	1.32	75.00	376.30
0.60	0.20	1.20	1.98	75.00	377.00
0.80	0.27	1.60	2.64	75.00	377.60
1.00	0.33	2.00	3.30	75.00	378.30
2.00	0.67	4.00	6.59	75.00	381.60

*60.7 weight percent of sodium chloride is chloride ions.
**12.5 lb of water per bag.
***6 bags × 50 lb per bag + 75 lb of water + sodium chloride.

Proportional amounts of sodium chloride were admixed for the trial mixes as shown in table 4. After they were cured for 10 days in ambient condition, acid-soluble and water-soluble chloride analyses were made with the grout powder samples obtained by drilling the hardened grout cylinders. The former was done by American Association of State Highway and Transportation Officials (AASHTO) T260 and the latter by ASTM C1218.[15,16] The entire acid-soluble chloride test results reported in this report was done according to AASHTO T260 standards. The chloride test results are presented in chapter 4 of this report.

A perfect agreement existed between admixed chloride concentrations and extracted chloride concentrations in the trial mixes. The grout mixing and pumping was performed in an industrial grade grout mixing system.

ENVIRONMENTAL CHAMBERS

To accelerate corrosion of fabricated PT specimens, one large and one small walk-in environmental chamber were employed by converting two commercial grade walk-in freezers. The smaller chamber had an interior footprint of 6 ft, 4 inches × 12 ft, 4 inches, and the larger one had an interior footprint of 11 ft, 4 inches × 12 ft, 4 inches. The interior height of both chambers was 6 ft, 11.5 inches. In addition to a standard freezer evaporator and refrigeration unit, each chamber had infrared heat lamps, a humidifier, a dehumidifier, and a digital thermostat to control the temperature between -10 and 120 °F and RH between 30 and 100 percent. Figure 3 through figure 6 show exterior and interior views of the chambers, respectively. A data collection terminal cabinet and fabricated specimens are also shown in figure 4 through figure 6.

Figure 3. Photo. Environmental chambers.

Figure 4. Photo. Inside the small environmental chamber.

Figure 5. Photo. Inside the large environmental chamber.

Figure 6. Photo. Data collection terminal cabinet.

INTRODUCTION TO ACCELERATED CORROSION TESTING PROGRAM

An accelerated corrosion testing protocol was developed to produce discernible test results within 6 months. Because corrosion reaction is greatly influenced by temperature and moisture level (RH), cyclic temperature and humidity variations simulating outdoor environmental condition to which the PT bridges are exposed in field were maintained inside the environmental chambers.

Fabricated specimens were exposed for a full cycle of 8 weeks in the following sequence:

- **Sub-cycle 1**: Ambient environment (77 °F + 60 percent RH) for 2 weeks.
- **Sub-cycle 2**: Hot and humid (H & H) environment (104 °F + 90 percent RH) for 2 weeks.
- **Sub-cycle 3**: Ambient environment (77 °F + 60 percent RH) for 2 weeks.
- **Sub-cycle 4**: Freezing and dry (F & D) environment (14 °F + 40 percent RH) for 2 weeks.

Therefore, the specimens were subjected to three full-cyclic exposures during the 6-month accelerated corrosion testing program. As will be discussed later, the last F & D cycle was replaced with another H & H cycle because corrosion activity during the F & D cycles was insignificant.

Temperature and RH in the chambers were recorded continuously using universal serial bus-based monitoring sensors. Ambient temperature and temperature/RH in the chambers were also manually measured at the time of performance data collection. At the same time, specimen interior temperature was measured using thermocouples placed in the two specimens. The experimental data were collected twice per cycle: the first one in the middle (end of the first week) and the second one at the end of the exposure cycle (end of the second week). After the second data collection was completed, the exposure cycle was switched to the next scheduled one. Data collection from the single-strand control specimens was made bi-weekly at end of the second week as they did not show noticeable changes in the corrosion activity due to their exposure to only room temperature. Condition of strands exposed in the void were also occasionally inspected and photographed. More discussion will be made in the Corrosion Performance Tests and Data Collection section in this chapter.

Weekly corrosion performance of the accelerated corrosion testing specimens was monitored with two types of electrochemical measurements. These non-destructive data are commonly used to characterize corrosion behavior of metallic specimens embedded in cementitious materials non-destructively subjected to various levels of chloride contamination and environmental loading.

The first experimental dataset collected in this study was corrosion potential. It indicates the thermodynamic tendency of the specimens to determine whether corrosion initiation is possible or not. ASTM C876 provides three corrosion potential criteria with respect to copper/copper

sulfate reference electrode (CSE) to determine corrosion tendency of steel embedded in concrete as follows:[17]

- More positive than -200 mV versus CSE: 90 percent of probability having no corrosion.
- More negative than -350 mV versus CSE: 90 percent of probability having corrosion.
- Between -200 and -350 mV versus CSE: uncertain state.

These criteria are not applicable in many circumstances, but they are still useful references to evaluate unknown thermodynamic state of metallic objects in cementitious medium. Its usefulness increases when it is used along with corrosion rate information.

The second experimental dataset in this study reviewed the instantaneous corrosion rate of single-strand specimens. It provided kinetic information about the intensity of corrosion once corrosion started. This information is vital to predict remaining life of a system or a structure by estimating how fast corrosion takes place. As the word "instantaneous" implies, it determines the rate of corrosion at the moment of measurement, and it can change anytime depending on external and internal conditions including temperature and moisture content. It is calculated from experimentally determined polarization resistance (R_p) with the assumption that corrosion occurs uniformly over the entire surface area. Corrosion rate is usually expressed by mils per year. In reality, active-passive metals like PT strands exposed to highly alkaline environment are damaged at finite fixed spots. This form of localized corrosion includes pitting corrosion and crevice corrosion. Although the underlying assumption of uniform corrosion is incorrect, the present study uses the collected nominal corrosion rate data with caution because there are no other alternatives to provide the corrosion rate information.

The next section briefly discusses electrochemistry of localized corrosion caused by a breakdown of passive film on reinforcing steel and strand exposed to uncarbonated concrete, mortar, or grout. The passive film is formed during anodic polarization, as shown in figure 7.

The anodic polarization process of a metal involves moving electrical potential of the metal (working electrode of an electrochemical test cell) toward more a positive direction from its reversible potential, as illustrated by the green arrows in figure 7. One way of achieving anodic polarization is through a potentiodynamic polarization technique using advanced electrochemical instruments. They enable researchers to conduct specific anodic polarization experiments with great precision and predetermined polarization limits, scan rates, etc. During the initial upward anodic polarization, corrosion current density increases (i.e., corrosion rate of the metal increases). This region is defined as the active zone as indicated in figure 7. When continuous anodic polarization process makes current density exceed a critical value ($i_{critical}$), current density drops substantially to a passive current density level ($i_{passive}$). At this current density level, passive film starts to build up on the metal surface in the presence of oxygen, and, consequently, corrosion rate of the metal decreases. With further anodic polarization in the positive potential direction, quality of the passive film is increasingly enhanced, and corrosion rate remains low. This region is called the passive zone, as indicated in figure 7. When the anodic potential reaches the pitting potential (E_{pit}) and beyond, pits start to form on the metal surface and grow as function of anodic potential. Above a certain potential, oxygen gas also evolves by water

dissociation. This region is labeled the transpassive zone, as indicated in figure 7. A cyclic potentiodynamic anodic polarization technique can be also employed to investigate pitting corrosion behavior of a particular metal. Basically, it is a reversed anodic polarization process once the anodic polarization curve reaches a pre-set limit in the transpassive zone. This step is shown as the blue line and blue arrows in figure 7. The area surrounded by the hysteresis loop indicates the degree of susceptibility to pitting corrosion. A larger area is more susceptible to pitting corrosion. The potential where the reversed anodic polarization curve and the upward anodic polarization curve intersect is called the protection potential (E_{prot}) or repassivation potential. No pitting occurs below E_{prot}, whereas pits can nucleate and grow above E_{pit}. Between E_{prot} and E_{pit}, no pits can form, but existing pits can grow.

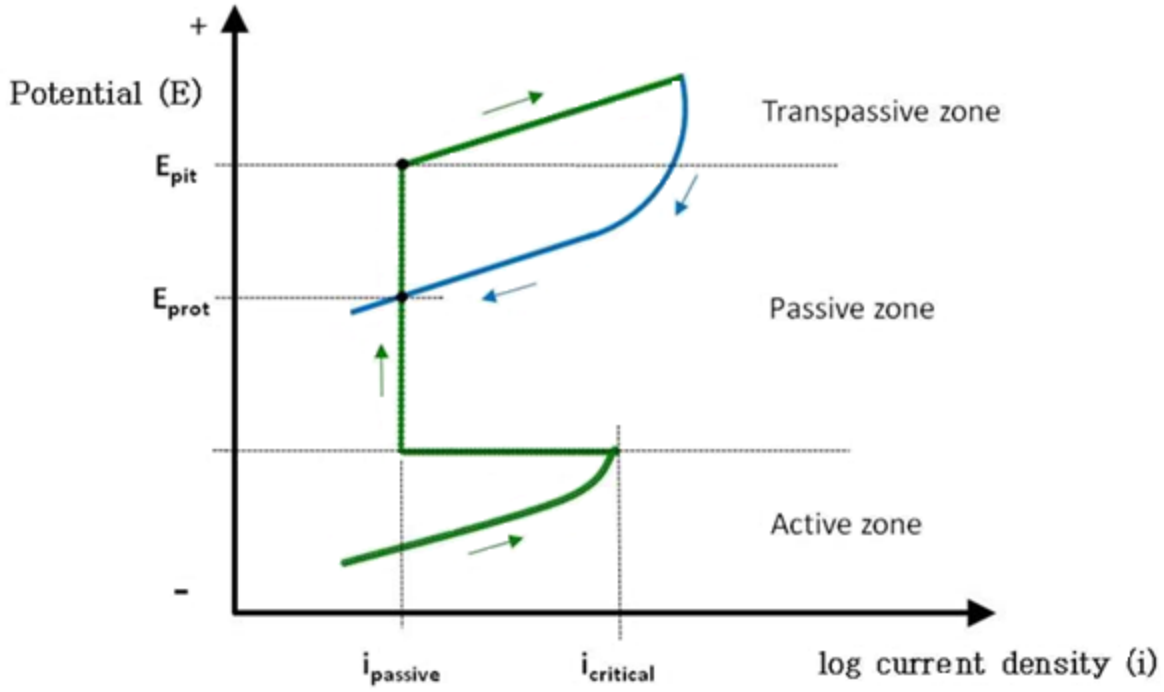

Figure 7. Graph. Major characteristics of active-passive metals presented in a potential-log current density (*E*-log *i*) diagram.

Figure 8 illustrates the effect of chloride ions on passivity of steel. As the chloride concentration increases, the passive zone shrinks, and both $i_{passive}$ and $i_{critical}$ increase due to weakened or compromised passive film. Consequently, a much higher corrosion rate should be expected at any corrosion potential for steel exposed to chloride contaminated concrete, mortar, and grout.

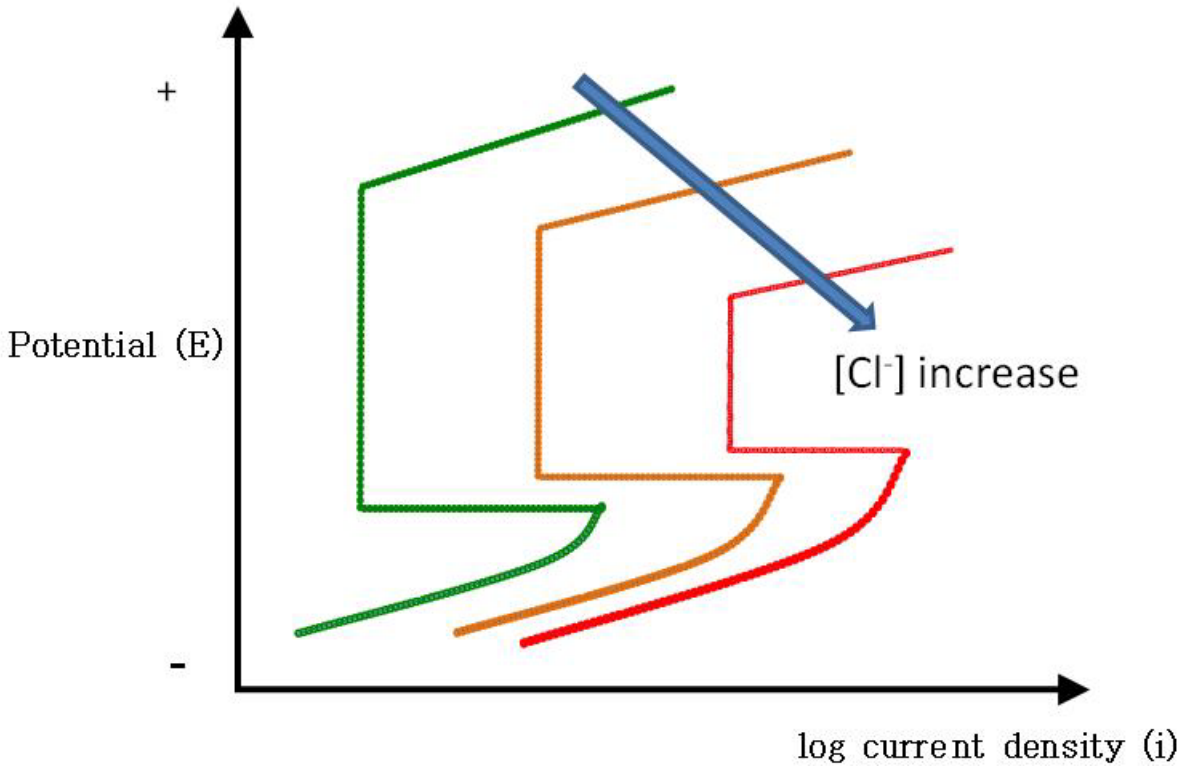

Figure 8. Graph. Effect of chloride ions on passivity.

The passive metals and alloys, including steel embedded in cementitious materials, are most susceptible to localized corrosion which can have three forms: pitting corrosion, crevice corrosion, and intergranular corrosion. They occur in two stages: corrosion initiation and corrosion propagation. Pitting corrosion, the first and most common localized corrosion, can initiate by four mechanisms, but this report only discusses one of them—passive film breakdown. This is because passive film breakdown is mainly responsible for chloride-induced corrosion of steel and strand in concrete, mortar, and grout. Pitting corrosion driven by this mechanism initiates when a corrosion cell is established between a small active area having damaged passive film and a large passive area covered with intact passive film. Schematic of such a corrosion cell is shown in figure 9. In the illustration, the following notations are used:

- OH^-: Hydroxyl ion.
- H^+: Hydrogen ion.
- O_2: Oxygen molecule.
- $2e^-$: Two electrons.
- Fe^{2+}: Ferrous ion.
- Cl^-: Chloride ion.

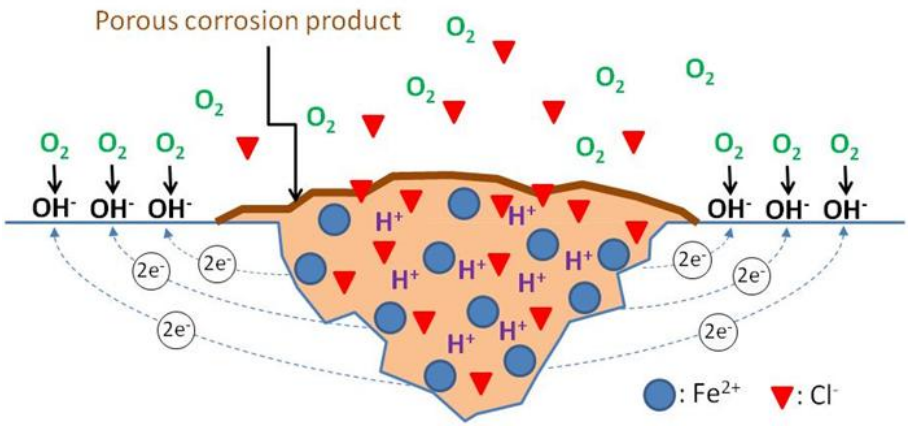

Figure 9. Illustration. Pitting corrosion mechanism.

Two electrochemical reactions occur simultaneously as follows:

$$Fe \rightarrow Fe^{2+} + 2e^-$$

Figure 10. Equation. Oxidation reaction at anode.

$$1/2O_2 + H_2O + 2e^- \rightarrow 2OH^-$$

Figure 11. Equation. Reduction reaction at cathode.

The equations in figure 10 and figure 11 show that the corrosion process liberates numerous positively charged ferrous ions (Fe^{2+}) into the pits and negatively charged hydroxyl ions ($2OH^-$) elsewhere.

Crevice corrosion, the second form of localized corrosion, initiates at geometrically confined areas where electrolytes are stagnant. This condition can establish a differential aeration cell when dissolved oxygen in the crevice is depleted by figure 11, whereas electrolytes outside the crevice in contact with bulk electrolyte contain abundant oxygen. As a result, the former becomes anodic to the latter, and corrosion progresses in the crevice. Again, surface area ratio of the anode and cathode can influence the magnitude of the corrosion damage at the anode. An anodic reaction in the crevice is encouraged to liberate ferrous ions and provide electrons to the cathodic area outside the crevice. A specific case of crevice corrosion related to the PT strand is illustrated in figure 12.

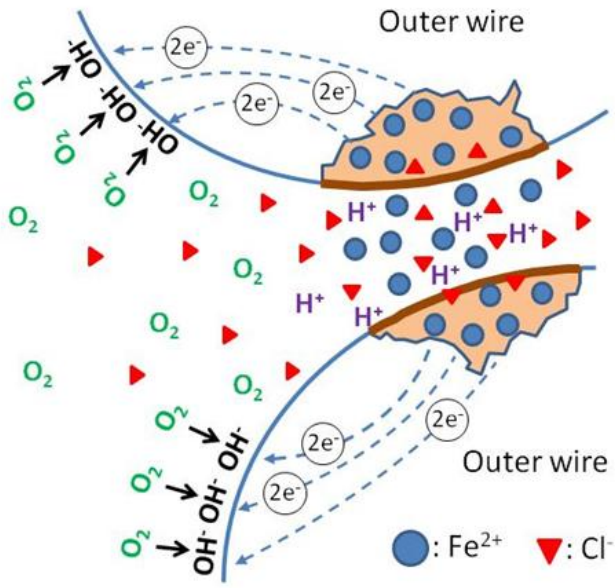

Figure 12. Illustration. Crevice corrosion mechanism.

During the corrosion propagation stage, the increased concentration of ferrous ions by metal dissolution within the pit or crevice attracts negatively charged anions, mainly chloride ions, into the pit or crevice to maintain charge neutrality, as shown by figure 13 as follows:

$$Fe^{2+} + 2Cl^- \rightarrow FeCl_2$$

Figure 13. Equation. Chemical reaction involving a ferrous ion and two chloride ions.

The ferrous chloride is then hydrolyzed by water to ferrous hydroxide and hydrochloric acid as follows:

$$FeCl_2 + 2H_2O \rightarrow Fe(OH)_2 + 2HCl$$

Figure 14. Equation. Chemical reaction for acidification.

The acidification process in figure 14 generates a highly corrosive local environment by lowing the pH within the pit or crevice and producing the acid product via an autocatalytic process. The outer corrosion product, ferrous hydroxide, can be converted to ferric hydroxide in contact with more dissolved oxygen as follows:

$$Fe(OH)_2 + 1/2H_2O + 1/4O_2 \rightarrow Fe(OH)_3$$

Figure 15. Equation. Chemical reaction involving ferric oxide formation.

As illustrated in figure 8, the accumulated chloride ions further compromise the passive film and lead to very active localized corrosion.

For multi-strand specimens, macro-cell corrosion current density data were collected (instead of corrosion rate data), as they also provide information about corrosion kinetics. Macro-cell corrosion current measurement is the other popular experimental technique to quantify the intensity of corrosion by measuring corrosion current from anode to cathode. The word “macro”

indicates that this type of corrosion involves physically separated anodes and cathodes as opposed to conventional micro-cell corrosion (or local action-cell corrosion). It was developed based on the field observations that reinforcing steel in concrete bridge decks corrodes by a macro-cell corrosion mechanism between salt-exposed top mat steel (macro-anode) and chloride-free bottom steel (macro-cathode). Numerous laboratory experiments have adopted this technique to simulate realistic corrosion of steel in concrete using small-scale macro-cell corrosion concrete slabs. It has been observed in the field PT bridges that macro-cell corrosion can induce serious damage to PT strands in a relatively short period of time. Figure 16 through figure 18 show three examples of corrosion-failed PT tendons by this corrosion mechanism. In the PT tendon cases, macro-cell corrosion can be established between macro-anode at cracks and holes in the ducts and infiltrated water in the grout voids and macro-cathode in the rest of the tendon. Figure 19 illustrates a specific macro-cell corrosion mechanism applicable to PT tendons. A macro-anode is connected to a nearby macro-cathode via metallic path (strands) and electrolyte (grout). This condition fulfills four components required for any operating macro-cell corrosion, that is, macro-anode, macro-cathode, metallic path, and electrolyte.

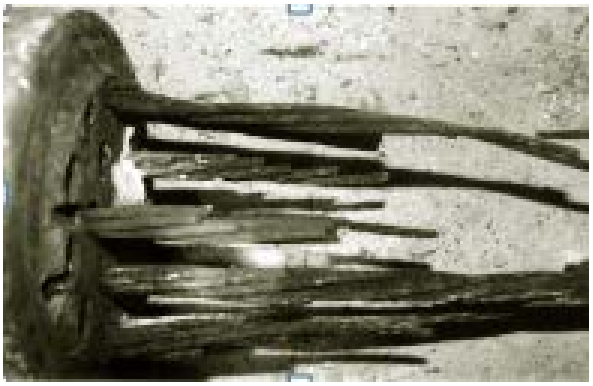

Credit: FDOT

Figure 16. Photo. Example of PT tendon failure due to macro-cell corrosion—Niles Channel bridge in Florida after 13 years in service.

Credit: FDOT

Figure 17. Photo. Example of PT tendon failure due to macro-cell corrosion—Sunshine Skyway bridge in Florida after 13 years in service.

Figure 18. Photo. Example of PT tendon failure due to macro-cell corrosion—Verina-Enon bridge in Virginia after 17 years in service.

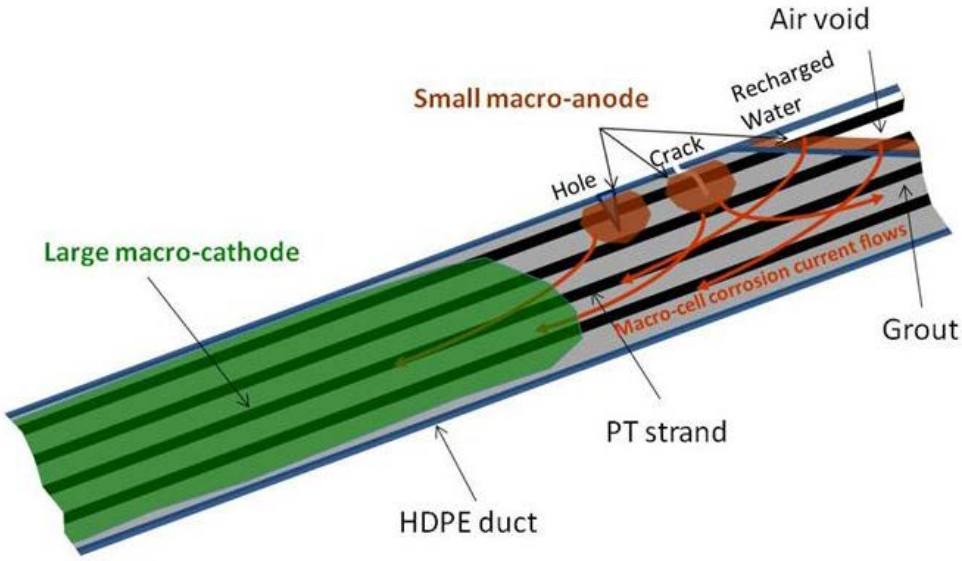

Figure 19. Illustration. Macro-cell corrosion mechanism in PT tendon.

Although the electrochemical reactions discussed are the same for any corroding steel in an aerated environment, the macro-anode and macro-cathode are physically separated, and their surface areas are much larger than ordinary micro-cell corrosion that consists of numerous tiny alternating anodes and cathodes. Consequently, intense corrosion can take place at the macro-anode by figure 10 and reduction of electrons at the macro-cathode by figure 11.

An Evans diagram (or *E*-log *i* diagram) illustrates how an anodic polarization diagram of a metal intersects with its cathodic polarization diagram. The intersection of two polarization diagrams determines the metal's corrosion potential and corrosion current density. Figure 20 shows four *E*-log *i* plots that describe several corrosion potential-corrosion current density relationships of active-passive metals, such as PT strands, depending on different anodic and cathodic behaviors. The four plots can be described as follows:

- Case (1) represents a non-corroding PT strand in normal grout. The passive anodic polarization curve (solid green line) intersects with the cathodic polarization curve

(solid blue line). In this case, relatively positive corrosion potential and low corrosion current density are observed.

- Case (1') also represents a non-corroding PT strand in normal grout, but more oxygen is supplied. The passive anodic polarization curve (solid green line) intersects with the more positively shifted cathodic polarization curve (dashed blue line). In this case, more positive corrosion potential and the same low corrosion current density are observed.

- Case (2) represents a corroding PT strand in defective grout. The active anodic polarization curve (solid magenta line) intersects with the cathodic polarization curve (solid blue line). In this case, negative corrosion potential and higher corrosion current density are observed.

- Case (2') also represents a corroding PT strand in defective grout, but more oxygen is supplied. The active anodic polarization curve (solid red line) intersects with the more positively shifted cathodic polarization curve (dashed blue line). In this case, slightly more positive corrosion potential and significantly higher corrosion current density than case (2) are observed.

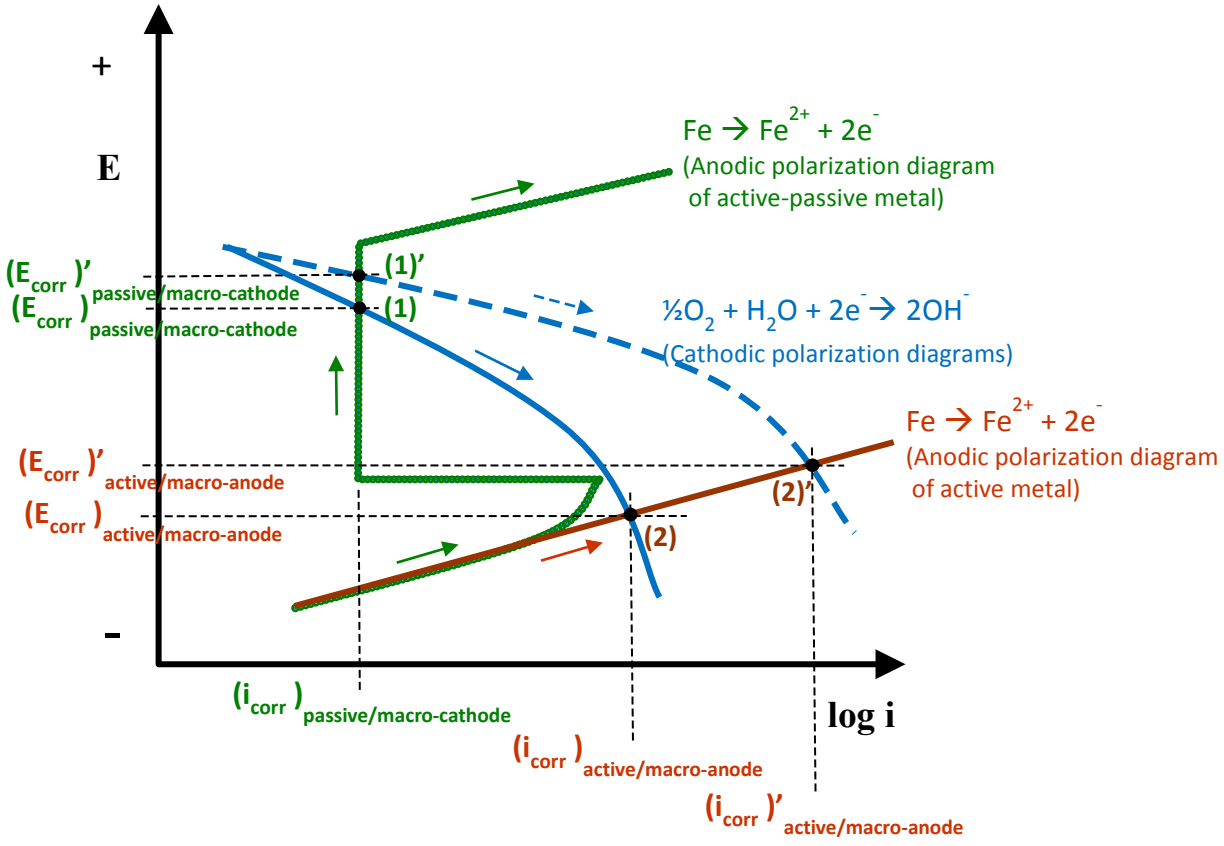

Figure 20. Graph. *E*–log *i* diagram describing different anodic and cathodic behaviors.

For macro-cell corrosion, cases (1) and (1') can relate to macro-cathode, while cases (2) and (2') can be related to macro-anode. The potential difference between any of them determines the driving force for macro-cell corrosion. In theory, electrical coupling between a macro-cathode in case (1') and a macro-anode in case (2') would yield the largest corrosion-induced damage as magnitude of

corrosion current density determines level of damage, and the coupled condition yields the highest macro-cell current density ($(i_{corr})'_{active/macro\text{-}anode} - (i_{corr})_{passive/macro\text{-}cathode}$). More severe corrosion damage at the macro-anode can occur if surface area ratio of the macro-cathode to the macro-anode becomes large (i.e., small anode-large cathode situation).

In addition, apparent grout resistivity and grout resistance data were also collected to provide additional information about corrosion environment. Less grout resistance allows the corrosion current to travel further distances. As a result, a larger macro-cathode surface area can be involved in the corrosion process.

SPECIMEN TYPE AND FABRICATION PROCESS

There were three types of test specimens employed in this study for each of three subtasks. They were designed to produce specific test results and, when analyzed together, provide comprehensive information regarding chloride threshold values.

Task 2.1: Single-Wire Specimens in Aqueous Solutions

The purpose of this subtask was to evaluate the effect of chloride concentration, stress level, and pH on corrosion of the PT strand. For this, corrosion potential and instantaneous corrosion rate of center wires exposed to various experimental conditions were measured.

A specially designed test cell was installed in the middle section of a 5-ft-long wire as shown in figure 21 and figure 22.

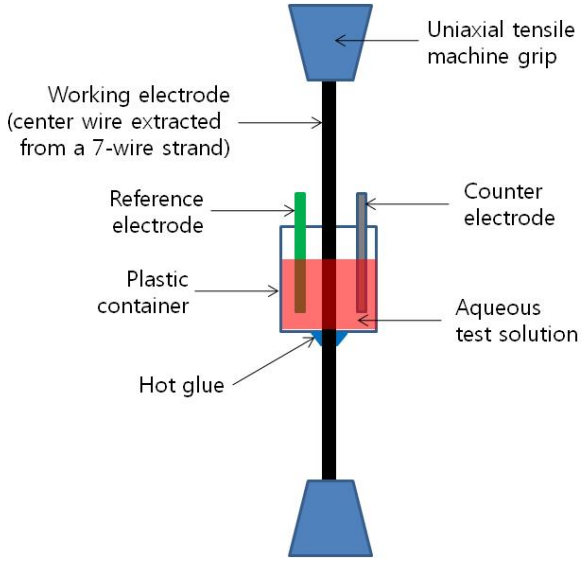

Figure 21. Illustration. Task 2.1 test setup for stressed wires.

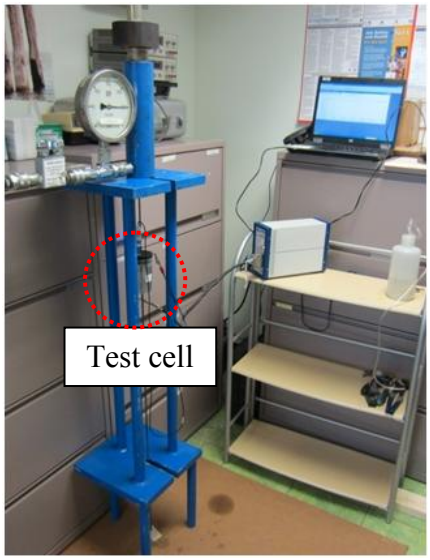

Figure 22. Photo. Test cell for stressed wires.

The original wire surface condition including lubricants applied during the manufacturing process was untouched to produce the corrosion data from the strands in the as-received condition. Some wires were tested under no stress, and the others were prestressed at 60 percent of guaranteed ultimate tensile strength (GUTS). For the stressed wires, a custom-made loading frame equipped with a load cell and hydraulic pump was used to apply the target stress. The loading frame is shown in figure 21 and figure 22. For the unstressed wires, a wooden frame was used to hold the test cell in place vertically as shown in figure 23.

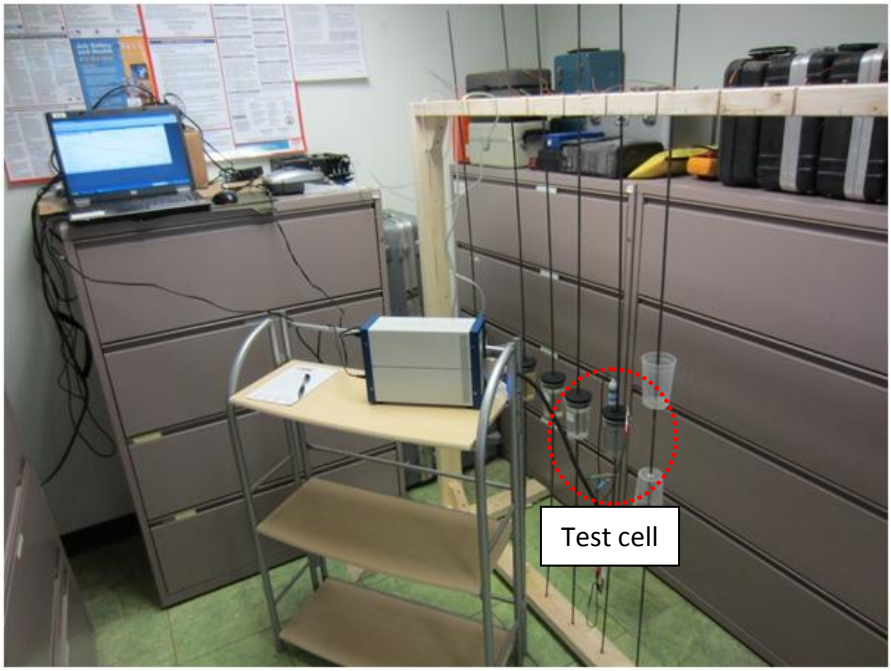

Figure 23. Photo. Task 2.1 test setup for unstressed wires.

The following test variables were employed to characterize electrochemical behaviors of stressed and unstressed wires at ambient temperature:

- **Temperature**: Ambient temperature was used.
- **Stress level**: 0 percent (unstressed) and 60 percent of GUTS (applied load of 35 kips based on nominal cross-sectional area of 0.032 inches^2).
- **Chloride concentration**: 0, 0.04, 0.08, 0.2, 0.4, 0.6, 0.8, 1.0, 2.0, and 5.0 percent by weight of cement (calculated for equivalent concentrations in aqueous solutions).
- **pH**: 13.6 (uncarbonated case) and 9.0 (carbonated case).

A combination of the test variables required 40 center wires (stress level × chloride concentration × pH = 2 × 10 × 2 = 40). However, some repeated measurements had to be made due to outliers. Consequently, more wires were tested during the actual experiment.

Task 2.2: Single-Strand Specimens in Grout

This specimen type was employed to understand the effect of chloride concentration, stress level, void, and crevice formed by adjacent wires on corrosion of single PT strands in chloride-contaminated grout. It has been observed that when actual PT strands corrode in the field, interstitial sites formed by twisted outer wires can encourage crevice corrosion.[14] Prestressing a strand also tightens all the interstitial spaces by stretching the wires and promoting capillary movement of water, thus enhancing corrosion activities there. A 12-inch single-strand specimen type was developed to measure corrosion rate on a short PT strand encased in hardened grout and a counter electrode.

Four rigid-loading frames were constructed to accommodate three 48-inch-long PT strands in each frame. A loading frame contained two stressed strands and one unstressed strand, as shown in figure 24.

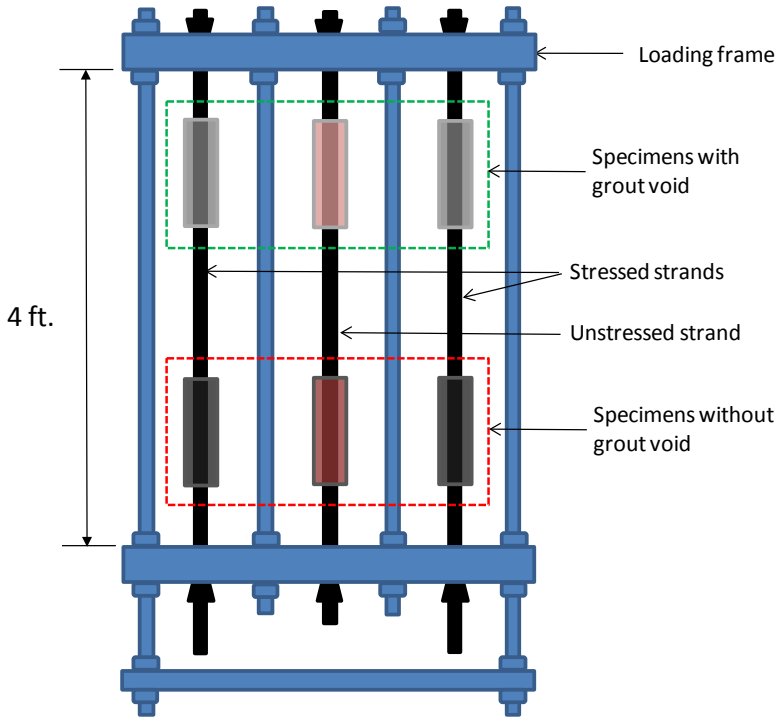

Figure 24. Illustration. Task 2.2 loading frame for single-strand specimens.

Each strand had two mock-up clear polyvinyl chloride (PVC) ducts in the middle, as shown in figure 24. Therefore, a total of six mock-up tendon specimens (four stressed and two unstressed) were tested per loading frame. The upper duct specimens simulated tendons containing a grout void, and the lower ones simulated fully grouted tendons. Later, the lower and upper ducts were filled with a grout mix containing the same chloride concentration.

Details of the mock-up specimens are shown in figure 25. Inner diameter and length of each duct were 2.0 and 12 inches, respectively. The inner wall of the duct was surrounded with a cylindrical-shaped grade 316 stainless steel mesh, which served as the counter electrode for the linear polarization resistance (LPR) measurement. Such a confined test cell design was intended to capture a very low measurement current (i.e., nano-ampere (10^{-9} A) range) in (cathodic direction) and out (anodic direction) of the strand during the LPR measurement.

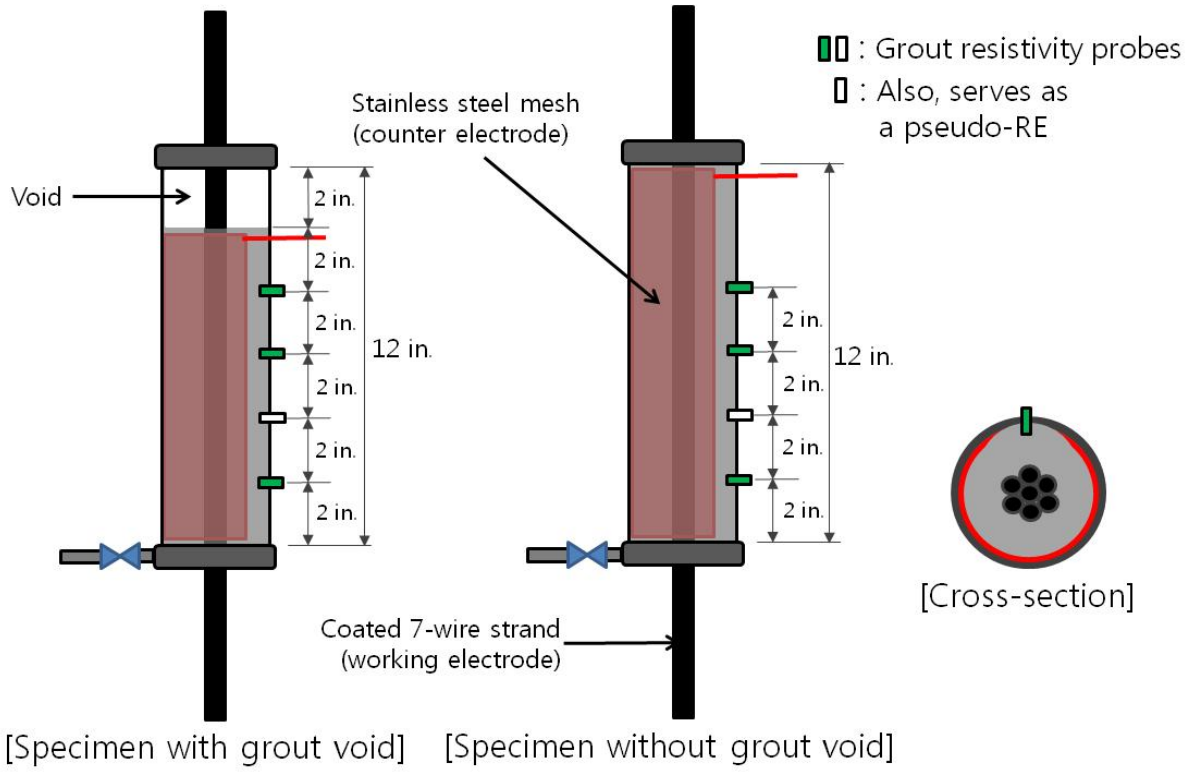

Figure 25. Illustration. Single-strand test cells.

The duct also had four resistivity probes at 2-inch spacings. The probes were made out of 0.25-inch diameter and 1-inch-long mixed metal oxide titanium, and they were installed as illustrated in figure 26 and figure 27.

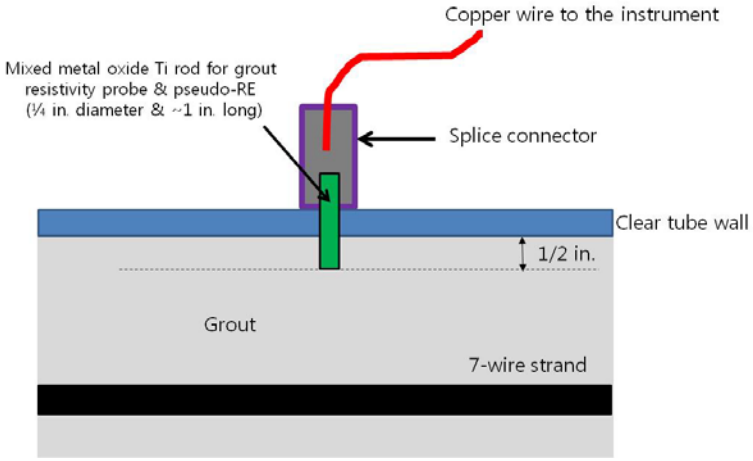

Figure 26. Illustration. Pseudo-reference electrode (PSE) probe.

Figure 27. Photo. Actual PSE probe.

The probes were used to measure apparent grout resistivity using the Wenner four-pin method. The second probe from the duct bottom also served as the PSE for the corrosion potential measurement. The potential readings made with the PSE were converted to those with respect to a standard silver-silver chloride reference electrode (ACE). This is schematically presented in figure 28. Eight blank grout cylinders were used to measure corrosion potentials of PSEs in eight chloride concentrations.

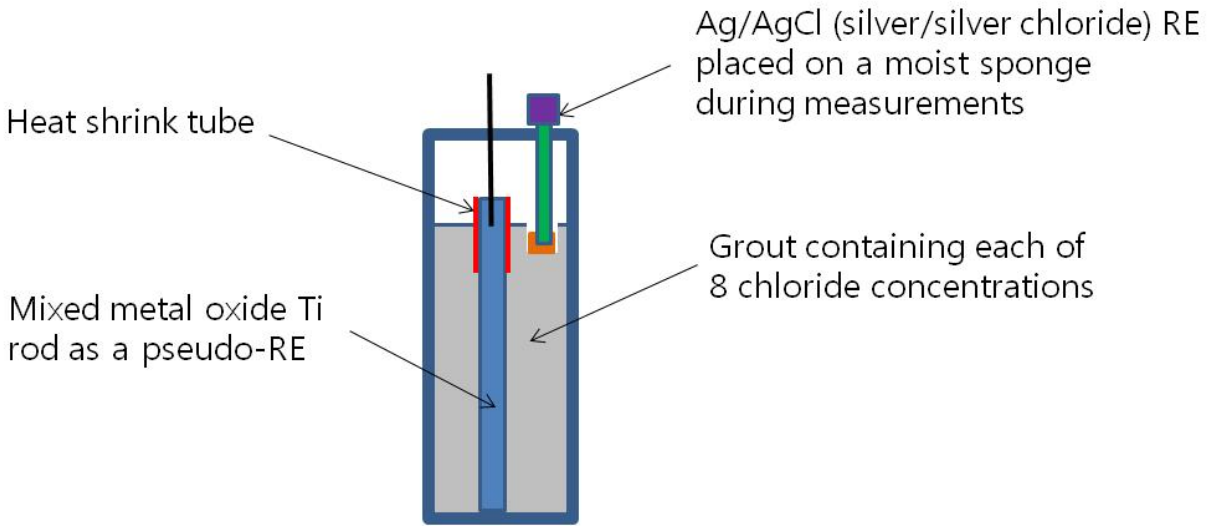

Figure 28. Illustration. PSE calibration cylinders.

An indirect potential measurement via a PSE was necessary to eliminate possible problems during the exposure testing when direct contact was made between grout and tip of the fragile ACE containing a liquid solution in a glass body.

The following variables were employed to characterize corrosion behaviors of stressed and unstressed PT strands:

- **Grout**: Pre-bagged grout product was used.
- **Stress level**: 0 and 60 percent of GUTS.

- **Grout void**: None and 2-by-2-inch cylindrical-shaped void.
- **Temperature and RH**: 77 °F + 60 percent RH, 104 °F + 90 percent RH, and 14 °F + 40 percent RH.
- **Chloride concentrations**: 0, 0.08, 0.2, 0.4, 0.6, 0.8, 1.0, and 2.0 percent by weight of cement.
- Ingress of water and oxygen into some voided specimens in the middle of exposure testing.

Combination of test variables required 40 single-strand specimens as follows:

- **Stressed single-strand specimens**: Grout void (2) × chloride concentrations (8) = 16.
- **Unstressed single-strand specimens**: Grout void (2) × four chloride concentrations (0, 0.2, 0.6, and 1.0 percent by weight of cement) = 8.
- **Extra unstressed single-strand specimens**: Grout void (2) × chloride concentrations (8) = 16.

After the counter electrodes and resistivity probes were installed in the ducts, the assembled duct specimens were placed at the fix positions along the strands, and the bottom openings between the strands and PVC caps were sealed with a silicon caulking material. The top openings were used as air vents during grout pumping. The strands were then installed in the loading frame. For the strands designated as stressed specimens, prestressing was done at 60 percent of GUTS from the upper end of the strands. For the unstressed ones, the strands were gently placed onto the loading frame using steel wedges. The target stress level was selected to avoid possibilities of overstressing while reflecting a typical working stress in the field PT bridges. After grout pumping, the top openings of the ducts were sealed with hot glue. Figure 29 and figure 30 show the stressing work, and figure 31 shows task 2.2 specimens prepared for grout installation.

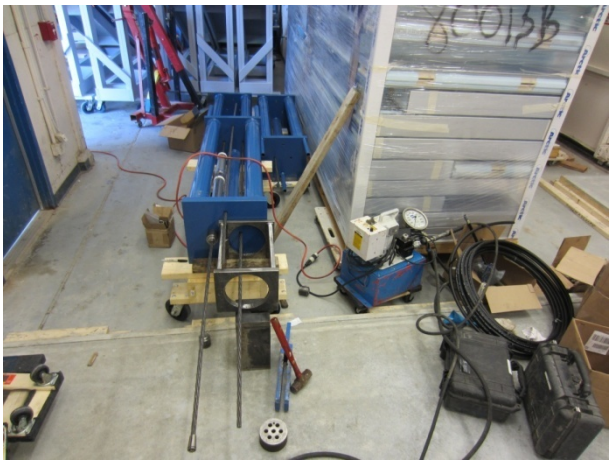

Figure 29. Photo. Stressing of single-strand specimens.

Figure 30. Photo. Stressing of multi-strand specimens.

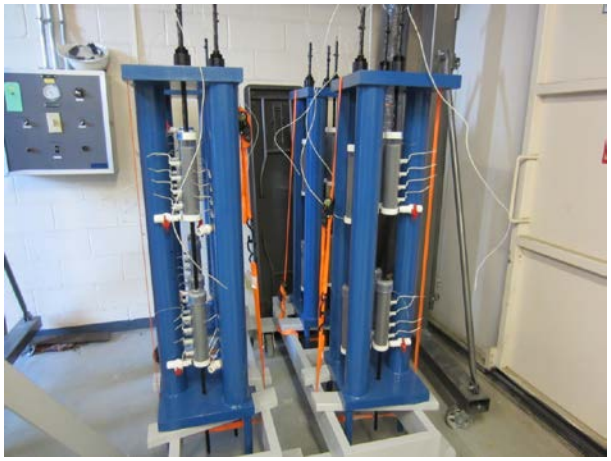

Figure 31. Photo. Fully assembled single-strand specimens.

The grouting work was completed in a single day. For each grout mix, six bags of the grout material, a predetermined amount of sodium chloride as listed in table 4, and 75 lb of distilled water were prepared in advance. The sodium chloride was dissolved in the mixing water just before mixing.

After pouring the dry grout powder into the grout mixer, mixing water was added (see figure 32). Once desirable grout consistency was achieved, the grout mix was pumped to the mock-up tendons (see figure 33). For the specimens without void, the duct was completely filled with the grout until it came out of the vent hole slightly. For those containing a void, 10 inches of the duct from the bottom was filled with the grout, and the remaining top 2 inches were left empty to simulate an entrapped air void. For each chloride concentration grout mix, casting was done with the same batch.

Figure 32. Photo. Grout mixing.

Figure 33. Photo. Grout pumping into a single-strand specimen.

Random grout samples were taken from each mix to perform standard grout tests (see figure 34).

Figure 34. Photo. In-situ grout testing.

The 28-day grout compressive strength data are listed in table 5. Batch #9 was the only batch producing 28-day compressive strength below 8,000 psi, the advertised 28-day strength by the grout manufacturer.

Table 5. 28-day compressive strength data of grout mixes.

Batch ID	Admixed Chloride Concentration by Weight of Cement (percent)	Cube Compressive Strength (psi)			
		1	2	3	Mean (psi)
Batch #1	0	10,040	10,290	10,400	10,243
Batch #2*	0	10,910	10,540	11,280	10,910
Batch #3	0.08	8,780	10,140	10,580	9,833
Batch #4	0.2	8,800	7,810	8,300	8,303
Batch #5	0.4	10,060	9,220	9,080	9,453
Batch #6	0.6	8,760	9,090	9,030	8,960
Batch #7	0.8	9,420	9,500	9,020	9,313
Batch #8	1.0	9,500	8,860	9,060	9,140
Batch #9	2.0	6,350	5,810	7,350	6,503

*Repeated casting due to grout leaking problem.

Batch #9 exhibited normal fluidity (7 s) and wet density (126 lb/ft^3). Mix and ambient temperatures were also within the recommended guidelines. Batch #9 was also the only one with specimens

cured in plastic molds instead of cast iron molds. Plastic molds are known to reduce compressive strength compared to cast iron molds.

When the specimens were cured for 10 days, two baseline data collections were made at ambient condition for all 40 single-strand specimens. After that, 24 specimens (16 stressed and 8 unstressed) designated for the accelerated corrosion testing were placed in the smaller environmental chamber. The other 16 unstressed single-strand specimens were kept in the ambient condition to serve as controls as well as backup specimens, if necessary. In order to collect the data efficiently without disturbing the temperature and RH inside the chamber, all the lead wires from the specimens were organized in several bundles and were run to a data collection panel mounted on the exterior wall of the chamber (see figure 4 through figure 6).

Task 2.3: Multi-Strand Specimens in Grout

The last specimen type was a large-scale multi-strand PT mock-up tendon. It was introduced to investigate the effects of chloride concentration, void, charging water, and macro-cell corrosion on PT strand corrosion. In this sub-task, reproduction of the worst PT corrosion problem caused by macro-cell corrosion was attempted using an innovative specimen design. Such a unique approach was necessary because conventional specimen configurations could not mimic the real macro-cell corrosion situation due to experimental limitations such as lab space and complexities involving fabricating long stressed tendon specimens in the confined environmental chambers. The multi-strand specimens were intended to simulate the principle of macro-cell corrosion mechanism as close as practical: macro-anode passing through a grout void with rechargeable water and macro-cathode embedded in normal grout. The intended macro-cathode was made with unstressed short strands surrounded by the intended macro-anode that was made with four stressed strands. Nearly equal surface areas were adopted for macro-anode and macro-cathode, thus surface effect (small macro-anode and large macro-cathode) could not be investigated in this study. This configuration also allowed comparing corrosion behaviors of stressed strands versus unstressed ones. This type of specimen could create more positive corrosion potential at the intended macro-cathode (case (1) or case (1') in figure 20) compared to the intended macro-anode (case (2) or case (2') in figure 20) and large driving force between them.

Each multi-strand specimen was 10 ft long and 6 inches in diameter. They were supported by a 25-degree inclined wooden support structure to simulate typical inclined tendons in the field. They contained four 10-ft stressed strands that served as a macro-anode and that were partially buried in the grout and five 7-ft unstressed strands that served as a macro-cathode and that were completely embedded in the grout. Both groups of strands were electrically isolated from each other with the exception of being coupled via an external toggle switch. Sufficient clearance among nine strands was maintained by three plastic circular plates with nine holes for the strands to run through. Four resistivity titanium probes identical to those used in task 2.2 specimens were installed at the 12-inch spacing along the 2 o'clock line starting from the lower anchor plate. The titanium probes were also used as the PSEs to measure the strand potentials at the probe locations. Figure 35 and figure 36 show specimen configuration and some of its details, respectively.

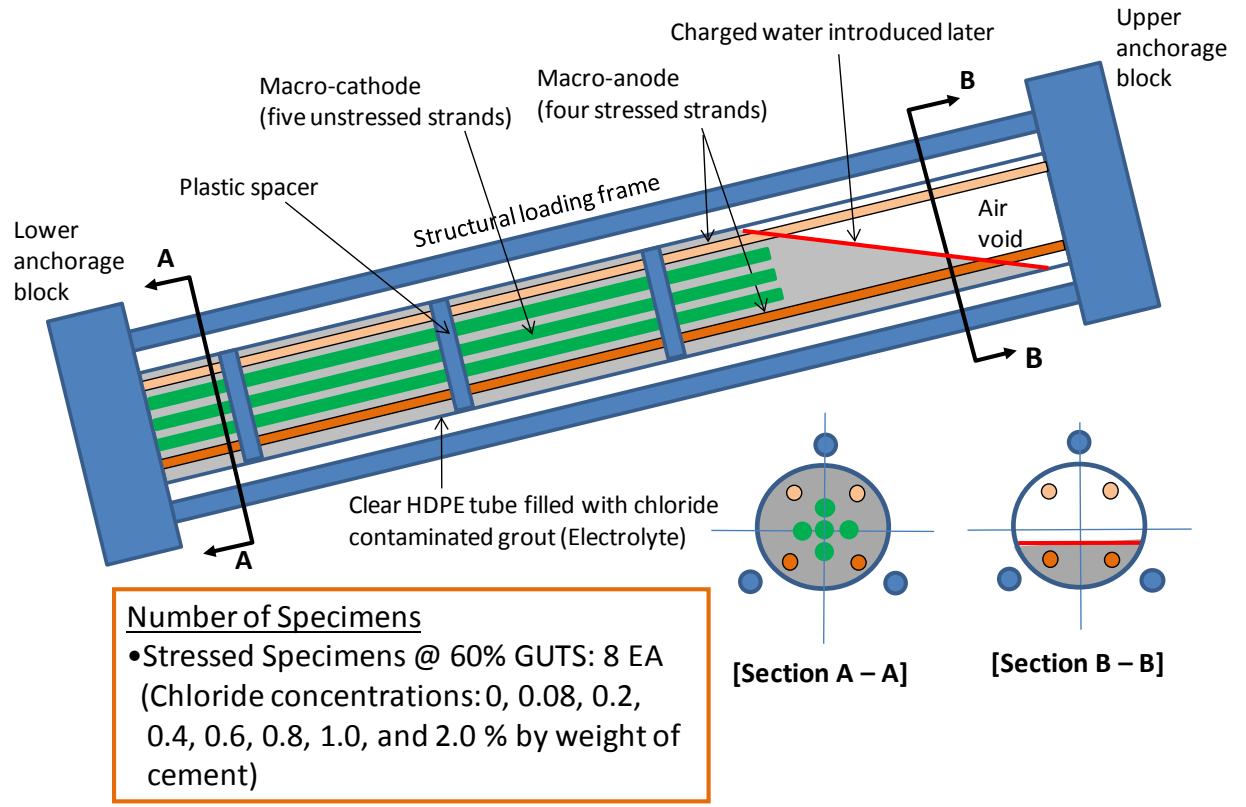

Figure 35. Illustration. Task 2.3 multi-strand specimens.

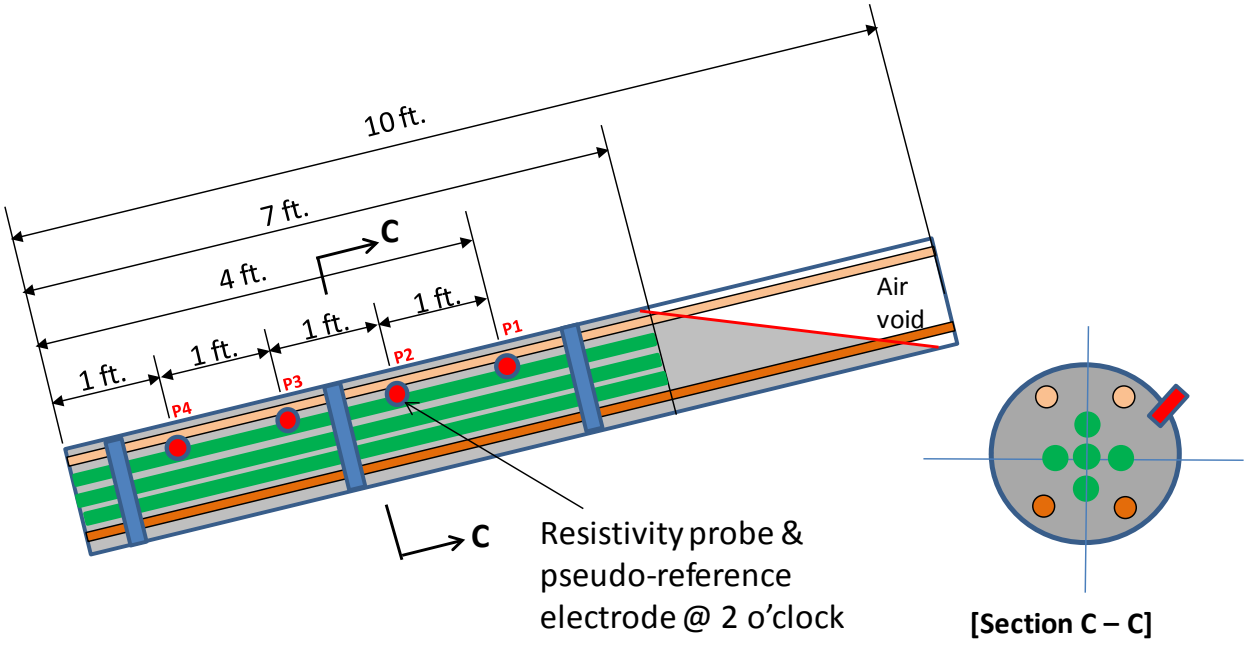

Figure 36. Illustration. Details of multi-strand specimens.

Figure 37 identifies the position of 12-inch-long strand segments with respect to the upper anchor plate. To monitor temperature inside specimens, two thermocouples were installed in the

0 percent chloride specimen placed in the smaller chamber and 1.0 percent chloride specimen placed in the larger chamber. The strand orientation was indicated as follows:

- Top-left strand (TL).
- Top-right strand (TR).
- Bottom-left strand (BL).
- Bottom-right strand (BR).

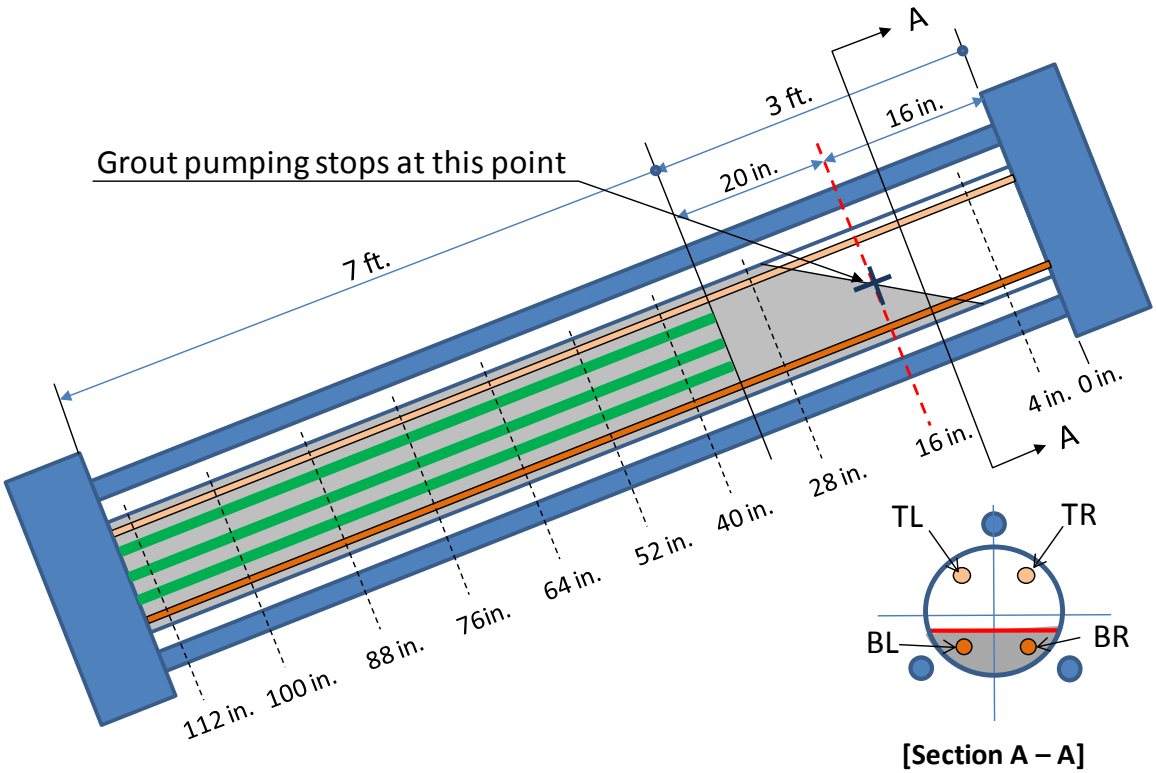

Figure 37. Illustration. Segment designation of multi-strand specimens.

A total of eight specimens were fabricated based on the following test variables:

- **Grout**: Pre-bagged grout product.
- **Stress level**: 60 percent of GUTS.
- **Temperature and RH**: 104 °F + 90 percent RH, 77 °F + 60 percent RH, and 14 °F + 40 percent RH.
- **Chloride concentrations**: 0, 0.08, 0.2, 0.4, 0.6, 0.8, 1.0, and 2.0 percent by weight of cement.
- Ingress of water and oxygen into the simulated air void.

Figure 38 shows some multi-strand specimens prepared for grouting.

Figure 38. Photo. Fully assembled multi-strand specimens.

As described for task 2.2, eight chloride contaminated grout mixes were made per table 4. The fresh grout mix was pumped into the inclined duct until the horizontal void/grout interface reached 16 inches down from the upper anchor plate. This stopping point is indicated with a cross mark in figure 37. In this way, five unstressed strands were buried completely in the grout, and four stressed ones were partially embedded in the grout such that the top 18.5-inch section of two upper stressed strands (TL and TR in figure 37) and the top 13.5-inch section of two lower stressed strands (BL and BR in figure 37) were exposed in the void. Figure 39 shows grouting work in progress. It should be mentioned that the first specimen containing 0 percent chloride started to leak in the bottom grout cap area when about 30 percent of fresh grout was pumped into the duct. As a result, the first batch was discarded, the leaky cap was replaced, and new batch of fresh grout was installed in the specimen.

As explained in task 2.2, three data collections following the 10-day curing were made at ambient condition before they were placed in the environmental chambers to commence the first H & H cycle. The smaller chamber housed two specimens having the lowest chloride concentrations, and the larger chamber had the other six specimens (see figure 4 through figure 6).

Figure 39. Photo. Grout pumping into a multi-strand specimen.

CORROSION PERFORMANCE TESTS AND DATA COLLECTION

Task 2.1: Electrochemical Testing of Single-Wire Specimens in Aqueous Test Solutions

When an experiment was about to begin for a king wire in a particular test condition, a test cell mounted on the wire was filled with an aqueous test solution so that the immersed test area was 1.78 inches^2, as listed in table 6. The test area is calculated as follows:

$$S = \pi \times d \times l$$

Figure 40. Equation. Calculation of surface area.

Where:

S = Surface area.
π= Constant (3.14).
d = Wire diameter.
l = Immersion depth.

Table 6. Test surface area used in this study.

Category	Single PT Strand		Task 2.1 (Center Wire)	Task 2.2 (Single-Strand Specimens)		Task 2.3 (Multi-Strand Specimens)	
	Diameter (inch)	Surface Area (inch^2)		Full	Void	Macro-Anode	Macro-Cathode
Outer six wires	0.198						
Center (king) wire	0.199						
Calculated test surface area		52.3	3.14 × 0.199 inch × 2.85 inch = 1.8 inches^2	1 strand × 1 ft/strand × 52.3 inches^2/ft = 52.3 inches^2	1 strand × 0.83 ft/strand × 52.3 inches^2/ft = 43.6 inches^2	4 strands × 8.7 ft/strand × 52.3 inches^2/ft = 1,813.1 inches^2	5 strands × 7 ft/strand × 52.3 inches^2/ft = 1,830.5 inches^2

Note: Blank cells indicate no data were relevant to the cell.

After 24 h of initial conditioning in the quiescent test solution, the three-electrode LPR test was performed using the experimental setup shown in figure 21 through figure 23. The first step of a LPR measurement determined a corrosion potential of a wire specimen. Once the stable corrosion potential was obtained, R_p was determined through a series of step-wise potentiostatic polarizations. Finally, R_p was used to calculate an instantaneous nominal corrosion rate. For steel embedded in mortar or concrete, intensity of corrosion is usually classified into four corrosion rates, either by corrosion current density ($\mu A/cm^2$) or by mils per year. These criteria are listed in table 7. Since test medium for task 2.1 is aqueous solutions, direct application of the criteria listed in table 7 is not feasible.

Table 7. Corrosion rate criteria.

Degree of Corrosion	Corrosion Rate Criteria	
	Corrosion Current Density ($\mu A/cm^2$)	**Corrosion Penetration Rate (mils/year)**
Negligible	< 0.1	< 0.046
Low	0.1–0.5	0.046–0.230
Moderate	0.5–1.0	0.230–0.460
High	> 1.0	> 0.460

1 cm^2 = 0.155 $inch^2$

Task 2.2: Single-Strand Specimens

Corrosion performance of single-strand specimens was nondestructively monitored once a week using the following methods:

1. Corrosion potential measurement.

2. Instantaneous corrosion rate measurement by LPR method.

3. Apparent grout resistivity.

The condition of the strands in the void was occasionally inspected. Corrosion potential and instantaneous corrosion rate were measured using the setup shown in figure 41. Apparent grout resistivity data were collected as supplementary information using the Wenner four-pin method with 2-inch pin spacings as shown in figure 42.

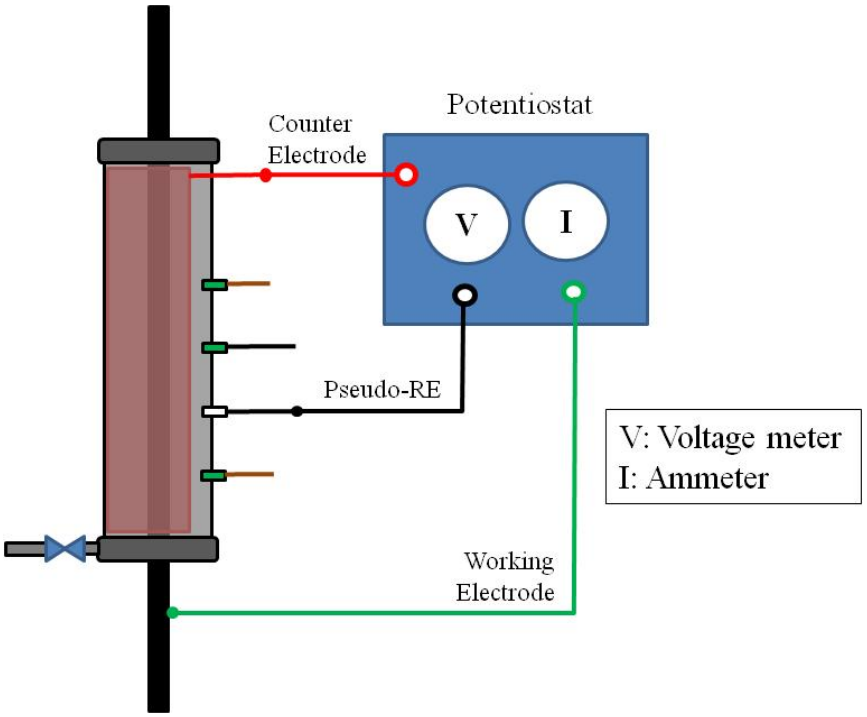

Figure 41. Illustration. LPR measurement for single-strand specimens.

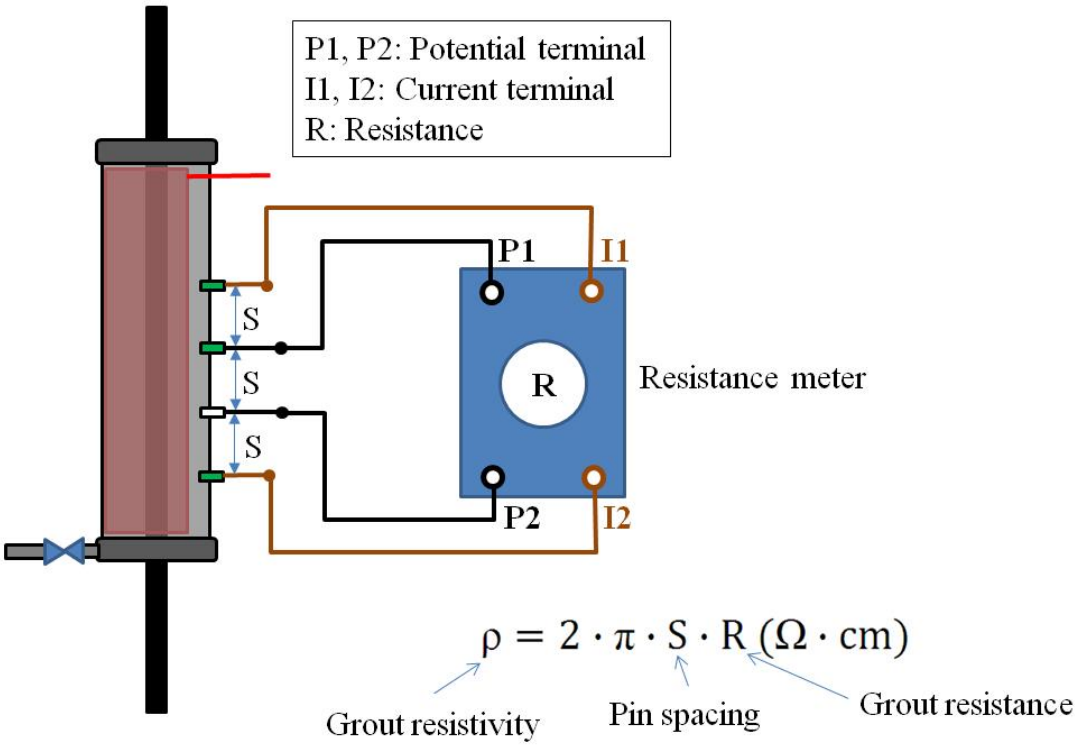

Figure 42. Illustration. Grout resistivity measurement for single-strand specimens.

Since test surface area should be known in order to calculate instantaneous corrosion rate, the following method was used to calculate PT strand surface area per unit length. The diameter of the outer wire was 0.198 inch, and the diameter of the center wire was 0.199 inch, as seen in figure 43.

$$S_6 = \pi \times d \times l \times 6 = 3.14 \times 0.198 \times 12 \times 6 = 44.8 \text{ inches}^2$$

Figure 43. Equation. Surface area of six outer wires.

As such, the following calculation was used to determine the surface area of the center wire:

$$S_c = \pi \times d_c \times l = 3.14 \times 0.199 \times 12 = 7.5 \text{ inches}^2$$

Figure 44. Equation. Surface area of the center wire.

Where:

S_c = Surface area of the center wire.
d_c = Diameter of the center wire.

Strictly speaking, the length of the outer wires should be longer than that of the center wire, but the additional length is ignored in this study to simplify the calculation.

$$S_7 = S_6 + S_c = (44.8 + 7.5) \text{ inch}^2 = 52.3 \text{ inches}^2$$

Figure 45. Equation. Total surface area of seven wires.

As listed in table 6, surface areas of 52.3 and 43.6 inches^2 were adopted for fully grouted specimens and those having a 2-inch void, respectively.

Task 2.3: Multi-Strand Specimens

Corrosion performance of multi-strand specimens was nondestructively monitored using the following methods once a week:

1. Polarized potential measurement.

2. Macro-cell corrosion current ($I_{macro\text{-}cell}$) measurement.

3. Corrosion potential measurement.

4. Grout resistance measurement.

Condition of strands in the void were also occasionally inspected. When $I_{macro\text{-}cell}$ was flowing between macro-anode and macro-cathode, both electrodes polarized away from their natural corrosion potentials and established a mixed potential somewhere between the corrosion potentials. A corrosion cell's relative proximity to a particular electrode's corrosion potential can indicate if it is under cathodic or anodic control. The polarized potential was measured with respect to a PSE, as illustrated in figure 46. $I_{macro\text{-}cell}$ quantifies intensity of corrosion between the macro-anode and the macro-cathode at the time of measurement. In order to avoid interruption in the circuit, an electrical connection was made between the macro-anode and the macro-cathode through a toggle switch. If

current interruption occurred, it would have taken a significant amount of time to regain electrochemical stability within the corrosion cell.

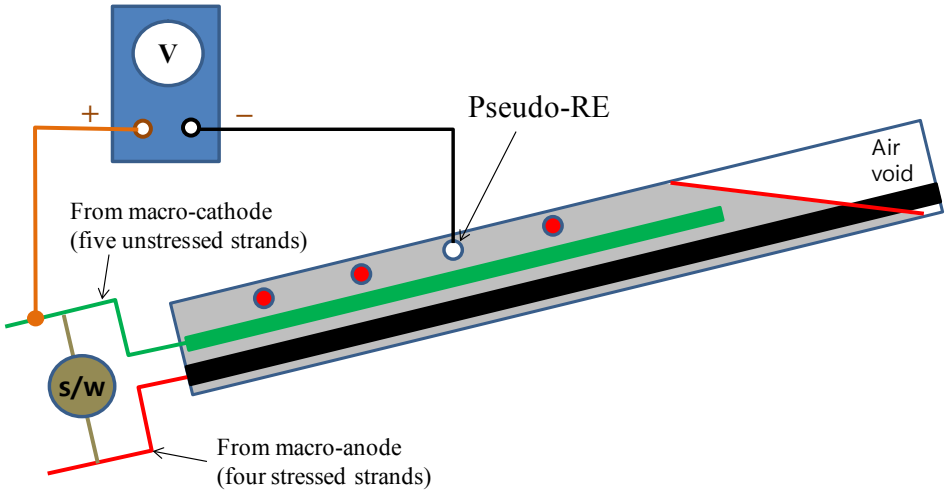

Figure 46. Illustration. Polarized potential measurement for multi-strand specimens.

Therefore, $I_{macro\text{-}cell}$ was measured after a zero resistance ammeter (ZRA) was temporarily inserted in the circuit and then the toggle switch was turned off. This step is shown in figure 47.

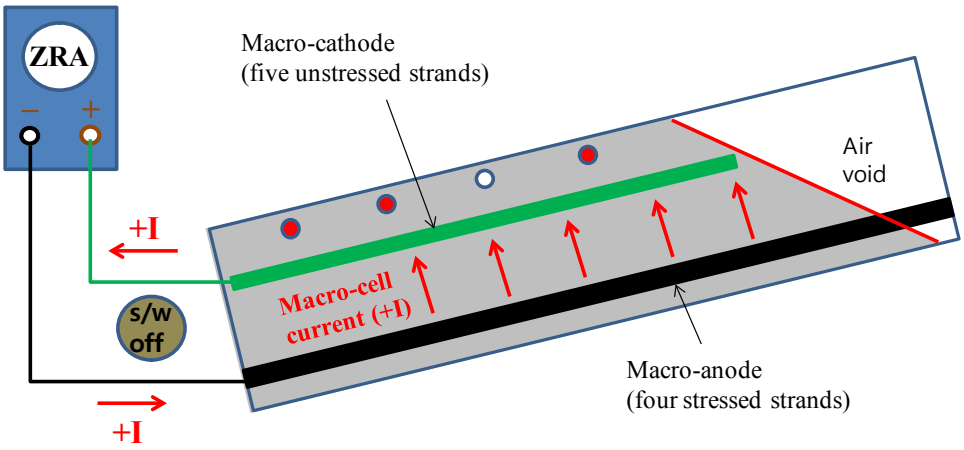

Figure 47. Illustration. Macro-cell corrosion current measurement for multi-strand specimens.

Later, the measured $I_{macro\text{-}cell}$ was divided by macro-anode surface area of 1,813.19 inches^2 from table 5 to calculate the macro-cell corrosion current density ($i_{macro\text{-}cell}$) that is a normalized form of corrosion intensity. After the polarized potential and $I_{macro\text{-}cell}$ were measured, ZRA was removed, and the electrical connection was left disconnected for several hours until the macro-anode and macro-cathode returned to their natural corrosion potentials. Once stable corrosion potentials were achieved, they were measured with respect to four PSEs. This step is shown in figure 48.

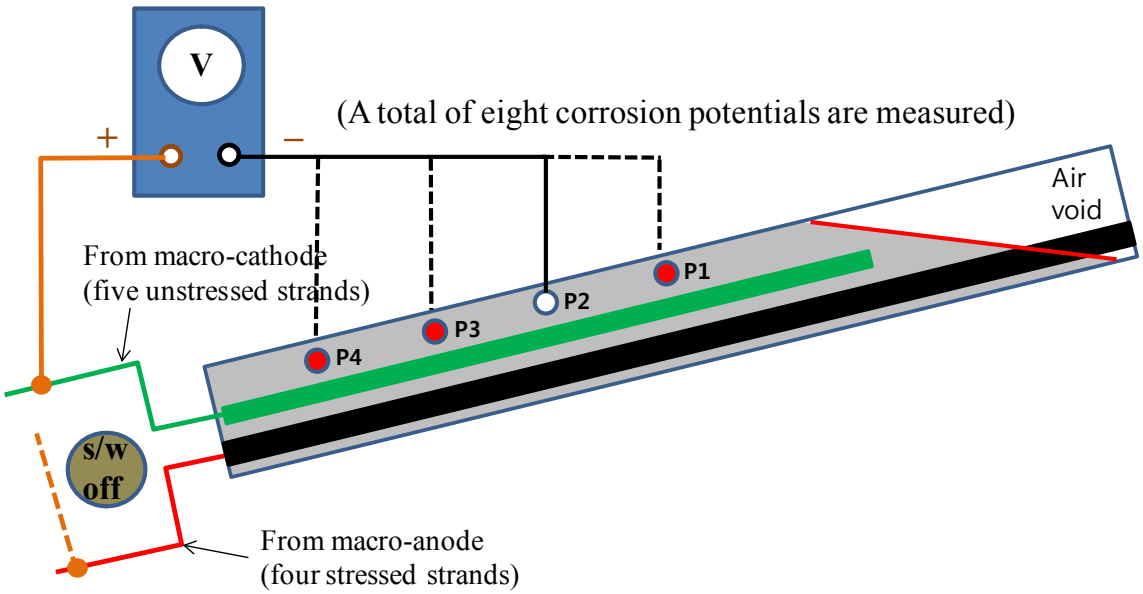

Figure 48. Illustration. Corrosion potential measurement for multi-strand specimens.

Grout resistance data were collected as supplementary information. Grout resistance was measured using four resistivity probes. The internal duct diameter with respect to resistivity probe spacing was too small to measure a valid apparent resistivity. As a result, the resistivity probes were used in two pairs to measure grout resistance in the upper and lower sections of the grouted duct as described in figure 49.

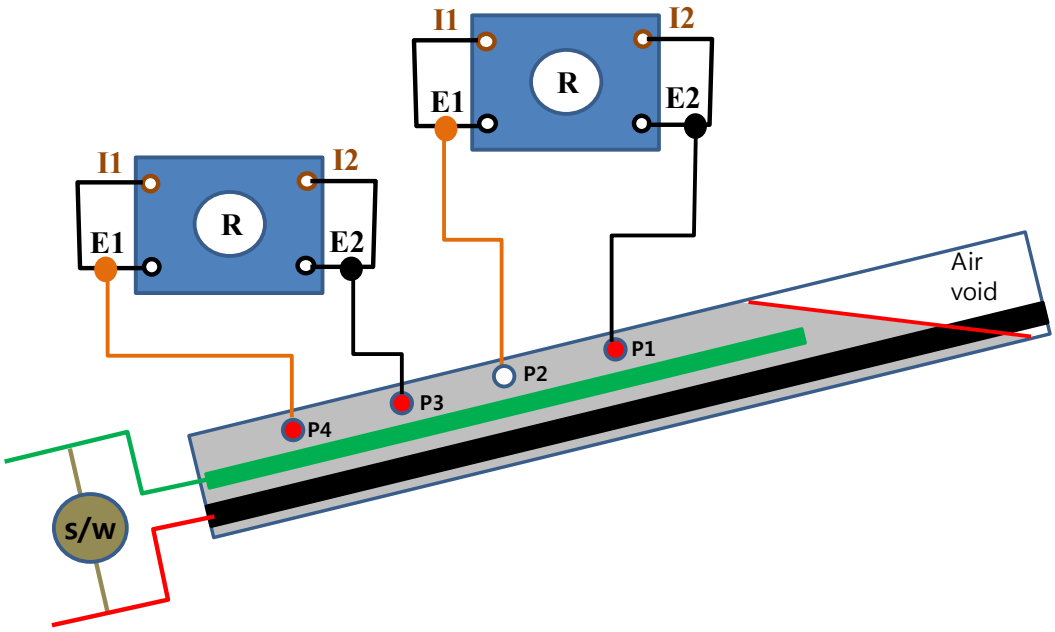

Figure 49. Illustration. Grout resistance measurement for multi-strand specimens.

DUCT CRACKING

The PVC duct of a 0.8 percent chloride multi-strand specimen was abruptly cracked upon minor impact. It happened when a researcher tried to inspect the void condition of the specimen during the second F & D cycle. Emergency repair was made using a special wrapping tape to minimize the impact of cracks. Figure 50 and figure 51 show the specimen before and after repair.

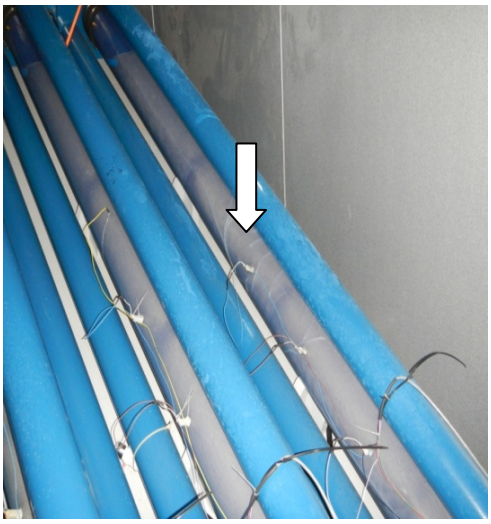

Figure 50. Photo. Cracked duct of 0.8 percent chloride multi-strand specimen before repair.

Figure 51. Photo. Cracked duct of 0.8 percent chloride multi-strand specimen after repair.

WATER RECHARGING EVENT

In order to replicate the water collecting problem from external sources into the voided area of duct in the field PT bridges, a small volume of water was added to the void space in five single-strand specimens and all eight multi-strand specimens after approximately 4 months of accelerated corrosion testing as follows:

- Stressed voided single-strand specimens: 0.08, 0.4, 0.8, and 2.0 percent chloride.

- Unstressed voided single-strand specimen: 0.6 percent chloride.
- Multi-strand specimens: All eight chloride concentrations.

This was done to duplicate the PT corrosion problem reported in the field. A total of 0.17 fl oz of distilled water was injected into each of five void single-strand specimens after a 0.25-inch hole was drilled through the clear duct in the void space. For multi-strand specimens, 5.1 fl oz of distilled water was fed through a pre-introduced hole in the void space. Figure 52 through figure 55 show this step. The filling holes were left open for the remainder of testing so that oxygen could enter.

Figure 52. Photo. Water charging into a multi-strand specimen.

Figure 53. Photo. Water charging into a single-strand specimen.

Figure 54. Photo. Multi-strand specimen 1 h after water charging.

Figure 55. Photo. Single-strand specimen 1 h after water charging.

Researchers at the University of South Florida and FDOT also performed a similar laboratory study to investigate the same problem using a macro-cell corrosion test setup between PT anchorage assemblies and strands.[18] They were able to produce marked current increases as shown in figure 56 upon repeated water charging events.

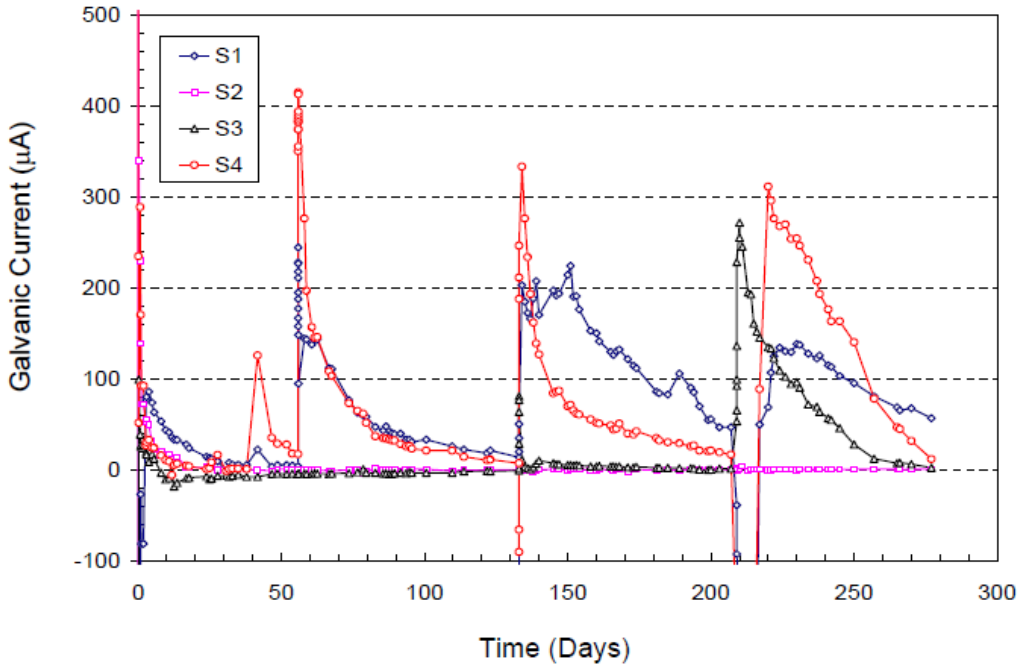

Figure 56. Graph. Relationship between water charging and macro-cell corrosion current jump.[18]

INTRODUCTION OF AIR HOLES

Right after water was added to the specimen voids, 4 0.5-inch-diameter holes were introduced to each of the 6 voided single-strand specimens, and 24 0.5-inch-diameter holes were introduced to one of the multi-strand specimens that was cracked and repaired. The specimens included the following:

- Stressed voided single-strand specimens: 0.08, 0.4, and 0.8 percent chloride (all three concentrations had water and air holes).
- Unstressed voided single-strand specimens: 0.08, 0.4, and 0.8 percent chloride, which were the control and kept in room temperature.
- Multi-strand specimen: 0.8 percent chloride (had water and air holes).

Figure 57 and figure 58 show a single-strand specimen and a multi-strand specimen that were introduced with 0.5-inch holes, respectively. This effort was to see if more oxygen could enhance corrosion activities of the strands.

Figure 57. Photo. Drilled single-strand specimen.

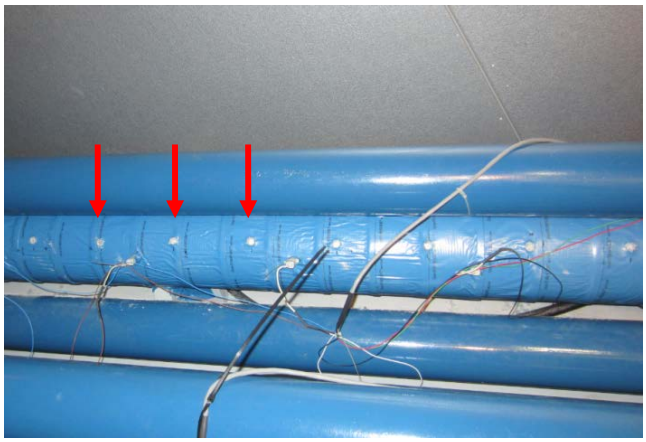

Figure 58. Photo. Drilled multi-strand specimen with 0.8 percent chloride.

AUTOPSY PROCEDURE

At the completion of the 6-month data collection period, the specimens were taken out of the environmental chambers, and an autopsy was carried out. One day before performing the autopsy, final data collection was performed at ambient condition. Following the data collection, all of the stressed specimens were detensioned, and destructive autopsy work began.

Task 2.2: Single-Strand Specimens

The detensioned and originally unstressed single-strand specimens were cut out from their loading frames followed by the autopsy. As the first step, three grout powder samples along the length were extracted for chloride analysis at 0- to1-inch depth from each specimen (see figure 59). A total of 72 samples were taken from 16 stressed and 8 unstressed specimens. Then, a right angle grinder equipped with a diamond blade was used to split each specimen open (see figure 60). Every strand was extracted, and their grout/strand interfaces were examined and photographed (see figure 61). Some of the strands exhibited minor corrosion (see figure 62), and the others exhibited heavy corrosion (see figure 63). The as-extracted condition was documented on a mapping sheet. The extracted PT strands were dismantled, and the individual wires were cleaned with a scrubbing pad (see figure 64). Superficial rust stains could be removed by this method, but those having stubborn

corrosion products associated with severe corrosion damage had to be cleaned further with an acid cleaning solution per ASTM G1 (see figure 65).[19] The cleaned wires were visually examined with occasional use of a magnifier.

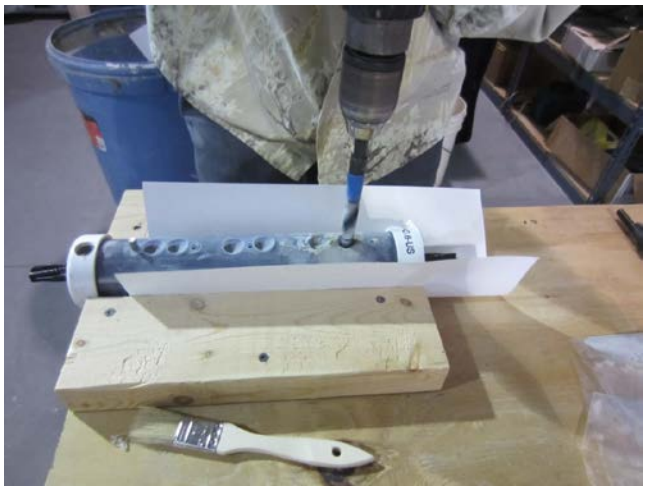

Figure 59. Photo. Grout powder sampling from a single-strand specimen.

Figure 60. Photo. Splitting a single-strand specimen using a circular saw.

Figure 61. Photo. Single-strand specimen longitudinally cut in half.

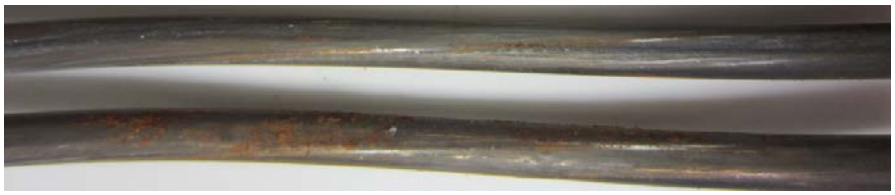

Figure 62. Photo. Example of superficial rust on the extracted wires.

Figure 63. Photo. Example of heavy rust on the extracted wires.

Figure 64. Photo. Cleaning individual wires using a scrubbing pad.

Figure 65. Photo. Acid cleaning of moderately to severely corroded wires.

Task 2.3: Multi-Strand Specimens

After stress in a multi-strand specimen was released, the upper anchor plate was removed (see figure 66). Following it, 12 grout power samples per specimen were taken along the 3 and 9 o'clock lines by drilling at two depths (0 to 1 and 1 to 2 inches) and three locations (14, 48, and 96 inches) from the lower anchor plate (see figure 67). As a result, a total of 96 grout powder samples were extracted to determine spatial distribution of the admixed chloride in the multi-strand specimens. As soon as grout sampling was completed, the destructive dismantling process started by cutting the clear duct along the 3 and 9 o'clock lines (see figure 68), removing the two duct halves, and chipping the grout away (see figure 69). Initially, great caution was exercised in anticipation of residual stress in the strands embedded in grout, but the stress dissipated quickly as the grout chipping work progressed from one specimen end. Some large grout pieces in direct contact with the strands were retrieved from the upper, middle, and lower sections of each specimen (see figure 70). These chunks were later used to collect powder samples at the strand imprints by carefully removing portions of the grout with a hammer and chisel to determine chloride concentrations at the grout/strand interface. Some grout fragments were also used to examine grout quality. After grout was completely removed, the strands were cut one by one near the lower anchor plate (see figure 71), and they were taken out of the loading frame (see figure 72). The removed strands were preserved in the smaller chamber which maintained a RH lower than 50 percent (see figure 73). After all the destructive work was completed, examination of the multi-strands started on a specially constructed autopsy table (see figure 74).

Figure 66. Photo. Removal of the upper anchor bearing plate of a multi-strand specimen.

Figure 67. Photo. Grout powder sampling for chloride analysis from a multi-strand specimen.

Figure 68. Photo. Cutting the clear duct to expose grout.

Figure 69. Photo. Chipping grout to expose PT strands.

Figure 70. Photo. Retrieved grout pieces from multi-strand specimens.

Figure 71. Photo. Cutting PT strands near the lower anchor bearing plate.

Figure 72. Photo. Extracting a multi-strand bundle from a loading frame.

Figure 73. Photo. Storing the retrieved multi-strand samples in a chamber.

Figure 74. Photo. Inspecting PT strands removed from a multi-strand specimen on an autopsy table.

The as-extracted condition of each strand was carefully inspected and documented on a mapping sheet. As indicated in figure 37, the reference point in the mapping sheet was 16 inches, the mean distance to the void/grout interface from the upper anchor plate. From the reference point moving toward the lower anchor plate, 12-inch-long segments were marked on the stressed and unstressed strands. This is also depicted in figure 37. Every 12-inch segment that exhibited rust spots was identified on the mapping sheet. With this marking system, four stressed strand segments passed through the void/grout interface: two 4-to-16-inch segments of the BL and BR strands and two 16- to 28-inch segments of the TL and TR strands as labeled in figure 37. A total of eight strand segments close to the upper anchor plate were situated near the void/grout interface, and all the other stressed and unstressed strand segments were contained in the grout. It was observed during the autopsy that some of the interface segments exposed to unintentional sulfate ions exhibited more corrosion damage compared to the rest. This situation resembled severe corrosion failures observed in the defective tendons in service.

Many segments of the stressed strands exhibited signs of corrosion, and they were cut out for further examination (see figure 75). Individual wires removed from the cut-out segments were cleaned with a scrubbing pad first. Similar to single-strand specimens, the wires with stubborn corrosion products were cleaned further with an acid cleaning solution. The unstressed strands exposed to grout with moderate to high levels of chloride contamination often showed rust stains in the localized areas. Each unstressed strand with this condition was dismantled as one 7-ft-long piece, and the wires were also cleaned with a scrubbing pad. No significant corrosion damage requiring acid cleaning was observed on any of the unstressed wires (see figure 76).

Figure 75. Photo. Several 12-inch-long cut-out segments exhibiting various corrosion conditions.

Figure 76. Photo. Cleaning and visual inspection of 7-ft-long unstressed strands.

CORROSION DAMAGE ASSESSMENT

The cleaned wires were first examined visually to classify them in two groups. The minor corrosion group included the wires exhibiting superficial corrosion or shallow pits (less than 2 mil deep). The wires that appeared to contain pits deeper than 2 mil were placed in the moderate to severe corrosion group. Most of the acid cleaned wires fell into the latter group.

Figure 77 shows a pit depth measurement in progress. The particular spot showed a pit depth of 13.5 mil. A digital pit depth gauge capable of measuring the lowest depth of 1.0 mil was used. A custom-made magnet-based measurement bed was a convenient means to hold the curved wire being measured steady in any orientation. Excessive section loss was measured with a digital micrometer as shown in figure 78.

Figure 77. Photo. Pit depth measurement using a digital pit gauge.

Figure 78**. Photo. Section loss measurement in a severely corroded area.**

CHAPTER 4. TEST RESULTS AND DISCUSSION

This chapter presents electrochemical data that were collected weekly, other laboratory test results, autopsy results, and discussion with the outcomes of the indepth data analyses. The first set of test results is presented with experimental data versus time plots to show data changes as a function of time. In each plot shown in figure 88 through figure 90, figure 108 through figure 115, figure 120 through figure 127, figure 144 through figure 151, figure 154, figure 155, and figure 164 through figure 171, the duration of individual H & H and F & D cycles is highlighted with red and blue columns, respectively. White columns indicate either initial ambient or ambient cycles. The second set of test results shown in figure 100 through figure 107 is related to individual mean values of experimental datasets collected over time to show major trends associated with admixed chloride concentration, stress level, existence of void, and/or exposure conditions (i.e., initial ambient, ambient, H & H, and F & D). The first three datasets collected during the first ambient cycle were treated separately as the initial ambient cycle because they indicated more active electrochemical behavior than those collected in the other ambient cycles at later times. It is thought that most strands experienced active corrosion during the initial ambient exposure as they were first in contact with fresh grout and then started to corrode. The initial corrosion process continued until the formation of protective oxide layers (passive film) on the strands was completed. Once the stable passivity was established, the strands maintained a low corrosion state as discussed in figure 7. The third set of test results shows photographs that were taken throughout the study. Lastly, corrosion damage of the autopsied specimens is documented with pit depth measurements, photographs, and condition mapping sheets.

From all of the results, a comparative analysis of the collected non-destructive data and the observed physical corrosion damage data was performed to determine chloride threshold values for PT tendons in chloride-contaminated grout.

TASK 2.1: ELECTROCHEMICAL TESTING OF SINGLE-WIRE SPECIMENS IN AQUEOUS TEST SOLUTIONS

Preliminary tests were conducted to become familiar with experimental setup and select the initial conditioning parameters for king wires prior to performing actual electrochemical testing. These parameters were maintained throughout the task 2.1 experiment. Physical aspects of the experiment setup such as installing test cells and applying target stress in the wires were finalized after several trials. The immersion time in the test solutions and solution agitation were two main issues. After reviewing the preliminary test results, initial conditioning of 24-h immersion time without agitating solution was selected for actual specimens. Figure 79 and figure 80 present corrosion potential data and corrosion rate data of king wires, respectively.

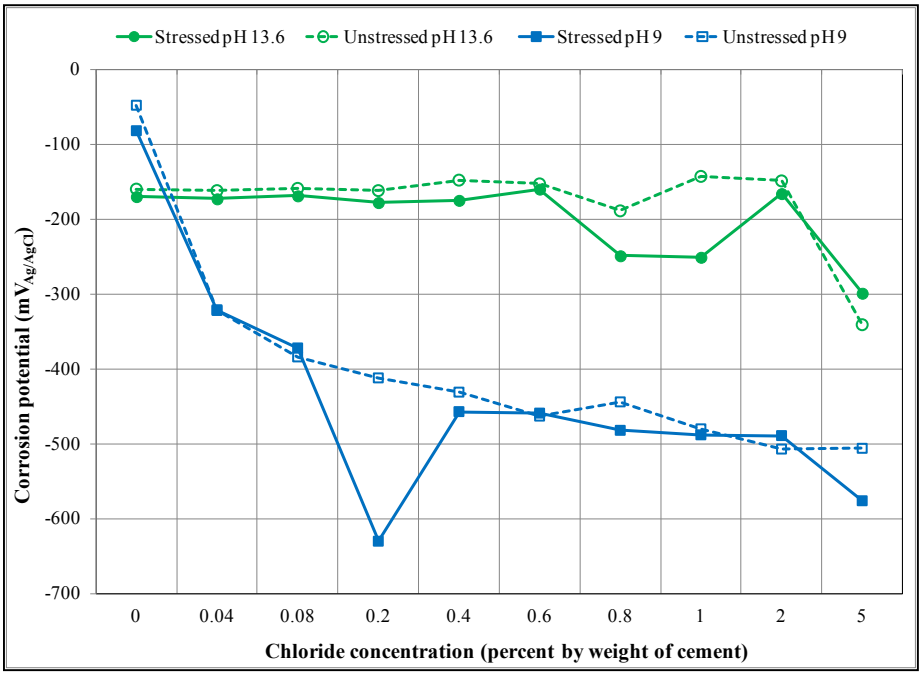

Figure 79. Graph. Corrosion potentials of center wires in different test environments.

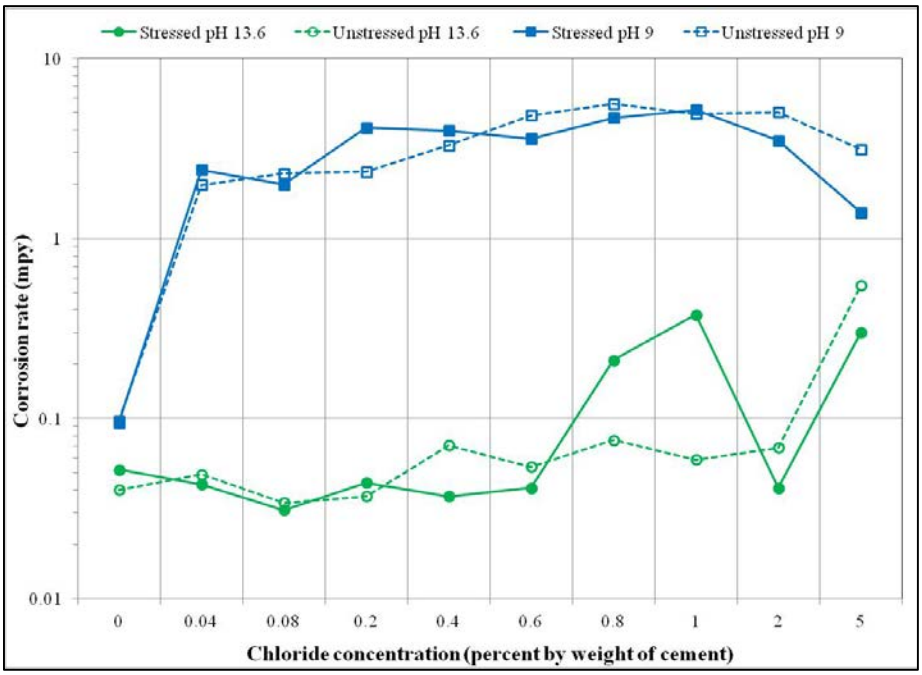

Figure 80. Graph. Corrosion rates of center wires in different test environments.

As expected, the wires immersed in the 13.6 pH solutions were protected by the passive film formed in the high pH environment. Their performance was characterized by relatively positive corrosion potentials, indicating an inactive thermodynamic state for corrosion and low corrosion rates indicating slow metal dissolution rate. In the high pH environment, the corrosion rate was virtually 0 mil/year up to an equivalent chloride concentration of 0.6 percent by weight of cement and then slightly increased at higher chloride concentrations. Corrosion products observed on the

tested wires and in the solutions were also negligible. The effect of stress was not apparent in a low chloride concentration up to 0.6 percent, but the stressed wires exposed at 0.8 and 1.0 percent chloride concentration showed slightly higher corrosion rates than the unstressed counterparts in the same test conditions. However, conflicting data from corrosion behavior at 2.0 and 5.0 percent chloride concentrations indicated that there was no trend. Additional tests are suggested to yield statistically significant results in the future.

For the specimens tested in the pH 9.0 solutions containing an equivalent chloride concentration of 0.04 percent by weight of cement and higher concentrations, corrosion potentials became progressively more negative as chloride concentration increased. Conversely, the matching corrosion rates went up sharply compared to the electrochemical data obtained in the chloride-free 9.0 pH solutions and all 13.6 pH solutions. The corrosion products deposited on the tested wires and bottom of the test cells were much more visible and abundant compared to the high pH counterparts. Also, color of the solutions became darker by dissolved corrosion products as corrosion rate increased. The observed reduction of corrosion rate at 5.0 percent chloride concentration is thought to be caused by a lack of dissolved oxygen in the low pH solutions due to excessive chloride ions. Again, there was no consistency observed regarding the effect of stress on corrosion rate regardless of chloride concentration.

The observed passive behavior of king wires in the high pH solutions signifies the importance of maintaining a high pH environment to prevent corrosion of PT strands. Formation of sound passive film is only possible on PT strands completely surrounded by high-quality grout that offers the high pH environment. The protective film will eventually become compromised when chloride ions exceed threshold values. The electrochemical data in figure 79 and figure 80 suggest that PT strands can tolerate chloride contamination without significant corrosion up to 0.6 percent by weight of cement in carbonation-free (high pH) grout, whereas PT strands with as low as 0.04 percent chloride by weight of cement can initiate active corrosion in the carbonated (low pH) grout. This is below the AASHTO specified chloride limit of 0.08 percent by weight of cement. Any air getting through the grout voids and cracked duct/grout will likely expose PT strands to a lower pH environment through carbonation process. Once corrosion starts in the low pH environment, the level of corrosion damage will depend on chloride concentration.

ADMIXED VERSUS EXTRACTED CHLORIDE CONTENTS

Figure 81 shows chloride analysis results of the 10-day trial mixes. Mean background acid-soluble chloride content in the grout powder was determined to be 0.009 percent (90 ppm) by weight of sample. It was small enough to consider the acquired grout chloride-free. The 0.009 percent by weight of sample is equivalent to 0.017 percent by weight of cement. The conversion was made based on known cement weight of 33.33 lb per 50-lb grout bag and 12.5 lb of mixing water added per bag.

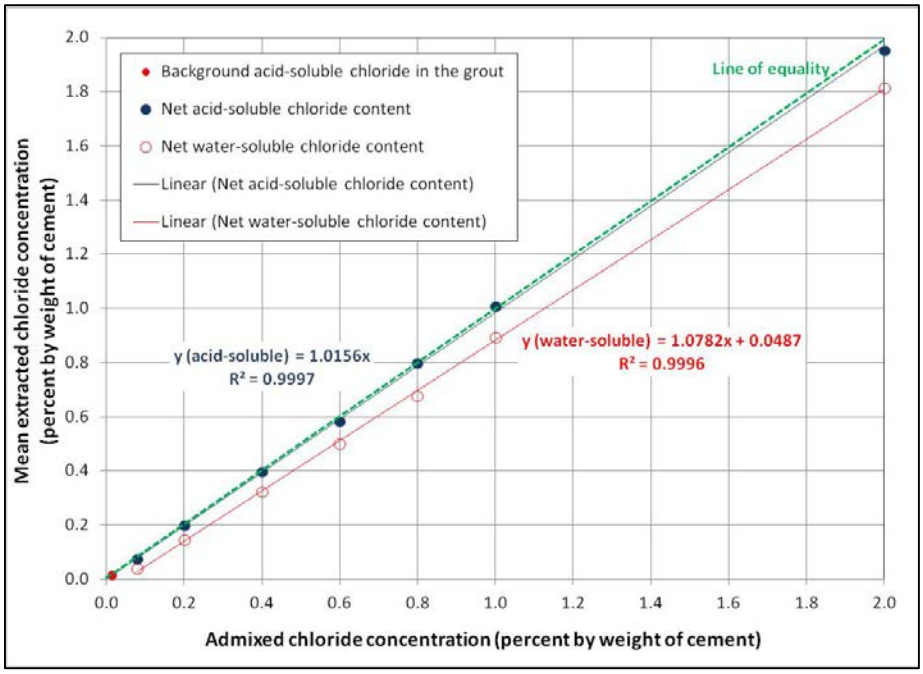

Figure 81. Graph. Relationship between admixed chloride contents and actual concentrations in the trial grout mixes extracted by ASTM water-soluble and AASHTO acid-soluble methods.[15,16]

As shown in figure 81, mean extracted acid-soluble chloride concentrations were virtually identical to the admixed chloride concentrations in that a linear regression line runs nearly over the line of equality with almost perfect coefficient of determination ($R^2 = 0.9997$). This means that nearly all admixed sodium chloride contents were extracted through the acid-soluble titration method. It is also true that the calculated sodium chloride weights listed in table 2 were accurate. For water-soluble chloride data, the extracted amounts were somewhat less compared to the acid-soluble results, and the difference increased as chloride concentration increased. Nonetheless, the water-soluble data also yielded $R^2 = 0.9996$. After confirming adequacy of the mix proportions, actual grout mixes were made to cast tasks 2.2 and 2.3 specimens.

Figure 82 shows acid-soluble chloride analysis results, expressed in three different units, of grout powder samples taken from single-strand specimens and multi-strand specimens after the accelerated corrosion testing was terminated. It can be seen that the extracted acid-soluble chloride contents were virtually the same between single-strand specimens and multi-strand specimens. This finding confirms that the admixed sodium chloride was uniformly dispersed in the fresh grout, and both types of specimens were tested in the identical chloride concentrations.

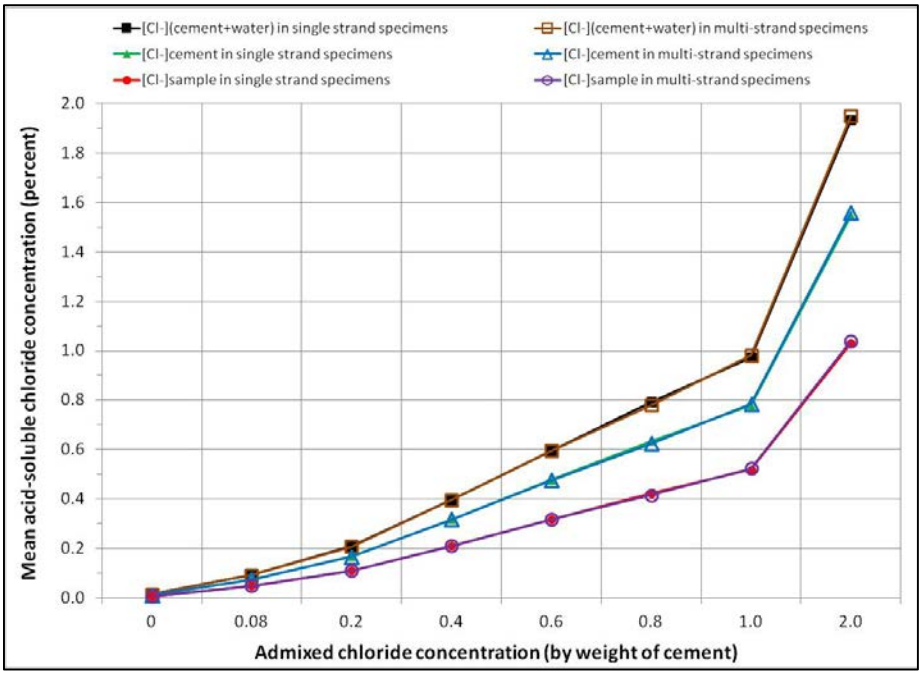

Figure 82. Graph. Mean acid-soluble chloride contents in grout powder samples calculated by three conversion methods.

It can be also seen in figure 82 that three different chloride concentration units yielded three different extracted concentrations for a given admixed chloride concentration (see table 8).

Table 8. Different chloride concentration units reported in this study.

Notation	Description of Acid-Soluble (Total) Chloride Concentration Units
$[Cl^-]_{(cement + water)}$	Percent by weight of cement plus weight of mixing water
$[Cl^-]_{cement}$	Percent by weight of cement excluding weight of mixing water
$[Cl^-]_{sample}$	Percent by weight of grout powder sample

Mean extracted acid-soluble chloride concentrations expressed by $[Cl^-]_{(cement + water)}$ accounted for almost 100 percent of the admixed chloride concentrations. Those expressed by $[Cl^-]_{cement}$ and by $[Cl^-]_{sample}$ resulted in approximately 75 and 50 percent of the admixed chloride concentrations, respectively. The following example exemplifies the 1.0 percent admixed chloride concentration case to demonstrate why different concentration units yield different concentration values.

As listed in table 2, a six-bag grout mix containing 1.0 percent chloride by weight of cement requires 2.0 lb of chloride ions (60.6 percent of 3.3 lb sodium chloride) dissolved in 75 lb distilled water and six 50-lb grout bags. Theoretical acid-soluble chloride concentration in the hardened grout powder sample should be as follows:

$$[Cl^-]_{acid\text{-}soluble} = \frac{2.0 \text{ lb}}{(300 \text{ lb} + 75 \text{ lb} + 3.3 \text{ lb})} = 0.005287 = 0.5287 \text{ percent} = 5{,}287 \text{ ppm by weight of sample}$$

Figure 83. Equation. Example of calculating acid-soluble chloride concentration in the hardened grout powder sample.

Mean acid-soluble chloride concentration in the grout powder samples taken from 1.0 percent chloride multi-strand specimen was 0.5235 percent, or 5,235 ppm by weight of sample. This is close to the theoretical value and is also about 50 percent of the original chloride concentration by weight of cement.

There are two correction factors to convert the chloride concentration $[Cl^-]_{sample}$ back to either $[Cl^-]_{(cement + water)}$ or $[Cl^-]_{cement}$. If weight of mixing water is considered, use a correction factor of 1.875 as follows (see figure 84):

- Weight of cement in six 50-lb grout bags = 2/3 × 300 lb = 200 lb.
- Weight percentage of cement in six 50-lb grout bag and mixing water = 200 lb/(300 lb + 75 lb) = 53.33 percent by weight of cement plus water.

$$[Cl^-]_{acid\text{-}soluble} = 0.5235 \text{ percent} \times \frac{1}{0.5333} =$$

$$0.5235 \text{ percent} \times 1.875 = 0.9816 \text{ percent by weight of cement plus water}$$

Figure 84. Equation. Example of converting chloride concentration by weight of grout sample to chloride concentration by weight of cement plus weight of mixing water.

This can be considered 100 percent of the original chloride concentration by weight of cement. If weight of mixing water is not considered, use a correction factor of 1.5 as follows (see figure 85):

- Weight of cement in six 50-lb grout bags = 2/3 × 300 lb = 200 lb.
- Weight percent of cement in six 50-lb grout bags = 200 lb/300 lb = 66.67 percent.

$$[Cl^-]_{acid\text{-}soluble} = 0.5235 \text{ percent} \times \frac{1}{0.6667} = 0.5235 \text{ percent} \times 1.5 =$$

$$0.7853 \text{ percent by weight of cement without water}$$

Figure 85. Equation. Example of converting chloride concentration by weight of grout sample to chloride concentration by weight of cement without weight of mixing water.

This can be treated approximately 75 percent of the original chloride concentration by weight of cement.

Even though any of three chloride concentration units may be used interchangeably for hardened grout powder samples, each unit is suitable for different circumstances. Specifically, a chloride concentration expressed by $[Cl^-]_{(cement + water)}$ is the best if precise mix proportion including weight of mixing water is known like the present study. This is because it represents almost 100 percent of acid-soluble chloride concentration in the hardened grout. For the particular grout product used in this study, a correction factor of 1.875 should be used. If weight of cement is known and weight of mixing water is unknown, concentration expressed by $[Cl^-]_{cement}$ can be used; however, it accounts for approximately 75 percent of acid-soluble chloride concentration in the hardened grout. In the same grout case, use a correction factor of 1.5. If none is known, concentration expressed by $[Cl^-]_{sample}$ is the only choice. In practice, the last option may be the most frequently used and easy to

use because no conversion is necessary. However, it is important to indicate that a chloride concentration expressed by this unit represents only 50 percent of true acid-soluble chloride concentration in the hardened grout.

To illustrate differences in these concentration units, figure 86 plots fractions of mean acid-soluble chloride data presented in figure 82 to their respective admixed chloride concentrations. Fractions of 0.08 and 0.2 percent data exceeded those of the higher chloride concentrations because background chloride concentration was significant for the two lowest chloride concentrations. For the other commercially available pre-bagged grout products, similar conversion relationships can be developed provided that exact weight of cement in a bag is known.

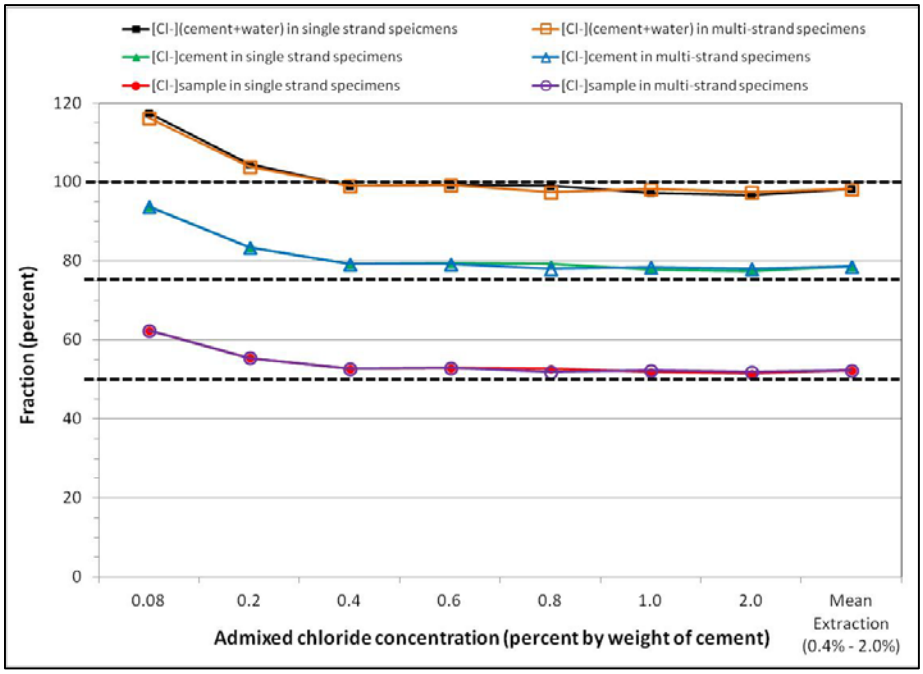

Figure 86. Graph. Mean chloride extraction rates based on three conversion methods.

Figure 87 provides detailed chloride data analysis results of multi-strand specimens. It shows mean chloride data grouped by sampling location and depth. It can be seen in the figure that mean extracted chloride concentrations were identical within each sample group except for those at the grout/strand interface being slightly lower. The adherence of chloride ions to the steel surface might be responsible for the lower chloride concentration at the interface. The same trend is typical for reinforcing steel bar/concrete interface as well. From this dataset, the admixed chloride ions were confirmed to be evenly distributed in each grout mix, and no biased test results were originated from uneven chloride distribution. The single-strand specimens had the same level of even chloride distribution at each target concentration.

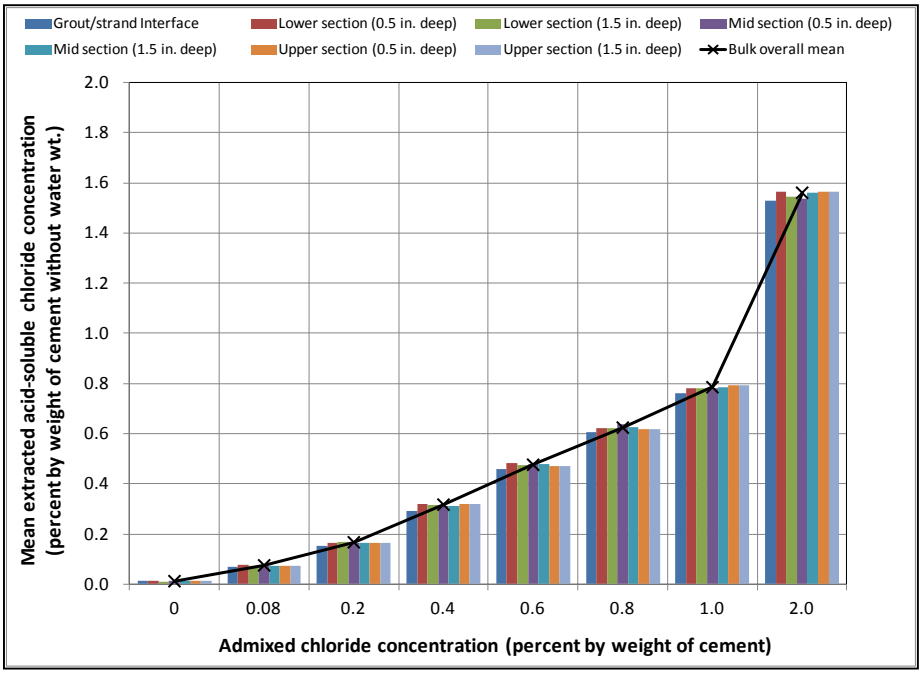

Figure 87. Graph. Mean extracted acid-soluble chloride concentrations at different locations of multi-strand specimens.

ENVIRONMENTAL DATA

Figure 88 shows temperature variations in the environmental chambers and interior of two multi-strand specimens during the accelerated corrosion testing.

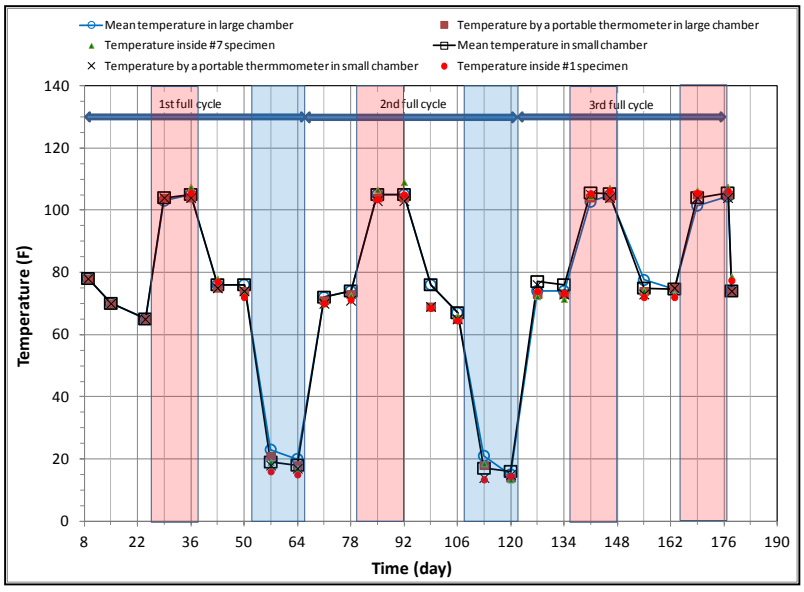

Figure 88. Graph. Sequence of exposure cycles and temperature changes during accelerated testing.

Figure 89 shows variations of mean RH readings in the environmental chambers. It can be seen that target temperatures were fairly well maintained, whereas target RHs were somewhat difficult to

control. Overall, environmental loading was thought to be adequate enough to expedite the corrosion process fairly well.

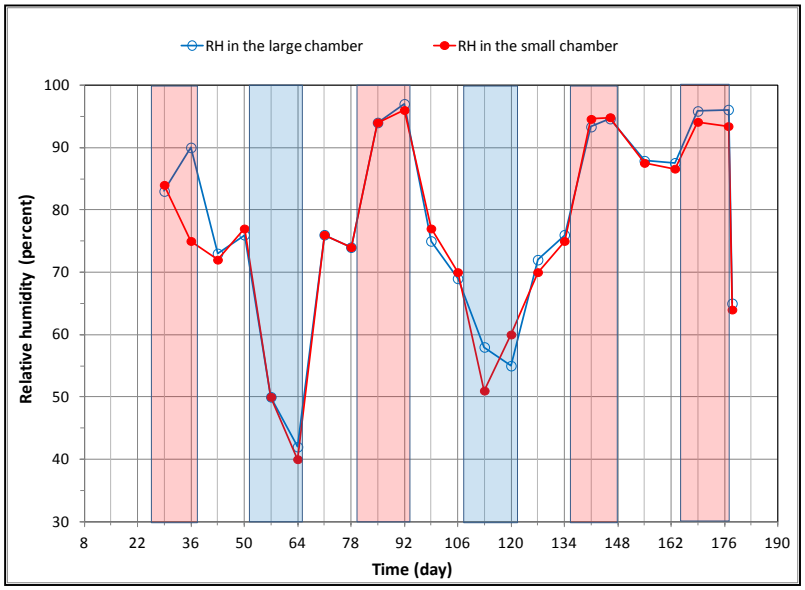

Figure 89. Graph. Recorded mean RH readings in the environmental chambers.

POTENTIAL DATA

PSE Versus ACE

The portable ACE and CSE are the most widely used and commercially available reference electrodes. They have finite potential differences at any given temperature with respect to the standard hydrogen electrode, a specially constructed reference electrode for all other reference electrodes. The potential readings taken with one type of reference electrode can be converted to those measured with other types as inherent potential difference between the two reference electrodes is known.

The PSE used in this study was a custom-made project-specific reference electrode used to collect potential data for the strand specimens. For the purpose of potential conversion to ACE, corrosion potentials of PSEs embedded in the calibration blocks containing eight chloride concentrations were measured weekly. These calibration blocks were subjected to the same temperature/RH cycles as the strand specimens in the environmental chambers. Figure 90 shows exemplary corrosion potential data of three PSEs versus ACE. The other PSE potential data fell within the ranges exhibited by these PSEs. It can be seen that 0 percent chloride PSE tended to show more temperature sensitive behavior than the others, especially during the F & D cycles. Also, 1.0 percent PSE exhibited nearly -220 mV versus ACE at an early measurement. The reason for the negative potential reading could not be identified.

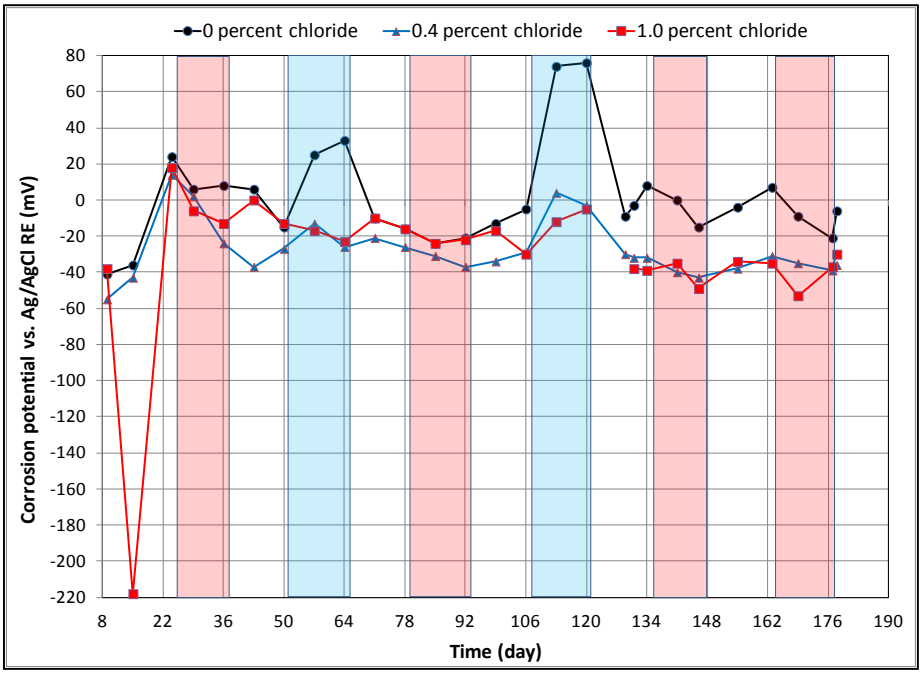

Figure 90. Graph. Corrosion potential versus time for three PSEs embedded in the calibration cylinders measured with respect to ACE.

Figure 91 shows PSE mean corrosion potentials for each chloride concentration calculated from individual corrosion potential data for 6 months in ambient, H & H, and F & D cycles. All exhibited relatively positive corrosion potentials during the F & D cycles. Since PSE potential can be influenced by many factors, it would be difficult to come up with an accurate, universal conversion factor. For the sake of simplifying the data analysis, a mean value of -30 mV versus ACE was chosen for this study as a single conversion factor regardless of chloride concentration and exposure condition. The number was selected based on a dominant trend observed during ambient and H & H cycles in figure 91. Since the potential data collected in ambient and H & H cycles account for majority of the potential data and corrosion activity observed in F & D was insignificant, use of the conversion factor should be considered reasonable. The converted potential values were used to compare them to the existing corrosion potential criteria given in ASTM C876.[18] With the -30 mV conversion factor, -100 mV versus PSE is equivalent to -130 mV versus ACE or -230 mV versus CSE. Conversely, -350 mV (90 percent probability of corrosion per ASTM C876) and -200 mV (90 percent probability of no corrosion per ASTM C876) versus CSE are equivalent to -220 and -70 mV versus PSE, respectively.

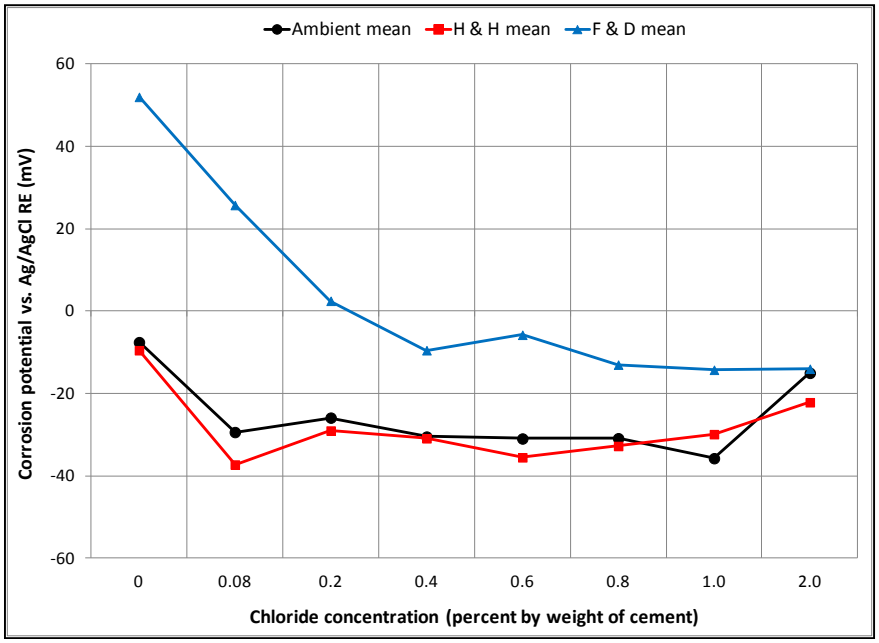

Figure 91. Graph. Mean corrosion potentials of PSEs versus ACE in three exposure conditions.

TASK 2.2: CORROSION POTENTIAL OF SINGLE-STRAND SPECIMENS

Figure 92 through figure 99 present corrosion potentials versus time plots for single-strand specimens. The first measurements after receiving water and/or air holes are indicated in the relevant plots. Most specimens in the environmental chambers exhibited fluctuating potentials as they were subjected to temperature and RH changes. The majority of corrosion potential data stayed between -70 and -220 mV versus PSE or -200 and -350 mV versus CSE. This range corresponds to uncertain corrosion state according to ASTM C876 criteria.[18]

While a voided specimen containing 0.08 percent chloride showed little change upon water recharging, the other specimens containing 0.4, 0.6, 0.8, and 2.0 percent chloride concentrations experienced a potential drop in the negative direction as soon as water entered the voids. Since more negative corrosion potential means more thermodynamically susceptible to corrosion, the added water should have made these voided specimens more corrosion active. The most negative corrosion potential, -380 mV versus PSE, was exhibited by a stressed specimen containing 2.0 percent chloride concentration (see figure 99), which is equivalent to approximately -410 mV versus ACE or -510 mV versus CSE. Such a negative potential is considered very active corrosion even for ordinary reinforced concrete.

Most control specimens in room temperature remained in the relatively positive potential range throughout the study, indicating enhanced passive behavior regardless of chloride concentration. Introduction of air holes (no water added) to 0.08, 0.4, and 0.8 percent chloride specimens did not influence their corrosion potential trends. One exception was noted for 1.0 percent chloride voided control specimen. This specimen exhibited a sudden potential drop to nearly -200 mV versus PSE or -330 mV versus CSE at the 177th day as shown in figure 87, indicating that corrosion might have just initiated in the specimen containing the highest chloride concentration among the voided specimens. Comparing corrosion potential data of the accelerated corrosion testing specimens to

those exposed in the room temperature reveals that alternating temperature and RH was effective to expedite strand corrosion in the former group.

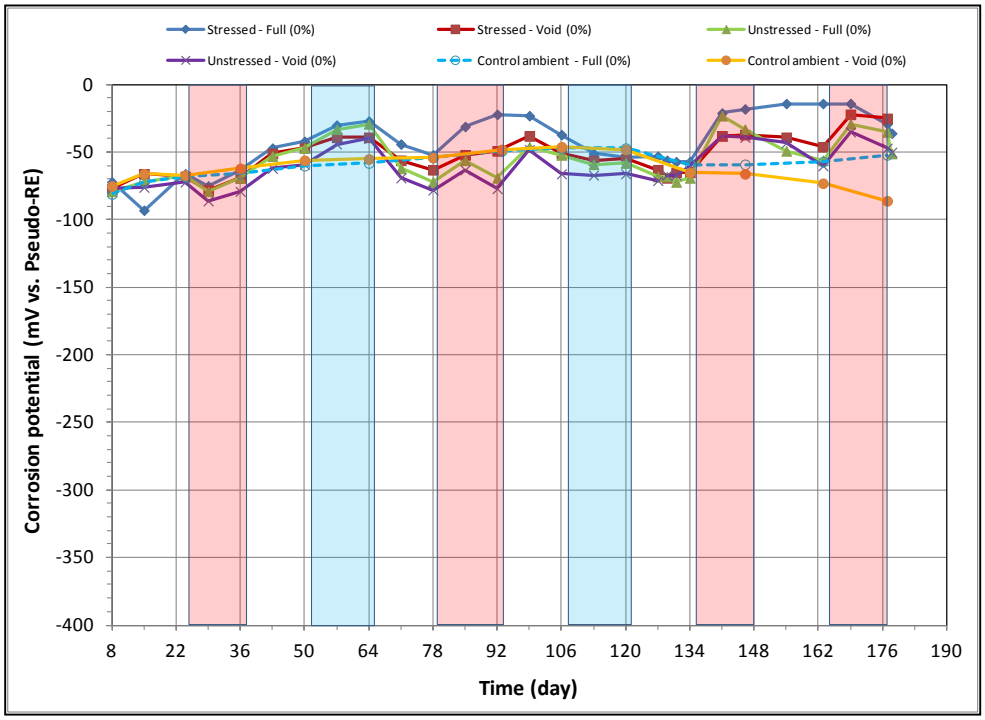

Figure 92. Graph. Corrosion potential versus time for 0 percent chloride single-strand specimens.

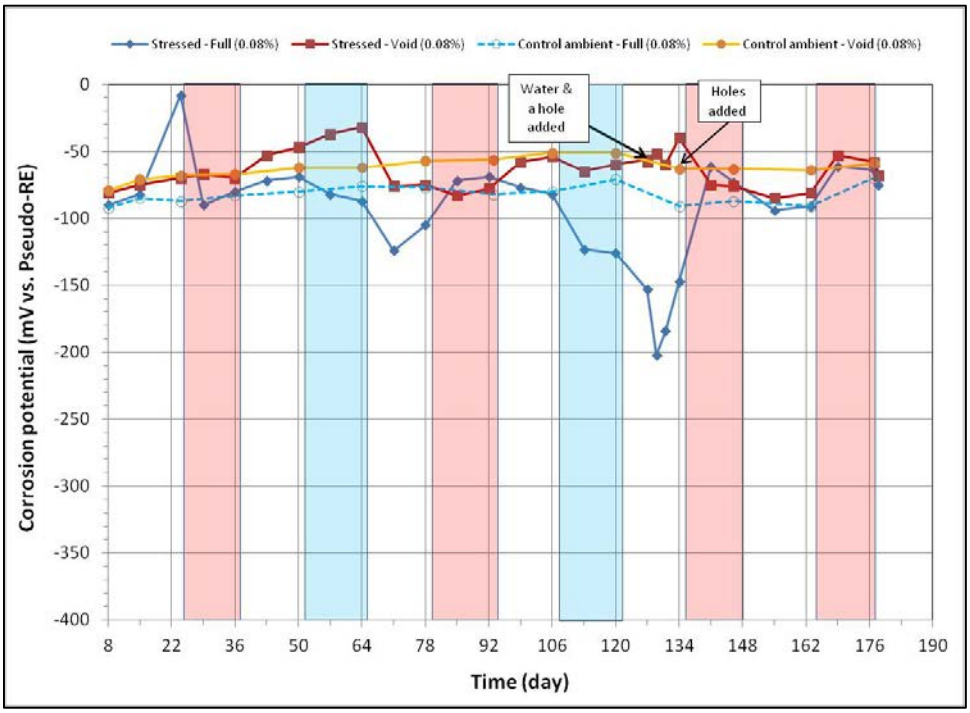

Figure 93. Graph. Corrosion potential versus time for 0.08 percent chloride single-strand specimens.

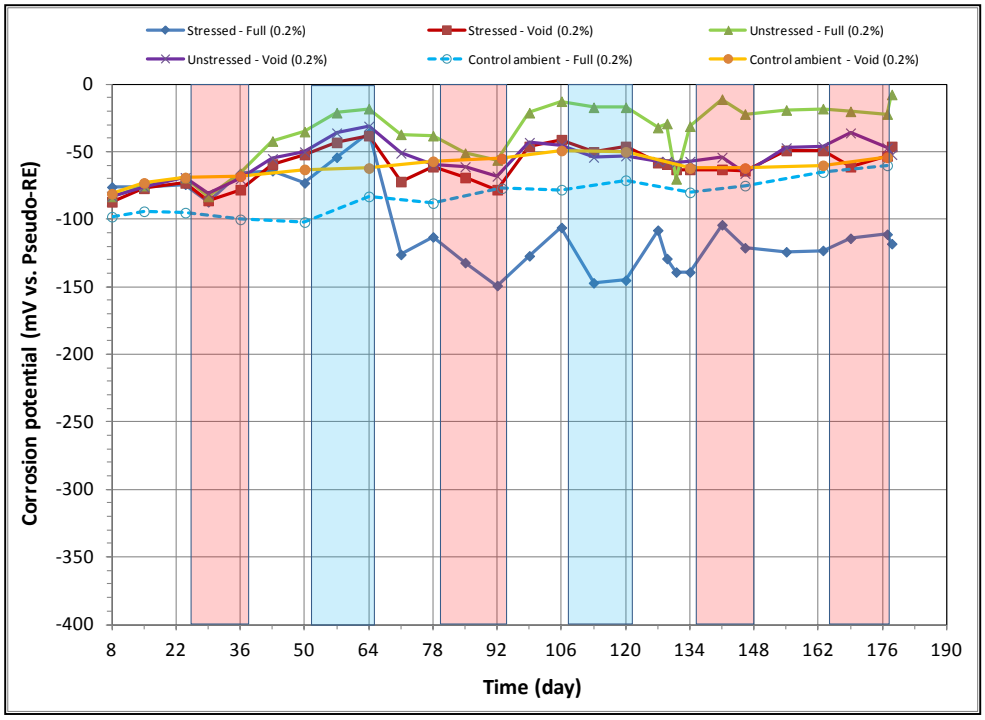

Figure 94. Graph. Corrosion potential versus time for 0.2 percent chloride single-strand specimens.

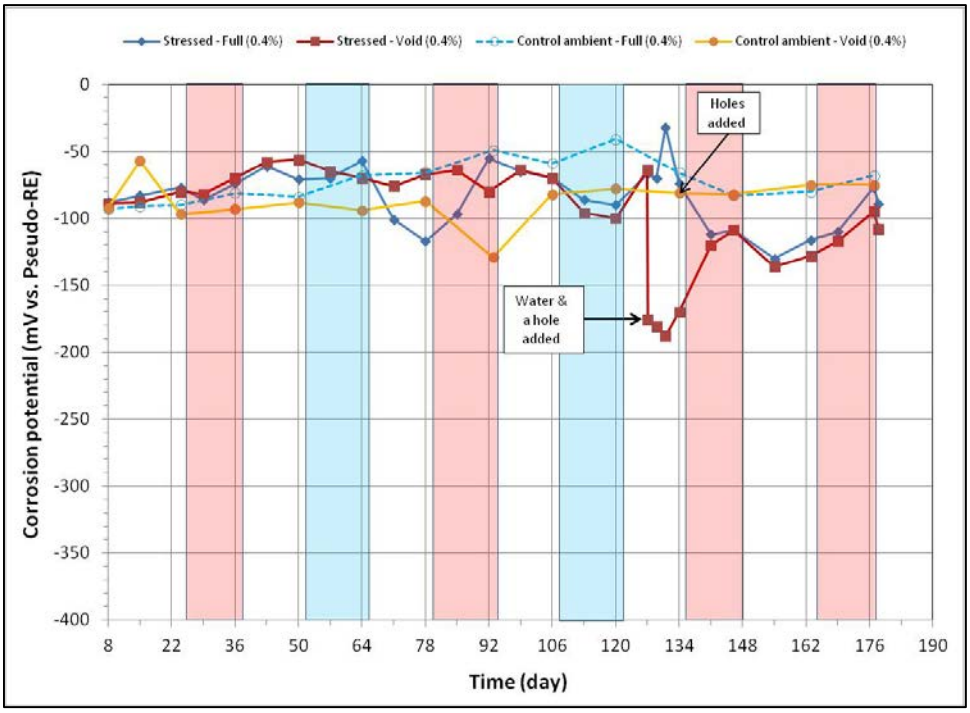

Figure 95. Graph. Corrosion potential versus time for 0.4 percent chloride single-strand specimens.

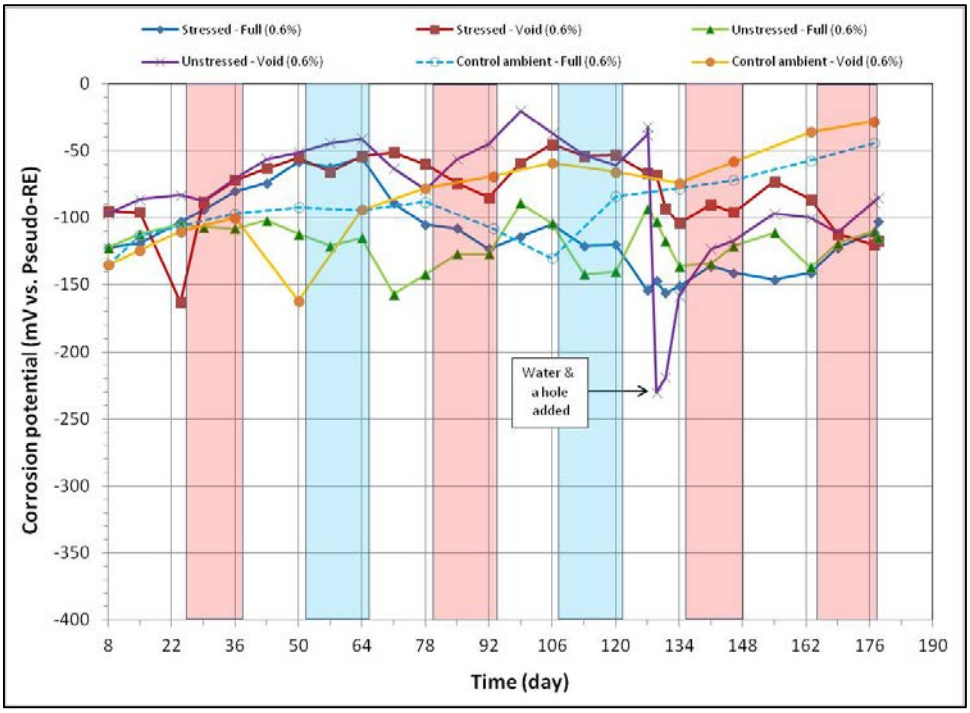

Figure 96. Graph. Corrosion potential versus time for 0.6 percent chloride single-strand specimens.

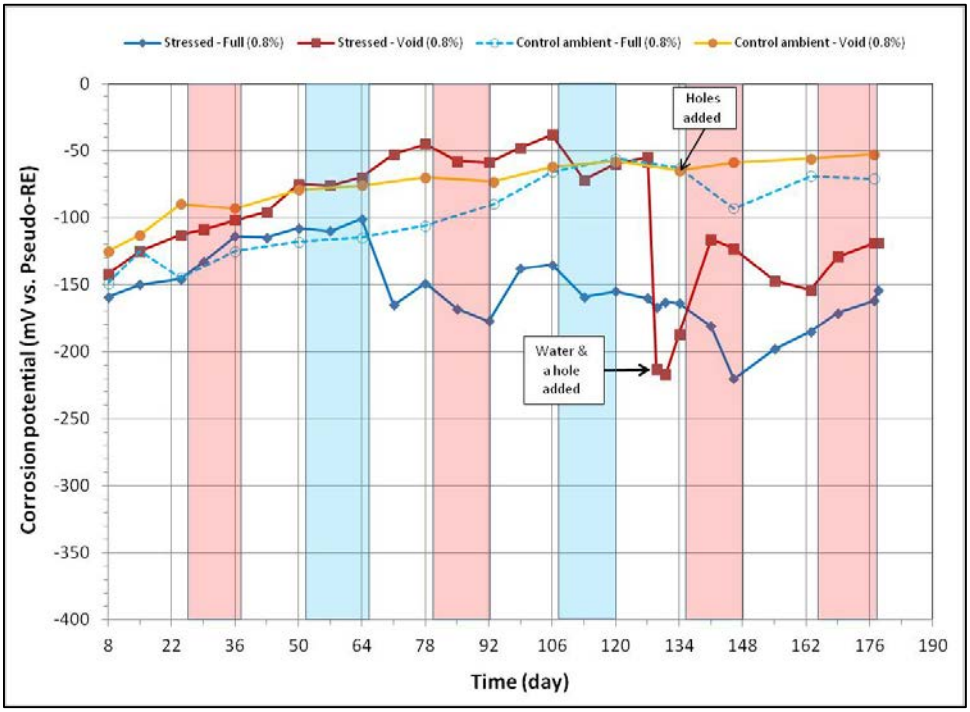

Figure 97. Graph. Corrosion potential versus time for 0.8 percent chloride single-strand specimens.

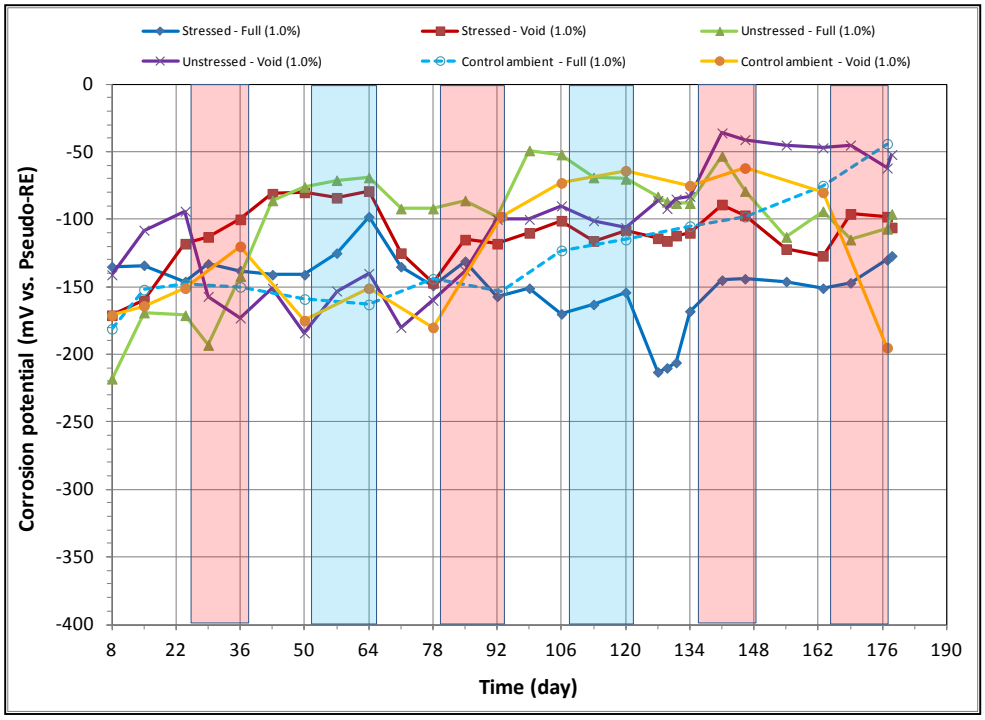

Figure 98. Graph. Corrosion potential versus time for 1.0 percent chloride single-strand specimens.

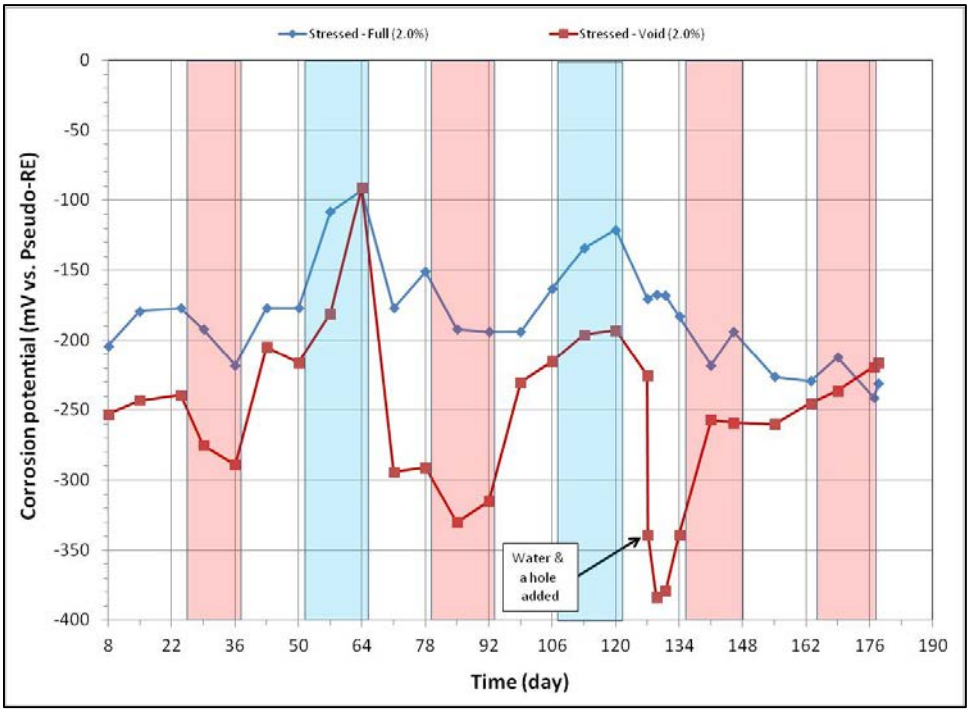

Figure 99. Graph. Corrosion potential versus time for 2.0 percent chloride single-strand specimens.

Fully Grouted Specimens Versus Voided Specimens

Figure 100 through figure 103 summarize mean corrosion potentials calculated for the stressed and unstressed strands in fully grouted specimens per chloride concentration in initial ambient, ambient, H & H, and F & D cycles, respectively. Similar plots for the voided specimens are presented in figure 104 through figure 107. Because water was added to some of the voided specimens after initial ambient and F & D cycles were completed, mean corrosion potential data related to post-water recharging event are presented in figure 105 (ambient) and figure 106 (H & H) only. In addition, control specimen data were also included in relevant initial ambient and ambient plots.

In general, mean corrosion potentials of both specimen types were gradually more negative as chloride concentration increased. As a result, the 2.0 percent chloride specimens exhibited the most negative mean corrosion potentials in each exposure condition except for F & D condition. Adding 0.17 fl oz of distilled water to the 0.08 percent chloride specimen did not change its mean corrosion potentials as shown in figure 105 and figure 106. Conversely, the voided specimens containing 0.4 to 2.0 percent chloride resulted in more negative mean corrosion potentials upon water recharging relative to those measured before adding water. The risk of corrosion is elevated with increasing chloride concentration if water enters voids in the grout containing higher acid-soluble chloride concentration than 0.08 percent by weight of cement, which is the current chloride limit specified by many design codes and specifications.[1]

The control specimens did not exhibit noticeable changes in corrosion potentials upon air hole introduction. Conversely, the specimens that received recharging water became active regardless of air holes. Therefore, it is concluded that presence of air holes alone did not impact corrosion potentials of the voided single-strand specimens.

The effect of stress on mean corrosion potential was not apparent for fully grouted specimens. For voided specimens after water recharging, stressed specimens containing 0.4 and 0.8 percent chloride experienced larger potential drops than a single unstressed specimen containing 0.6 percent chloride (see figure 105 and figure 106). The limited data suggest that stressed strands may be more susceptible to corrosion compared to the unstressed ones if the grout void is filled with water.

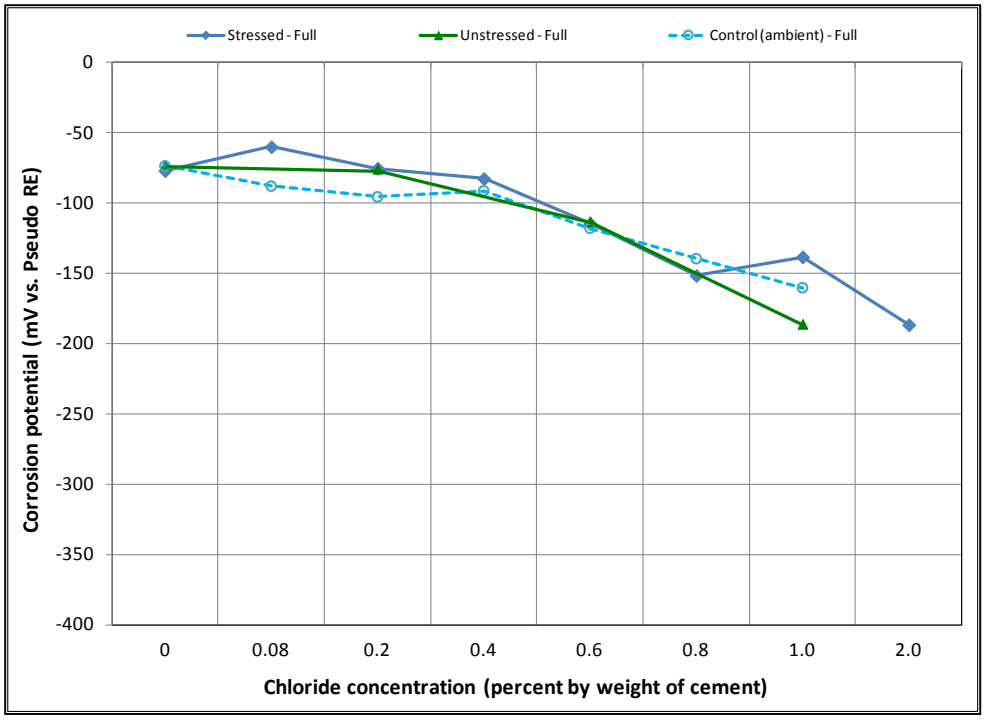

Figure 100. Graph. Mean corrosion potential of fully grouted single-strand specimens in initial ambient condition.

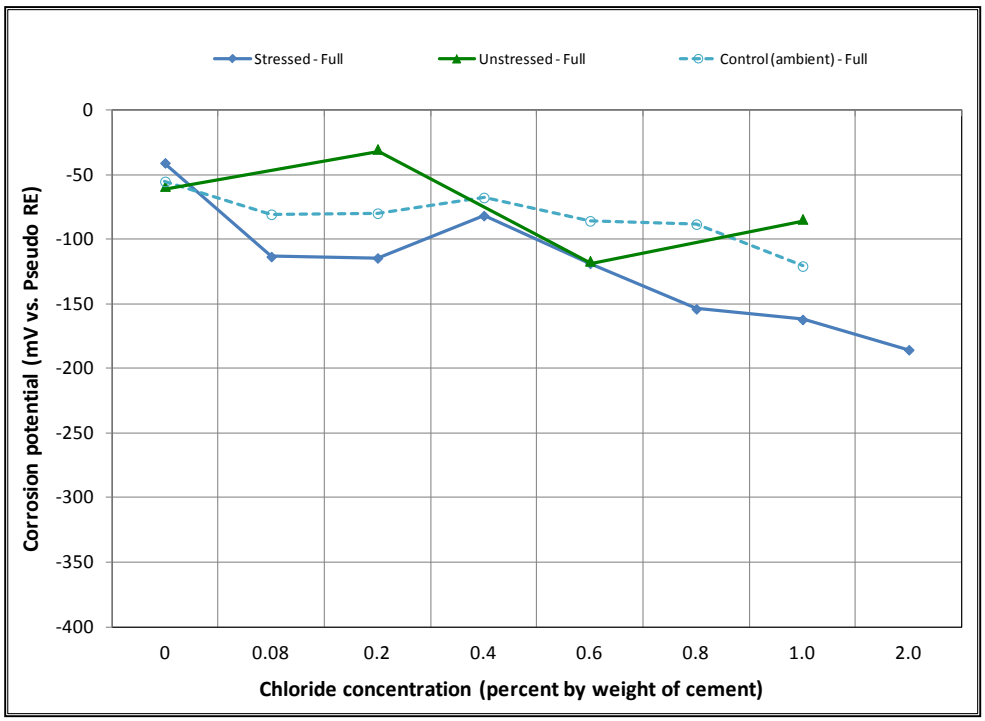

Figure 101. Graph. Mean corrosion potential of fully grouted single-strand specimens in ambient condition.

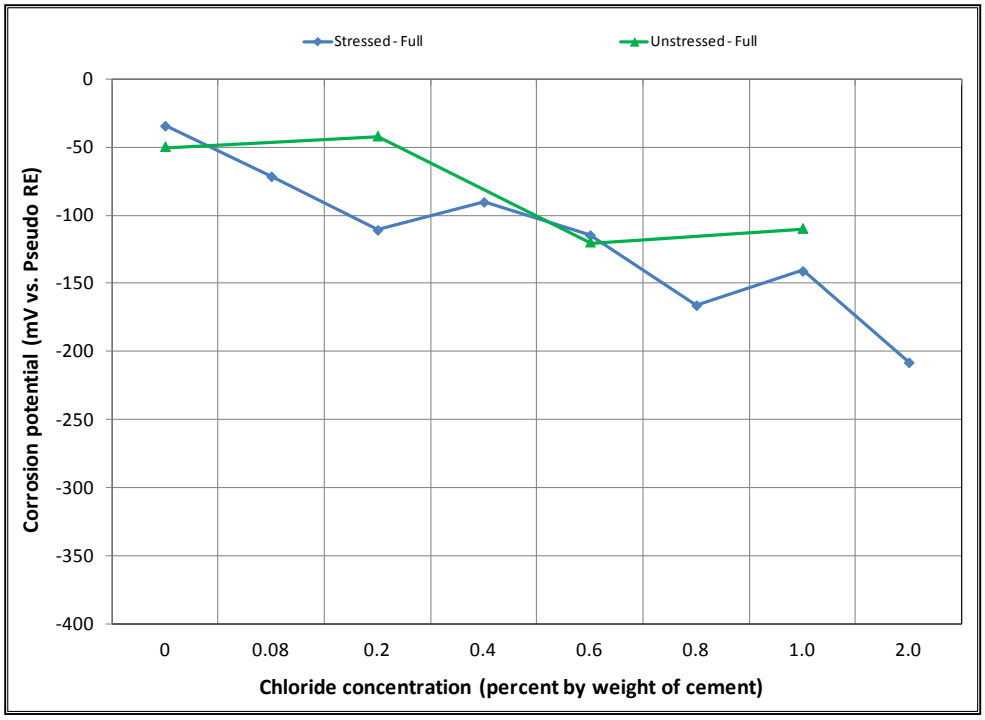

Figure 102. Graph. Mean corrosion potential of fully grouted single-strand specimens in H & H condition.

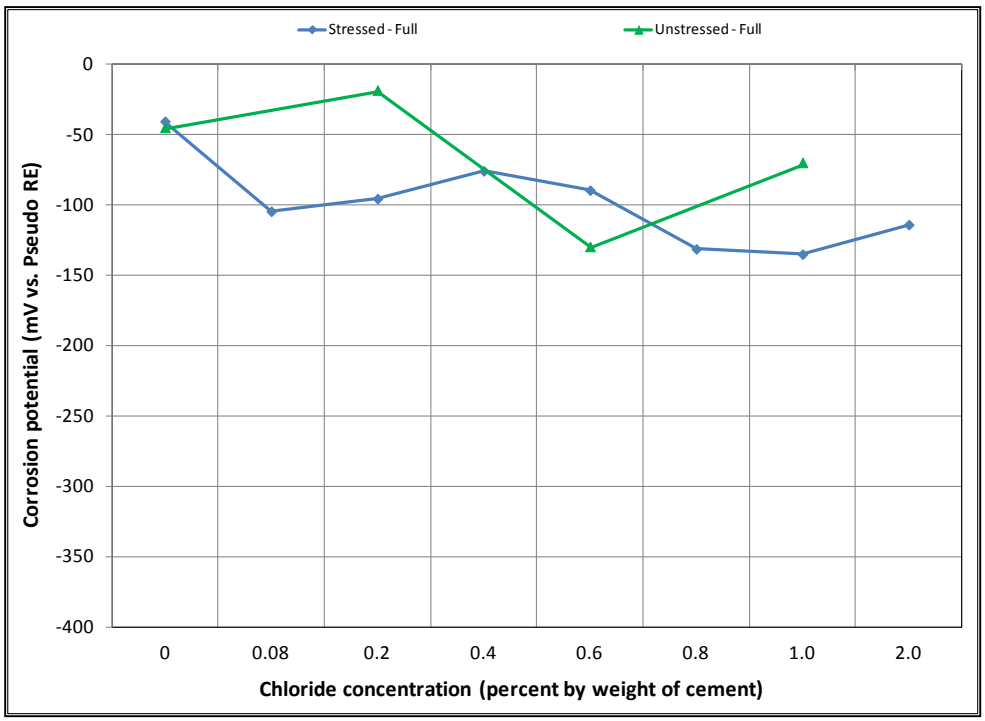

Figure 103. Graph. Mean corrosion potential of fully grouted single-strand specimens in F & D condition.

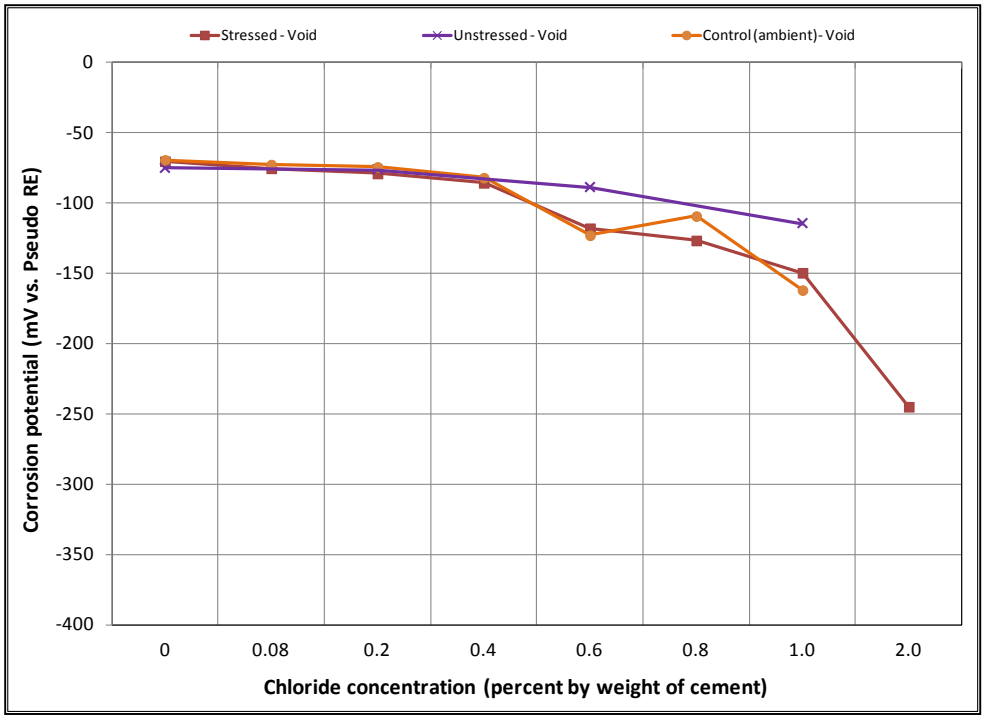

Figure 104. Graph. Mean corrosion potential of voided single-strand specimens in initial ambient condition.

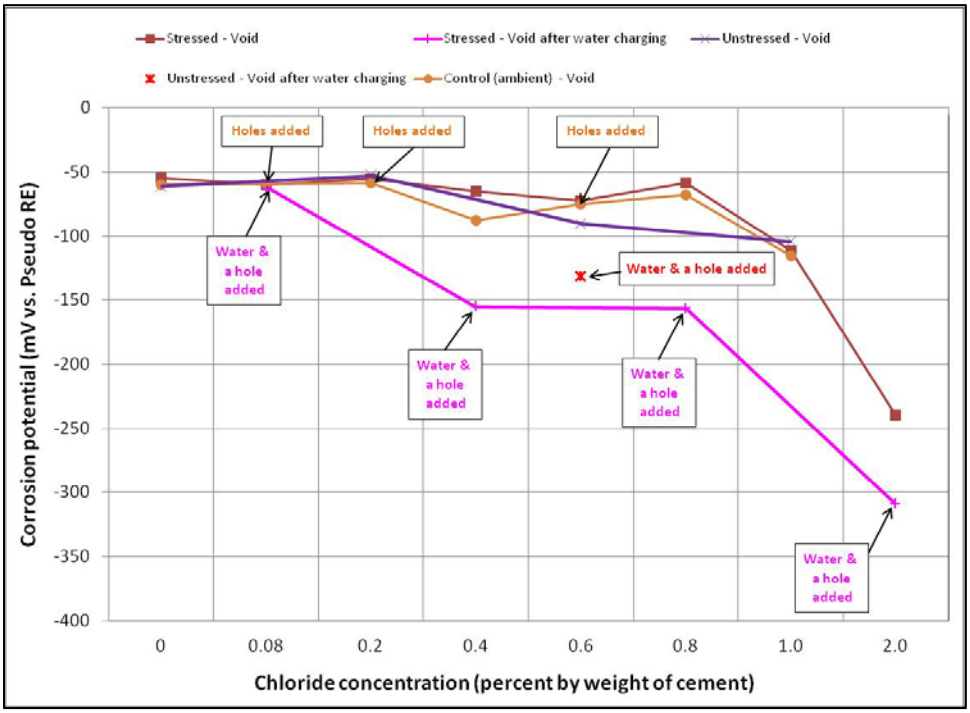

Figure 105. Graph. Mean corrosion potential of voided single-strand specimens in ambient condition.

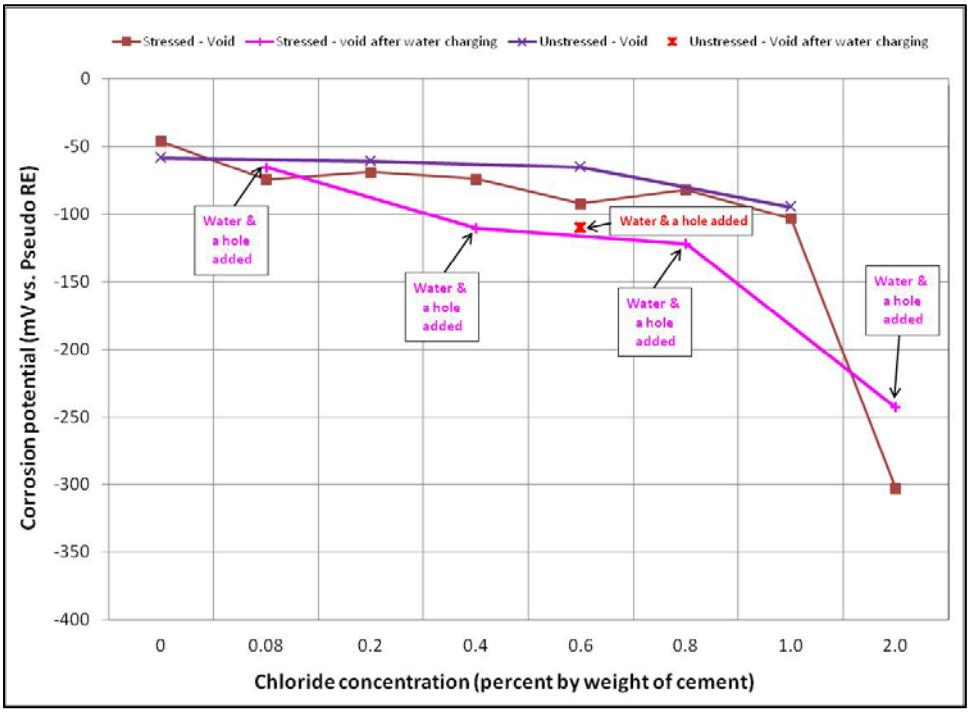

Figure 106. Graph. Mean corrosion potential of voided single-strand specimens in H & H condition.

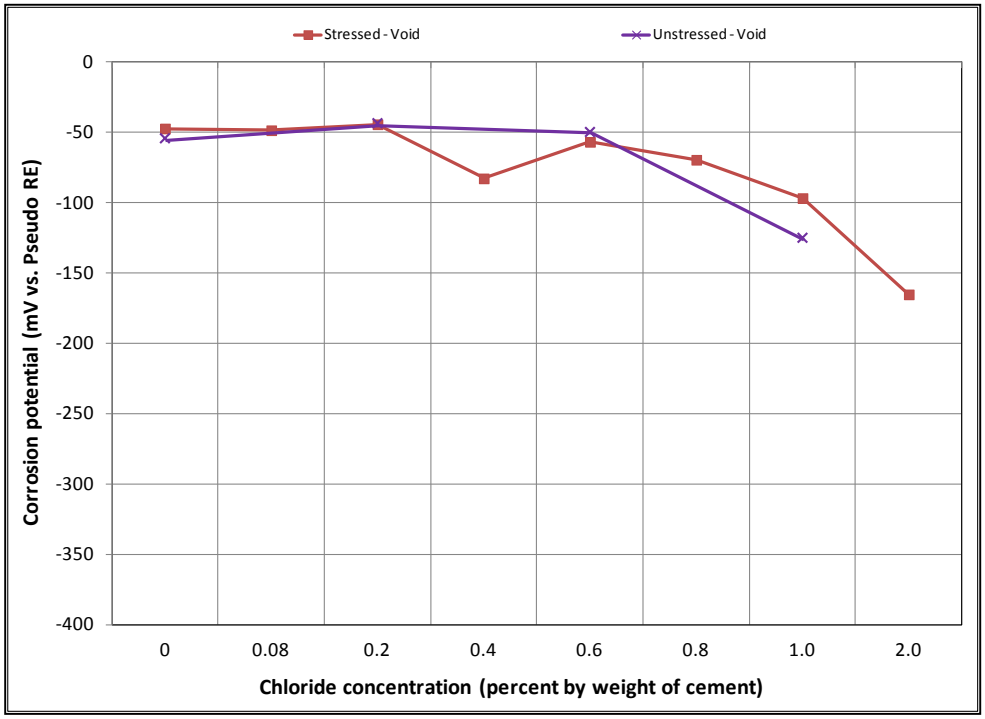

Figure 107. Graph. Mean corrosion potential of voided single-strand specimens in F & D condition.

TASK 2.3: CORROSION POTENTIALS AND POLARIZED POTENTIALS OF MULTI-STRAND SPECIMENS

Figure 108 through figure 115 present corrosion potentials of stressed strands (macro-anode) and unstressed strands (macro-cathode) versus time plots for multi-strand specimens. The plots also contain their polarized potentials. *Polarization in electrochemistry* is defined as a potential shift corresponding to a directional current flow. Anodic polarization occurs in the positive potential direction when current leaves the electrode into electrolyte, while cathodic polarization occurs in the negative potential direction if current enters the electrode from the electrolyte. Flow of electrons is opposite to the current flow by the known sign convention. The polarized potential is often called "mixed potential" because macro-anode is polarized from its corrosion potential in the positive direction, and macro-cathode is polarized from its corrosion potential in the negative direction until their polarized potentials intersect at a mid-point where steady state macro-cell current is maintained.

Corrosion potentials of macro-anode and macro-cathode of multi-strand specimens containing 0 to 0.2 percent chloride remained above -150 mV versus PSE, thus their potential difference was small (roughly less than 100 mV). Their data are shown in figure 108 through figure 110. When chloride concentration increased to between 0.4 and 1.0 percent, the majority of stressed strand corrosion potentials became more negative than -200 mV versus PSE. Since they were equivalent to more negative than -350 mV versus CSE, active corrosion of the stressed strands was evident. These data are shown in figure 111 through figure 114. The majority of unstressed strands corrosion potentials still remained above -150 mV versus PSE. As a result, potential difference became larger than 150 mV in many cases. A larger potential difference means a greater driving force for macro-cell corrosion current to flow. Subsequently, when acid-soluble chloride concentration was higher than 0.4 percent by weight of cement, multi-strand specimens developed large driving voltage between macro-anode (stressed strands) and macro-cathode (unstressed strands) to facilitate active macro-cell corrosion. Multi-strand specimens were intended to create intensive macro-cell corrosion by design, and actual data supported that the specimen design worked to produce realistic macro-cell corrosion damage on the stressed strands.

When 5.1 fl oz of distilled water was added in the voids, most specimens (0.08, 0.2, 0.4, 0.6, 1.0, and 2.0 percent chloride) experienced negative potential shifts immediately. The others experienced either no change (0 percent chloride in figure 108) or positive potential shifts (0.8 percent chloride in figure 113) upon water recharging. All three kinds of potentials of the 0.8 percent chloride specimen remained in the positive range afterwards. This specimen's duct cracked during the second F & D cycle, and emergency repair was made just before water recharging (see figure 50 through figure 55). In addition, 24 0.5-inch-diameter holes were introduced over the repaired duct along with the water recharging event to see whether more oxygen can diffuse to the strands (see figure 57 and figure 58). This is the only multi-strand specimen that received the air holes. As will be discussed later, the upward potential shifts might have been caused by increased oxygen levels at the strands.

Corrosion potential data of macro-cathode in 2.0 percent chloride specimen started to corrode approximately 1 month after accelerated corrosion testing began (see figure 115). Such an early corrosion of macro-cathode shifted its corrosion potential steadily toward the more negative direction approaching corrosion potential of macro-anode. Figure 115 shows that both corrosion

potentials became similar from the 106th day onward. Consequently, the intended macro-cell corrosion setup of 2.0 percent chloride specimen became less effective with time in association with the shrinking driving voltage.

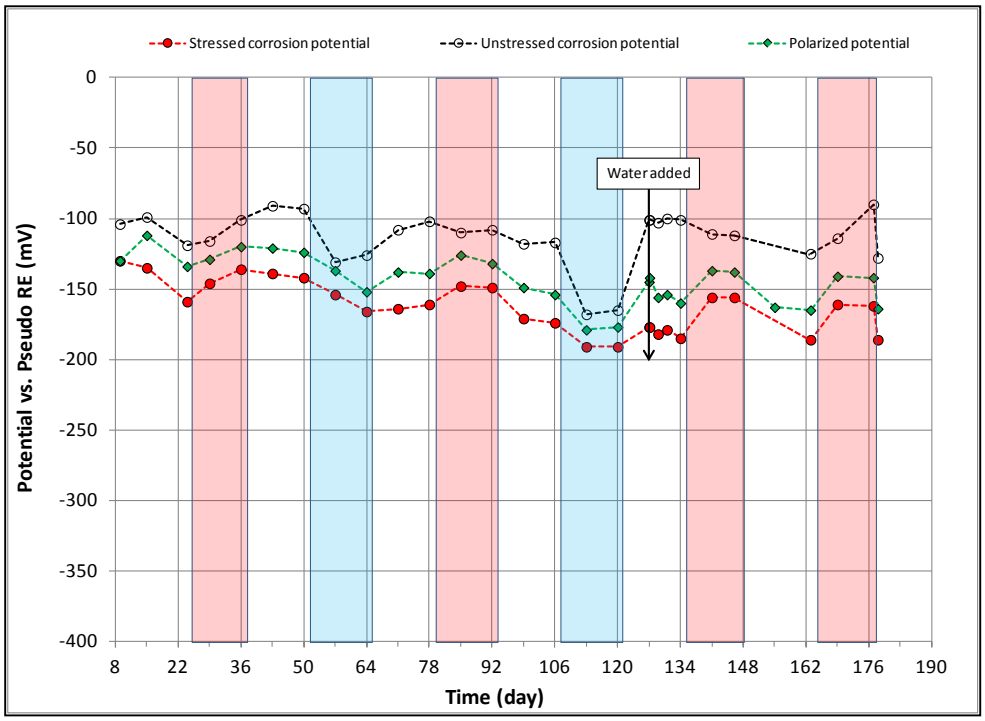

Figure 108. Graph. Potential versus time for 0 percent chloride multi-strand specimen.

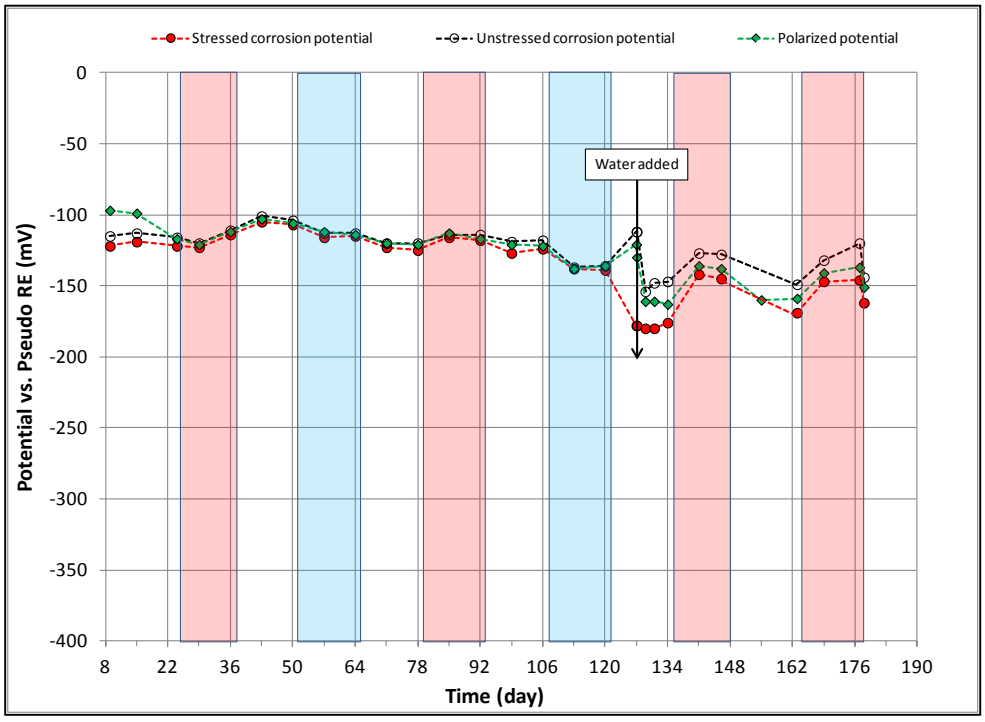

Figure 109. Graph. Potential versus time for 0.08 percent chloride multi-strand specimen.

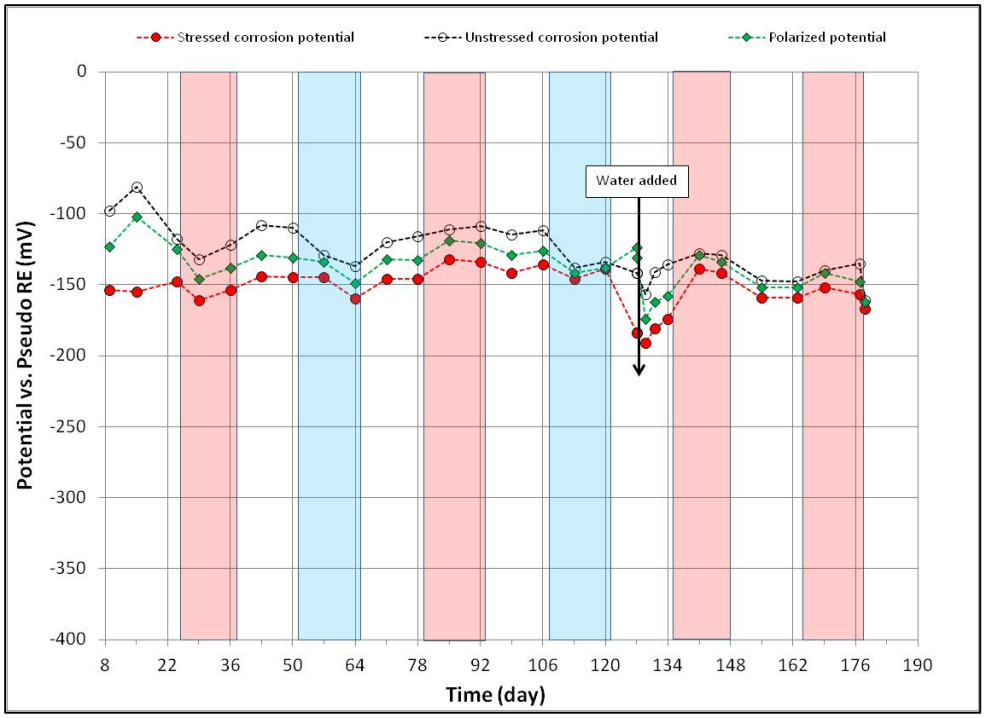

Figure 110. Graph. Potential versus time for 0.2 percent chloride multi-strand specimen.

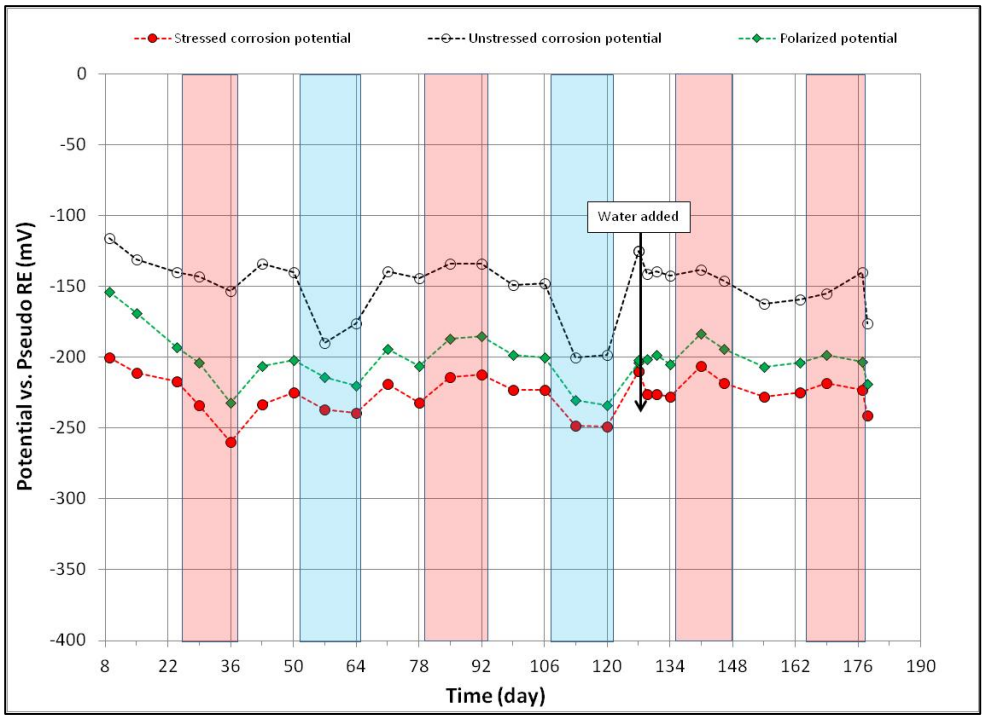

Figure 111. Graph. Potential versus time for 0.4 percent chloride multi-strand specimen.

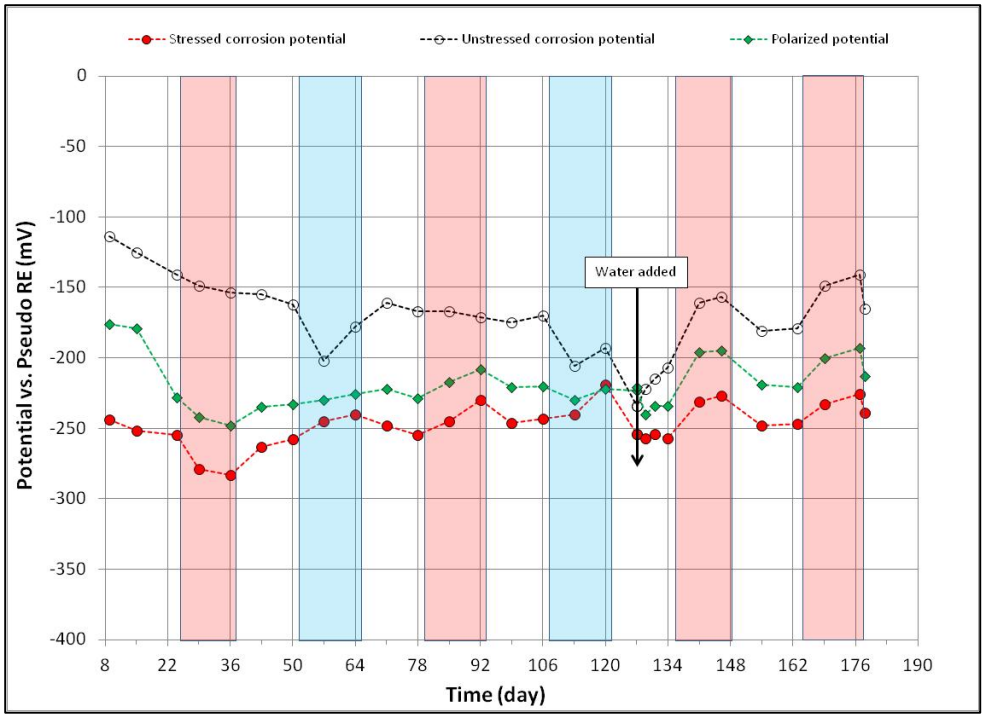

Figure 112. Graph. Potential versus time for 0.6 percent chloride multi-strand specimen.

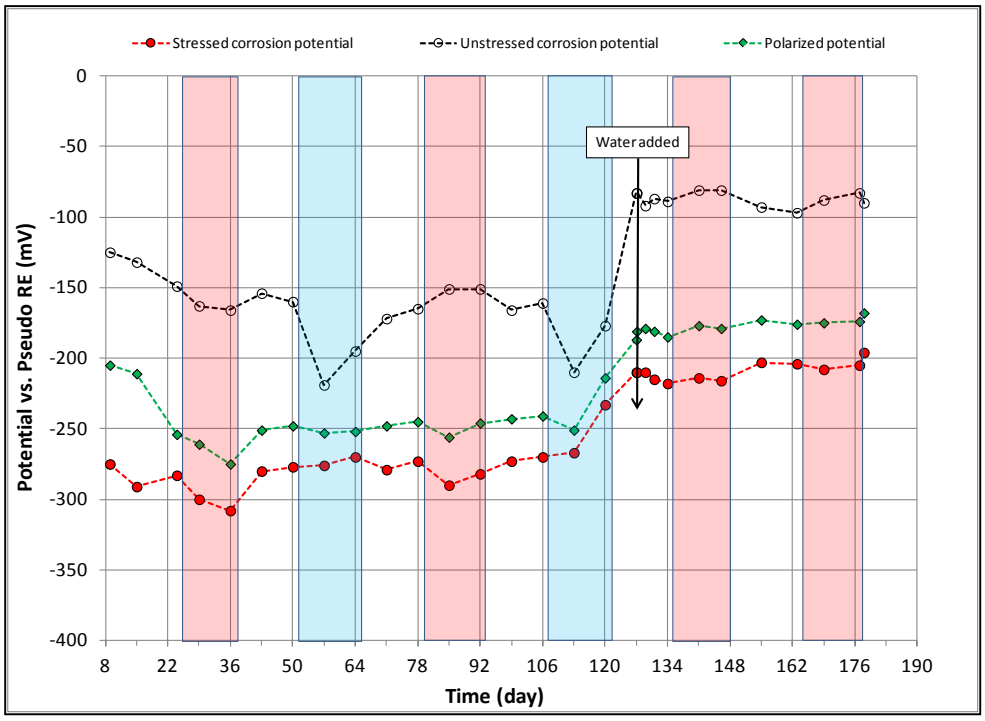

Figure 113. Graph. Potential versus time for 0.8 percent chloride multi-strand specimen.

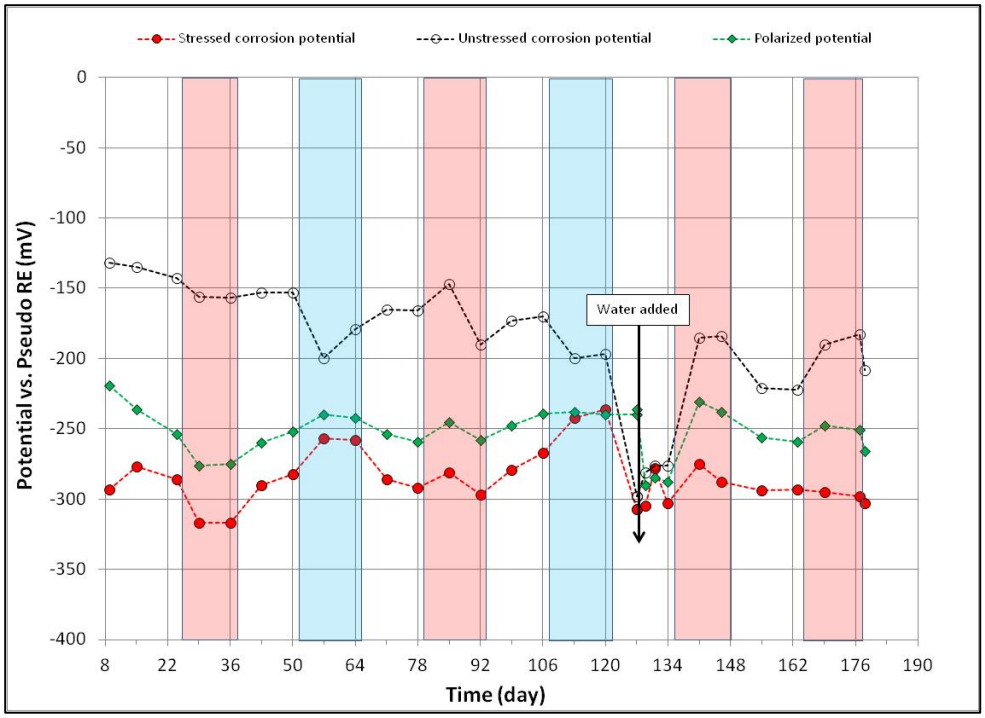

Figure 114. Graph. Potential versus time for 1.0 percent chloride multi-strand specimen.

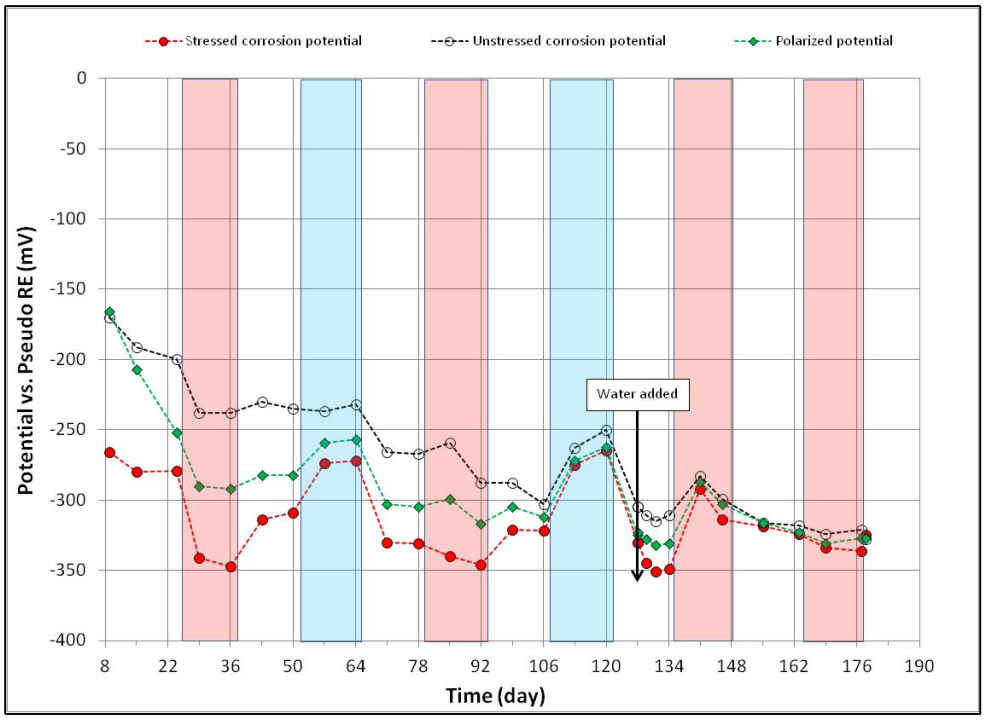

Figure 115. Graph. Potential versus time for 2.0 percent chloride multi-strand specimen.

Figure 116 through figure 118 present mean corrosion potentials per chloride concentration and exposure condition of stressed strands, unstressed strands, and mean polarized potentials, respectively. As discussed earlier, stressed strands (macro-anode) exhibited more negative mean corrosion potentials than unstressed ones (macro-cathode). Comparing all the plots in the figures, it

appears that the stressed strands exhibited the most negative potentials at any chloride concentration, irrespective of exposure condition and water in the void. It is unclear if presence of stress or localized corrosion at the void/grout interface or both factors made the entire stressed strands active. Although water recharging made the corrosion potentials of the stressed strands more negative, potential changes before and after water recharging were less than 50 mV in most chloride concentrations. Once chloride concentration increased to 0.4 percent, mean corrosion potentials of stressed strands fell into the 90 percent corrosion probability threshold, -220 mV versus PSE (-350 mV versus CSE), independent of exposure condition as shown in figure 116. The same situation occurred for unstressed strands only after chloride concentration reached 2.0 percent as shown in figure 117.

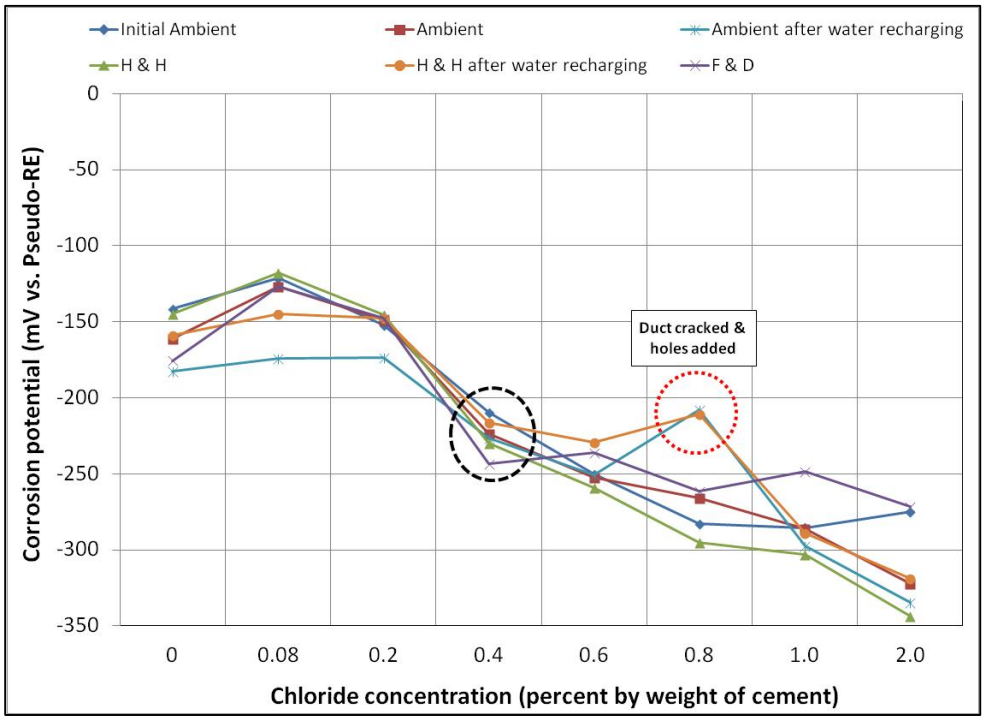

Figure 116. Graph. Mean corrosion potential of stressed strands in multi-strand specimens.

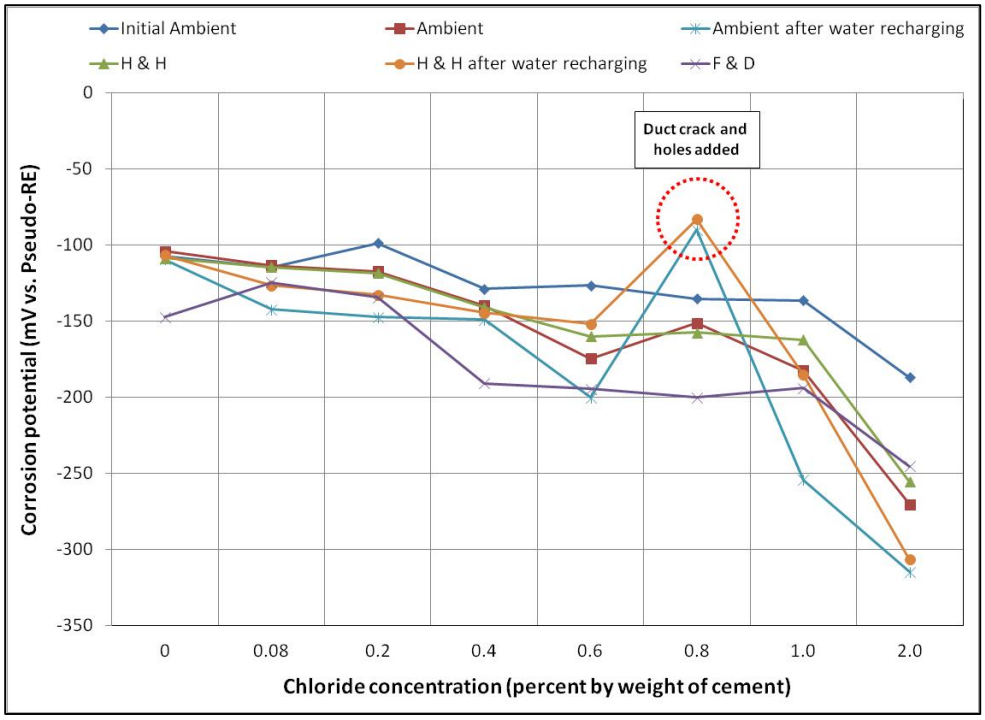

Figure 117. Graph. Mean corrosion potential of unstressed strands in multi-strand specimens.

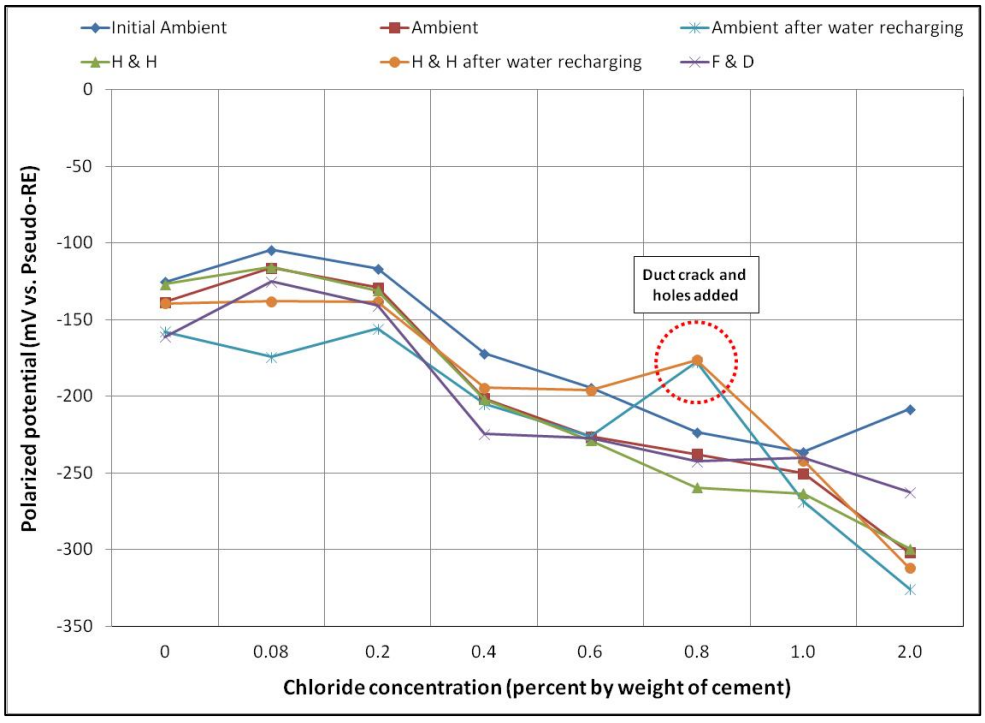

Figure 118. Graph. Mean polarized potential of multi-strand specimens.

Figure 119 shows overall mean corrosion potentials of stressed and unstressed strands and overall mean polarized potentials as a function of chloride concentration. Overall mean corrosion potentials of stressed strands decreased more than 120 mV when chloride concentration increased to 0.4 percent by weight of cement. Such a large decrease suggests that the stressed PT strands initiated active corrosion at 0.4 percent chloride concentration. At chloride concentrations between 0.4 and 1.0 percent, overall mean polarized potential was closer to overall mean stressed corrosion potentials instead of being near the overall mean unstressed corrosion potentials. This behavior suggests that the macro-cell corrosion process in these multi-strand specimens was under cathodic control. Under this condition, oxygen availability must have controlled the most common cathodic reaction given in figure 11.

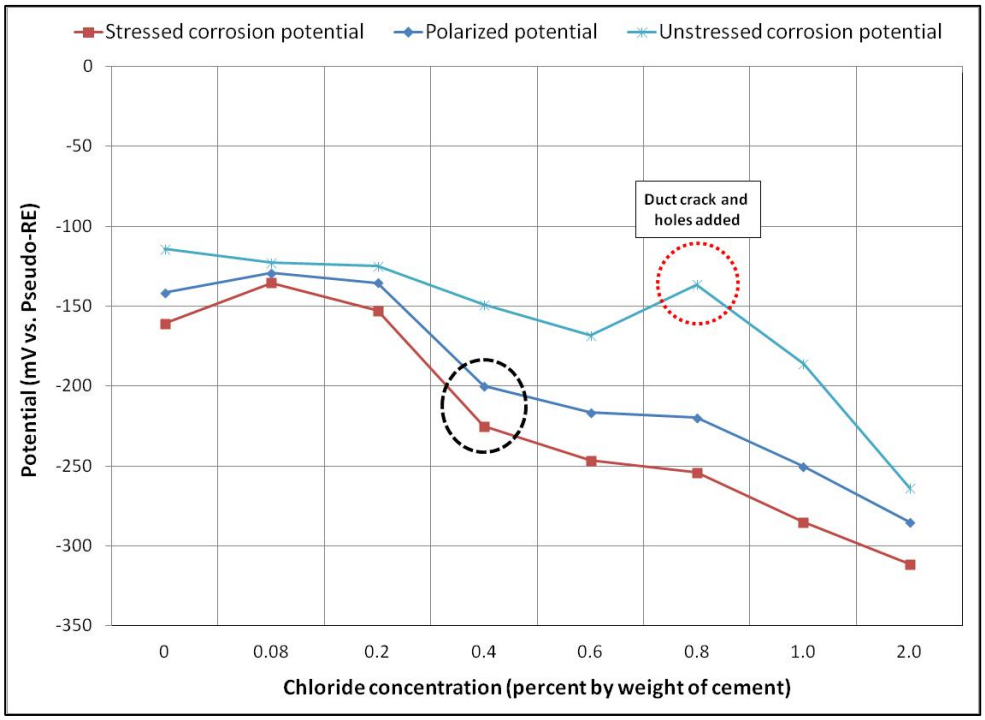

Figure 119. Graph. Overall mean potential of multi-strand specimens.

Figure 116 through figure 119 show data humps on 0.8 percent chloride specimen data. It was mentioned earlier that the PVC duct of 0.8 percent chloride specimen was cracked, and 24 artificial holes were introduced afterwards. These irregular potential jumps were only related to the data collected after the integrity of the PVC duct was compromised. It is speculated that the positive potential shifts were caused by more oxygen available at the strands that would move potentials in the positive direction by concentration polarization process. This phenomenon can be described with corrosion potential changes from case (1) to case (1') and from case (2) to case (2') in figure 20. This theory also suggests the opposite situation for the other multi-strand specimens, which were encased by tightly sealed ducts that created less oxygen environment.

As will be discussed in the Characterization of Corrosion Morphologies section, it was confirmed that 0 percent chloride concentration specimen corroded due to excessive free sulfate ions at the void/grout interface. In normal conditions without the unintended corrosion, the specimen should have experienced no corrosion, and its potential values should have increased in the positive

direction so that their data are placed in more positive positions in the plots than the 0.08 percent chloride potential data.

If the duct cracking problem and excessive sulfate ions in 0 percent chloride concentration specimen as discussed above had not occurred, the data trend lines would have looked more like linear as a function of chloride concentration.

CORROSION RATE AND MACRO-CELL CORROSION CURRENT DENSITY DATA

Task 2.2: Corrosion Rate Data of Single-Strand Specimens

Figure 120 through figure 127 present corrosion rates versus time plots for single-strand specimens. The first measurements after receiving water and/or introducing air holes are indicated in the relevant plots. Total surface area of a PT strand in contact with grout was used to calculate the nominal corrosion rate. The surface area information is listed in table 6. Since the actual size of corroding areas by pitting corrosion and crevice corrosion was relatively small compared to the total surface area, the calculated corrosion rates were low in all chloride concentrations. The corrosion rate data obtained in this study can fall into the negligible range if the corrosion rate criteria listed in table 7 are strictly applied. Since there is little published information available regarding corrosion rate of PT strands measured by the same technique, it is difficult to interpret the experimental data as they were collected. For this reason, data analysis in this section takes into account actual conditions of the extracted strands during the autopsy.

A general trend observed in figure 120 through figure 127 is that specimens subjected to accelerated corrosion testing experienced higher corrosion rates during the H & H cycles and much lower corrosion rates during the F & D cycles. Intermediate corrosion rates were observed in initial ambient and ambient cycles. The observed data confirmed the corrosion rate's dependency on temperature. However, the corrosion rates also gradually decreased with time. The 1.0 and 2.0 percent chloride specimens depict this trend well because it is easy to see their higher corrosion rates compared to the lower concentration specimens. As observed in corrosion potential data of the voided single-strand specimens, corrosion rate increased when water was added in the voids. As chloride concentration increased, the magnitude of the corrosion rate increase became proportionally larger. The lowest chloride concentration to induce noticeable increase was 0.4 percent (see figure 123). Increased corrosion rates decreased again in the subsequent measurements with time. Introduction of air holes did not change the corrosion rate.

All control specimens showed steadily decreasing corrosion rates with time as their corrosion potentials moved upward steadily in the more positive direction. Again, formation of passive film on the strand surface was thought to be responsible for the corrosion rate reduction under the mild room temperature environment in every chloride concentration.

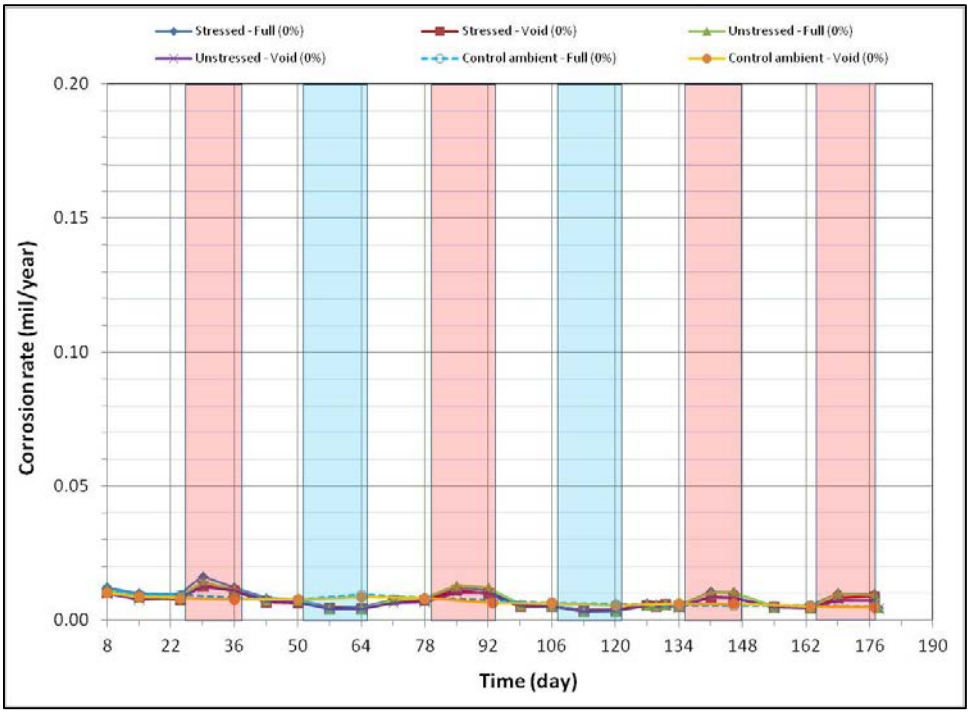

Figure 120. Graph. Corrosion rate versus time for 0 percent chloride single-strand specimens.

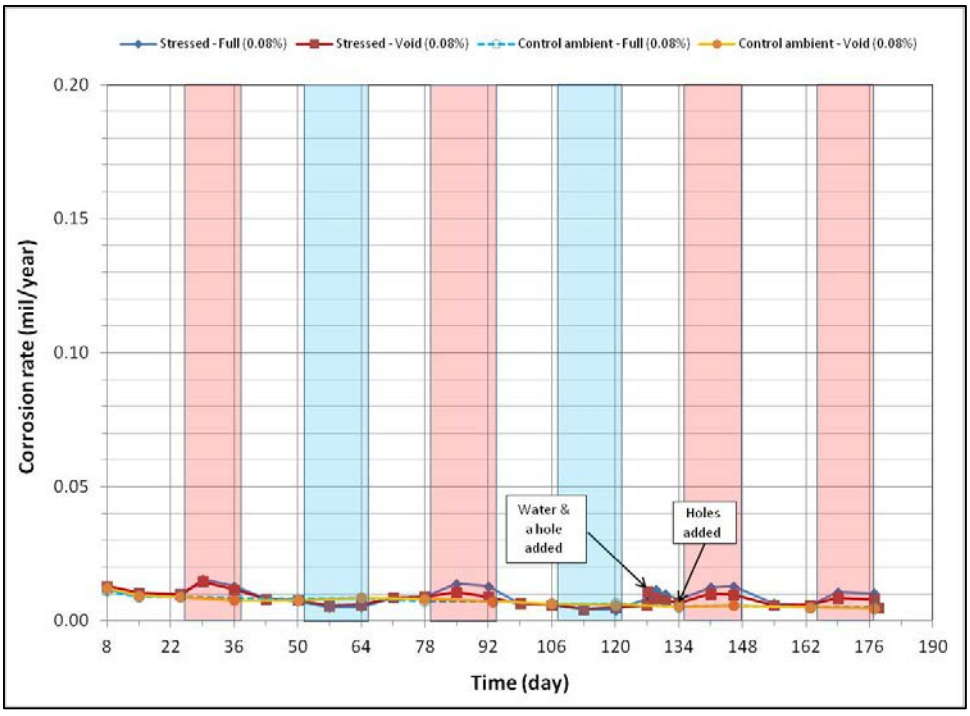

Figure 121. Graph. Corrosion rate versus time for 0.08 percent chloride single-strand specimens.

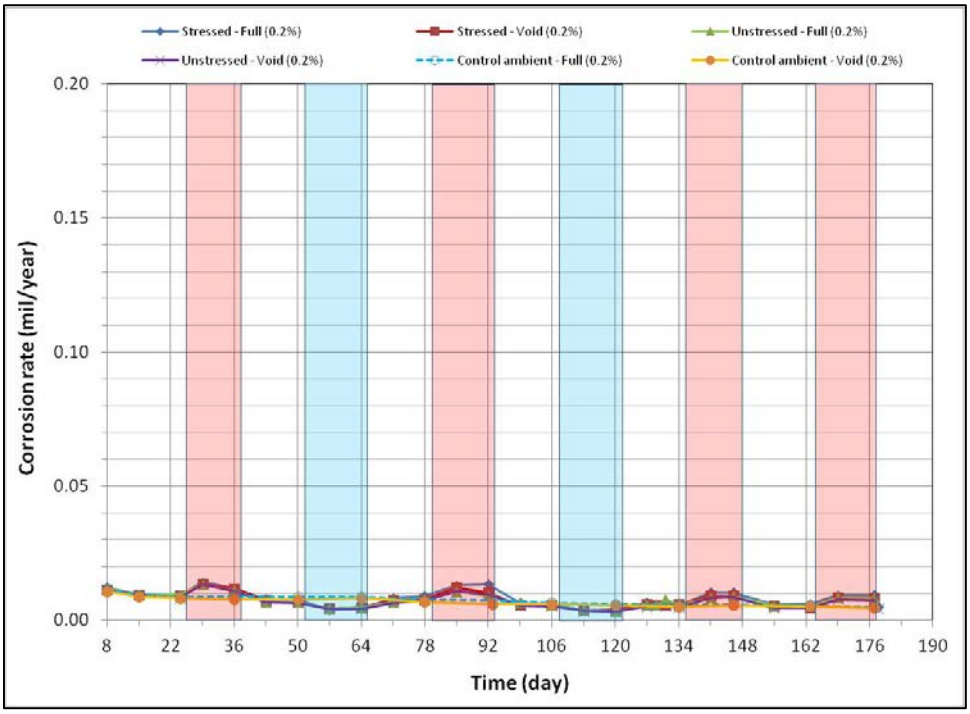

Figure 122. Graph. Corrosion rate versus time for 0.2 percent chloride single-strand specimens.

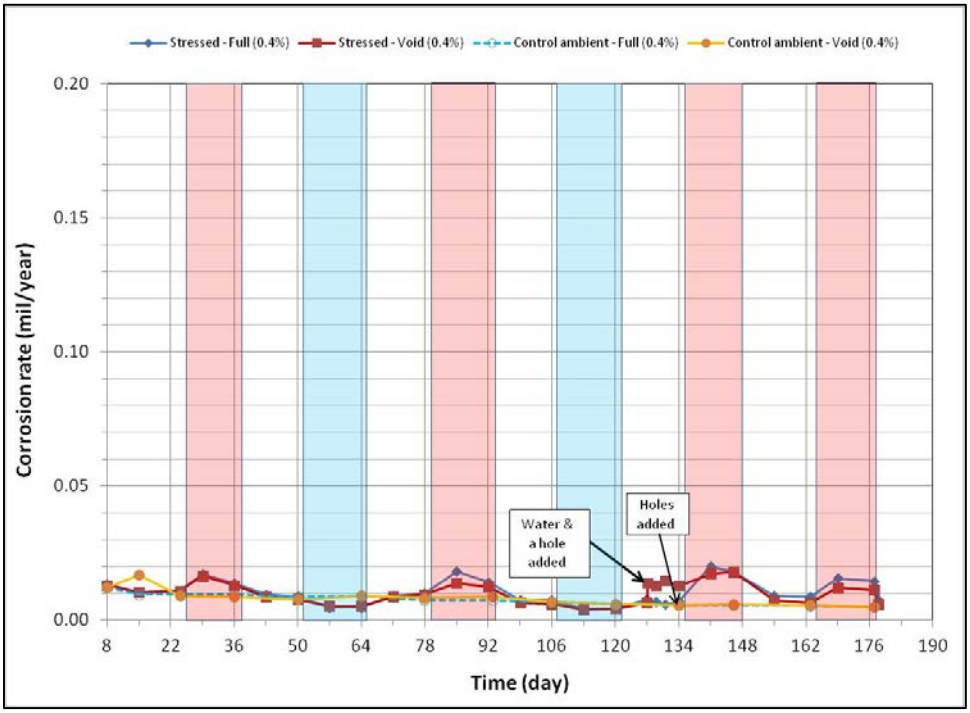

Figure 123. Graph. Corrosion rate versus time for 0.4 percent chloride single-strand specimens.

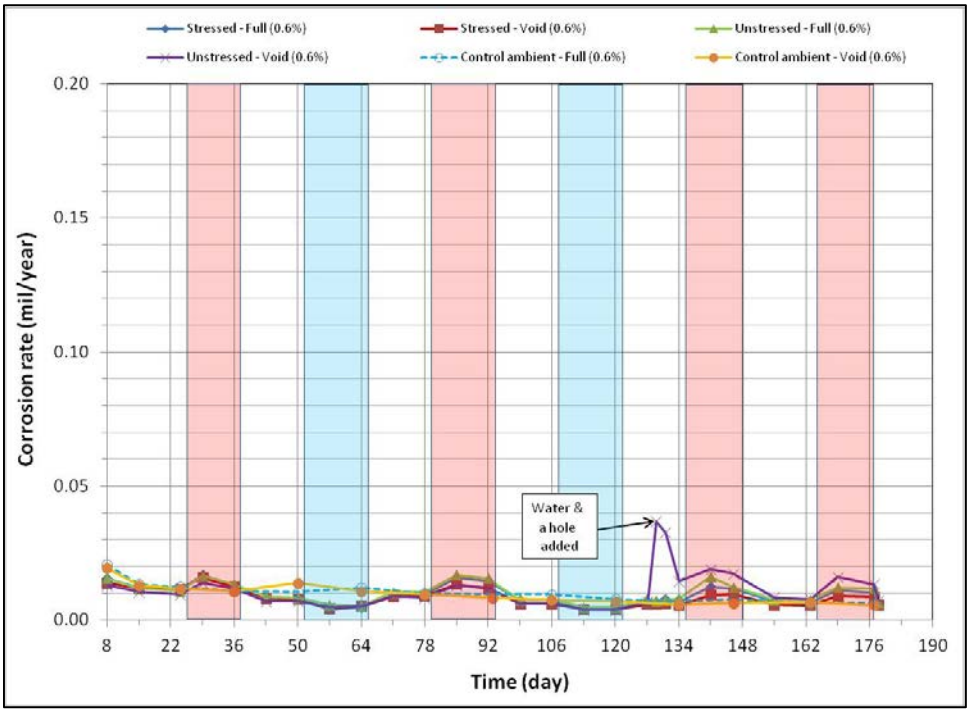

Figure 124. Graph. Corrosion rate versus time for 0.6 percent chloride single-strand specimens.

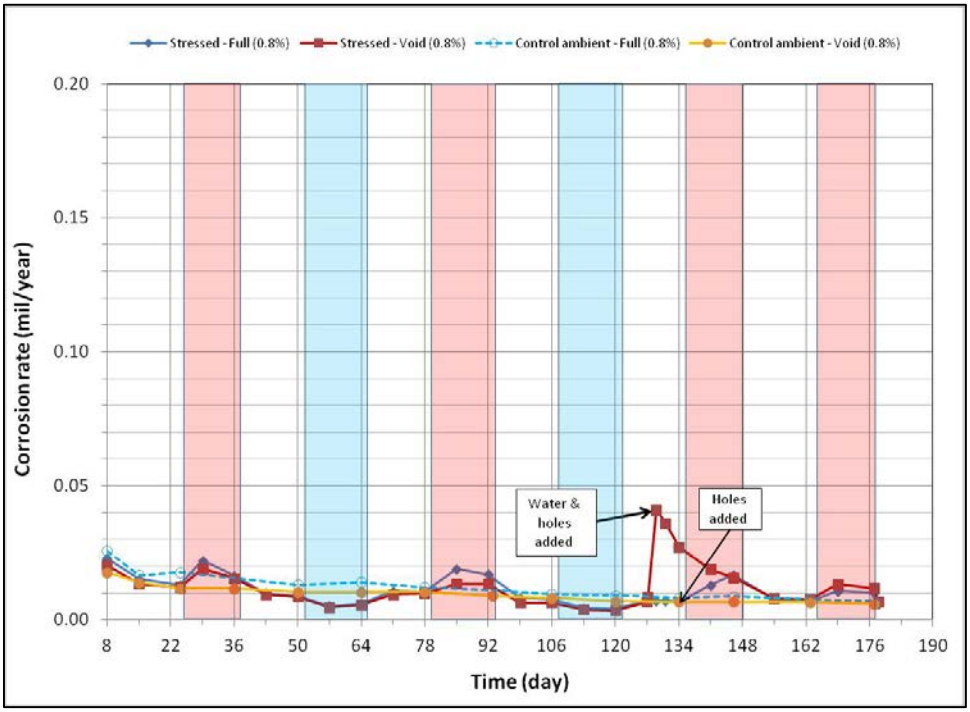

Figure 125. Graph. Corrosion rate versus time for 0.8 percent chloride single-strand specimens.

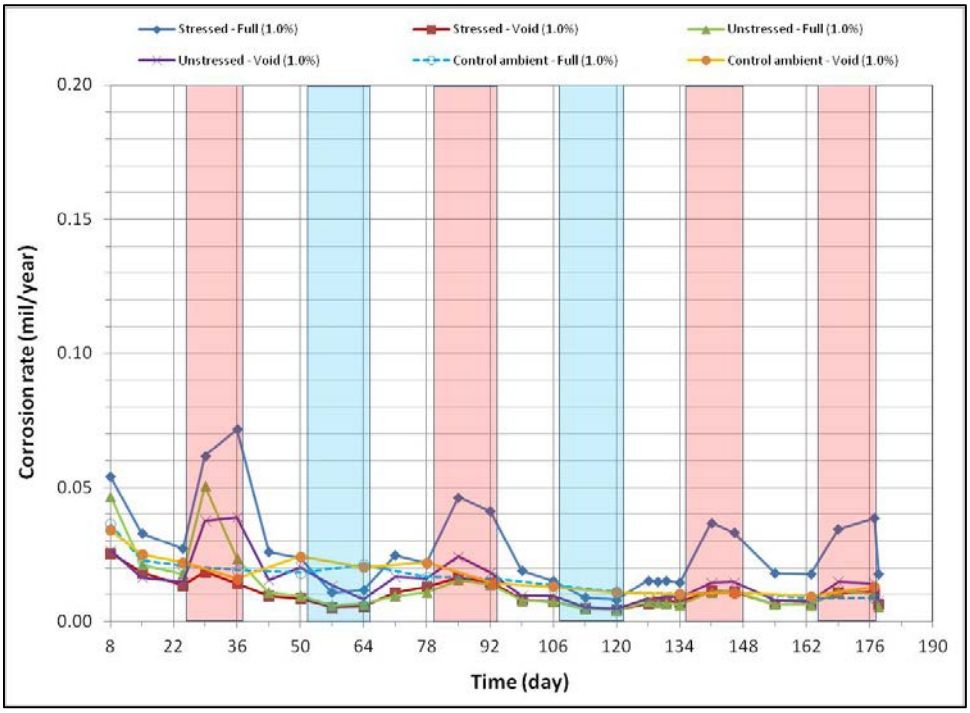

Figure 126. Graph. Corrosion rate versus time for 1.0 percent chloride single-strand specimens.

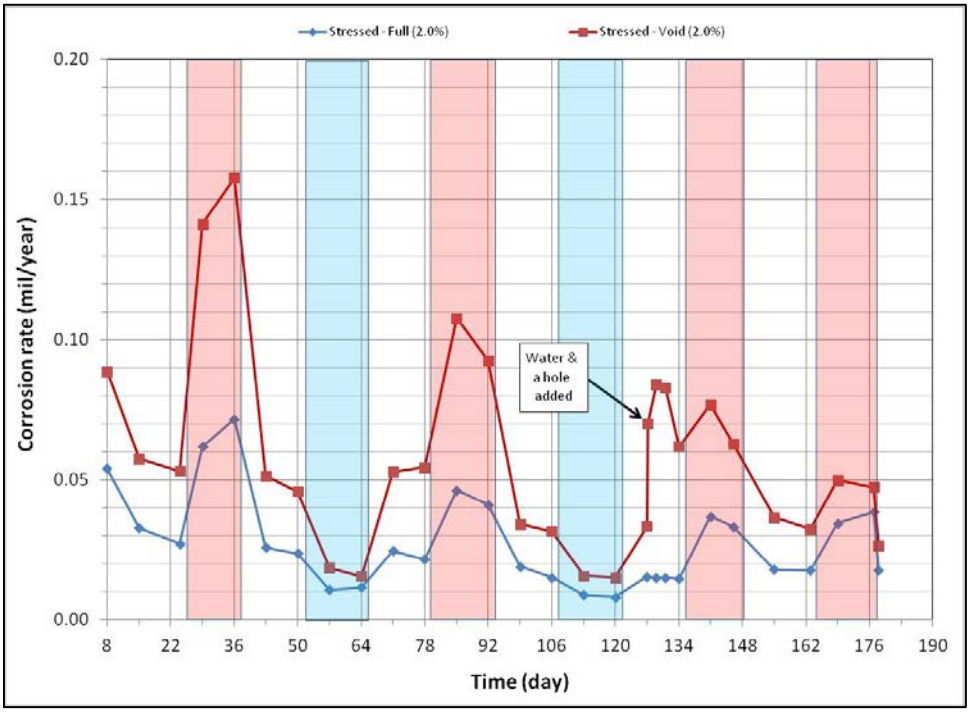

Figure 127. Graph. Corrosion rate versus time for 2.0 percent chloride single-strand specimens.

Fully Grouted Specimens Versus Voided Specimens

Figure 128 through figure 131 summarize mean corrosion rates calculated for the stressed and unstressed strands in fully grouted specimens per chloride concentration in initial ambient, ambient, H & H, and F & D cycles, respectively. The data for control specimens were also included in initial ambient and ambient plots. Similar plots for voided specimens are presented in figure 132 through figure 135. In each exposure condition, mean corrosion rates per chloride concentration were grouped by stress versus no stress. Because water was added to some of the voided specimens after initial ambient and F & D cycles were completed, mean corrosion rate data related to post-water recharging event are presented in figure 133 (ambient) and figure 134 (H & H) only.

To maintain the same scale in each plot, maximum corrosion rate was set at 0.2 mil/year, close to the highest corrosion rate reported in figure 127. As a result, it is hard to see subtle differences among different sets of corrosion rate data. There were no clear trends observed by stress level and presence of void except that voided specimens exhibited increased mean corrosion rates upon water recharging, and this trend is more pronounced at higher chloride concentrations as shown in figure 133 and figure 134. The effect of drilling air holes on corrosion rate was not observed.

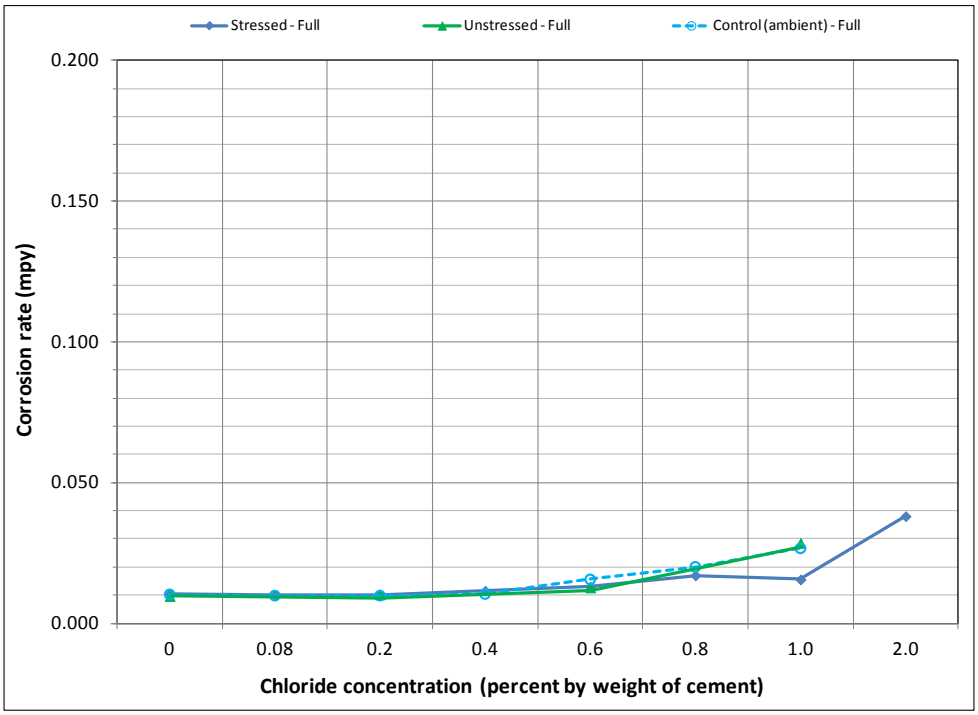

Figure 128. Graph. Mean corrosion rate of fully grouted single-strand specimens in initial ambient condition.

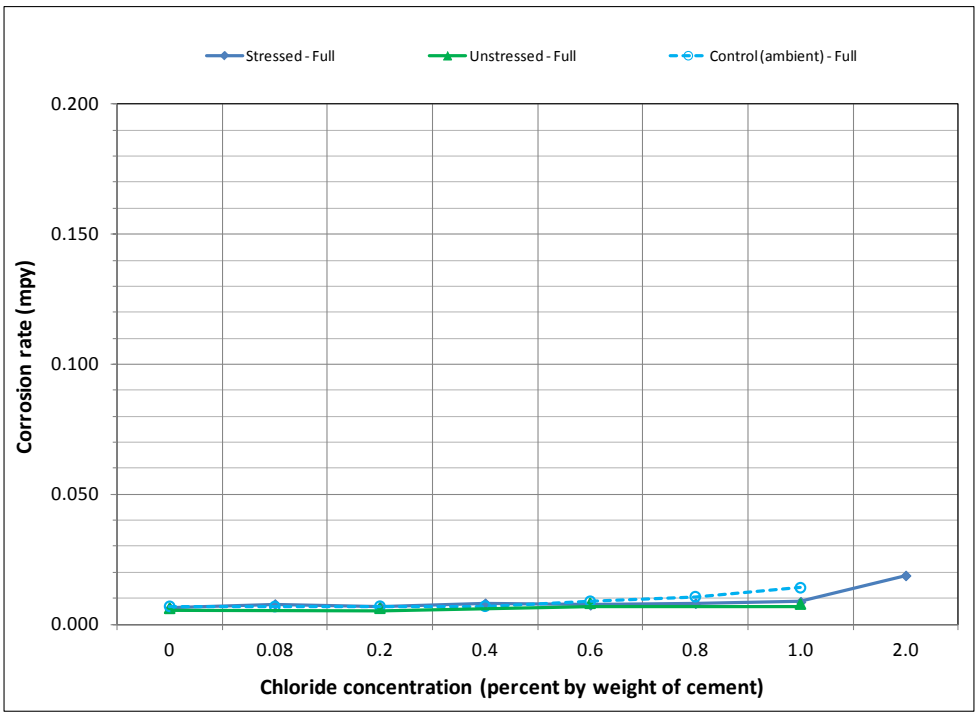

Figure 129. Graph. Mean corrosion rate of fully grouted single-strand specimens in ambient condition.

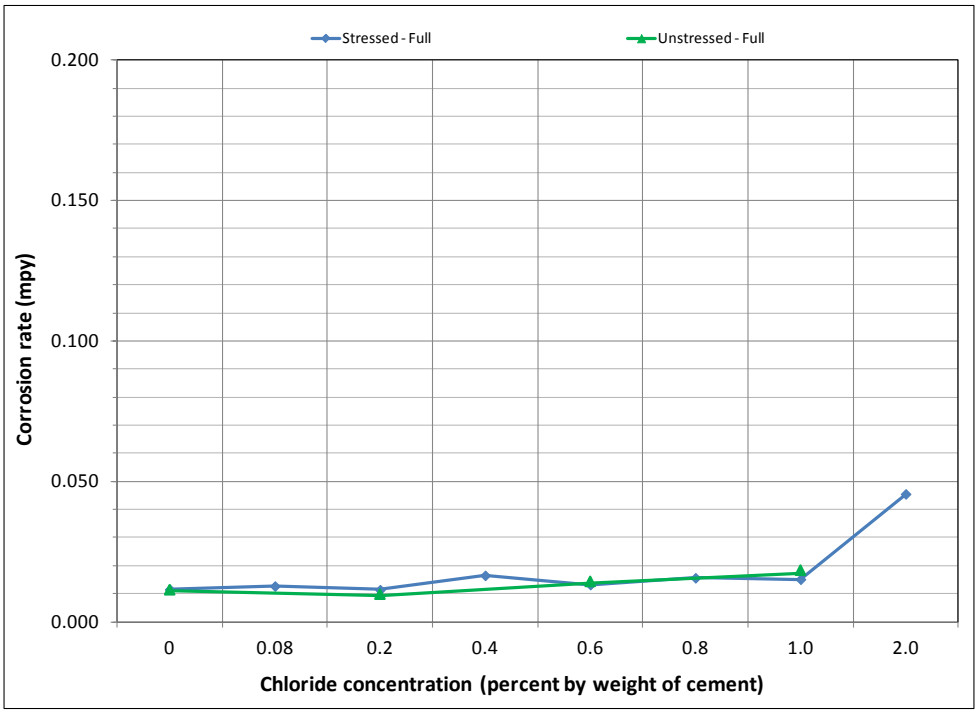

Figure 130. Graph. Mean corrosion rate of fully grouted single-strand specimens in H & H condition.

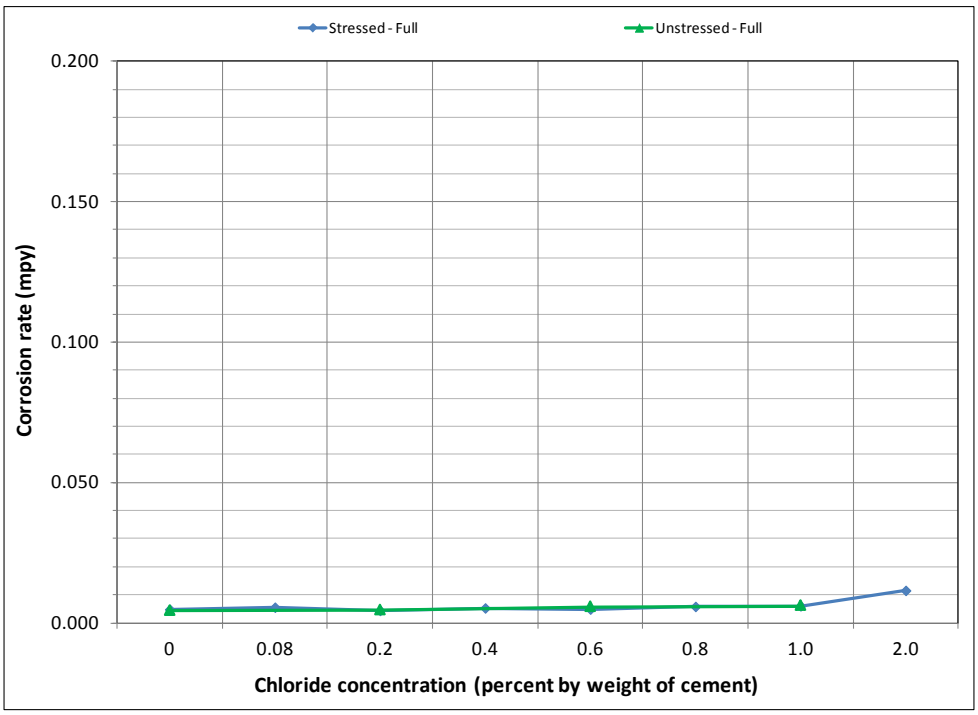

Figure 131. Graph. Mean corrosion rate of fully grouted single-strand specimens in F & D condition.

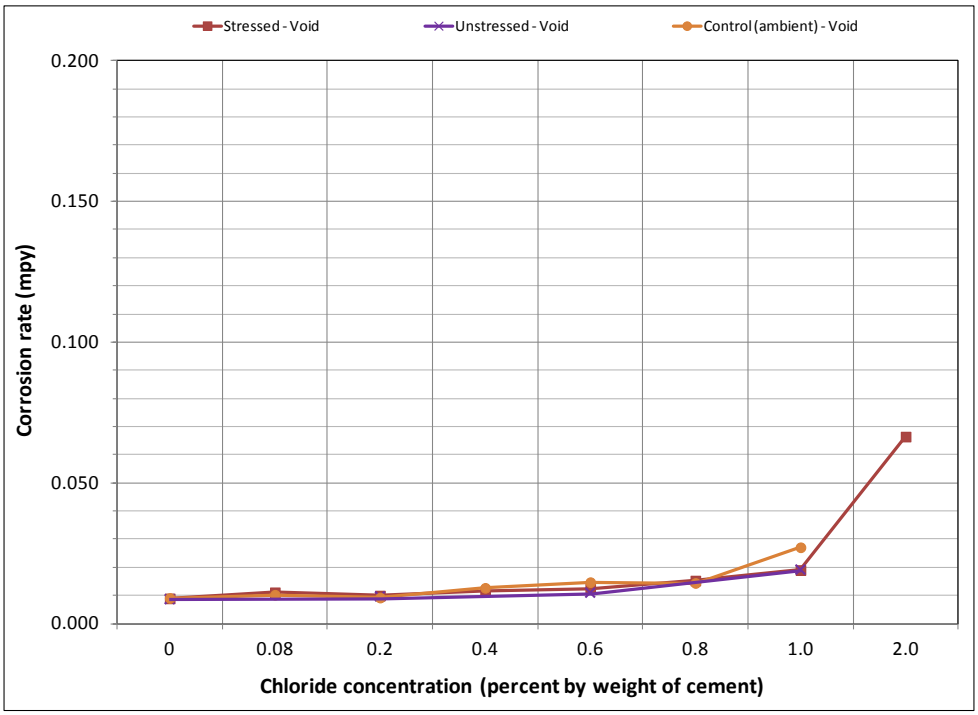

Figure 132. Graph. Mean corrosion rate of voided single-strand specimens in initial ambient condition.

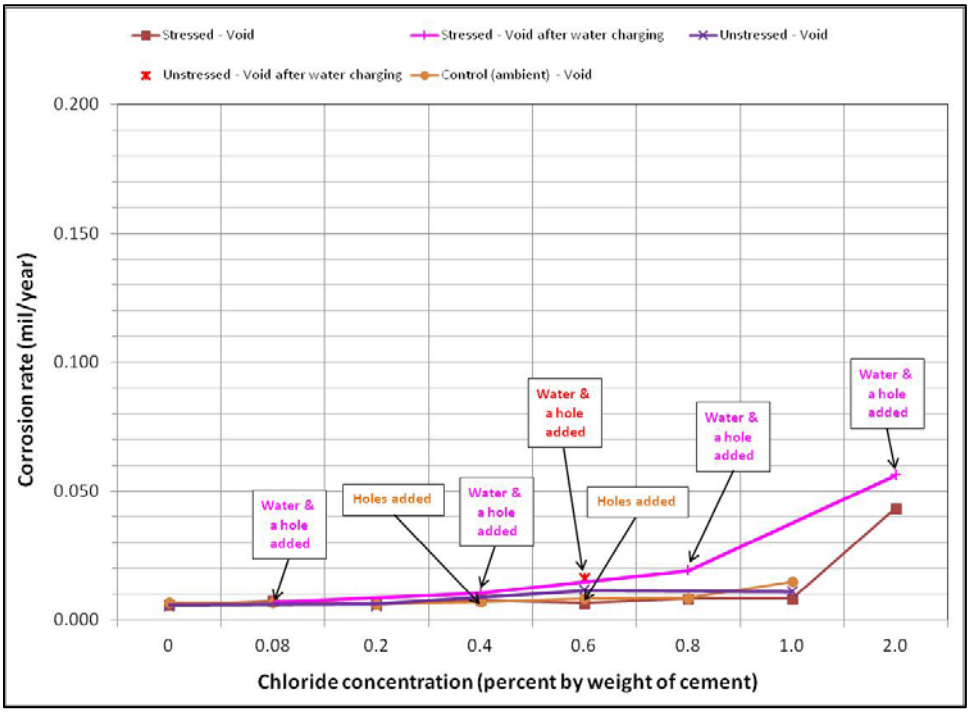

Figure 133. Graph. Mean corrosion rate of voided single-strand specimens in ambient condition.

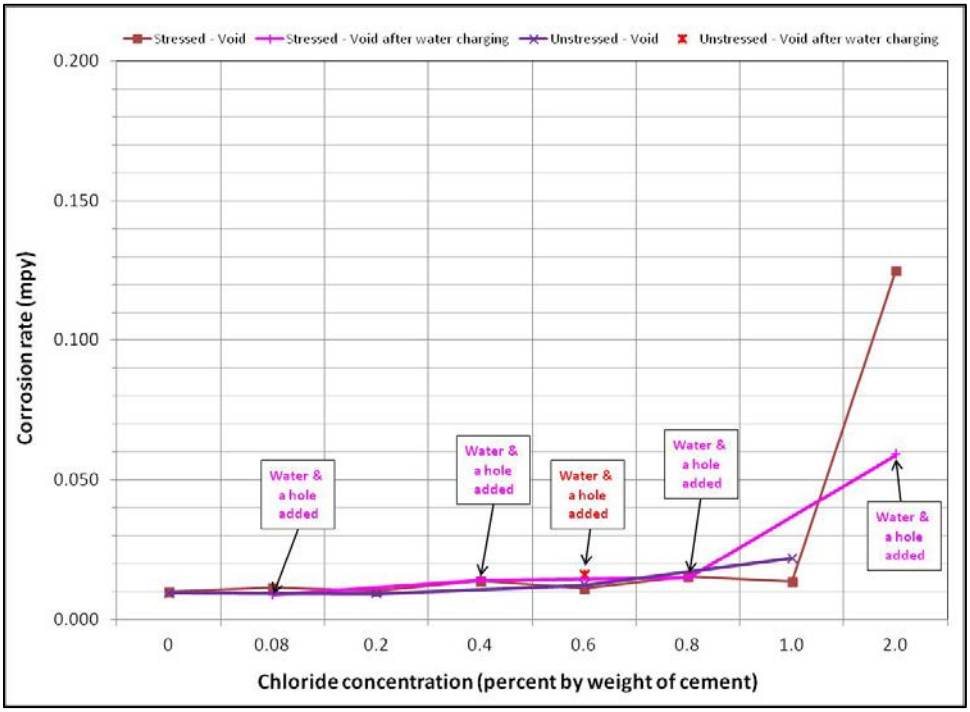

Figure 134. Graph. Mean corrosion rate of voided single-strand specimens in H & H condition.

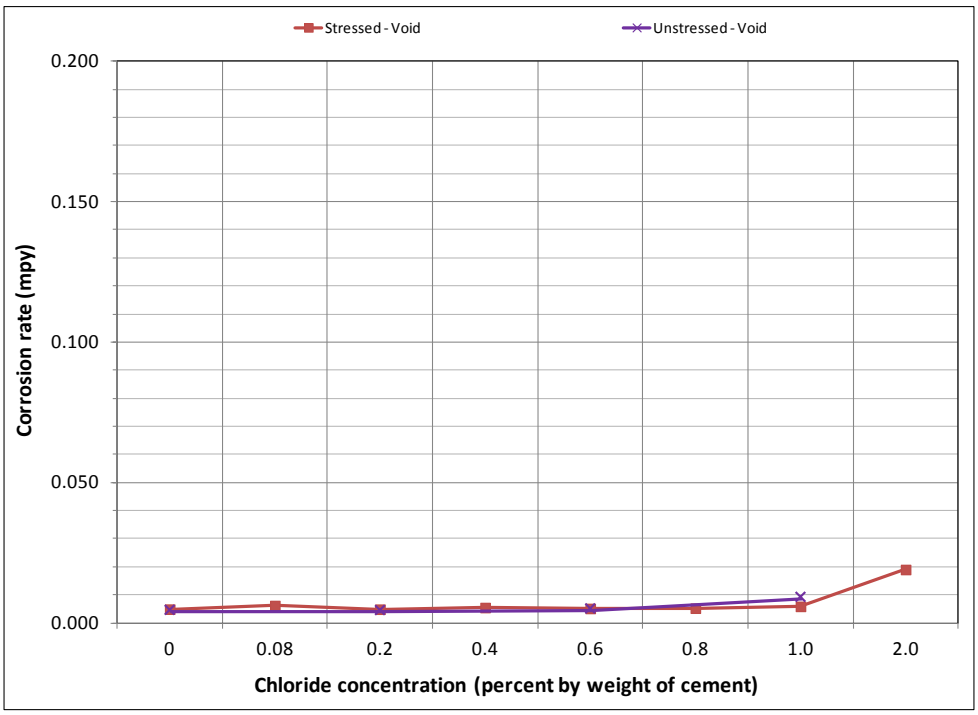

Figure 135. Graph. Mean corrosion rate of voided single-strand specimens in F & D condition.

Figure 136 through figure 141 present enlarged portions of mean corrosion rate plots related to initial ambient (see figure 128 and figure 132), ambient (see figure 129 and figure 133), and H & H (see figure 130 and figure 134) conditions. Since corrosion activity diminished in the F & D condition, their data were not included in figure 136 through figure 141. The plots in figure 136, figure 138, and figure 140 contain mean corrosion rate data of fully grouted specimens, and the plots in figure 137, figure 139, and figure 141 contain the same data for voided specimens. To capture subtle trends for undisturbed conditions, corrosion rate data after water recharging were removed from the original plots, and the maximum scale for the plots was set at 0.03 mil/year. Because the key point of the plots was to understand corrosion rate behaviors corresponding to chloride concentrations between 0 and 0.8 percent, losing some of the 2.0 percent chloride specimen data in the enlarged plots was accepted. Two more enlarged plots are presented in figure 142 and figure 143. The former is related to overall mean corrosion rates per chloride concentration, and the latter is related to mean corrosion rates grouped by stress level per chloride concentration. Careful examination of figure 136 through figure 143 leads to the following findings:

- No difference in mean corrosion rate was observed between fully grout specimens and voided specimens.
- There was no discernible difference between stressed specimens and unstressed specimens.
- Mean corrosion rates in ambient condition were slightly lower than those collected in initial ambient and H & H conditions.

- Mean corrosion rates of the accelerated corrosion testing specimens became almost the same as those of control specimens as low corrosion rates measured during the F & D cycles offset higher corrosion rates obtained during the H & H cycles.

- Mean corrosion rates of 0, 0.08, and 0.2 percent specimens were nearly the same. They were thought to be in sound passive state. At 0.4 percent chloride concentration, mean corrosion rates started to increase.

- According to the autopsy results, the lowest chloride concentration to initiate pitting corrosion was also the 0.4 percent chloride. Therefore, there is good agreement between corrosion morphology and the lowest chloride concentration that began to increase corrosion rate beyond the passive state.

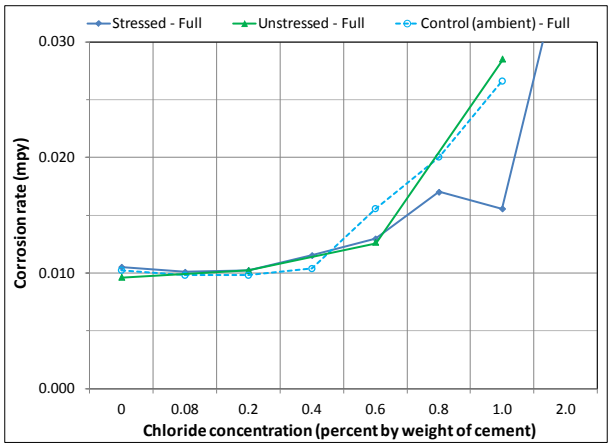

Figure 136. Graph. Magnified corrosion rate for initial ambient condition of fully grouted specimens.

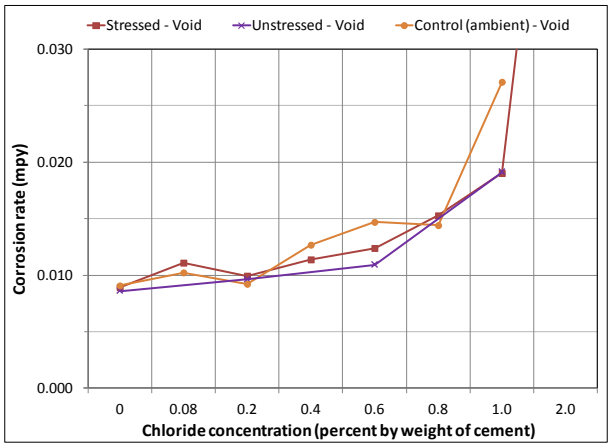

Figure 137. Graph. Magnified corrosion rate for initial ambient condition of voided specimens.

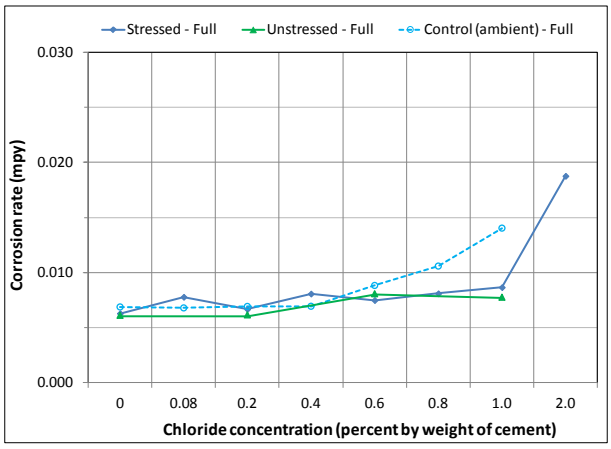

Figure 138. Graph. Magnified corrosion rate for ambient condition of fully grouted specimens.

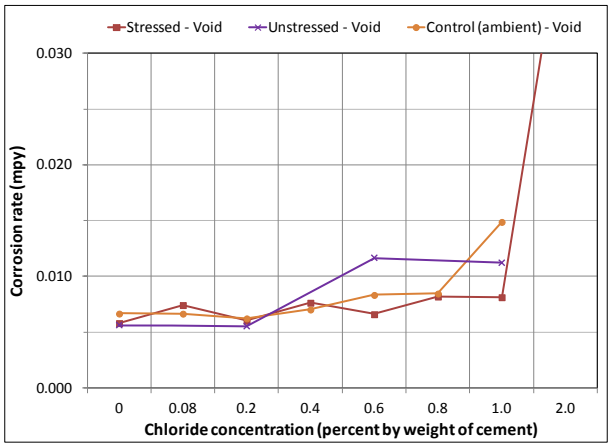

Figure 139. Graph. Magnified corrosion rate for ambient condition of voided specimens.

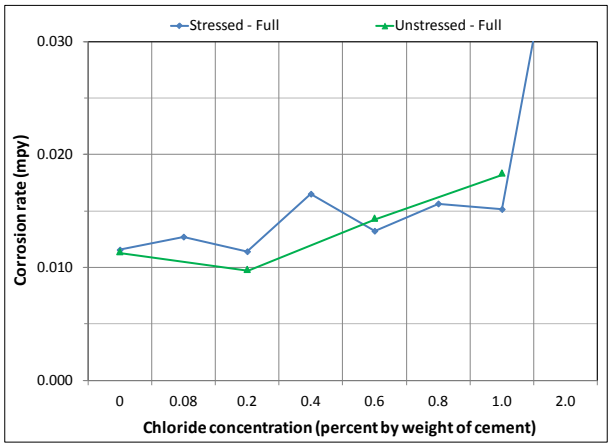

Figure 140. Graph. Magnified corrosion rate for H & H condition of fully grouted specimens.

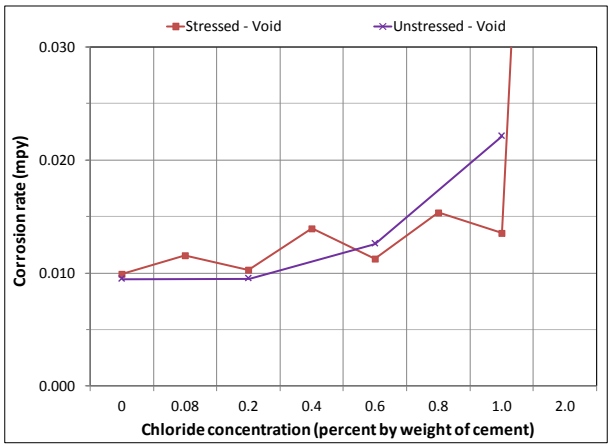

Figure 141. Graph. Magnified corrosion rate for H & H condition of voided specimens.

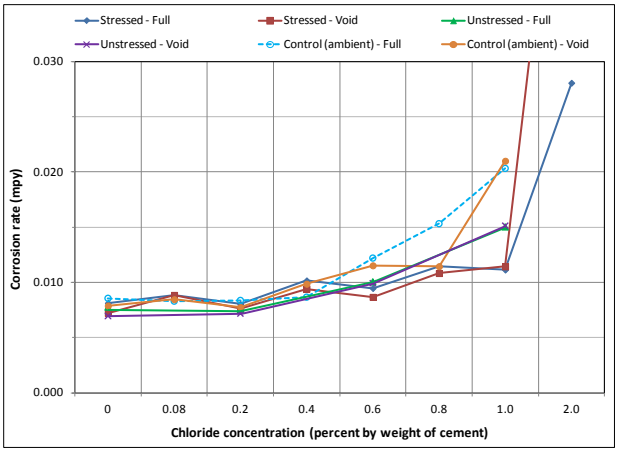

Figure 142. Graph. Overall mean corrosion rates of single-strand specimens.

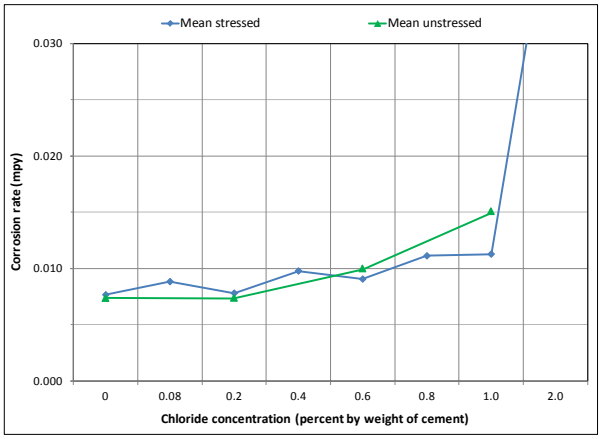

Figure 143. Graph. Overall mean corrosion rates of single-strand specimens grouped by stress level.

Task 2.3: Corrosion Current Density and Driving Voltage Data of Multi-Strand Specimens

Figure 144 through figure 151 present macro-cell corrosion current density ($i_{macro\text{-}cell}$) data and the corresponding driving voltage data versus time plots for multi-strand specimens. The *driving voltage* is the difference of corrosion potentials between macro-anode and macro-cathode. The magnitude of $i_{macro\text{-}cell}$ increases proportionally to that of driving voltage. Figure 144 through figure 146 show a small driving voltage (nearly zero macro-cell corrosion current density relationship (i.e., less than 50 mV and less than 0.01 µA/cm^2)) for 0, 0.08, and 0.2 percent chloride specimens. Figure 149 and figure 150 provide examples of a large driving voltage (substantial macro-cell corrosion current density relationship (i.e., over 100 mV and 0.10 µA/cm^2)) for 0.8 and 1.0 percent specimens. The relationships are particularly pronounced during the H & H cycles. As discussed previously in conjunction with figure 115, the 2.0 percent chloride specimen data shown in figure 151 indicated that unstressed strands were already corroding in the highest chloride contaminated grout mix. This situation resulted in reduction of driving voltage between macro-anode and macro-cathode. Such a reduced driving voltage attributed to the gradual reduction of $i_{macro\text{-}cell}$ to nearly zero and even a small current reversal at the end of testing.

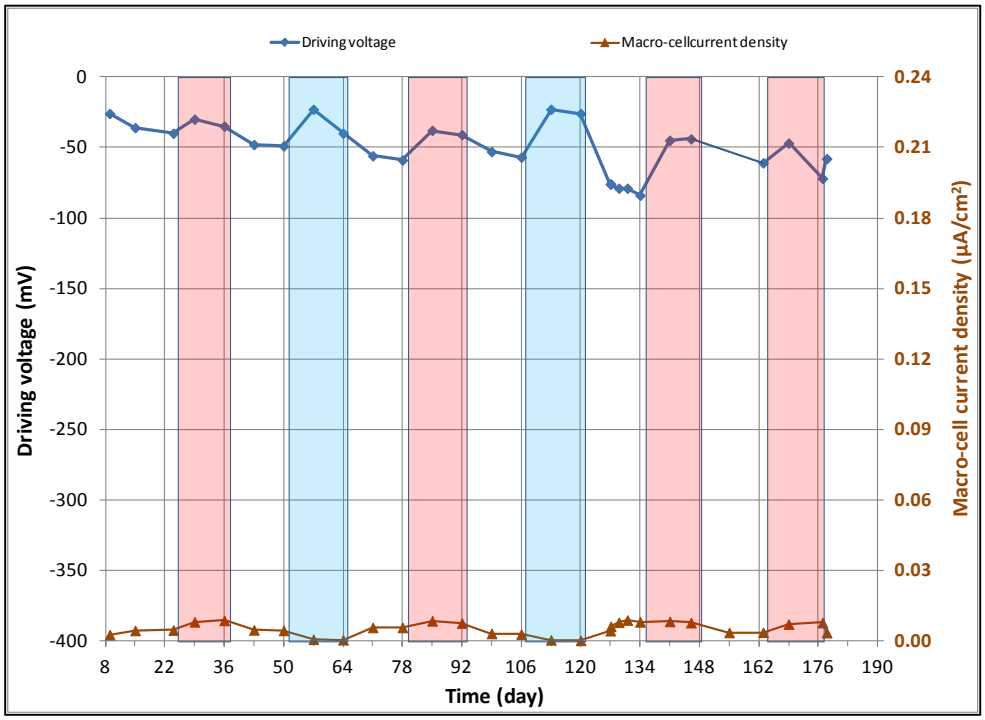

Figure 144. Graph. $i_{macro\text{-}cell}$ and driving voltage versus time for 0 percent chloride multi-strand specimen.

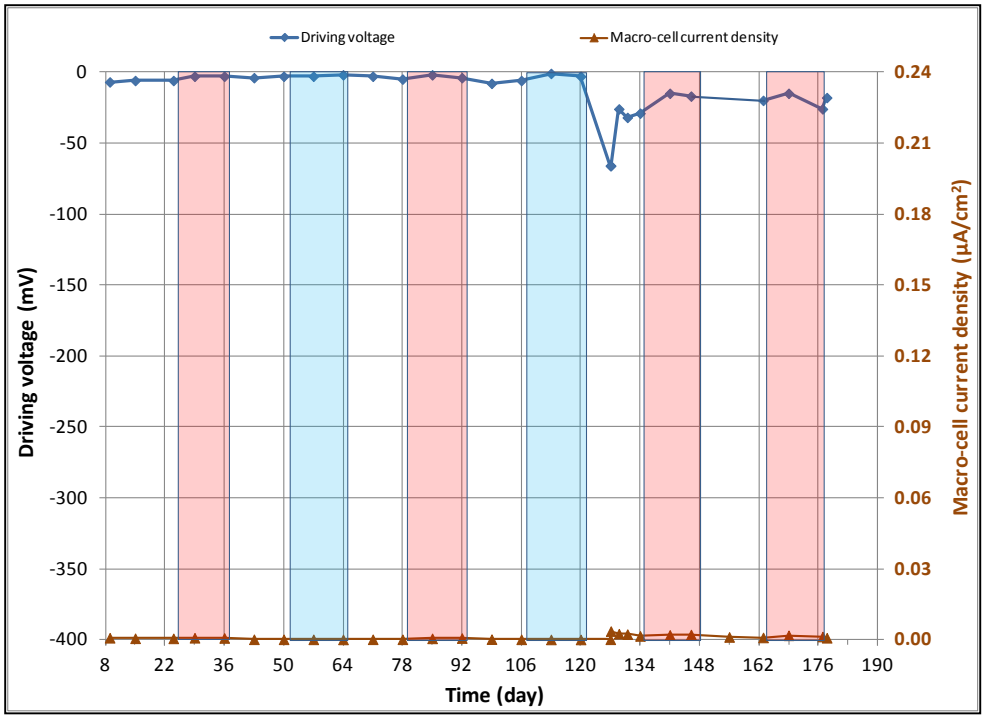

Figure 145. Graph. $i_{macro\text{-}cell}$ and driving voltage versus time for 0.08 percent chloride multi-strand specimen.

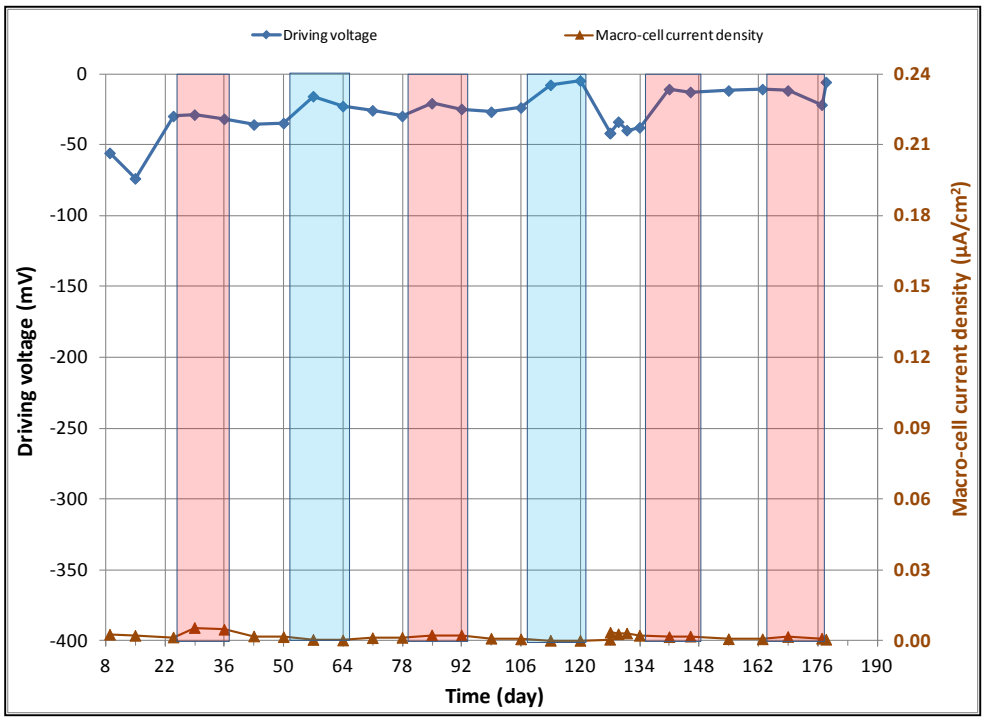

Figure 146. Graph. $i_{macro\text{-}cell}$ and driving voltage versus time for 0.2 percent chloride multi-strand specimen.

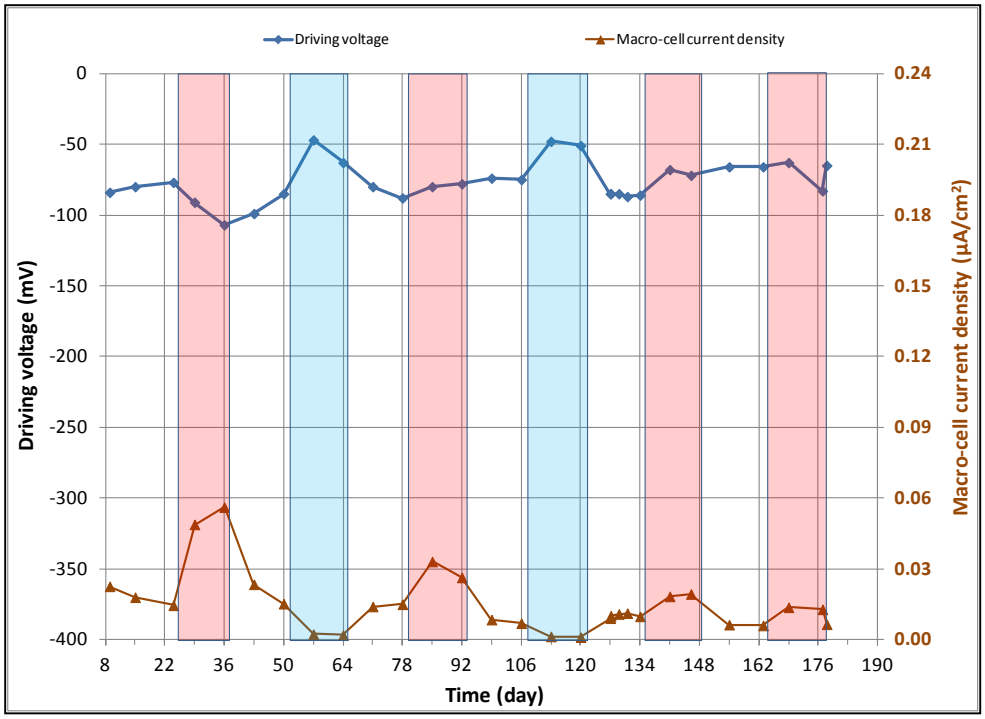

Figure 147. Graph. $i_{macro\text{-}cell}$ and driving voltage versus time for 0.4 percent chloride multi-strand specimen.

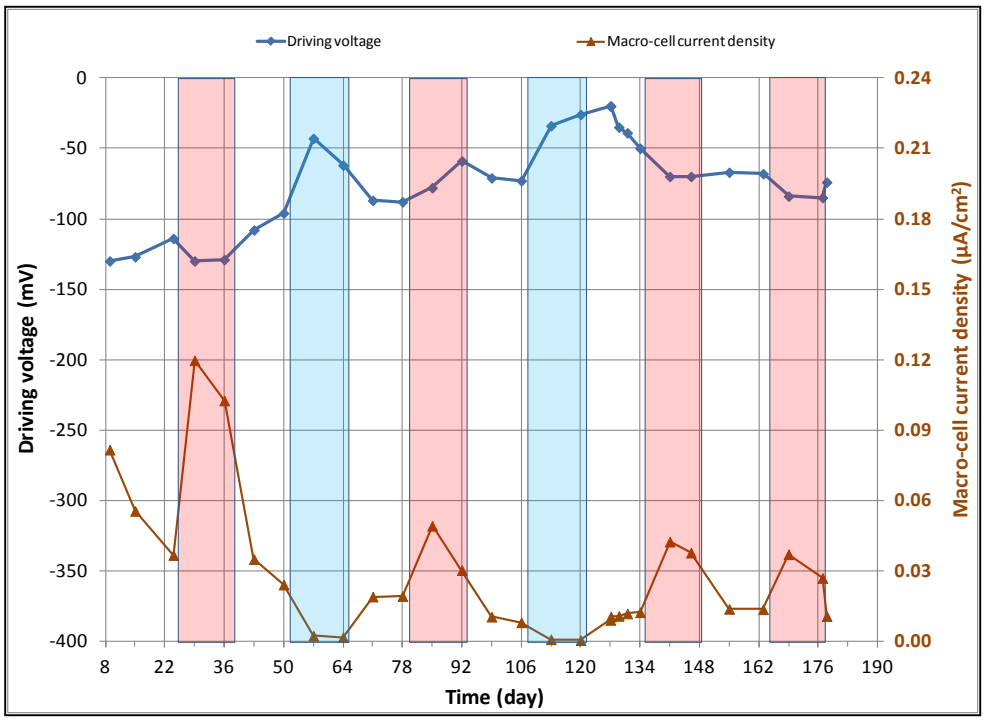

Figure 148. Graph. $i_{macro\text{-}cell}$ and driving voltage versus time for 0.6 percent chloride multi-strand specimen.

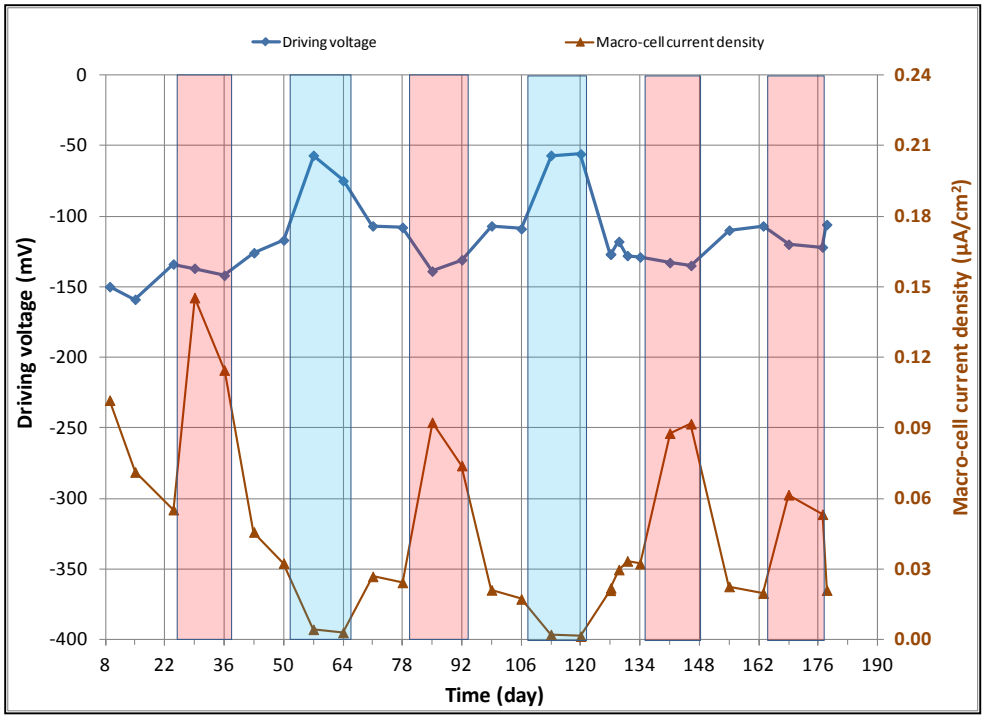

Figure 149. Graph. $i_{macro\text{-}cell}$ and driving voltage versus time for 0.8 percent chloride multi-strand specimen.

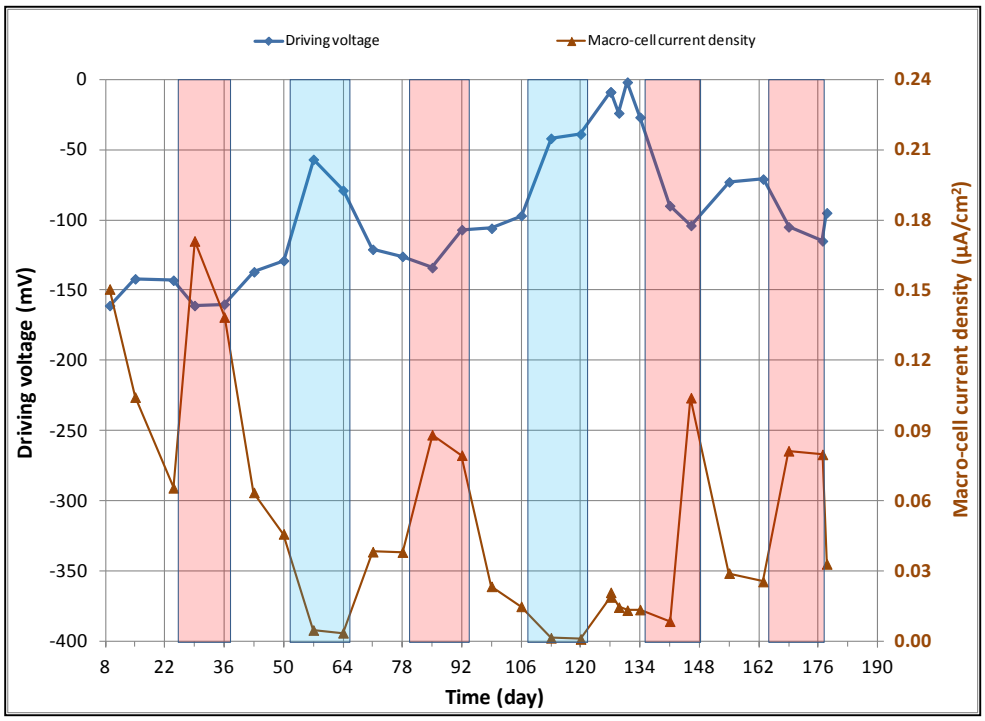

Figure 150. Graph. $i_{macro\text{-}cell}$ and driving voltage versus time for 1.0 percent chloride multi-strand specimen.

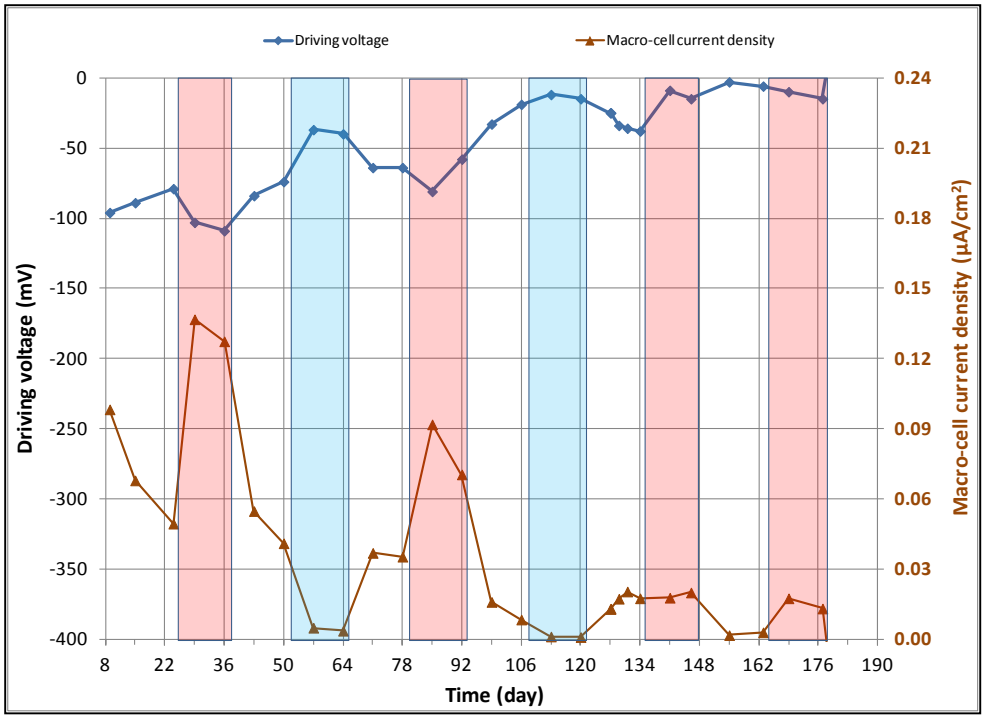

Figure 151**. Graph. $i_{macro\text{-}cell}$ and driving voltage versus time for 2.0 percent chloride multi-strand specimen.**

Figure 152 presents mean $i_{macro\text{-}cell}$ data grouped by exposure condition for each chloride concentration. It is clear that $i_{macro\text{-}cell}$ started to increase substantially once chloride concentration exceeded 0.4 percent. The H & H cycles produced the highest mean $i_{macro\text{-}cell}$ at all chloride concentrations in different environmental conditions: mean $i_{macro\text{-}cell}$ increased almost linearly as a function of chloride concentration up to 1.0 percent. In contrast, the lowest mean $i_{macro\text{-}cell}$ data were obtained during the F & D cycles independent of chloride concentration. Mean $i_{macro\text{-}cell}$ was also somewhat insensitive to chloride concentration under ambient exposure condition. Water recharging did not increase $i_{macro\text{-}cell}$ under the H & H and ambient cycles. Figure 153 summarizes overall mean $i_{macro\text{-}cell}$ data as a function of chloride concentration. It can be seen again that recognizable corrosion accompanied by $i_{macro\text{-}cell}$ over 0.010 µA/cm^2 began at 0.4 percent chloride.

Figure 154 shows the compiled $i_{macro\text{-}cell}$ changes as a function of time and temperature. Actual temperature recording data were overlapped in the figure to show that $i_{macro\text{-}cell}$ increased during the H & H cycles and decreased during the F & D cycles. The specimens containing more than 0.4 percent chloride concentration exhibited much higher $i_{macro\text{-}cell}$ than those containing lesser chloride. However, the differences gradually decreased with time. As discussed before, the specimen containing 2.0 percent chloride exhibited less $i_{macro\text{-}cell}$ than ones with 0.8 and 1.0 percent chloride due to the corroding macro-cathode. Figure 155 shows an enlarged section of the $i_{macro\text{-}cell}$ plot in figure 154, which shows the $i_{macro\text{-}cell}$ data before and after charging 5.1 fl oz of distilled water in the voids. Even though the 0.8 percent chloride specimen responded with increased $i_{macro\text{-}cell}$ upon water entry, the effect of water recharging was not considered significant compared to the data shown in figure 56. Some possible reasons for not being able to observe similar current surges in the present study include the following:

- The present study did not use enough water.
- Distilled water was not a strong oxidizer compared to salt water.
- Oxygen was limited in the grout to support cathodic reaction.

It is recommended to conduct follow-up tests by varying frequency of water recharging and type and volume of water used in the voids.

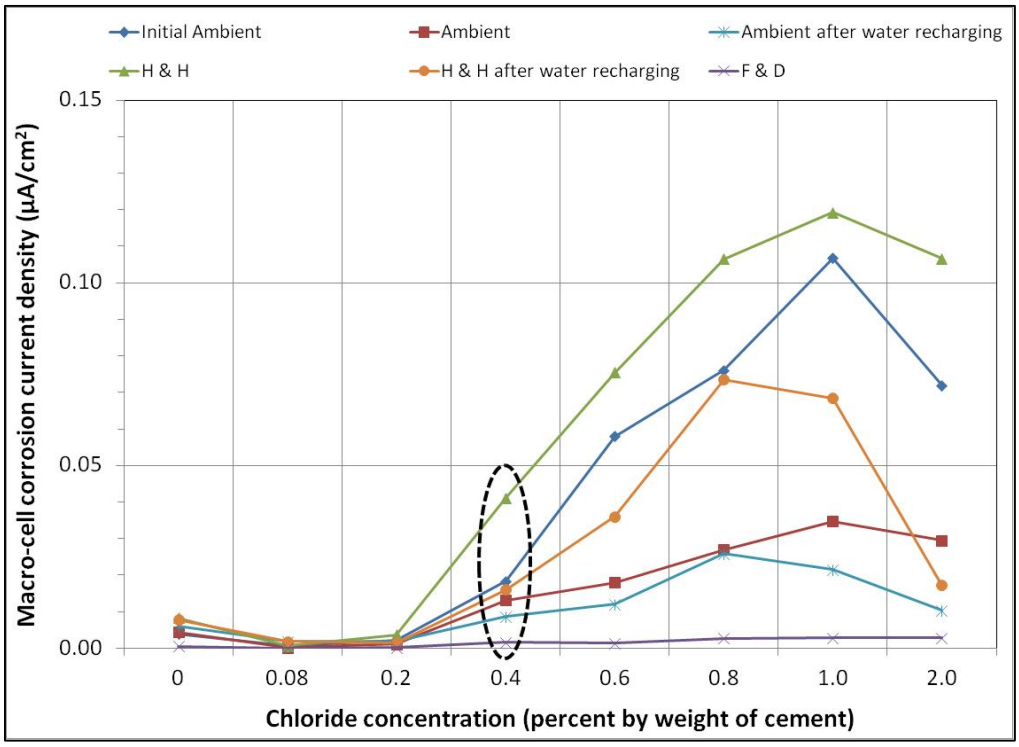

Figure 152. Graph. Mean $i_{macro\text{-}cell}$ data of multi-strand specimens by exposure condition.

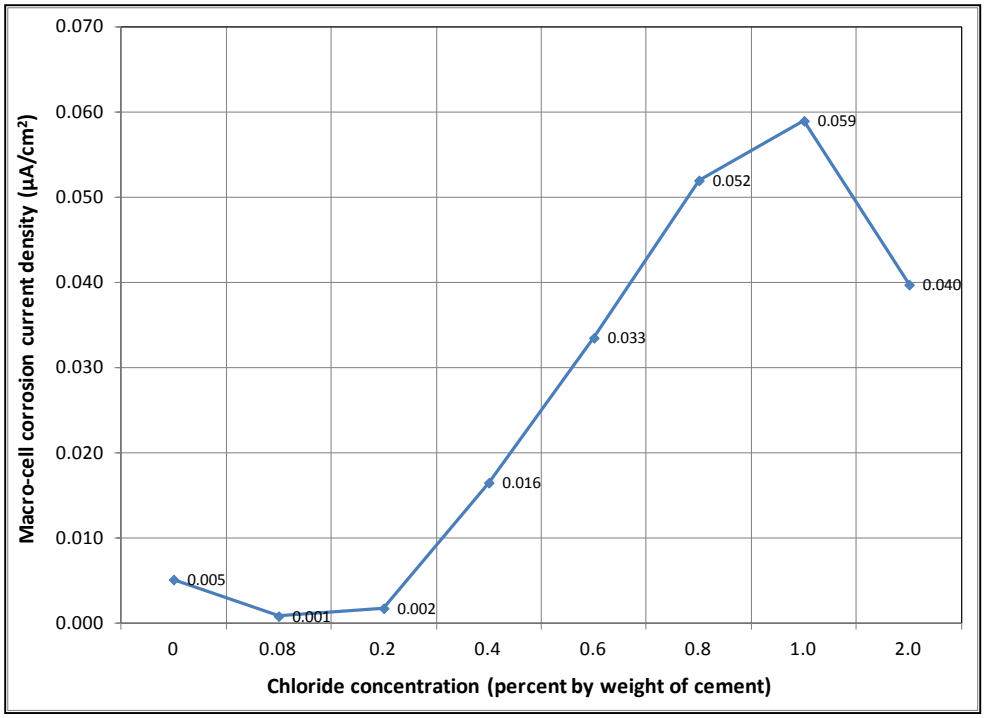

Figure 153. Graph. Overall mean $i_{macro\text{-}cell}$ data of multi-strand specimens.

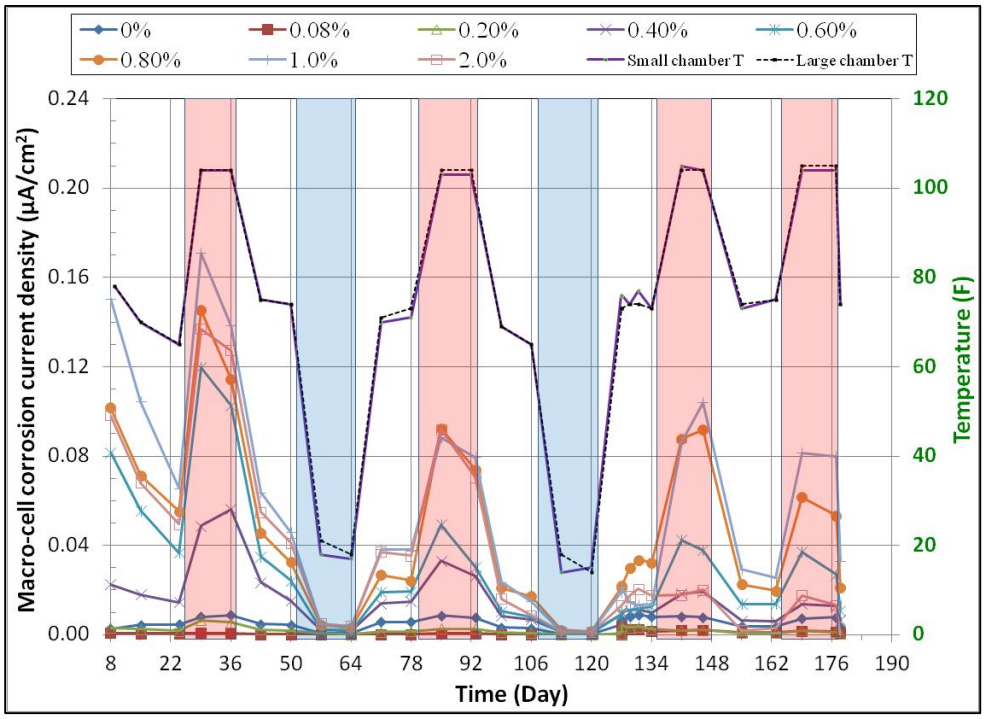

Figure 154. Graph. $i_{macro\text{-}cell}$ behavior responding to temperature variation.

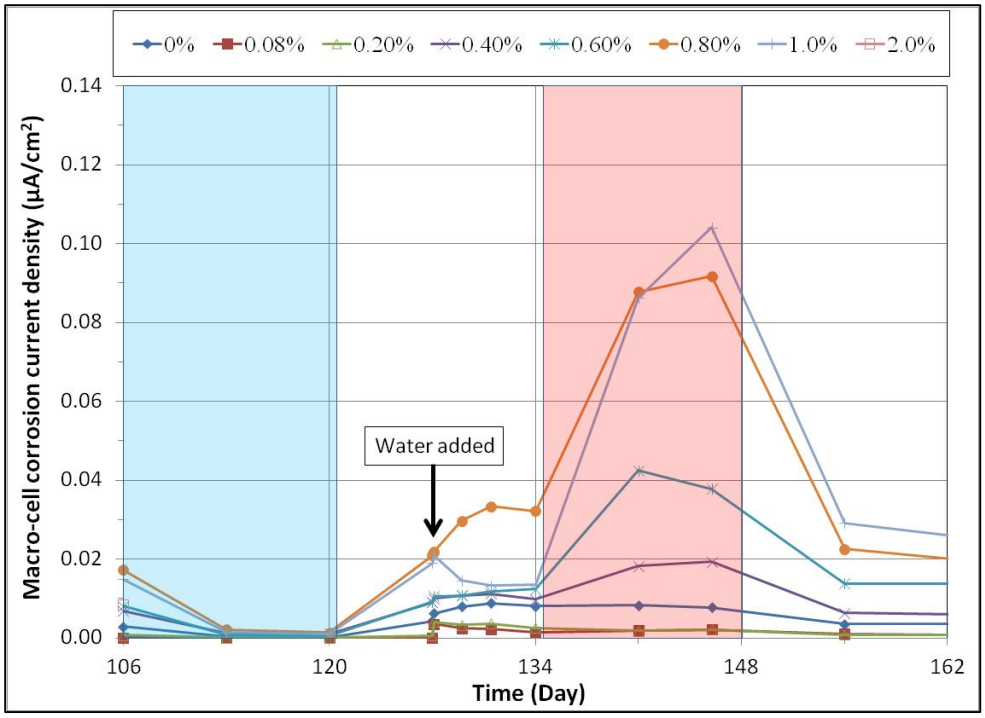

Figure 155. Graph. $i_{macro\text{-}cell}$ changes after water recharging.

Figure 156 through figure 163 show stressed strands in the voids. The photographs were taken 1 week after recharging water was added to the voids. It was observed even during early days of testing that three specimens containing 0 percent chloride (see figure 156), 0.4 percent chloride (see figure 159), and 2.0 percent chloride (see figure 163) showed black deposit on the void/grout interface where stressed strands passed through. The unknown deposit material is indicated with arrows in the figures. The specimens covered with the deposit layer also appeared to hold water longer than specimens without it. This mysterious layer turned out to be important, as the autopsy revealed that some strands in contact with the deposit layer suffered from severe corrosion. Three wires of 0.4 percent chloride specimen and one wire of 2.0 percent chloride specimen were corroded in two during the 6-month accelerated corrosion testing. The 0 percent chloride specimen had severely corroded strands at the interface during the same period. The other specimens showed only minor corrosion on the stressed strands near the interface. The encountered excessive corrosion problem was never expected. Consequently, data analysis became complicated as to what to include and what to exclude among the weekly collected electrochemical data.

Figure 156. Photo. Void condition of 0 percent chloride specimen.

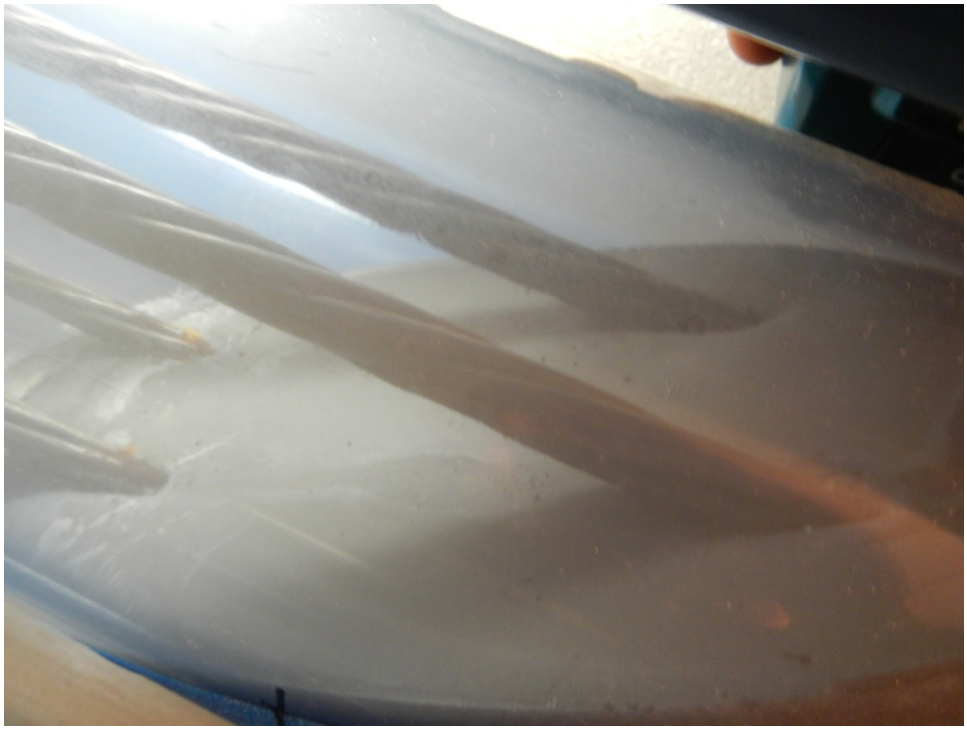

Figure 157. Photo. Void condition of 0.08 percent chloride specimen.

Figure 158. Photo. Void condition of 0.2 percent chloride specimen.

Figure 159. Photo. Void condition of 0.4 percent chloride specimen.

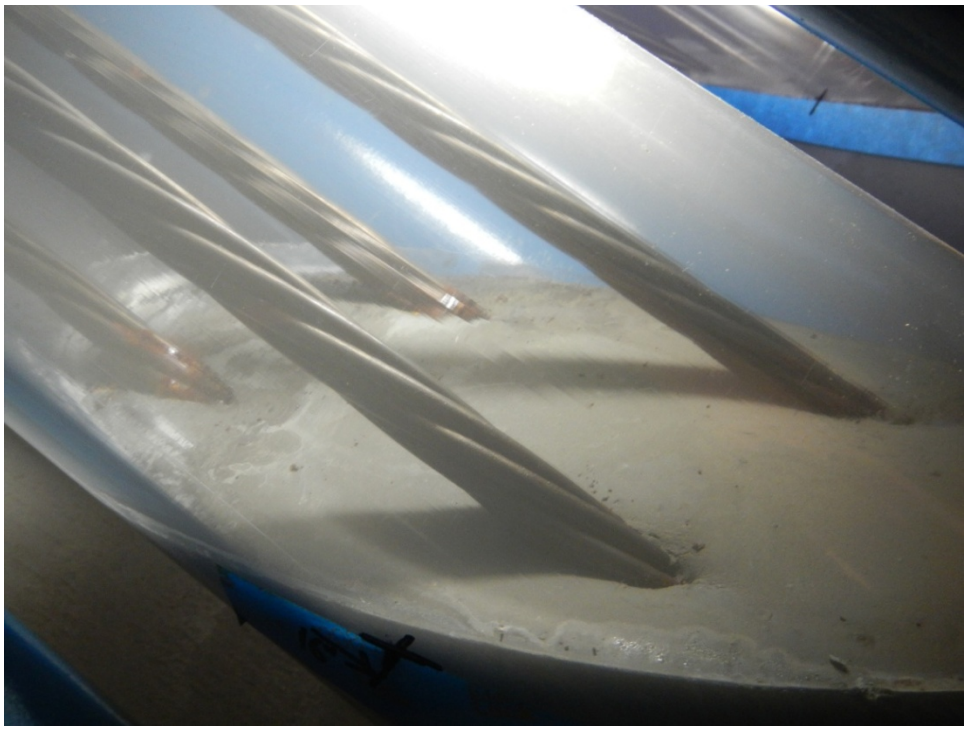

Figure 160. Photo. Void condition of 0.6 percent chloride specimen.

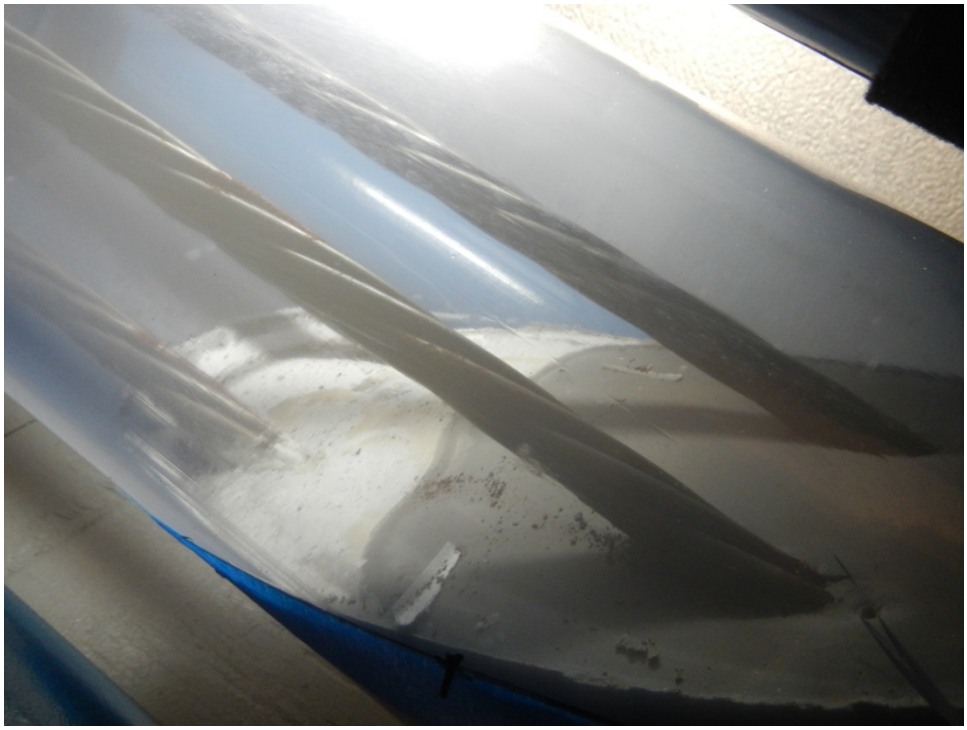

Figure 161. Photo. Void condition of 0.8 percent chloride specimen.

Figure 162. Photo. Void condition of 1.0 percent chloride specimen.

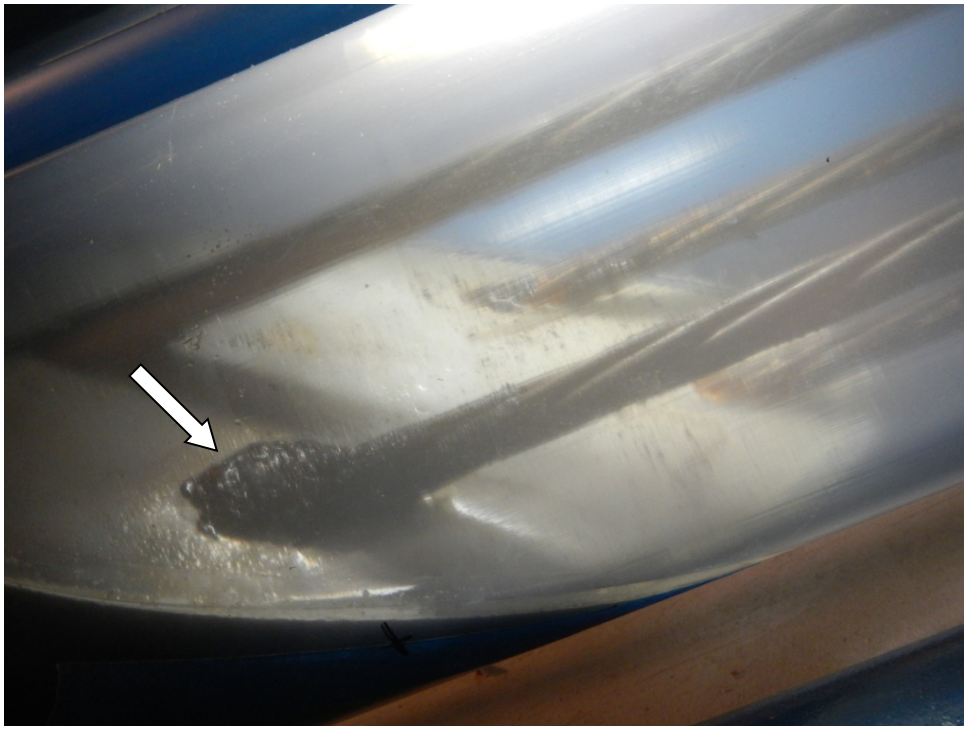

Figure 163. Photo. Void condition of 2.0 percent chloride specimen.

APPARENT GROUT RESISTIVITY AND GROUT RESISTANCE DATA

Task 2.2: Apparent Grout Resistivity of Single-Strand Specimens

Figure 164 through figure 171 present apparent grout resistivity versus time plots for single-strand specimens. Apparent grout resistivity increased when temperature decreased, and it decreased when temperature increased. Such a dependency of grout resistivity on temperature is also responsible for increased corrosion rate during the H & H cycles and suppressed corrosion rate during the F & D cycles. The control specimens maintained more or less their initial resistivity values at the ambient condition.

Figure 172 through figure 175 summarize mean apparent grout resistivity of fully grouted specimens per chloride concentration in initial ambient, ambient, H & H, and F & D conditions, respectively. Similarly, figure 176 through figure 179 summarize mean apparent grout resistivity of voided specimens per chloride concentration in initial ambient, ambient, H & H, and F & D conditions, respectively. Mean apparent grout resistivity data showed the same trend—the highest resistivity during the F & D cycles and the lowest during the H & H cycles. No definite relationship was found between apparent grout resistivity and chloride concentration. Grout void and stress did not appear to influence the apparent grout resistivity, either.

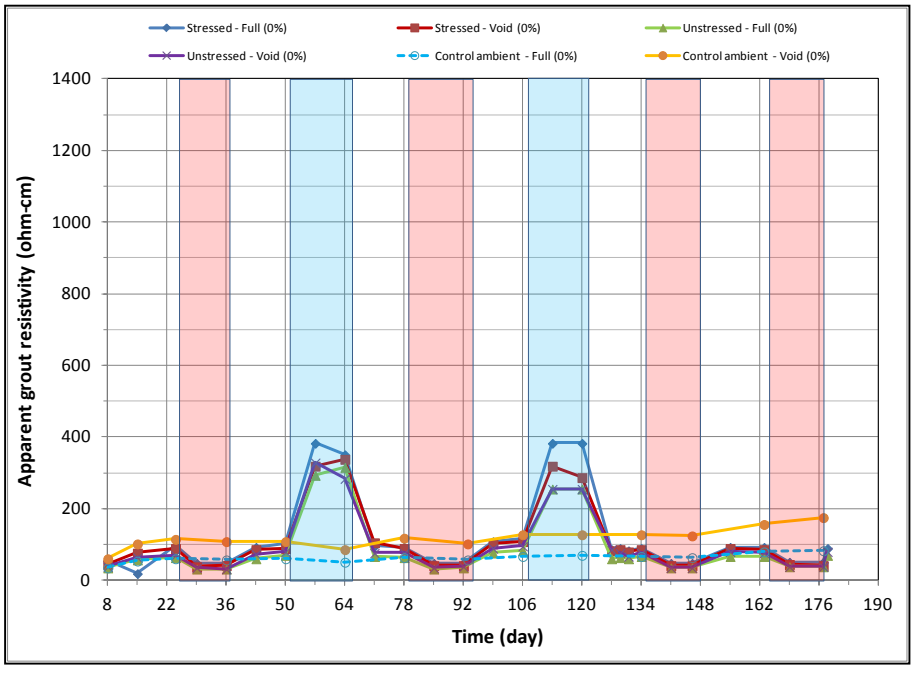

Figure 164. Graph. Apparent grout resistivity versus time for 0 percent chloride single-strand specimens.

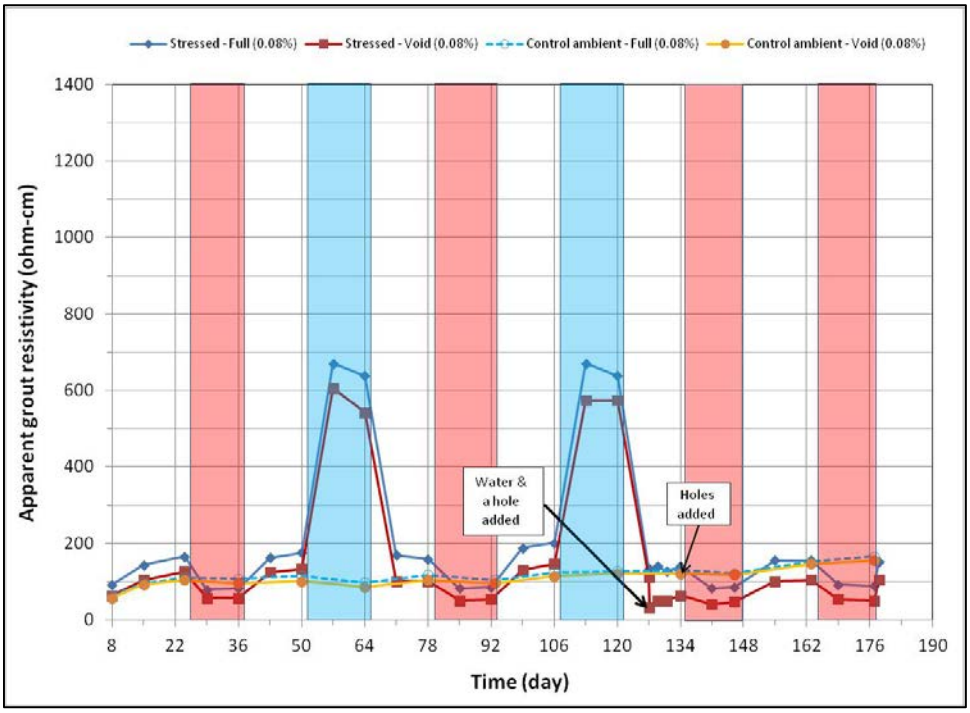

Figure 165. Graph. Apparent grout resistivity versus time for 0.08 percent chloride single-strand specimens.

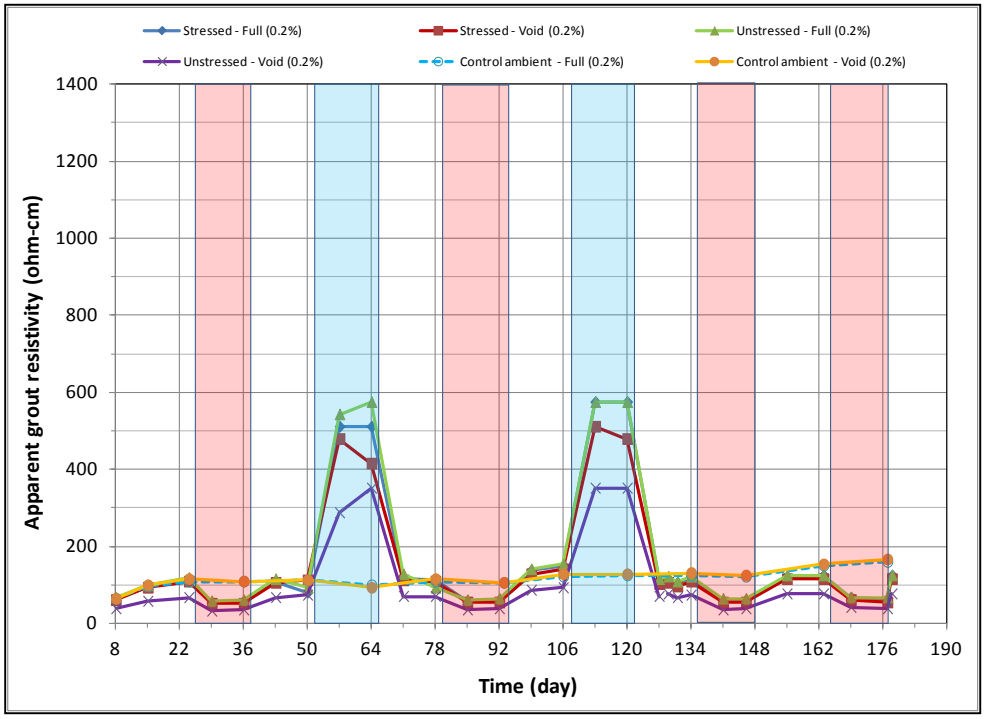

Figure 166. Graph. Apparent grout resistivity versus time for 0.2 percent chloride single-strand specimens.

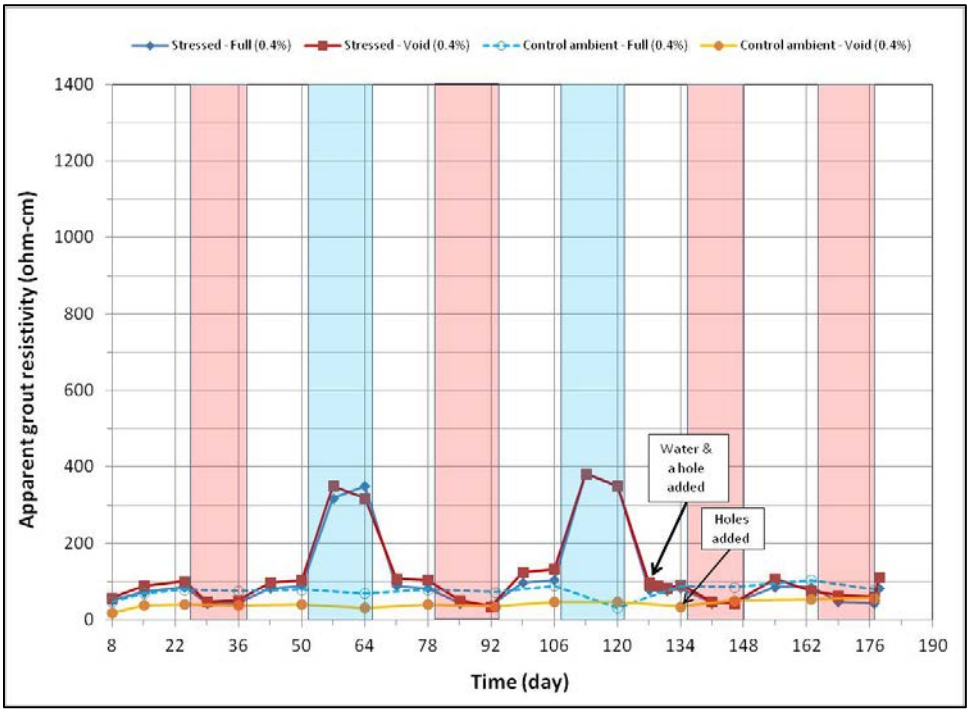

Figure 167. Graph. Apparent grout resistivity versus time for 0.4 percent chloride single-strand specimens.

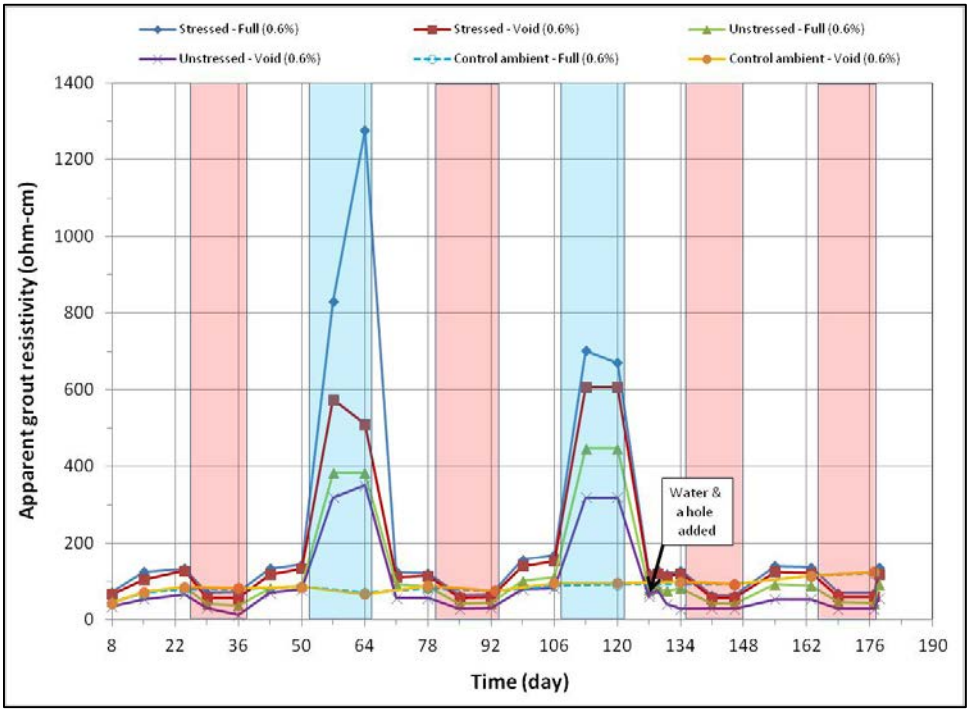

Figure 168. Graph. Apparent grout resistivity versus time for 0.6 percent chloride single-strand specimens.

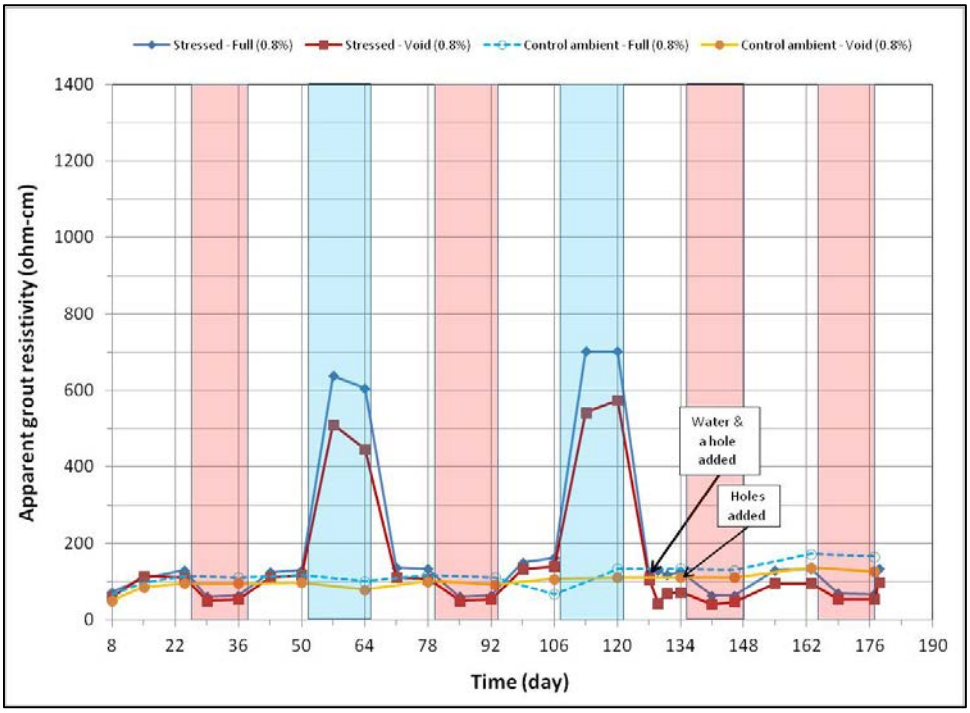

Figure 169. Graph. Apparent grout resistivity versus time for 0.8 percent chloride single-strand specimens.

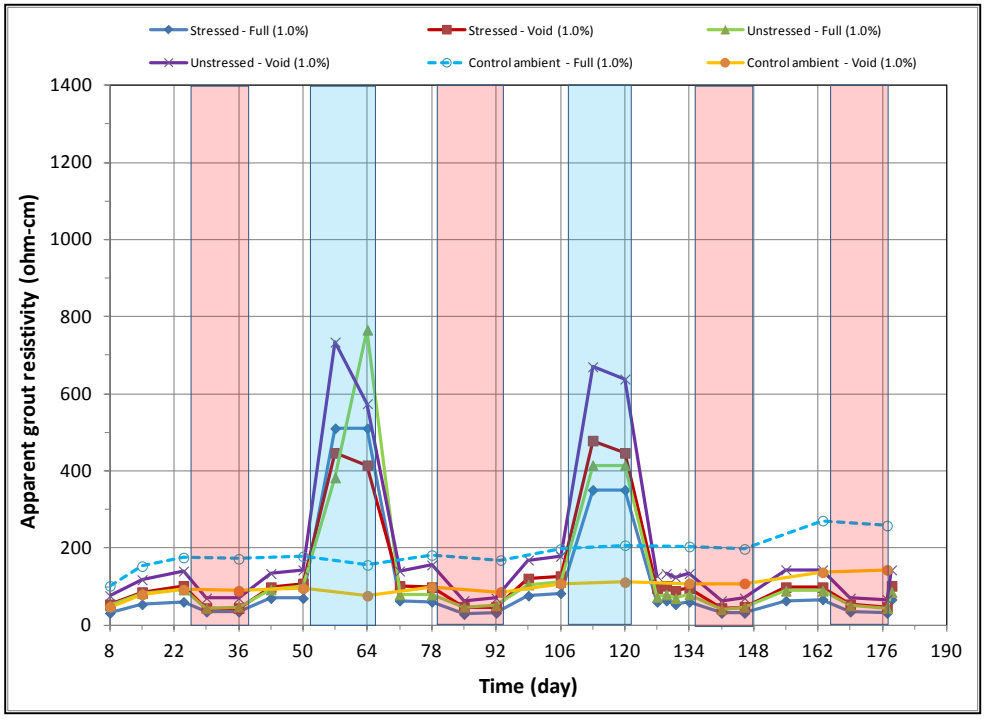

Figure 170. Graph. Apparent grout resistivity versus time for 1.0 percent chloride single-strand specimens.

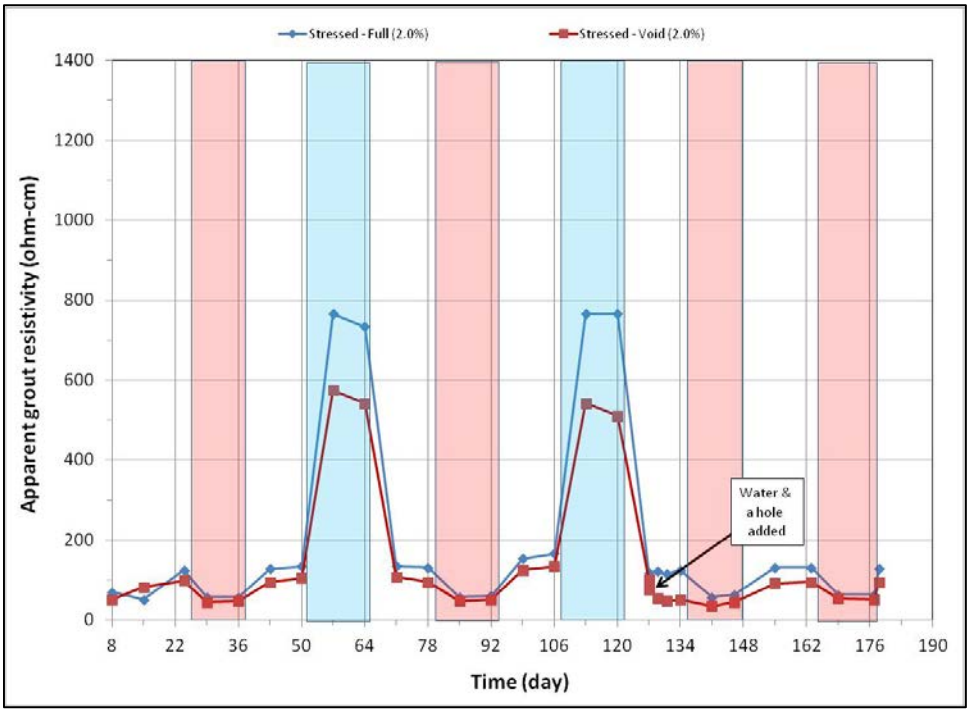

Figure 171. Graph. Apparent grout resistivity versus time for 2.0 percent chloride single-strand specimens.

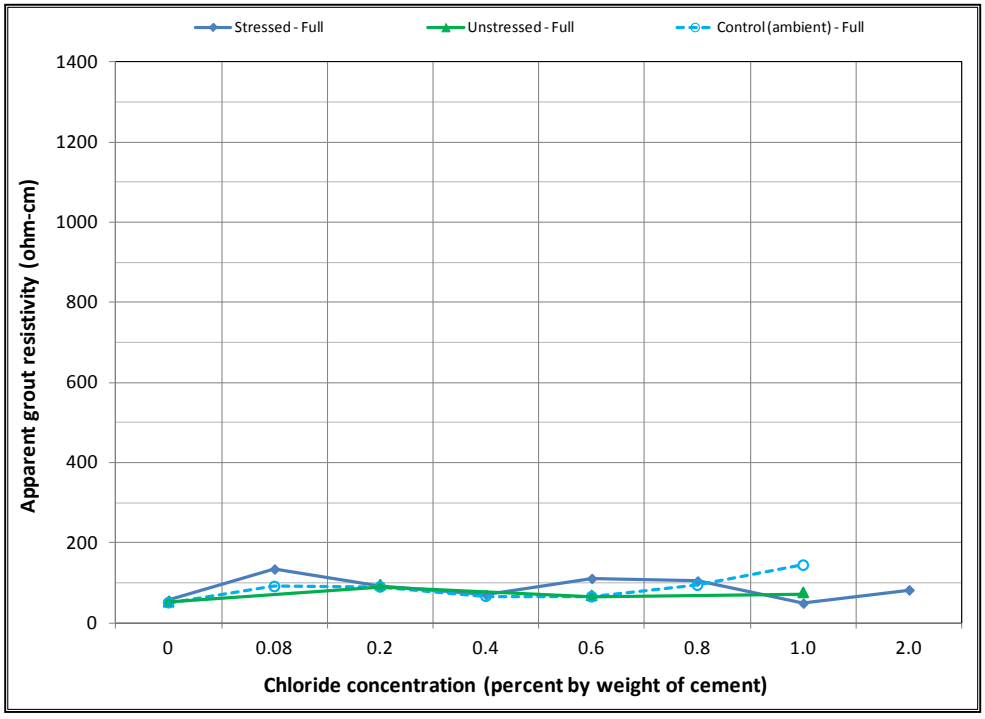

Figure 172. Graph. Mean apparent grout resistivity of fully grouted single-strand specimens in initial ambient condition.

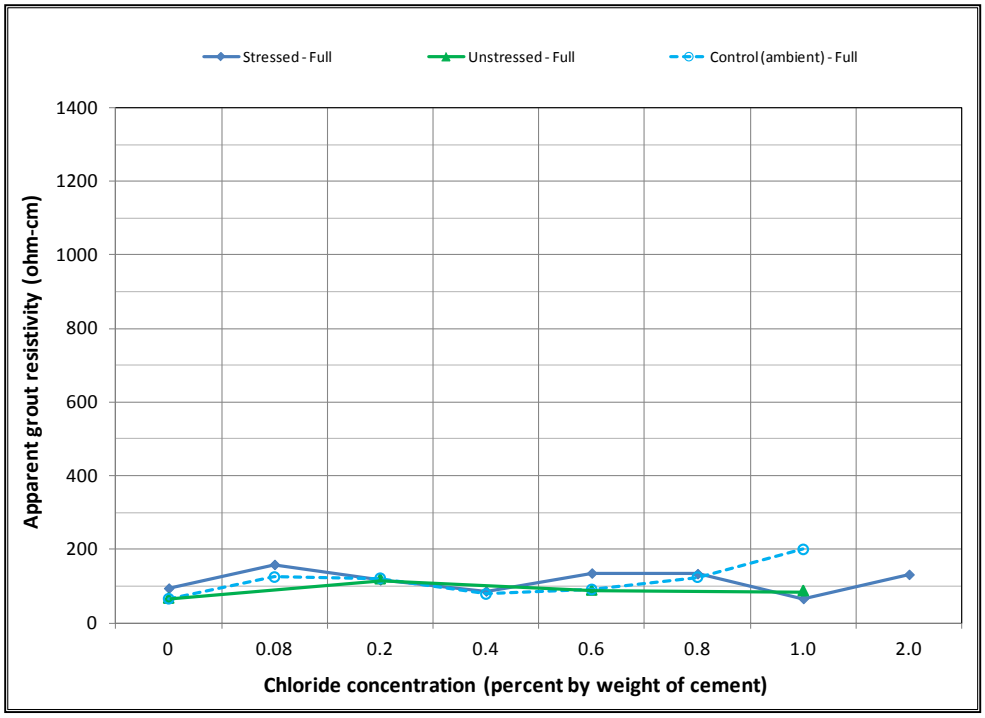

Figure 173. Graph. Mean apparent grout resistivity of fully grouted single-strand specimens in ambient condition.

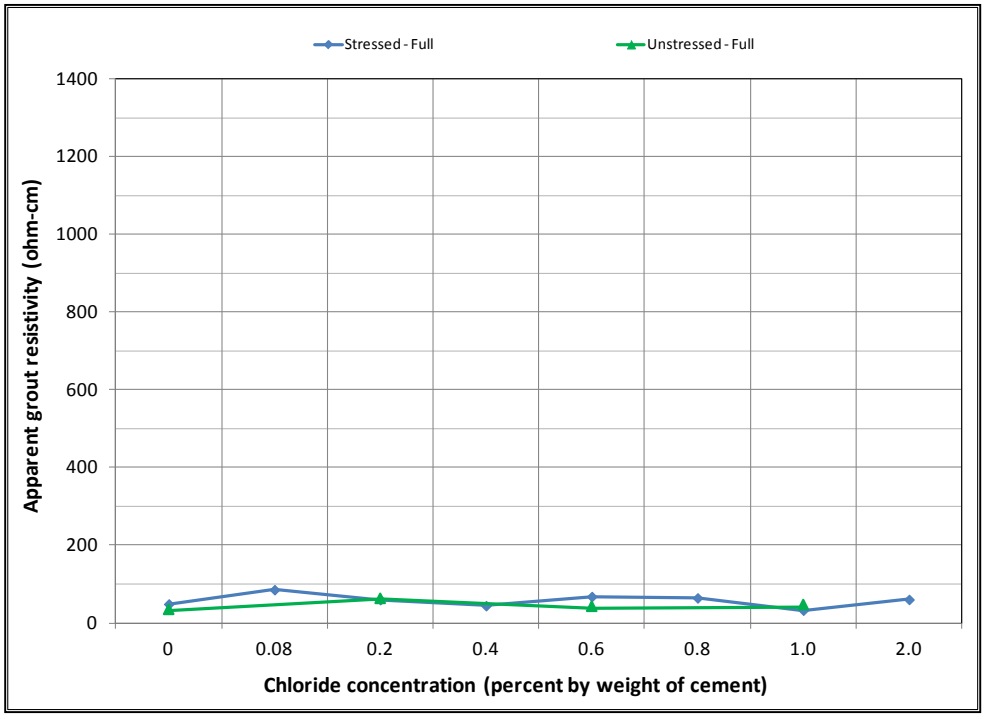

Figure 174. Graph. Mean apparent grout resistivity of fully grouted single-strand specimens in H & H condition.

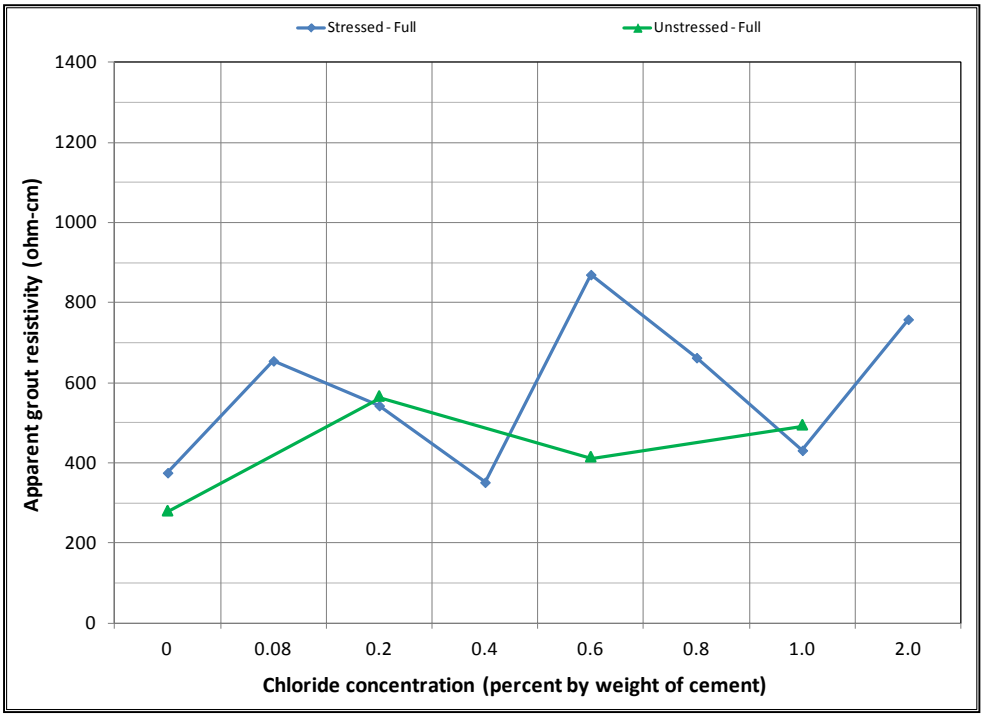

Figure 175. Graph. Mean apparent grout resistivity of fully grouted single-strand specimens in F & D condition.

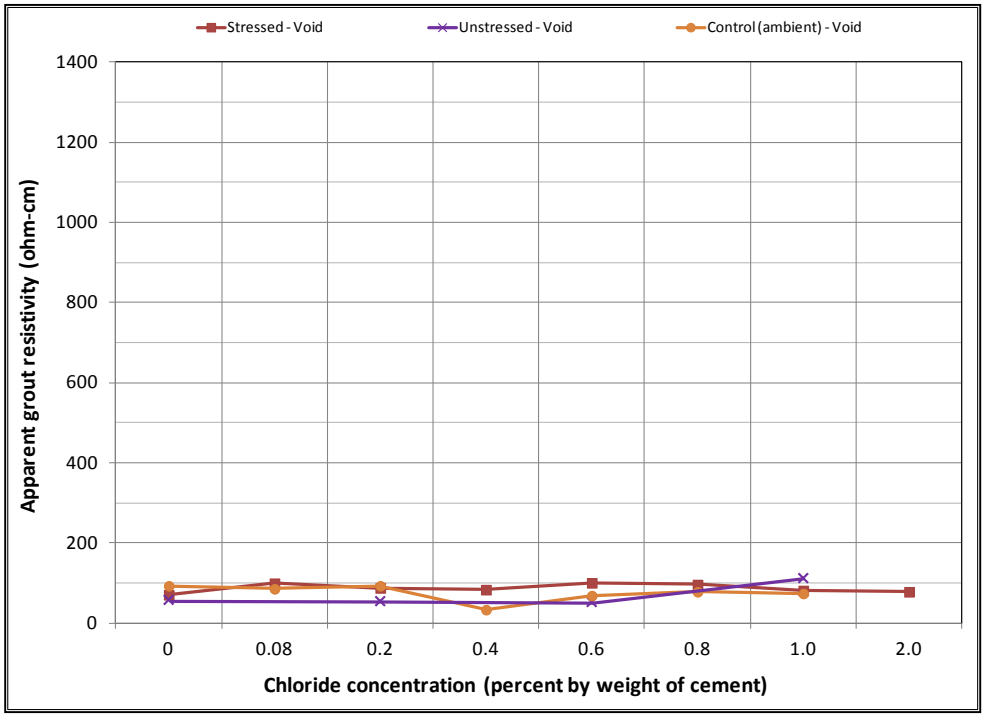

Figure 176. Graph. Mean apparent grout resistivity of voided single-strand specimens in initial ambient condition.

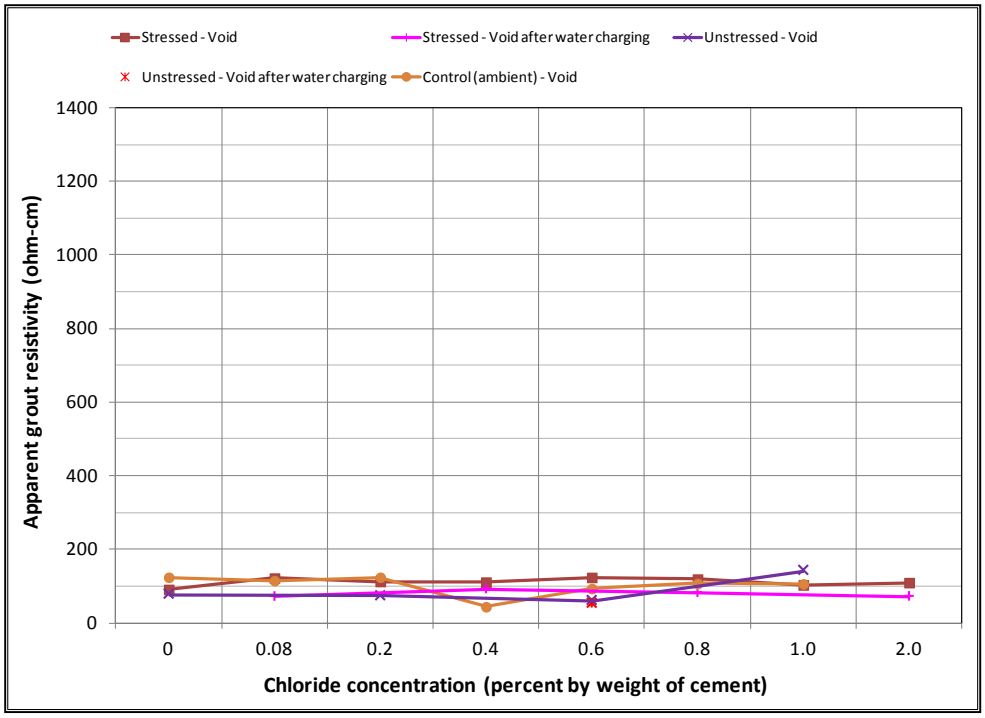

Figure 177. Graph. Mean apparent grout resistivity of voided single-strand specimens in ambient condition.

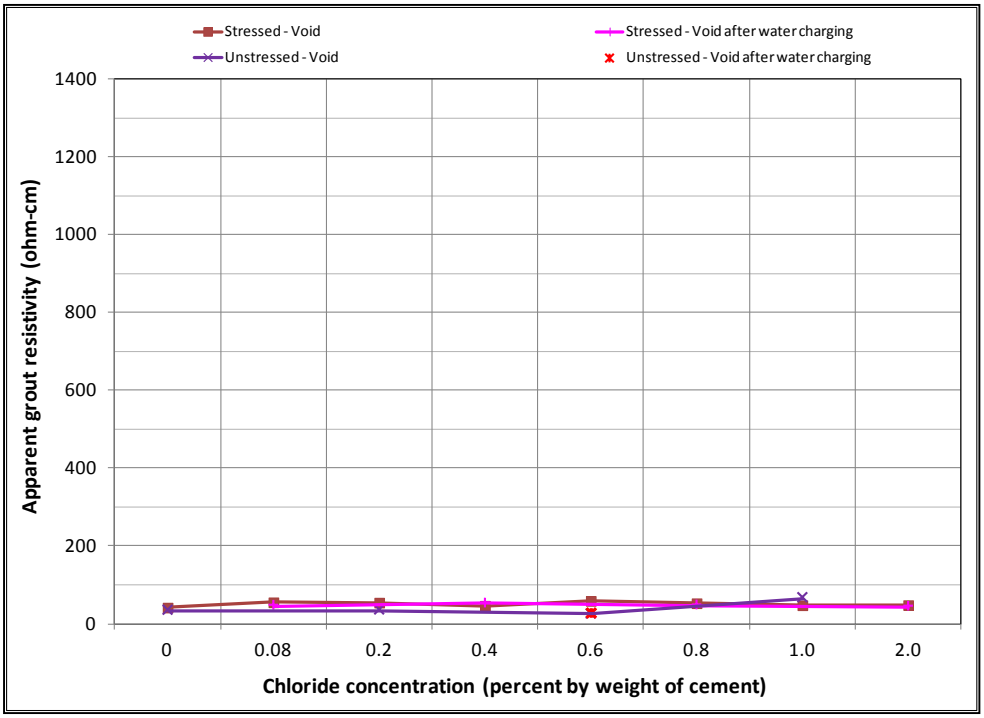

Figure 178. Graph. Mean apparent grout resistivity of voided single-strand specimens in H & H condition.

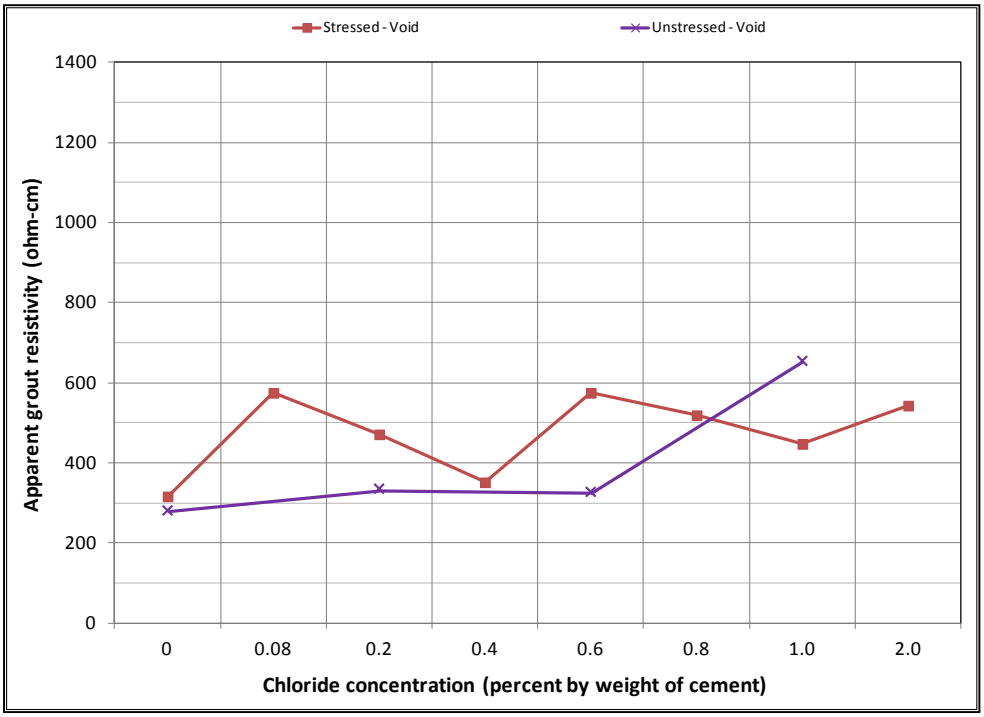

Figure 179**. Graph. Mean apparent grout resistivity of voided single-strand specimens in F & D condition.**

Task 2.3: Grout Resistance of Multi-Strand Specimens

Figure 180 and figure 181 summarize mean grout resistances of multi-strand specimens in different exposure conditions measured with upper pair (P1 and P2) and lower pair (P3 and P4) of resistance probes, respectively. Figure 182 shows overall mean grout resistances. As discussed in the apparent grout resistivity section, the F & D cycles yielded the highest grout resistance, and the H & H cycles yielded the lowest. The grout resistance's dependency on temperature should be partially responsible for increased macro-cell corrosion current density during the H & H cycles and suppressed macro-cell corrosion current density during the F & D cycles. The lower grout section associated with the P3 and P4 probes had much lower resistance than the upper section with P1 and P2 probes.

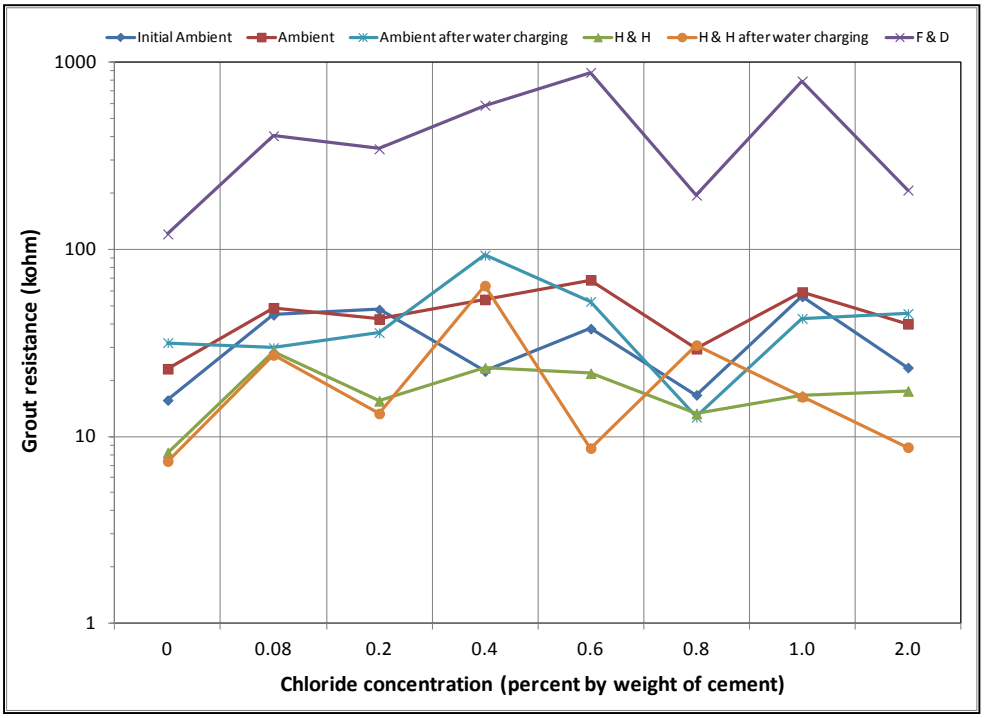

Figure 180. Graph. Mean grout resistances between P1 and P2 of multi-strand specimens.

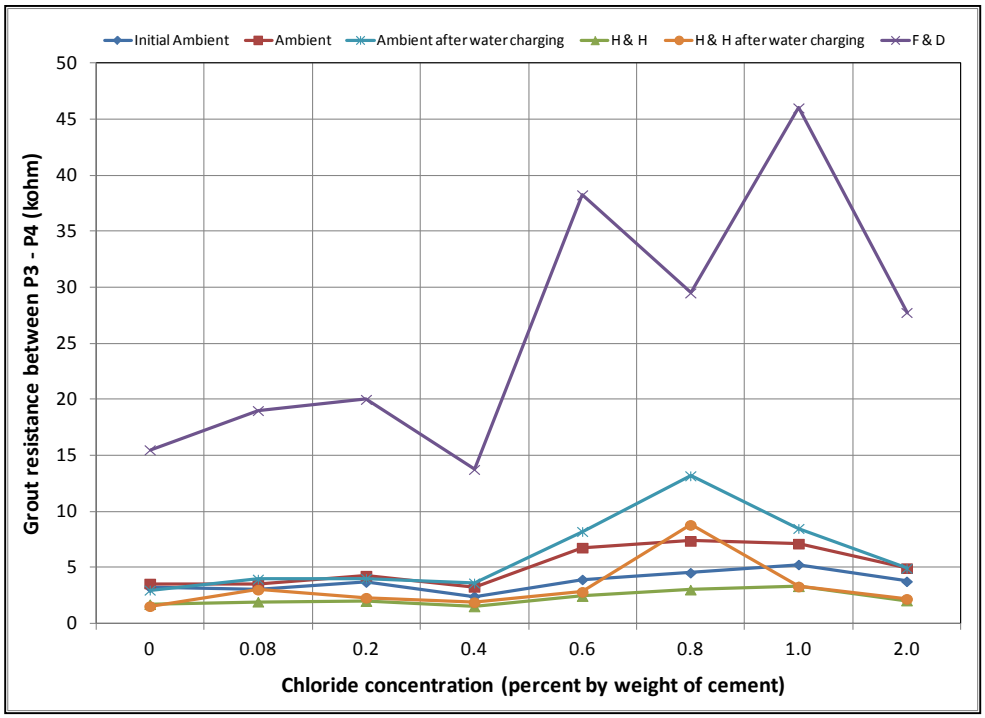

Figure 181. Graph. Mean grout resistances between P3 and P4 of multi-strand specimens.

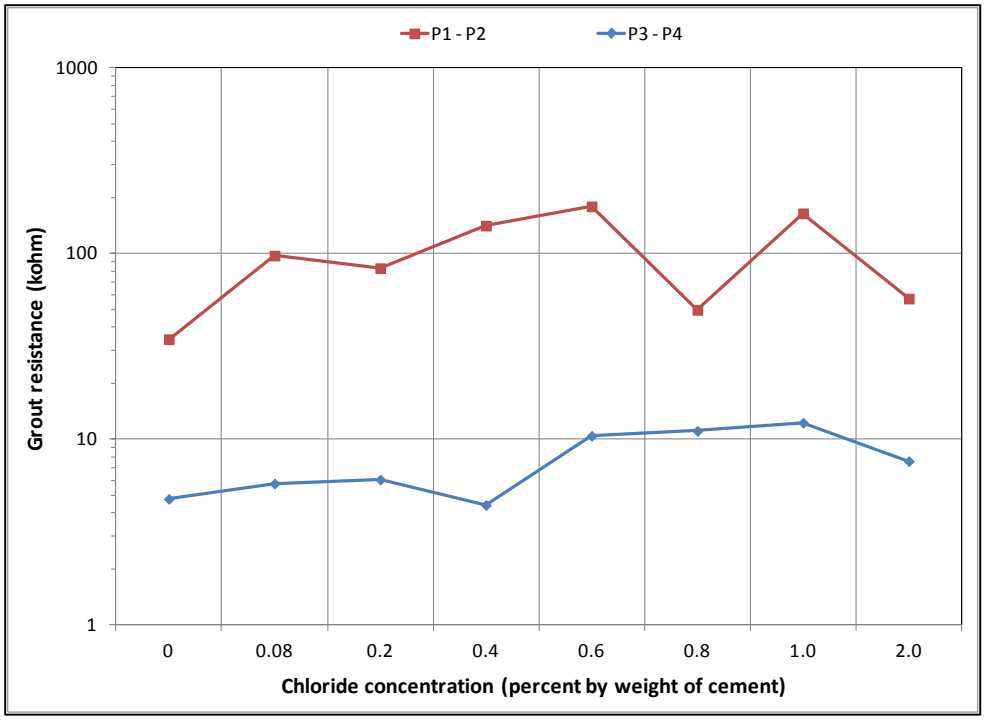

Figure 182. Graph. Overall mean grout resistances of multi-strand specimens.

CHARACTERIZATION OF CORROSION MORPHOLOGIES

Task 2.2: Single-Strand Specimens

Table 9 summarizes the number of rust spots and the number of pits counted on single-strand specimens. Physical condition of every extracted strand was documented schematically using a condition mapping sheet. Figure 183 through figure 190 show the mapped conditions of single-strand specimens. The red marks on the mapping sheets indicate where rust spots were observed. Length of the marks indicates relative surface area showing sign of corrosion. Figure 191 through figure 198 show as-extracted conditions of voided single-strand specimens. The first rust spot appeared on a stressed 0.4 percent chloride specimen with void (see figure 194). As chloride concentration increased, the number of rust spots increased. Although the 0.4 percent chloride specimen received 0.17 fl oz of distilled water in the void, the added water might not play a role to initiate corrosion. This is because other voided specimens containing a lower chloride concentration (0.08 percent) and a higher chloride concentration (0.6 percent) did not initiate corrosion even though they also received the same volume of distilled water. The fully grouted stressed specimens containing 0.8 and 2.0 percent chloride developed two and five rust spots, respectively. The voided stressed specimens containing the same chloride concentrations also developed the same number of rust spots despite having water in the voids. Measurable pits (≥ 2 mil) started to appear at 0.8 percent chloride concentration. More pits were observed on the strands exposed to higher chloride concentrations and voids. Markedly higher number of pits found in the stressed 2.0 percent chloride specimen with void suggests that a combination of a void, recharged water, and elevated chloride concentration can be detrimental.

Table 9. Summary of corrosion condition observed on single-strand specimens.

Chloride Concentration (Percent by Cement Weight)	Number of Rust Spots*				Number of Pits			
	Stressed-Full	Stressed-Void	Unstressed-Full	Unstressed-Void	Stressed-Full	Stressed-Void	Unstressed-Full	Unstressed-Void
0.00	0	0	0	0	0	0	0	0
0.08	0	**0**			0	0		
0.20	0	0	0	0	0	0	0	0
0.40	0	**1**			0	0		
0.60	1	2	1	**0**	0	0	0	0
0.80	2	**2**			0	0		
1.00	5	4	4	5	0	34	0	26
2.00	5	**5**			35	102		

*Size of individual rust spots varied.

Note: Bolded text indicates voids that were recharged with 0.17 fl oz of distilled water at day 127. Blank cells indicate no data were relevant to the cell.

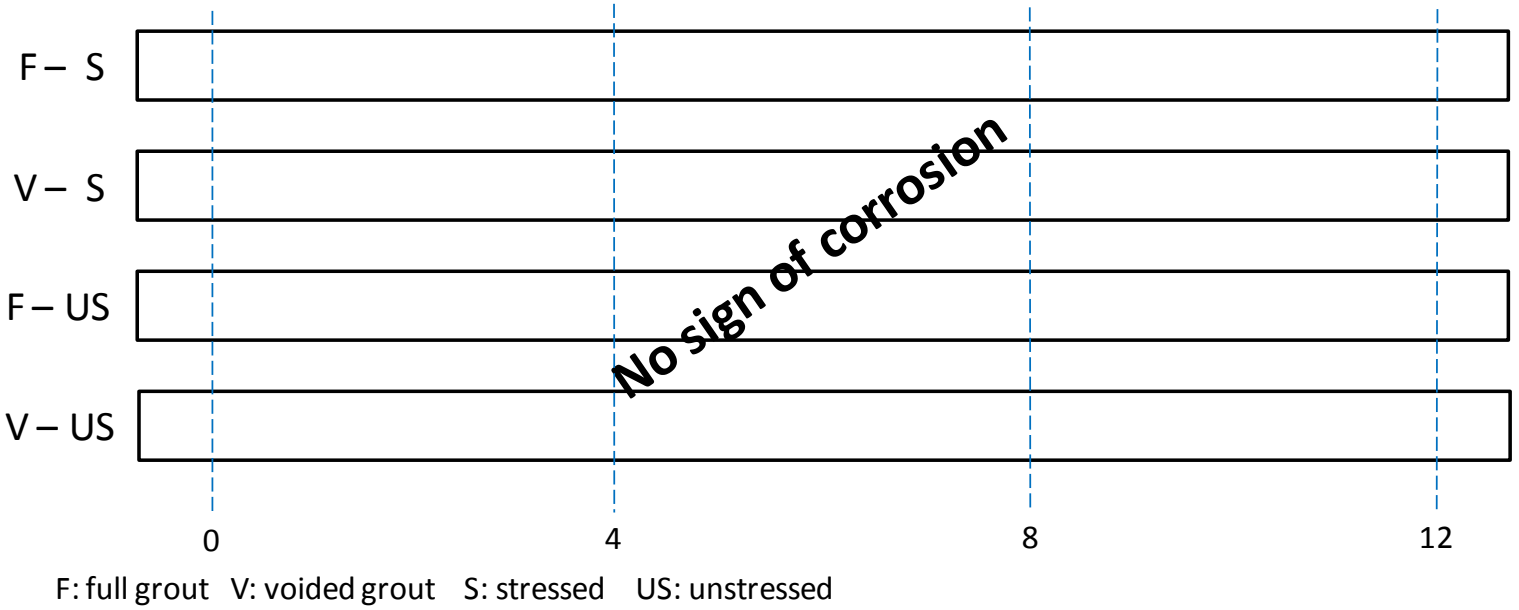

Figure 183. Illustration. Condition mapping of 0 percent chloride single-strand specimens.

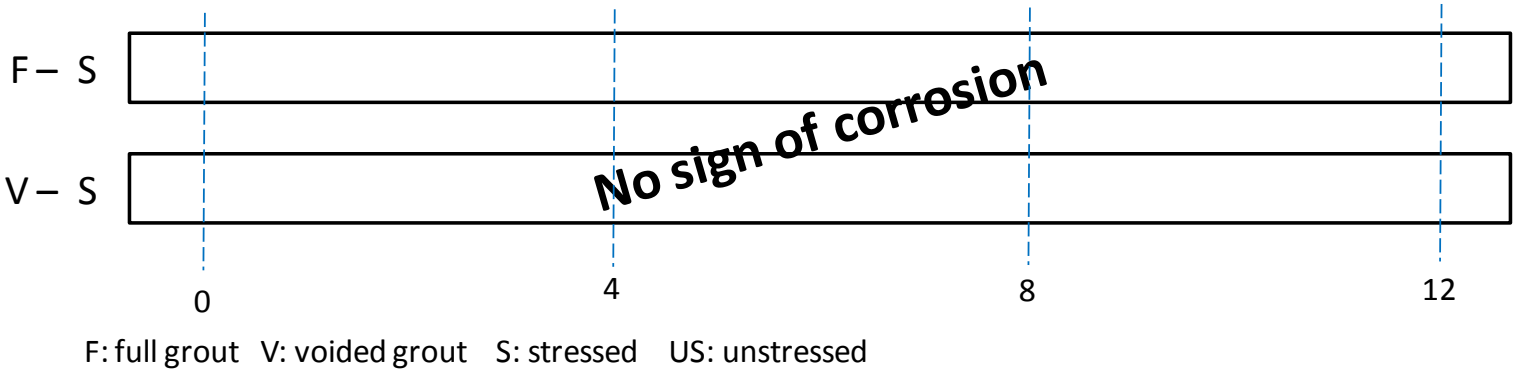

Figure 184. Illustration. Condition mapping of 0.08 percent chloride single-strand specimens.

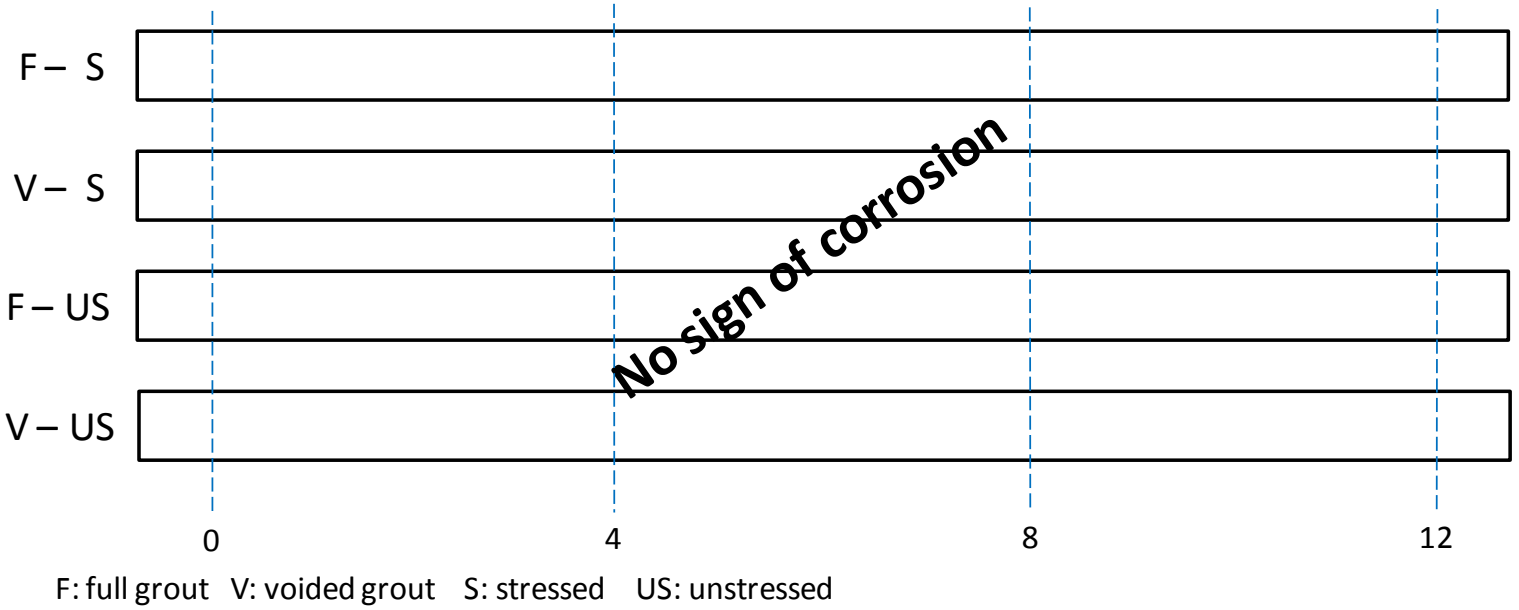

Figure 185. Illustration. Condition mapping of 0.2 percent chloride single-strand specimens.

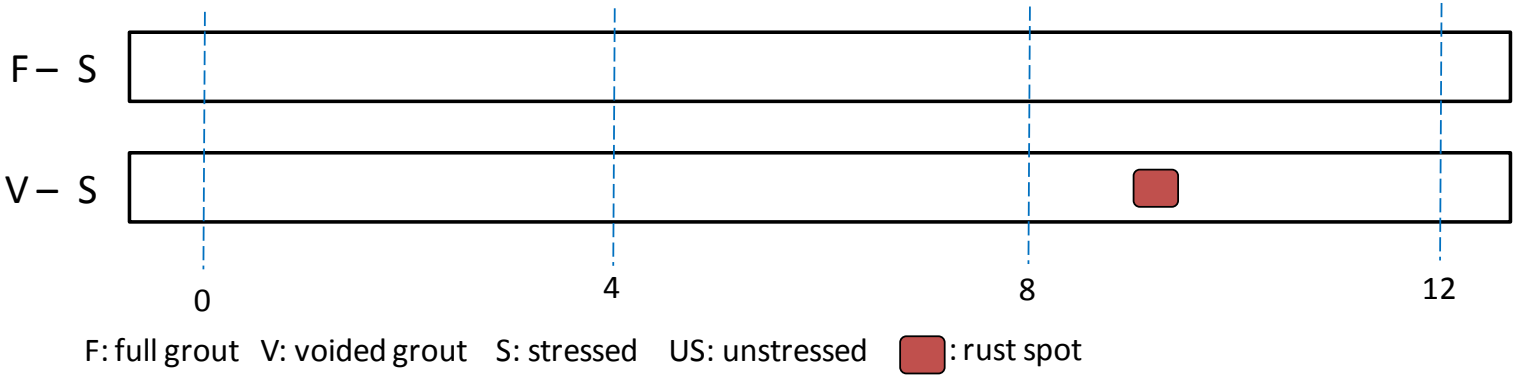

Figure 186. Illustration. Condition mapping of 0.4 percent chloride single-strand specimens.

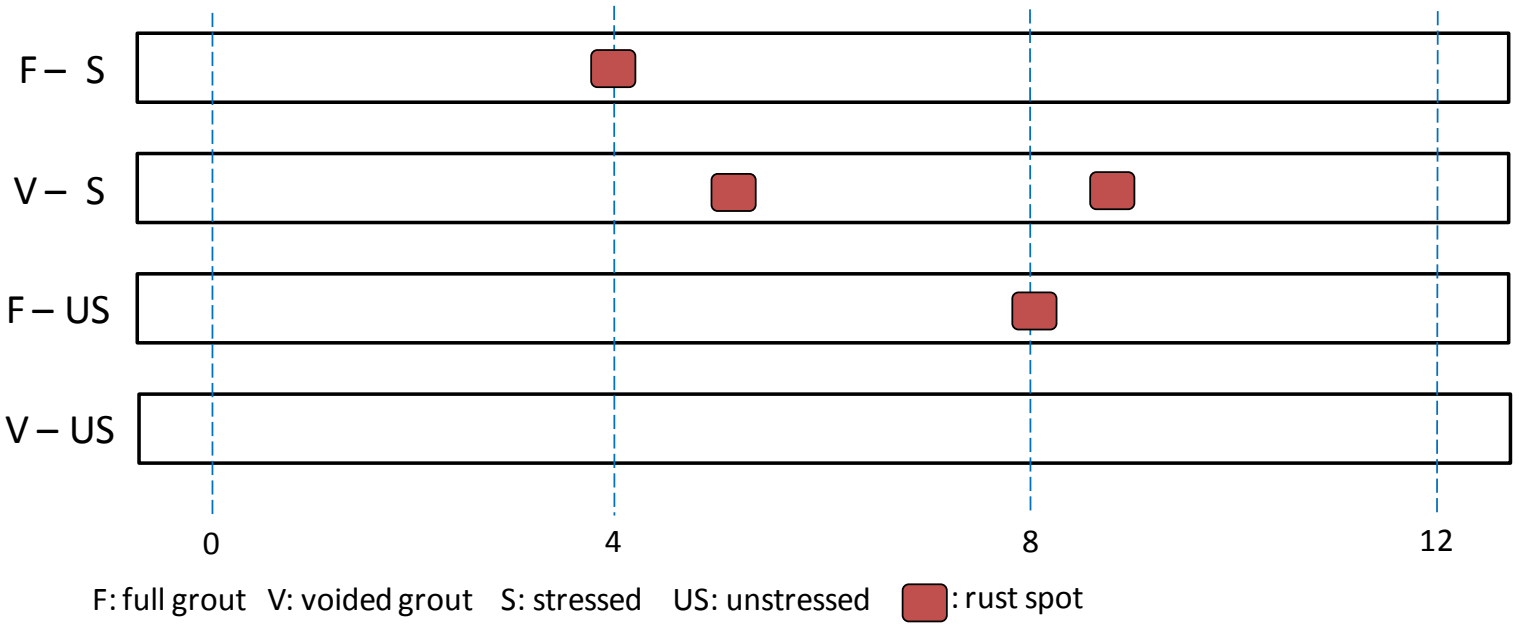

Figure 187. Illustration. Condition mapping of 0.6 percent chloride single-strand specimens.

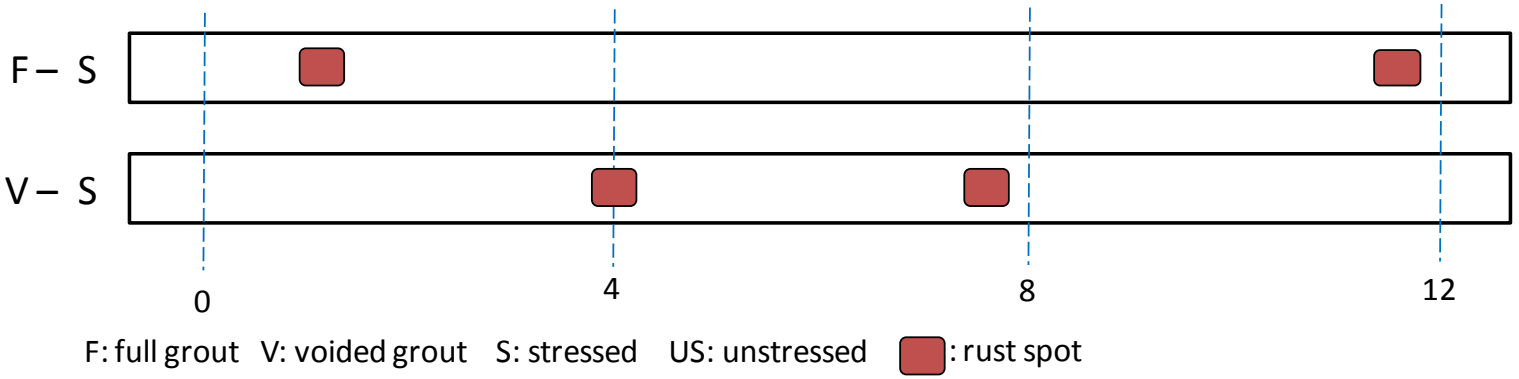

Figure 188. Illustration. Condition mapping of 0.8 percent chloride single-strand specimens.

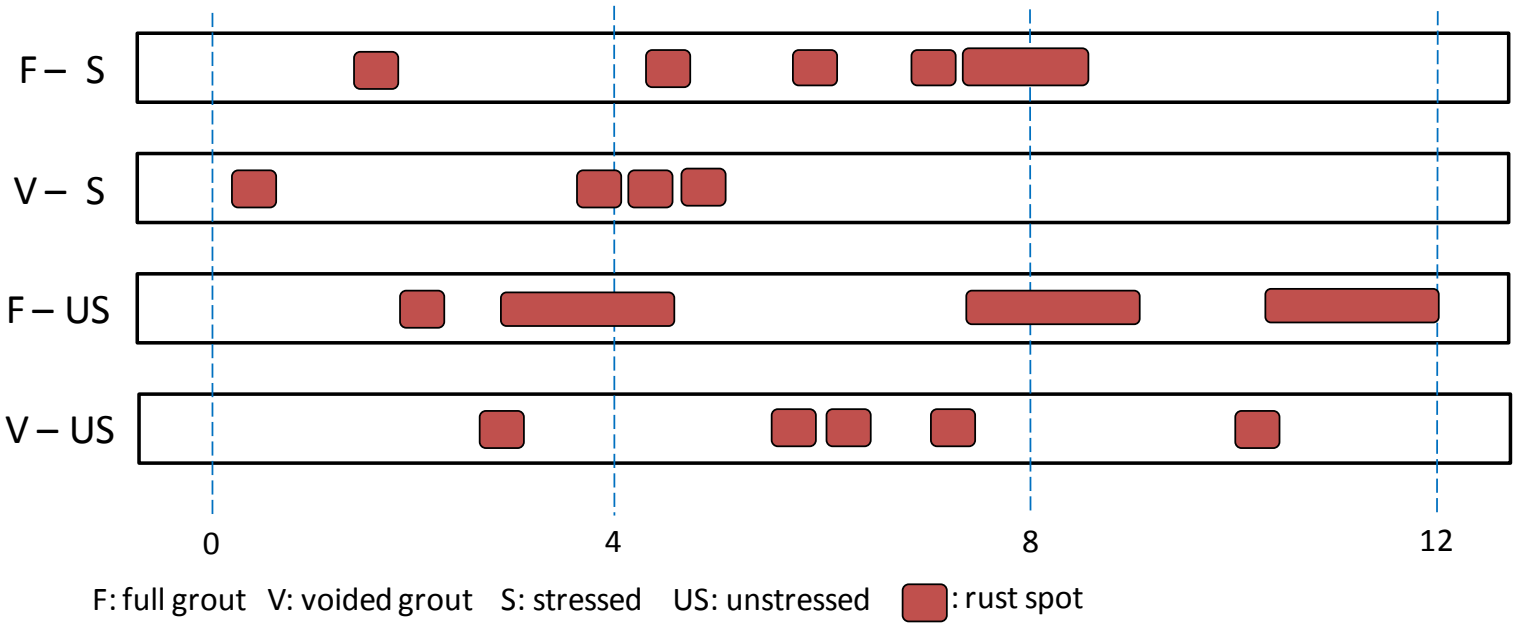

Figure 189. Illustration. Condition mapping of 1.0 percent chloride single-strand specimens.

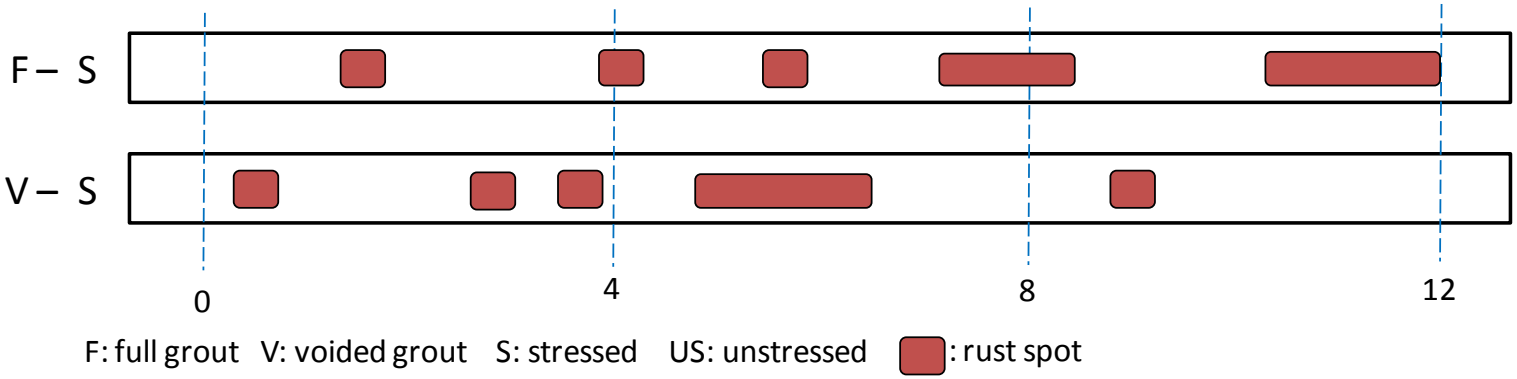

Figure 190**. Illustration. Condition mapping of 2.0 percent chloride single-strand specimens.**

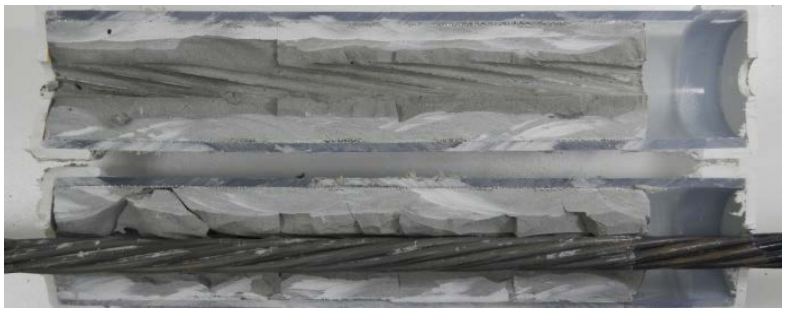

Figure 191. Photo. Stressed single-strand specimen with void and 0 percent chloride.

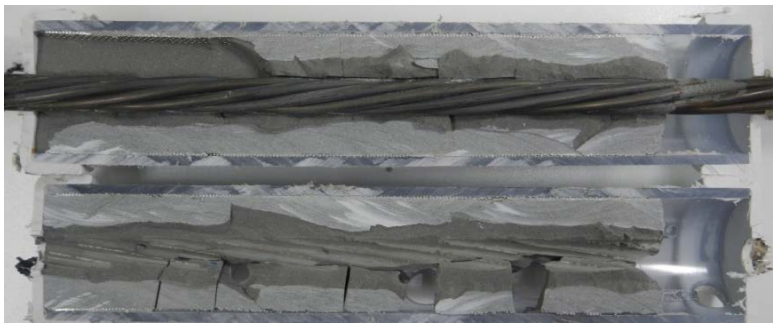

Figure 192. Photo. Stressed single-strand specimen with void and 0.08 percent chloride.

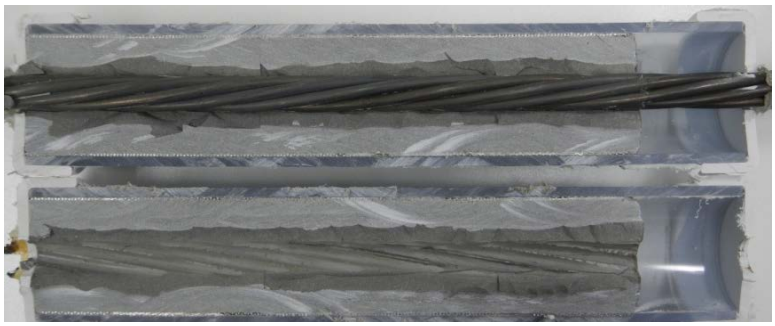

Figure 193. Photo. Stressed single-strand specimen with void and 0.2 percent chloride.

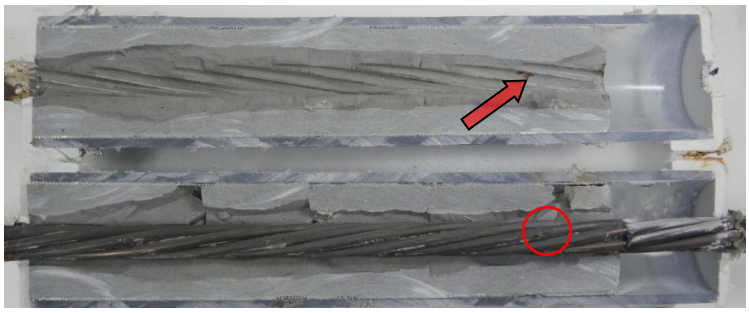

Figure 194. Photo. Stressed single-strand specimen with void and 0.4 percent chloride.

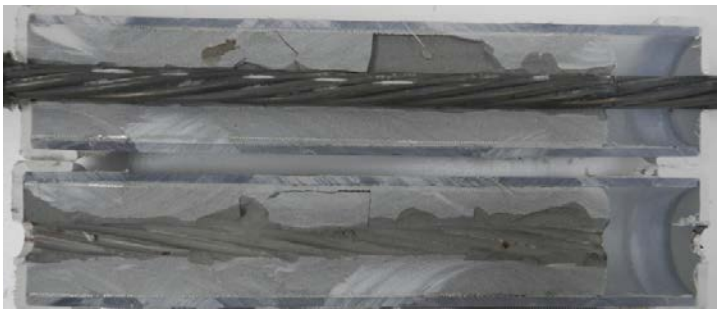

Figure 195. Photo. Stressed single-strand specimen with void and 0.6 percent chloride.

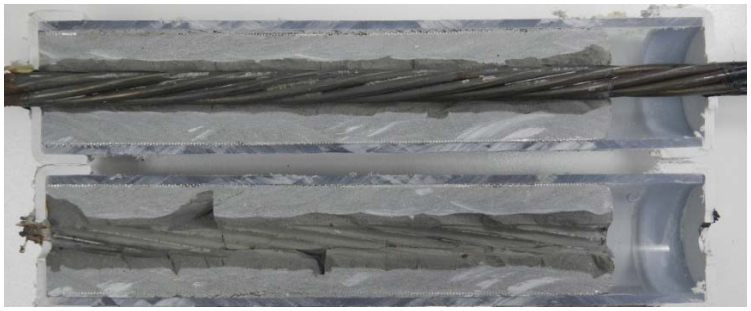

Figure 196. Photo. Stressed single-strand specimen with void and 0.8 percent chloride.

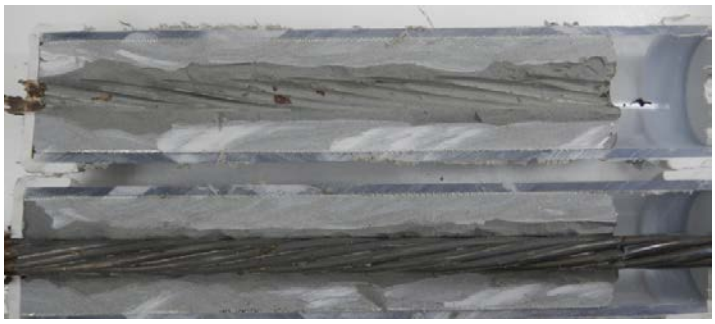

Figure 197. Photo. Stressed single-strand specimen with void and 1.0 percent chloride.

Figure 198. Photo. Stressed single-strand specimen with void and 2.0 percent chloride.

Task 2.3: Multi-Strand Specimens

After grout caps were removed from the lower anchor plates, the anchor plates and electrical connections inside the caps were inspected for any signs of corrosion that might have affected corrosion measurements. Figure 199 and figure 200 show exterior and interior conditions of a

lower anchor plate. Other than yellowish spray-on corrosion inhibitor film and residue of expansive foam that was used as filler, everything on the exterior face appeared clean without corrosion. Similarly, no corrosion was found on the interior face of the anchor plate. The other anchor plates showed similar conditions.

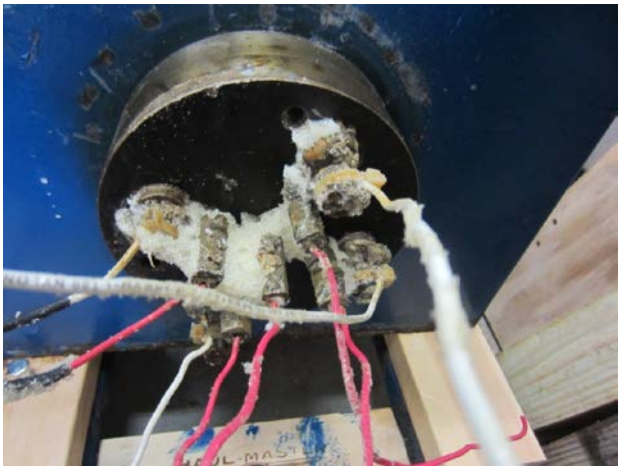

Figure 199. Photo. Exposed exterior side of lower anchor plate.

Figure 200. Photo. Exposed interior side of lower anchor plate.

Figure 201 through figure 208 show condition mapping results of multi-strand specimens in a 12-inch grid system. Individual marks indicate where rust spots were observed. They do not represent the extent of corrosion. Rather, they show locations of a rust spot or a group of rust spots. On the stressed strands, rust spots started to appear at 0 percent chloride concentration and increased with chloride concentration. On the unstressed strands, rust spots first appeared at 0.4 percent chloride, and more appeared proportionally at higher chloride concentrations. In theory, the unstressed strands served as a macro-cathode; therefore, they were not supposed to corrode. One possibility is that polarized potentials of unstressed strands might place the unstressed strands outside the corrosion immune zone of a Pourbaix diagram if sufficient amount of chloride ions exists, in this case, 0.4 percent by weight of cement. The Pourbaix diagram classifies various thermodynamic states for corrosion as a function of potential and pH.

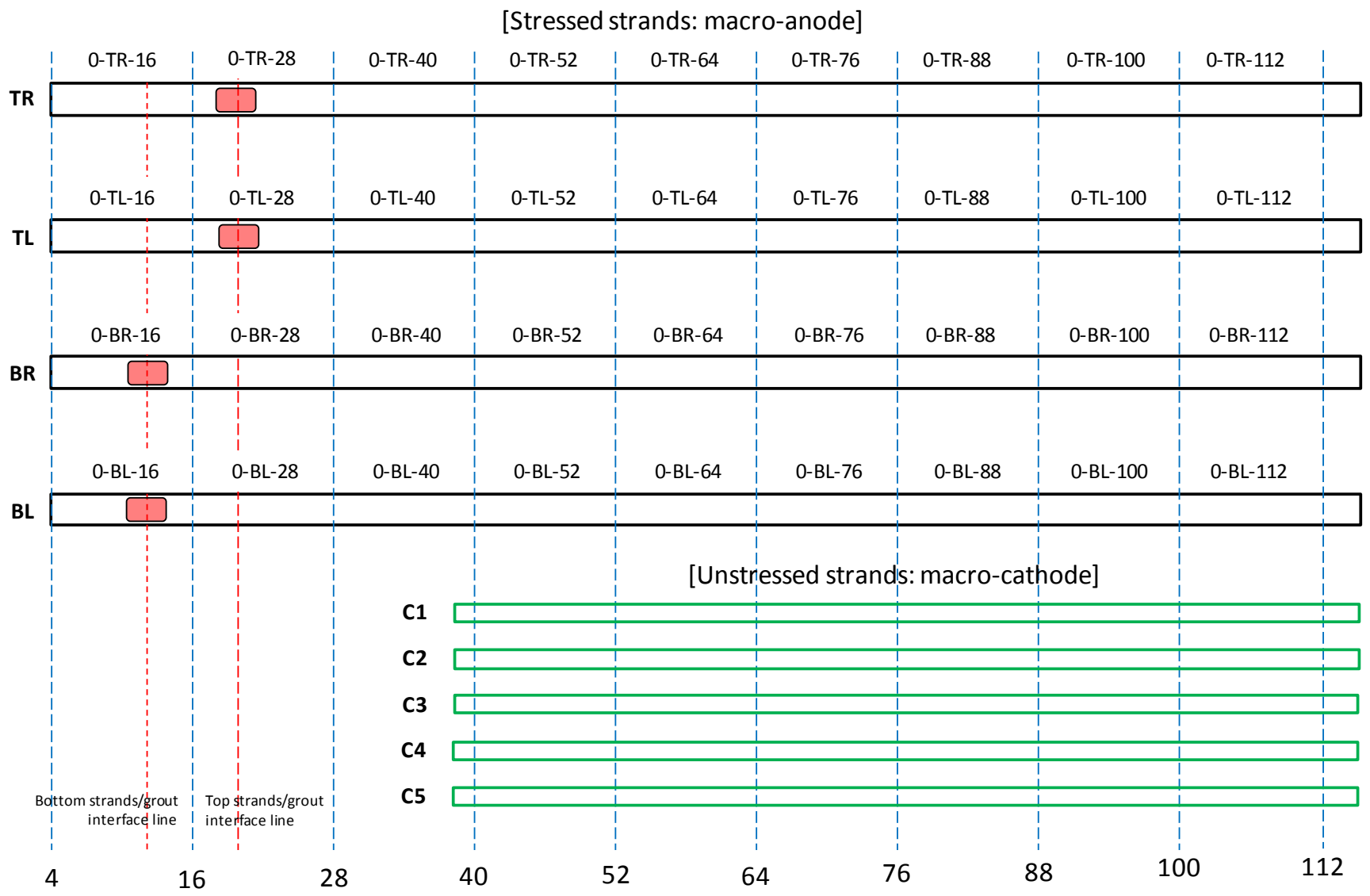

Figure 201. Illustration. Condition mapping of 0 percent chloride multi-strand specimen.

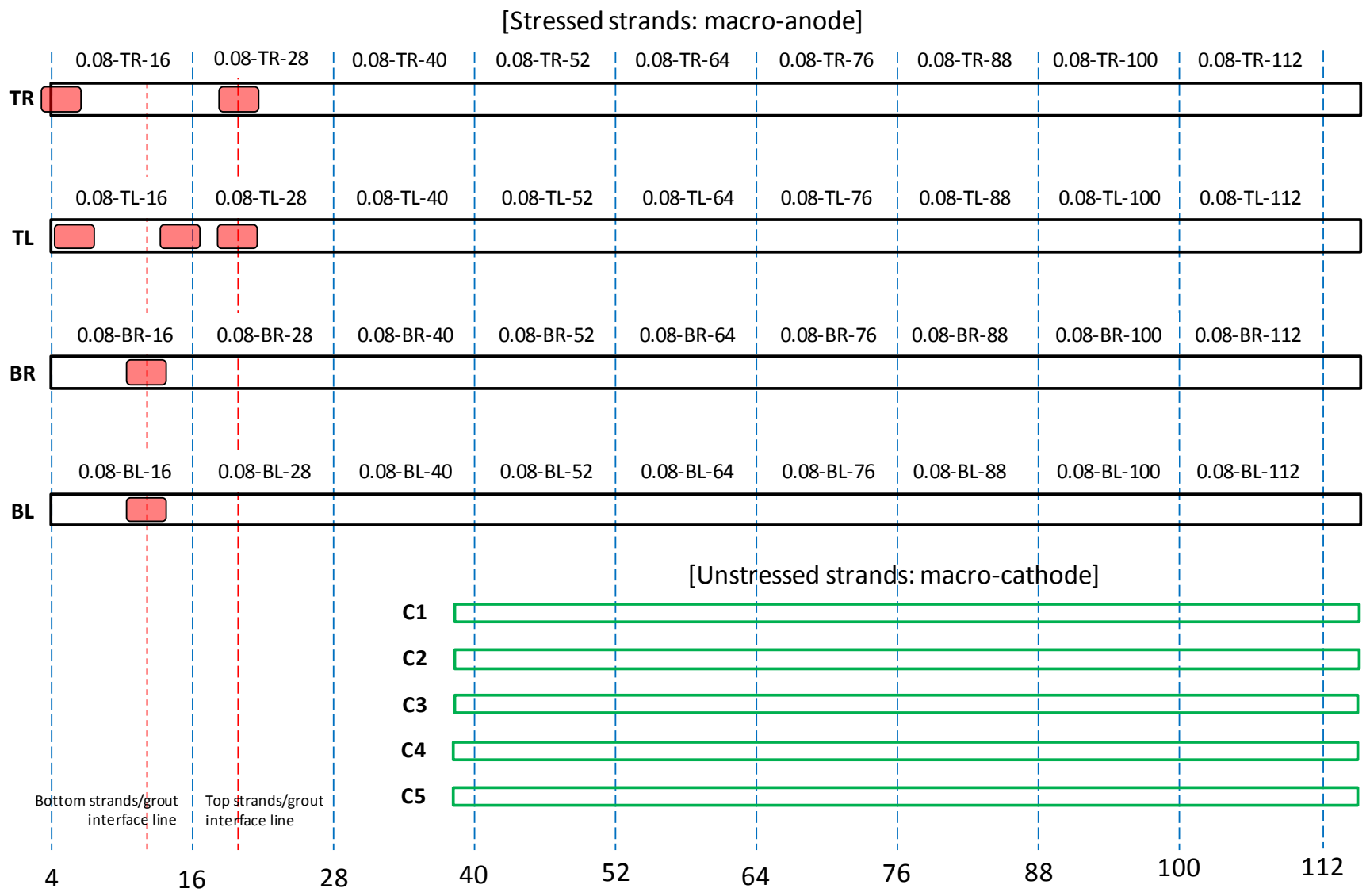

Figure 202. Illustration. Condition mapping of 0.08 percent chloride multi-strand specimen.

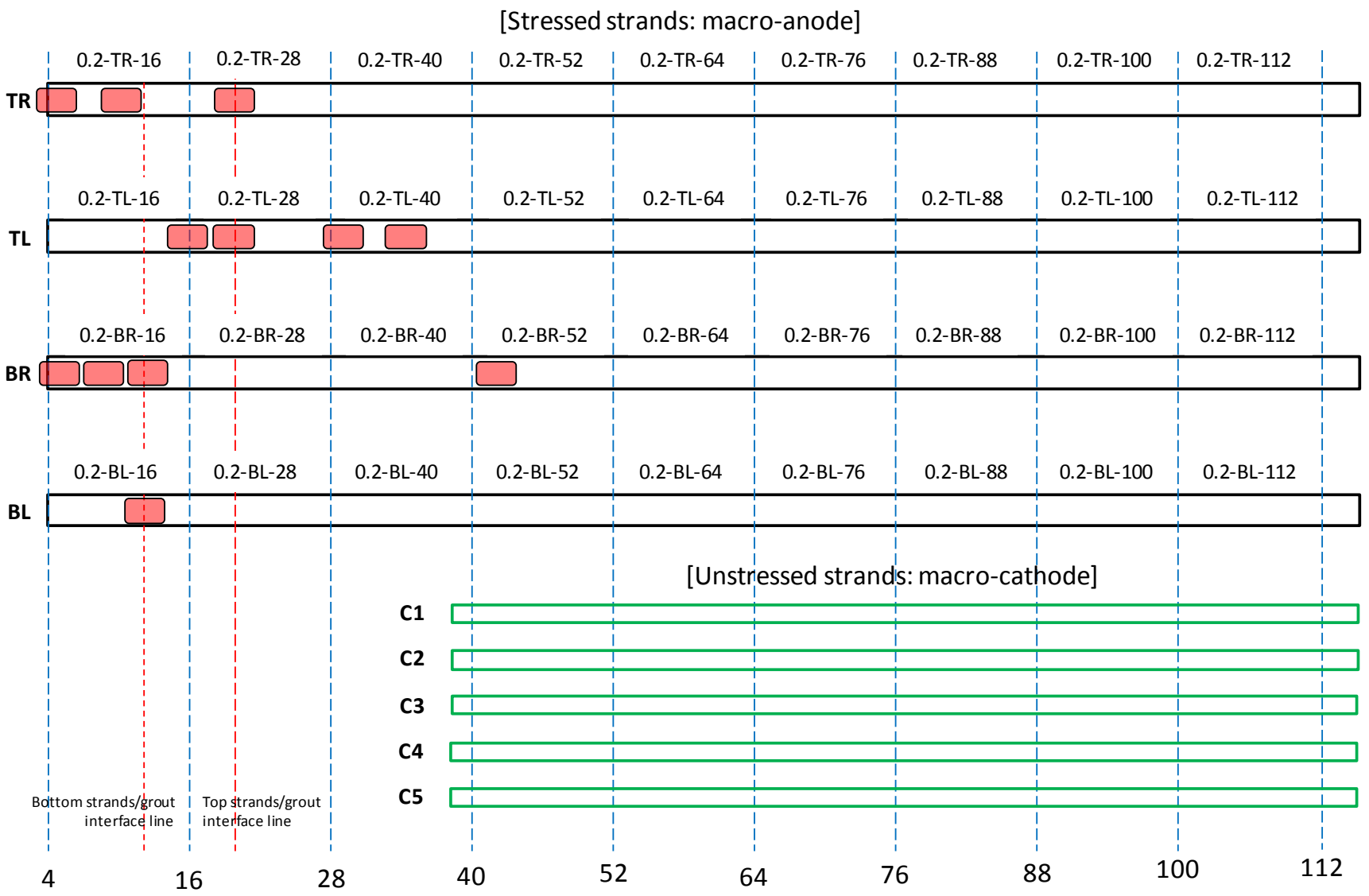

Figure 203. Illustration. Condition mapping of 0.2 percent chloride multi-strand specimen.

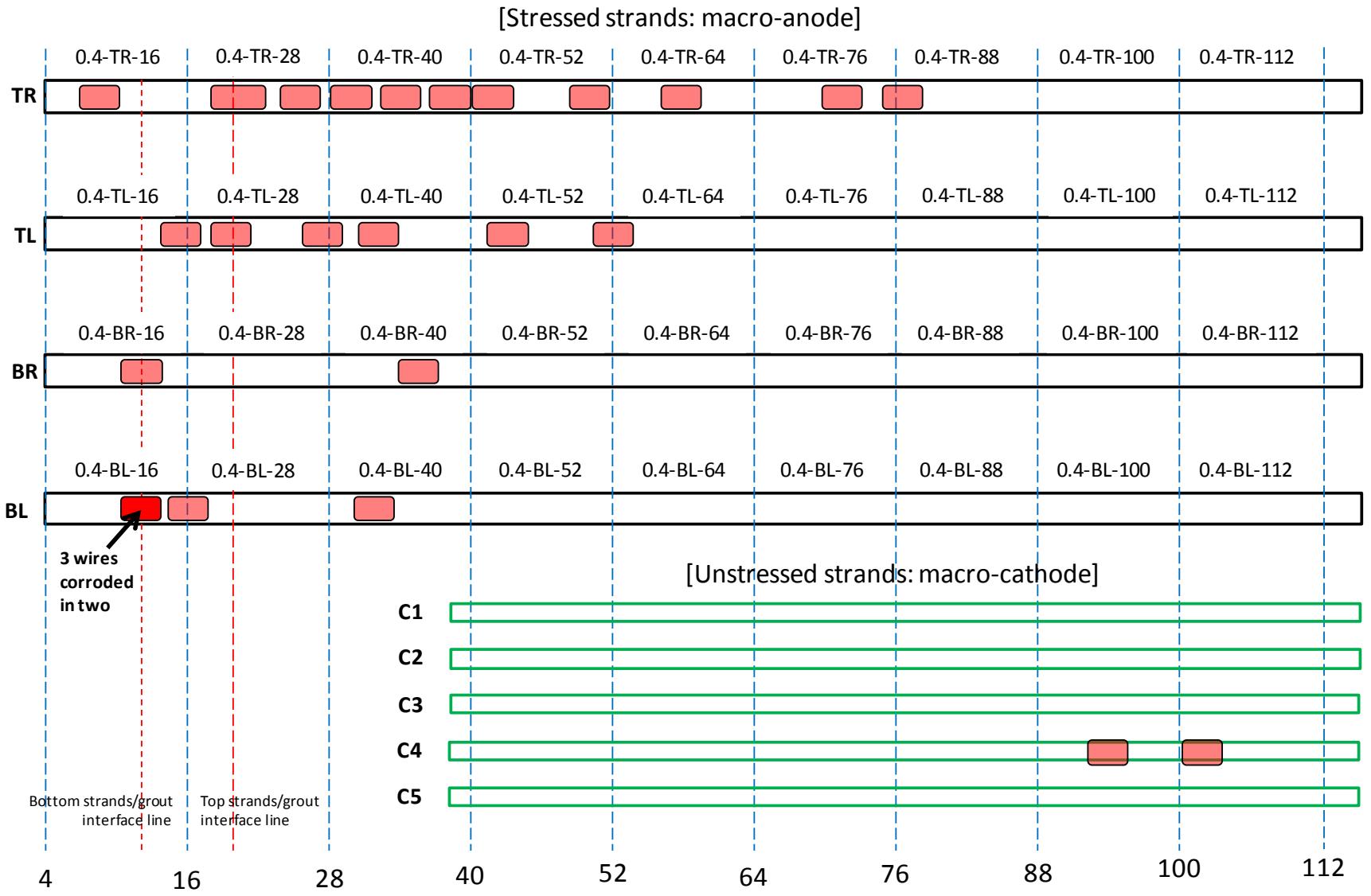

Figure 204. Illustration. Condition mapping of 0.4 percent chloride multi-strand specimen.

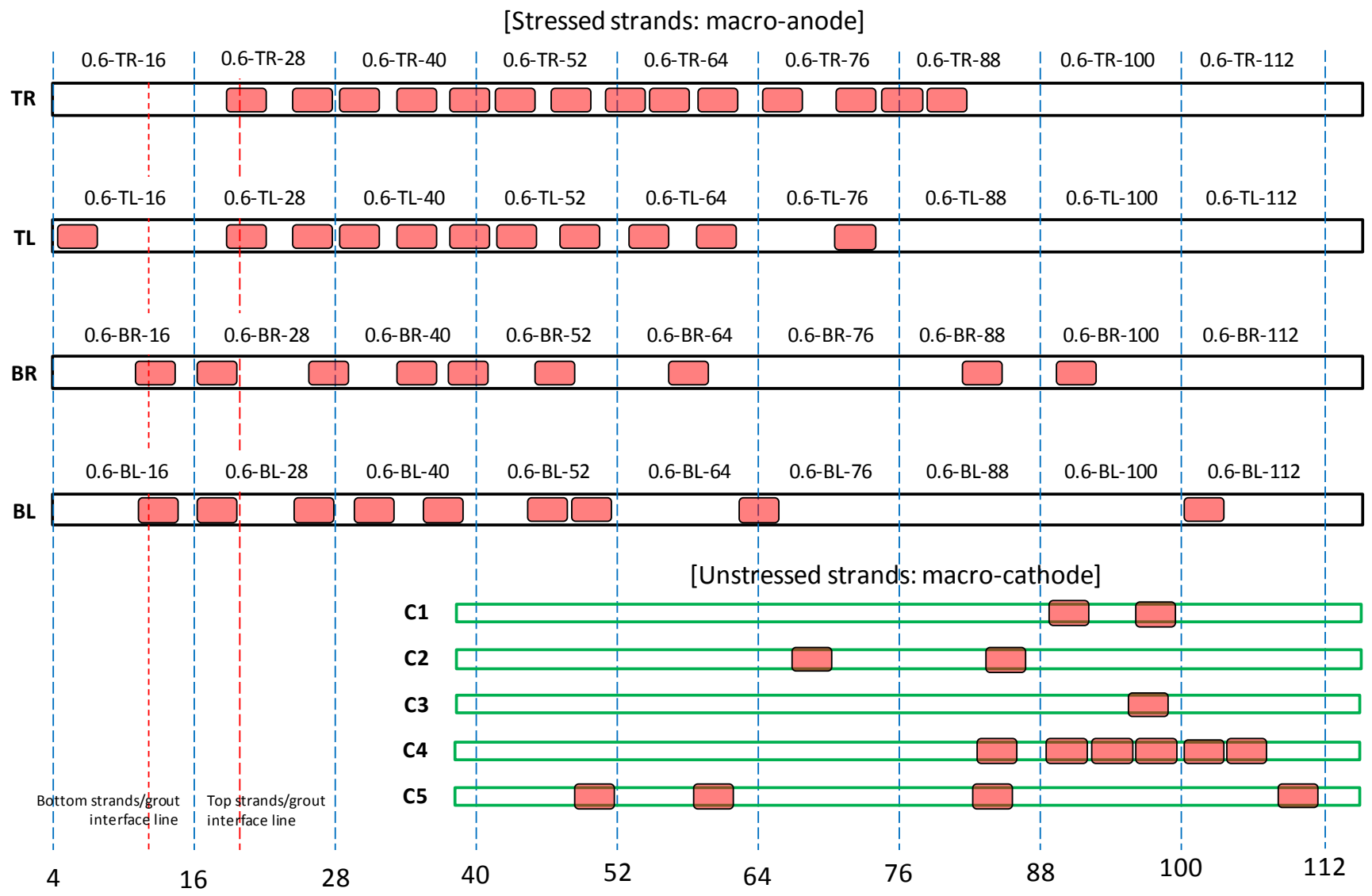

Figure 205. Illustration. Condition mapping of 0.6 percent chloride multi-strand specimen.

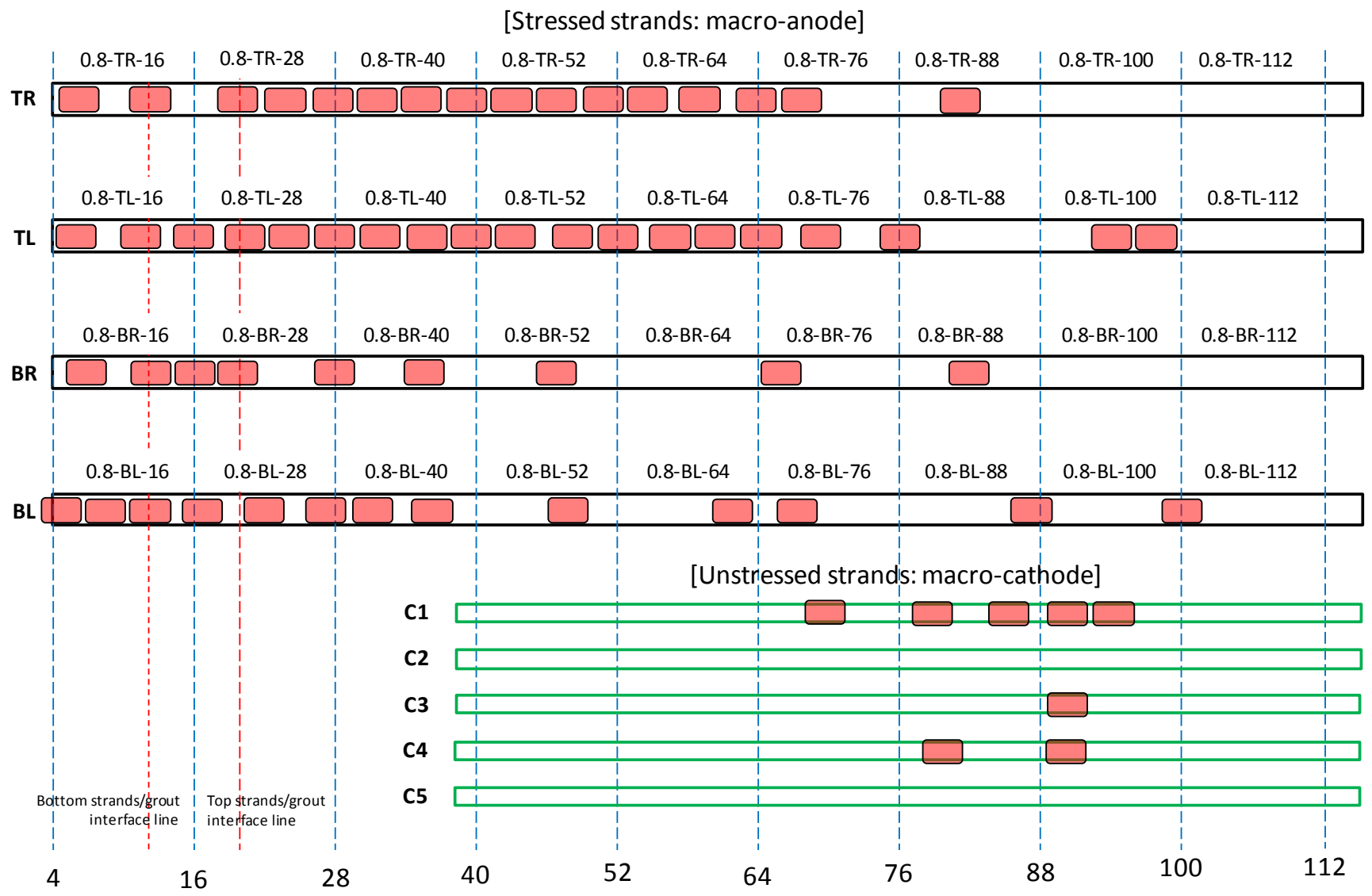

Figure 206. Illustration. Condition mapping of 0.8 percent chloride multi-strand specimen.

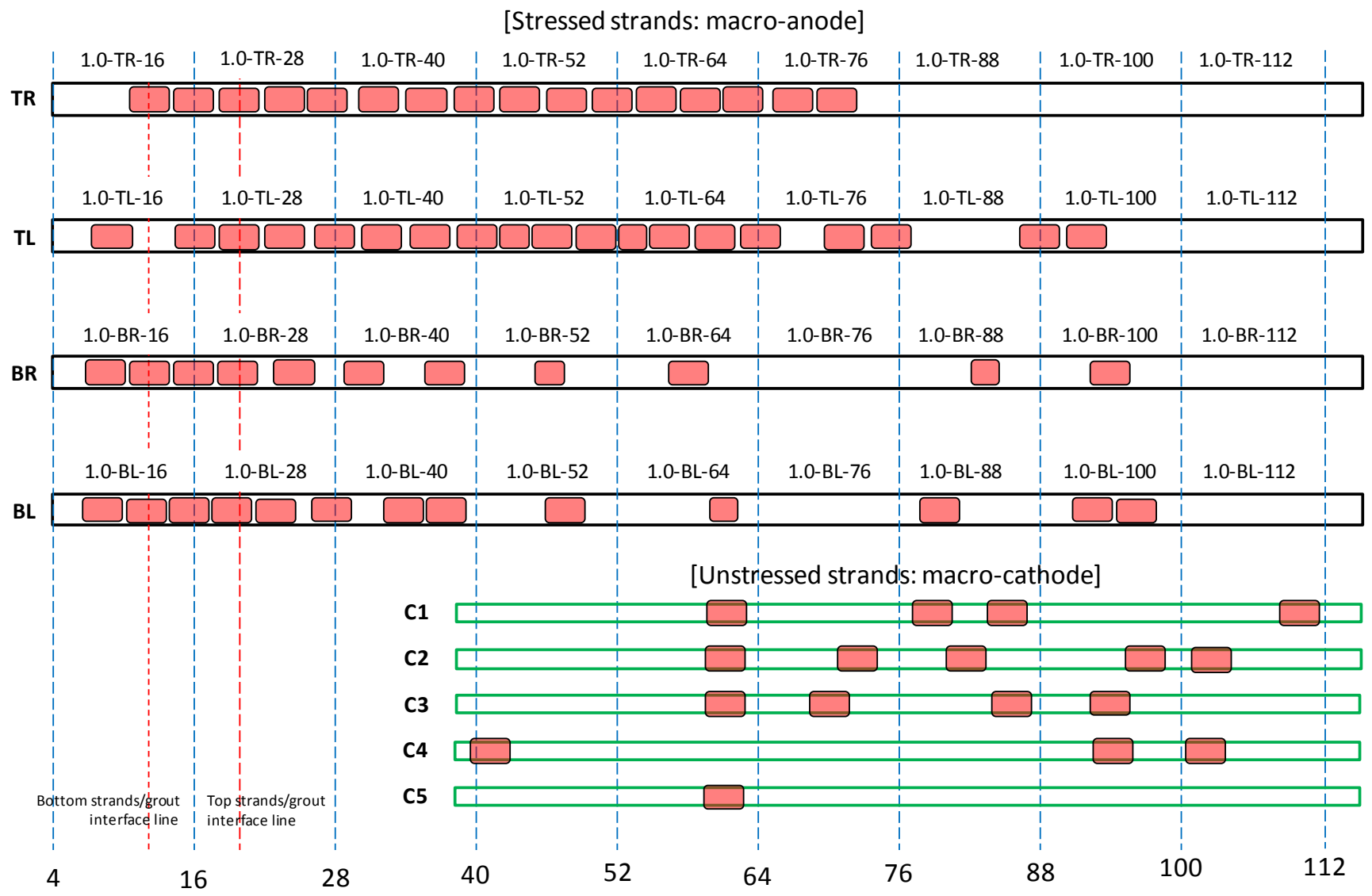

Figure 207. Illustration. Condition mapping of 1.0 percent chloride multi-strand specimen.

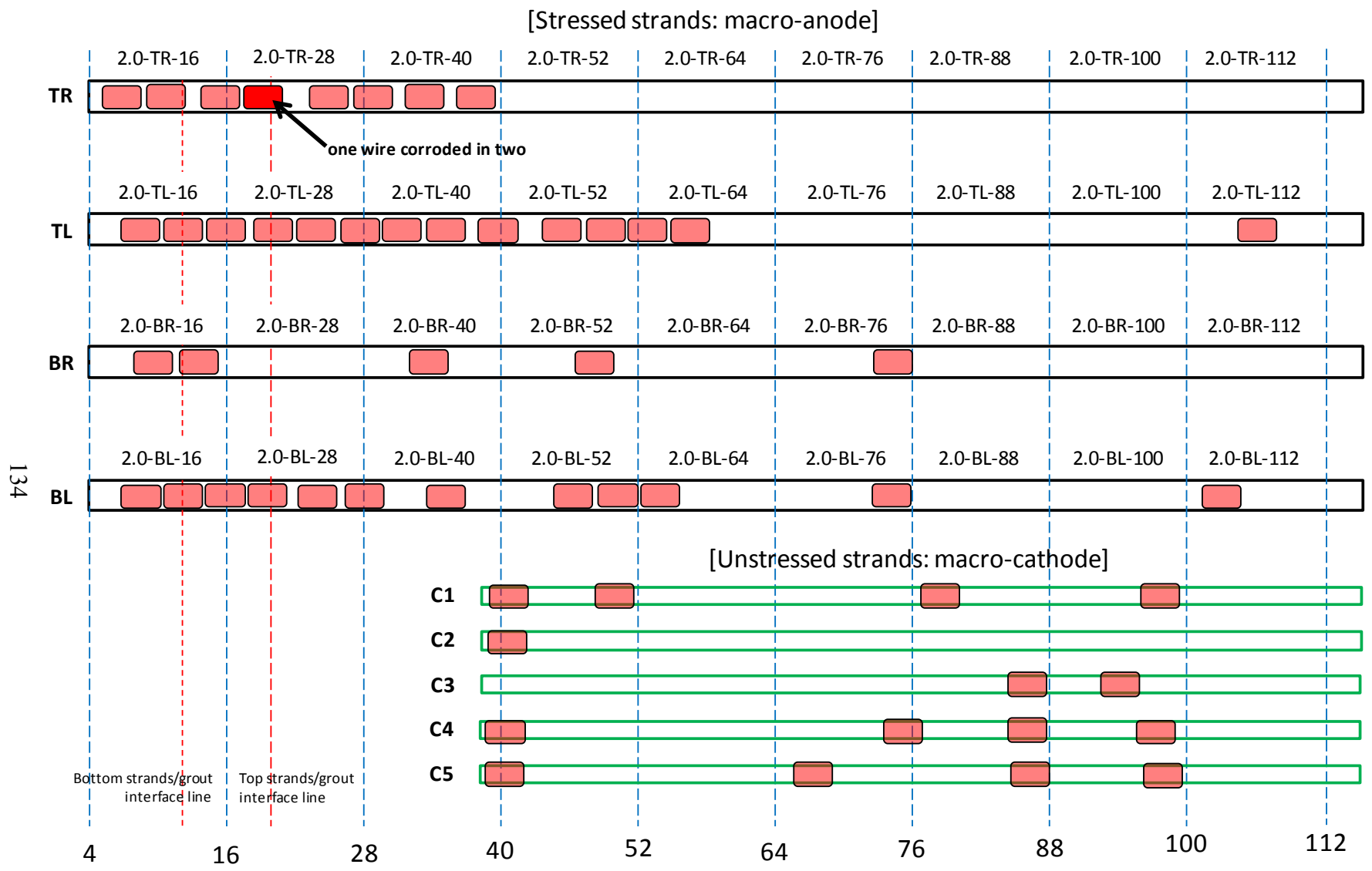

Figure 208**. Illustration. Condition mapping of 2.0 percent chloride multi-strand specimen.**

Figure 209 shows an intact strand near the void/grout interface of 0.08 percent chloride specimen, and figure 210 shows the as-extracted condition of four interface segments of the same specimen.

Figure 209. Photo. Exposed strand at the void/grout interface of 0.08 percent chloride multi-strand specimen.

Figure 210. Photo. As-extracted condition of four stressed strands near the void/grout interface of 0.08 percent chloride multi-strand specimen.

Since the void/grout interface was sloped at a 25-degree angle, the 4-to-16-inch segments of the BL and BR strands and 16-to-28-inch segments of the TL and TR strands were exposed at the interface (see figure 37). The labels included in figure 210 provide relative position of each segment with respect to the distance from the upper anchor plate and the interface. Only minor corrosion can be seen on the interface segments. Figure 211 shows a stressed strand of 0.8 percent chloride specimen showing moderate corrosion at the interface. Figure 212 shows the interface segments of the same specimen, with BL and BR exhibiting minor corrosion and TL and TR exhibiting moderate corrosion.

Figure 211. Photo. Exposed strand at the interface of 0.8 percent chloride multi-strand specimen.

Figure 212. Photo. As-extracted condition of four stressed strands at the void/grout interface of 0.8 percent chloride multi-strand specimen.

The specimens containing 0.08, 0.8, and 1.0 percent chloride showed overall good condition at the interface even after 5.1 fl oz of distilled water was added. Their interface conditions observed during the accelerated corrosion testing are shown in figure 157, figure 161, and figure 162, respectively. The specimens containing 0.2 and 0.6 percent chloride also showed good condition with minor corrosion at the interface. Their interface photographs are shown in figure 158 and figure 160, respectively.

Severe corrosion was observed at the interfaces of three other specimens containing 0, 0.4, and 2.0 percent chloride. Figure 213 shows the void/grout interface of 0 percent chloride specimen upon removal of the PVC duct. The interface was covered with a thick black deposit. Figure 214 and figure 215 show a top section of the interface and its cross section, respectively. The black deposit layer appeared to be porous and contained numerous small black particles. Figure 216 shows two pairs of the stressed strand segments that passed through the void/grout interface.

Figure 217 and figure 218 show close-up views of two interface segments shown in figure 216. Severe corrosion took place despite a chloride-free condition.

Figure 213. Photo. Strands at the void/grout interface of 0 percent chloride multi-strand specimen.

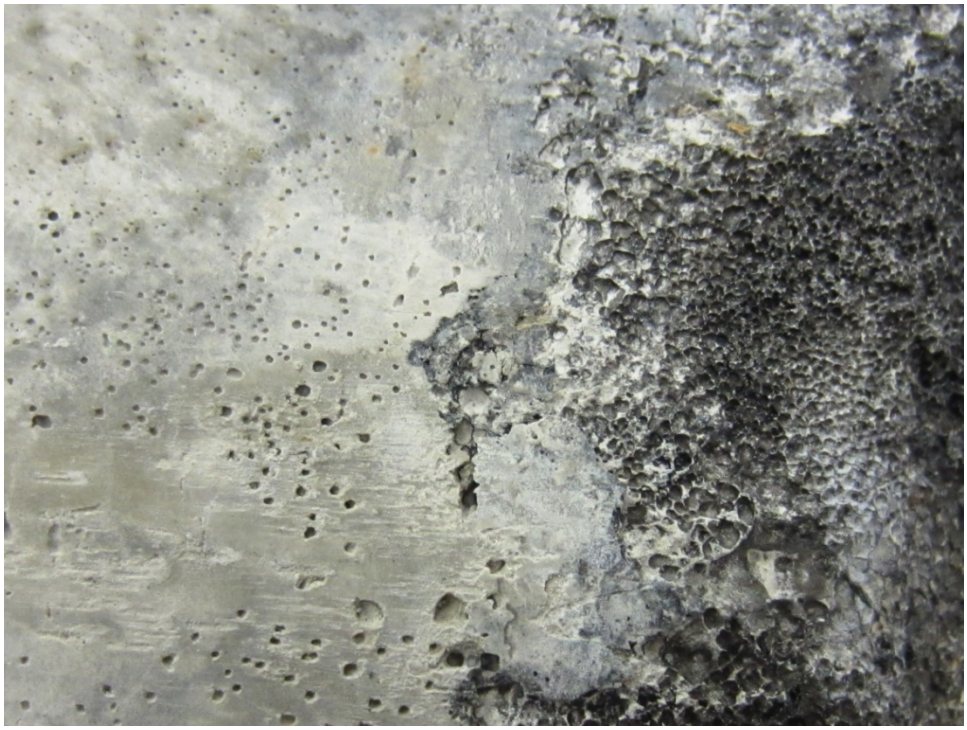

Figure 214. Photo. Close-up plan view of the void/grout interface (top section).

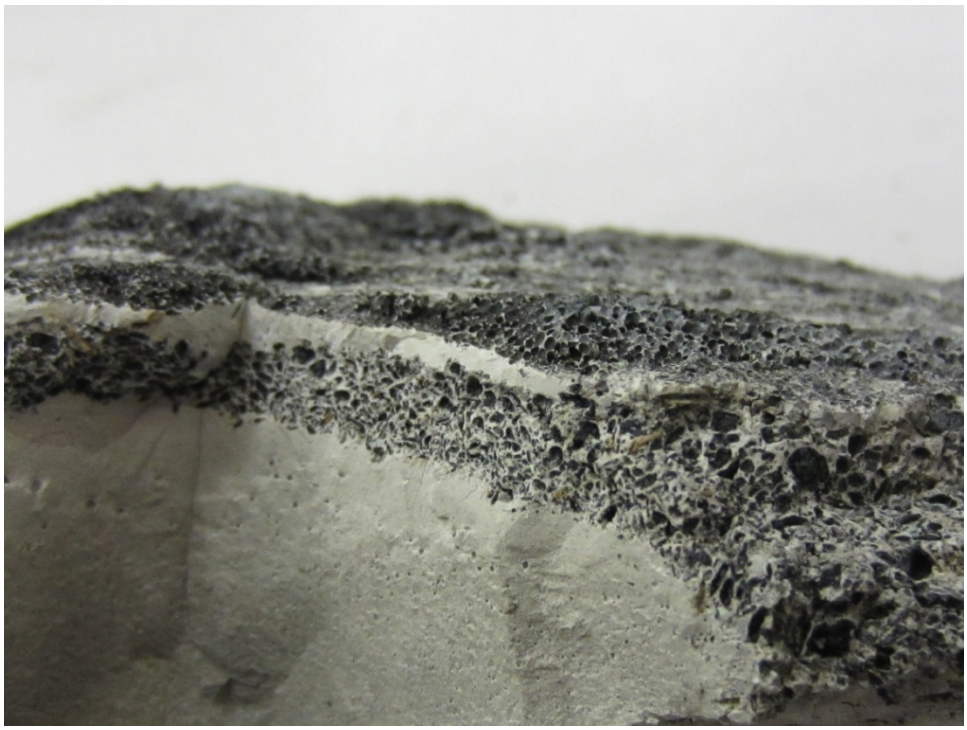

Figure 215. Photo. Cross section of the void/grout interface (top section).

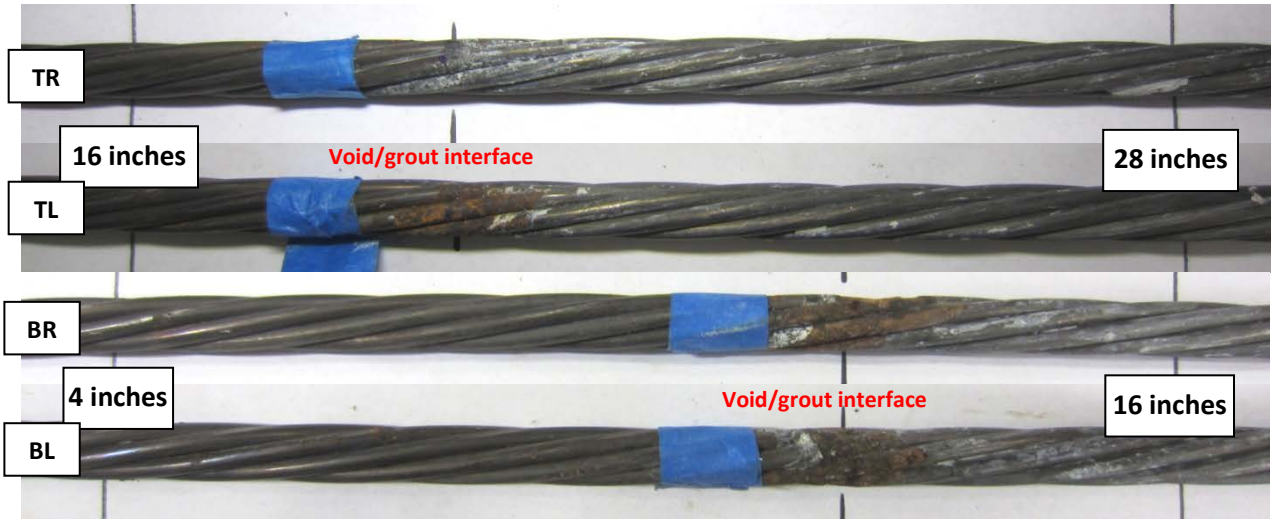

Figure 216. Photo. As-extracted condition of the stressed strands at the void/grout interface of 0 percent chloride multi-strand specimen.

Figure 217. Photo. As-extracted condition of a stressed segment passed through the contaminated void/grout interface of 0 percent chloride multi-strand specimen.

Figure 218. Photo. As-extracted condition of another stressed segment passed through the contaminated void/grout interface of 0 percent chloride multi-strand specimen.

Figure 219 shows the condition of stressed strands just behind the void/grout interface of the 0.4 percent chloride specimen. It was suspected in the middle of the detensioning process that some wires must have fractured under the tension. Upon grout removal, it was discovered that three wires of a stressed strand were indeed severed. The corroded strand is indicated by the red arrow in figure 219. Figure 220 and figure 221 show details of the broken wires. It was obvious that they failed during the detensioning process caused by excessive stress concentrated in the corroded areas with significant section loss. This specimen also had black deposit on the interface as indicated by the gray arrows in figure 219. Figure 222 shows a grout piece taken from the 12 o'clock orientation near the interface of the 0.4 percent chloride specimen. A bleed channel and poor grout condition can be seen. Figure 223 shows a cross section of the same piece, and a porous layer and black particles can be seen. They looked identical to the grout fragment of 0 percent chloride specimen shown in figure 215.

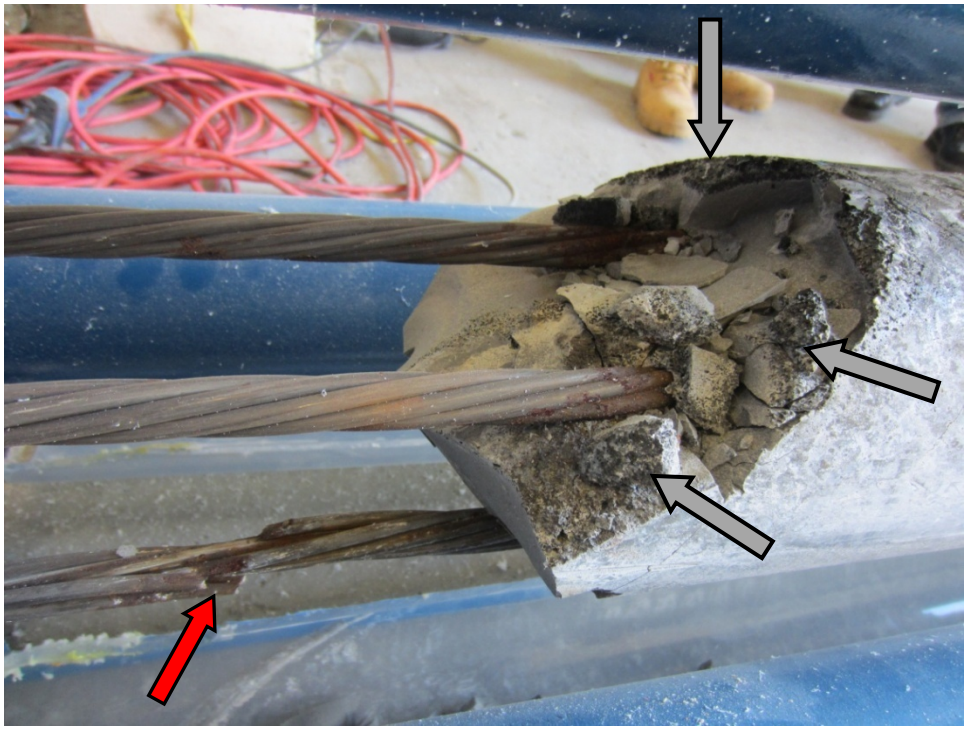

Figure 219. Photo. Severely corroded strand with three broken wires at the void/grout interface of 0.4 percent chloride multi-strand specimen.

Figure 220. Photo. Close-up view of the severely corroded strand shown in figure 219.

Figure 221. Photo. Close-up view of the broken wires shown in figure 220.

Figure 222. Photo. Top side grout piece exhibiting bleed channel and porous grout removed from 0.4 percent chloride specimen.

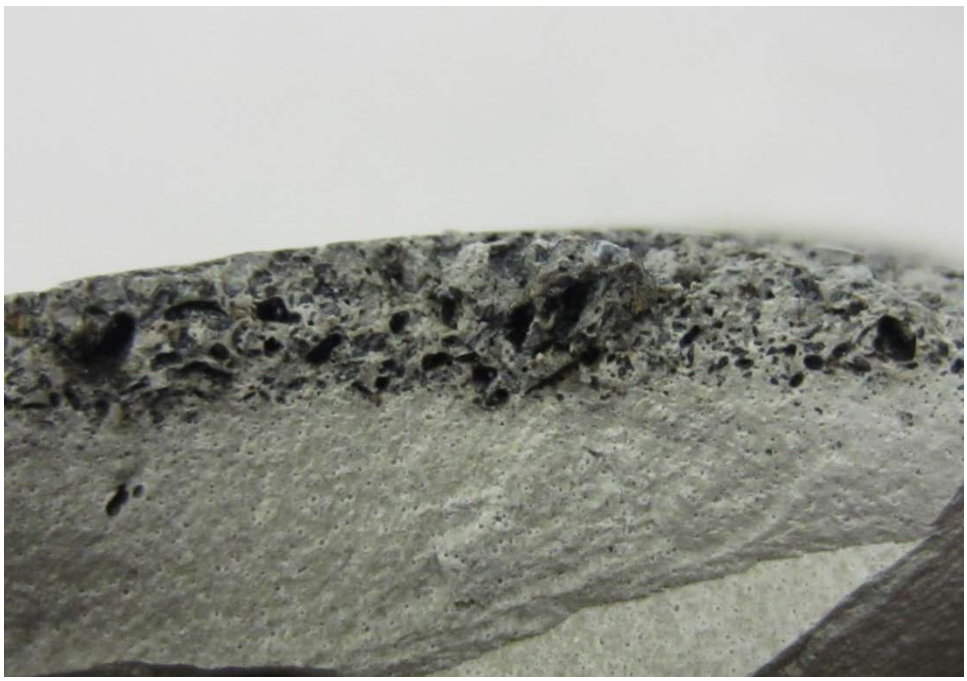

Figure 223. Photo. Cross section of the grout piece shown in figure 222.

The porous grout defect is not new. In fact, FDOT, the Texas Department of Transportation, and VDOT reported the same "grout segregation" phenomenon pertaining to a particular grout product. Figure 224 and figure 225, taken by the author of this report, show VDOT's field trial result of two grout products. As observed in the present study, the same grout product used in VDOT's trial

also exhibited the segregated grout along the bleed channel on the 12 o'clock orientation (see figure 224), while the other product yielded a good quality, hardened grout (see figure 225).

Figure 224. Photo. Defective grout along a bleed channel.

Figure 225. Photo. Normal grout.

Figure 226 shows another stressed strand of the same 0.4 percent chloride specimen that experienced similar significant section loss and black deposit, as indicated by the arrows.

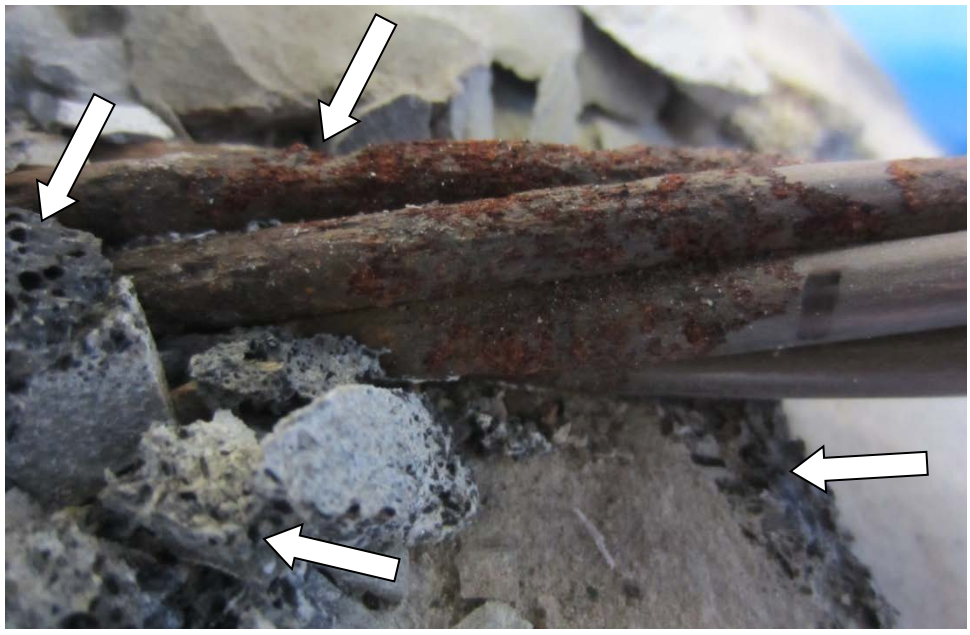

Figure 226. Photo. Another exposed strand at the void/grout interface of 0.4 percent chloride multi-strand specimen.

Discovery of severe corrosion in the absence of chloride triggered a small lab investigation using an ion chromatography instrument to analyze water-soluble (free) sulfate ions in the black particles removed from the 0 percent chloride specimen and grout fragments retrieved from the void/grout interfaces of the 0, 0.2, and 0.4 percent chloride specimens. Some bulk grout powder samples collected earlier for chloride analysis and original grout powder samples were also analyzed as controls. Table 10 summarizes the analysis results. It was determined that the grout powder contained 0.9 percent of water-soluble sulfate ions by weight of cement, whereas the black particles contained 2.8 percent water-soluble sulfate ions by weight of cement. The high sulfate concentration was also found in the black deposit sample scrapped off the interface of the 0 percent chloride specimen. The elevated level of free sulfate ions is thought to be responsible for the extraordinary corrosion damage observed in the chloride-free grout. The other interface samples (0.08 and 0.2 percent chloride) and grout powder samples did not reveal high levels of free sulfate ions because they did not contain the black particles. Although grout fragments of the 0.4 percent chloride specimen was also suspected to suffer the sulfate induced corrosion, they did not contain sufficient black deposit material to perform ion chromatography analysis, and it could not be confirmed that high concentration of free sulfate ions on its interface was also responsible for corrosion failure of three wires.

Table 10. Sulfate ion concentrations in the samples.

Sample ID	Sample Weight (oz)	Percent by Grout Weight	Percent by Cement Weight
Black particles collected from void/grout interface of 0 percent chloride specimen	0.07	1.5	2.8
Top layer scraped from void/grout interface of 0 percent chloride specimen	0.175	1.5	2.7
Top layer scraped from void/grout interface of 0.2 percent chloride specimen	0.175	0.4	0.7
Top layer scraped from void/grout interface of 0.4 percent chloride specimen	0.175	0.1	0.1
Grout powder sample from 0 percent chloride specimen	0.07	0.0	0.1
Grout powder sample from 0.08 percent chloride specimen	0.07	0.1	0.1
Grout powder sample from 0.4 percent chloride specimen	0.07	0.0	0.0
Original grout powder	0.175	0.5	0.9

If proper hydration of grout takes place, the sulfate ions in the dry grout should be chemically bound evenly in the cement paste, and little can be leached out in deionized water. This binding effect can be confirmed with 0 to 0.1 percent free sulfate concentrations by weight of cement in the hardened grout. It is speculated that when grout segregation occurs, free sulfate ions and black particles, presumably some sort of carbon black component of silica fume, can float to the top along the 12 o'clock bleed channel and form the corrosive deposit layer containing an excessive amount of free sulfate ions on top of the segregated and porous void/grout interface. The porous layer also appeared to hold water longer, as indicated by arrows in figure 156 and figure 159. It is unknown at this time how and why the segregated grout problem occurred only in some specimens even though the grouting work for every specimen was done in a consistent way.

Figure 227 and figure 228 show the condition of the exposed stressed strands in 2.0 percent chloride specimen after grout was removed near the void/grout interface. A severely corroded strand having a broken wire at the interface is shown. The broken wire must have been corroded for an extended period of time judging by the thick corrosion products formed on the failed section. The failed strand had been covered with black corrosion product formed at the interface, as shown in figure 163. It is not known whether the corrosion product contained a high level of free sulfate ions that could be also responsible for the intensive wire corrosion.

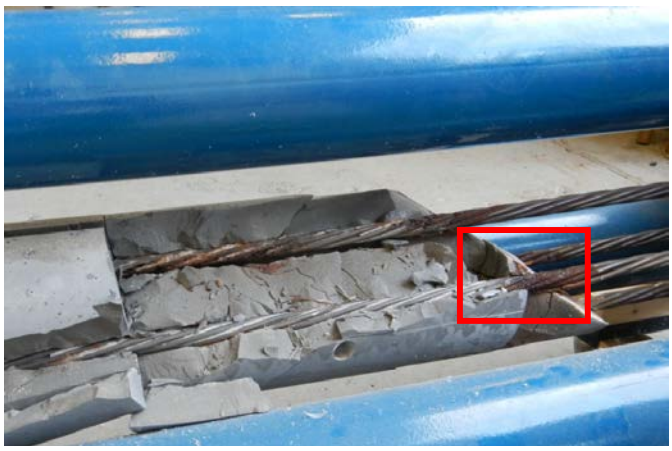

Figure 227. Photo. Severely corroded strand with one broken wire revealed at the void/grout interface of 2.0 percent chloride multi-strand specimen.

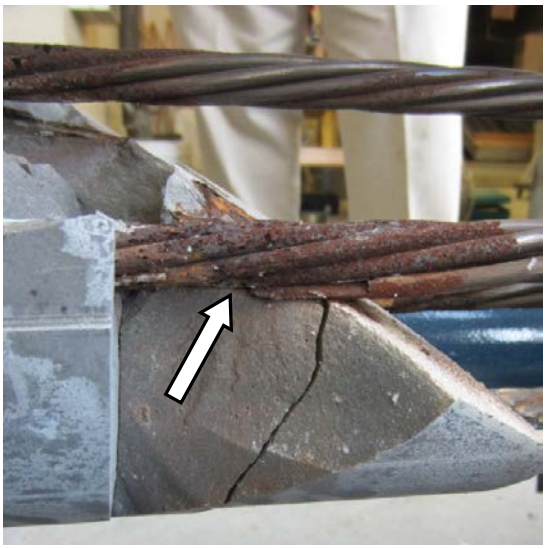

Figure 228. Photo. Close-up view of severely corroded strand with one broken wire revealed at the void/grout interface of 2.0 percent chloride multi-strand specimen.

Figure 229 also shows corrosion of a stressed strand developed in grout containing the highest chloride concentration. The 1.0 percent or less chloride concentration specimens did not exhibit such an active corrosion in the grout-covered section.

Figure 230 shows three corroding unstressed strands along with two stressed strands in 2.0 percent chloride specimen. As will be discussed later, all of the rust spots formed on the unstressed strands were superficial even in the highest chloride concentration.

Figure 229. Photo. Active corrosion of a stressed strand inside the 2.0 percent chloride grout 70 inches from the lower anchorage.

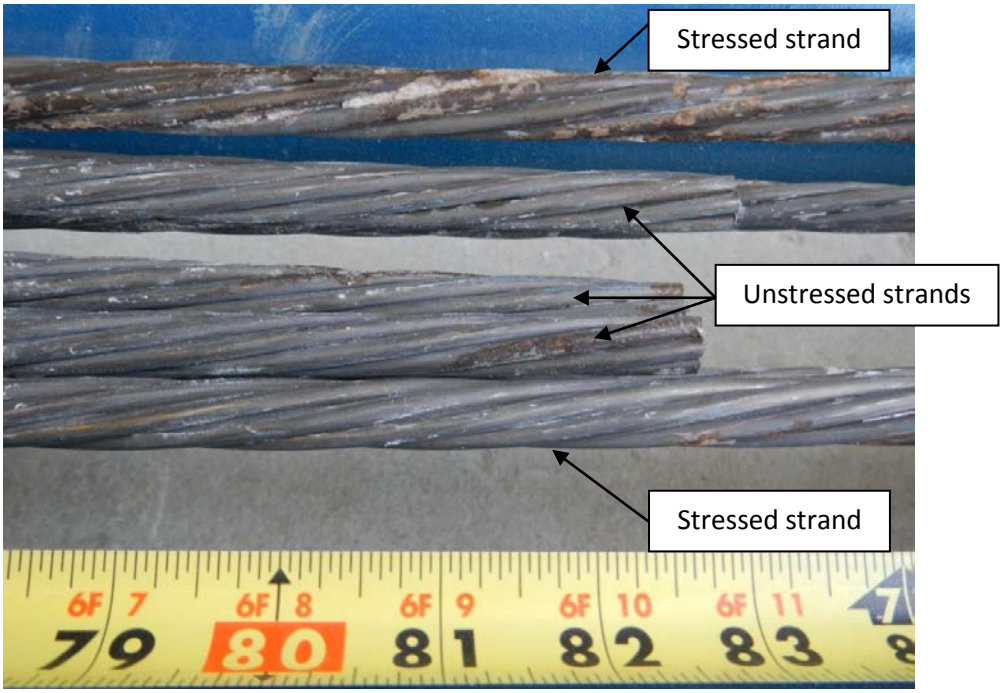

Figure 230. Photo. Corrosion of unstressed strands in 2.0 percent chloride multi-strand specimen.

Table 11 and table 12 summarize physical conditions of the 12-inch strand segments extracted from the void/grout interface (4 to 16 inches and 16 to 28 inches) and those embedded in the grout, respectively.

Table 11. Condition summary of interface segments of multi-strand specimens.

Chloride Concentration (Percent by Cement Weight)	Number of Segments Showing Superficial Rust (Percent)		Number of Segment Wires Showing Heavy Rust Requiring Acid Cleaning (Percent)	
	Stressed: Total 8 Segments per Specimen	Unstressed	Stressed: 56 Wires per Specimen (Total 8 Segments × 7 Wires/ Specimen)	Unstressed
0.00	4 (50.0 percent)	None	17 (30.4 percent)	None
0.08	6 (75.0 percent)		1 (1.8 percent)	
0.20	6 (75.0 percent)		0 (0 percent)	
0.40	7 (87.5 percent)		20 (35.7 percent)	
0.60	7 (87.5 percent)		2 (3.6 percent)	
0.80	8 (100 percent)		13 (23.2 percent)	
1.00	8 (100 percent)		23 (41.1 percent)	
2.00	8 (100 percent)		36 (64.3 percent)	

Table 12. Condition summary of in-grout strand segments of multi-strand specimens.

Chloride Concentration (Percent by Cement Weight)	Number of Segments Showing Superficial Rust (Percent)		Number of Segment Wires Showing Heavy Rust Requiring Acid Cleaning (Percent)	
	Stressed: Total 28 Segments per Specimen	Unstressed: Total 30 Segments per Specimen	Stressed: 196 Wires per Specimen (Total 28 Segments × 7 Wires/ Specimen)	Unstressed: 210 Wires per Specimen (Total 30 Wires × 7 Wires/Segment
0.00	0 (0 percent)	0 (0 percent)	0 (0 percent)	0 (0 percent)
0.08	0 (0 percent)	0 (0 percent)	0 (0 percent)	0 (0 percent)
0.20	2 (7.1 percent)	0 (0 percent)	0 (0 percent)	0 (0 percent)
0.40	10 (35.7 percent)	2 (6.7 percent)	2 (1.0 percent)	0 (0 percent)
0.60	19 (67.9 percent)	11 (36.7 percent)	0 (0 percent)	0 (0 percent)
0.80	22 (78.6 percent)	6 (20.0 percent)	30 (15.3 percent)	0 (0 percent)
1.00	20 (71.4 percent)	16 (53.3 percent)	44 (22.4 percent)	0 (0 percent)
2.00	12 (42.9 percent)	14 (46.7 percent)	34 (17.3 percent)	0 (0 percent)

Because the majority of the interface segments developed rust in every chloride concentration, only the in-grout strand conditions presented in table 12 are discussed here. Even though rust first appeared on two stressed segments (or 7.1 percent) of 0.2 percent chloride specimen, 0.4 percent chloride is considered the lowest concentration with appreciable number of segments exhibiting corrosion: 10 stressed segments (or 35.7 percent) and two unstressed segments (or 6.7 percent). Figure 231 and figure 232 show random carbonation test results of 0.6 and 0.8 percent chloride specimens. Based on the dark pink color, the pH of the grout was confirmed to be above 10.0. Therefore, it was concluded that carbonation did not occur during the accelerated corrosion testing.

Figure 231. Photo. Carbonation testing results of 0.6 percent chloride multi-strand specimens.

Figure 232. Photo. Carbonation testing results of 0.8 percent chloride multi-strand specimens.

During the grout demolition, localized wet and soft grout was uncovered in 0.8 and 1.0 percent chloride specimens. As-discovered conditions are shown in figure 233 and figure 234, respectively. Despite the abnormal (wet and soft) grout condition, no corrosion was found in these areas. FDOT observed severe corrosion beneath the same type of defective grout. It is unknown at this time how the wet grout was formed and why corrosion did not occur.

Figure 233. Photo. Wet and soft grout found in 0.8 percent chloride multi-strand specimen.

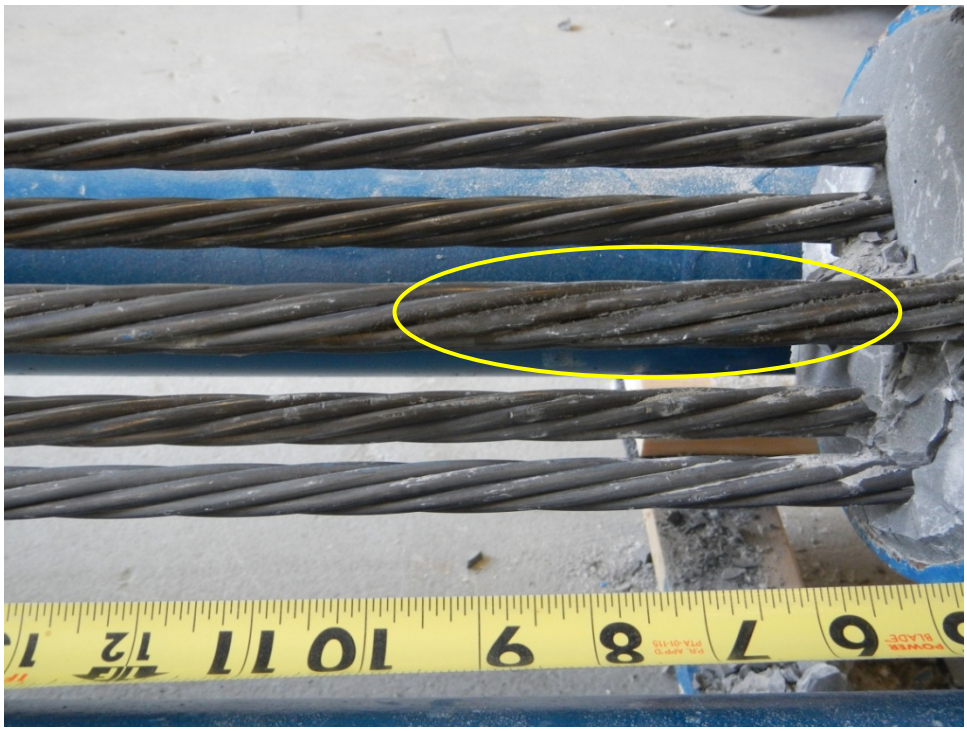

Figure 234. Photo. Wet and soft grout found in 1.0 percent chloride multi-strand specimen.

When the PT strands were dismantled, it was observed that hardened grout filled some interstices formed by the outer six wires and the center wire. Figure 235 shows a hardened grout layer stuck in an interstice when an outer wire was removed. Moderately corroded wires can be seen. Figure 236 shows a rust-stained small grout piece fell from the strand shown in figure 235. It has been known that water can get into the wire interstices and induce crevice corrosion. These photographs

document that chloride-contaminated fresh grout can also smear into the interstices to induce the same type of corrosion there.

Figure 235. Photo. Grout fragment found inside an interstice surrounded by corroding wires.

Figure 236. Photo. Heavily rust-stained grout fragment that fell from the strand shown in figure 235.

CORROSION DAMAGE MEASUREMENT DATA

The acid-cleaned wires were visually examined, and those that appeared to have pits deeper than 2 mil were set aside for pit depth measurement. Figure 237 through figure 246 show representative pitting corrosion morphologies exhibiting different levels of damage. Also, figure 247 and figure 248 show crevice corrosion damage found on a 0.4 percent and 0.8 percent chloride multi-strand specimen, respectively. The deepest pit found in this study was 60 mil, which is 30 percent of the wire diameter.

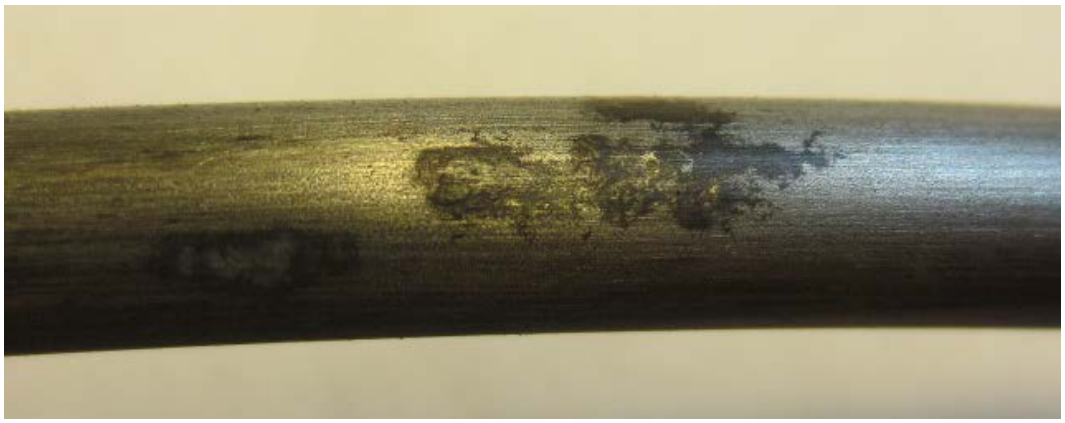

Figure 237. Photo. Stressed and voided 0.4 percent chloride single-strand specimen (pit depth < 2 mil).

Figure 238. Photo. Stressed and fully grouted 0.8 percent chloride single-strand specimen (pit depth ~2 mil).

Figure 239. Photo. Stressed and fully grouted 0.8 percent chloride single-strand specimen (pit depth = 4.7 mil).

Figure 240. Photo. 0 percent chloride multi-strand specimen at the void/grout interface (pit depth = 2–4 mil).

Figure 241. Photo. 0.08 percent chloride multi-strand specimen near the interface (pit depth = 2–10 mil).

Figure 242. Photo. 0.6 percent chloride multi-strand specimen in the grout (pit depth = 2–14 mil).

Figure 243. Photo. Stressed and voided 1.0 percent chloride single-strand specimen (pit depth = 2–18 mil).

Figure 244. Photo. 1.0 percent chloride multi-strand specimen in the grout (pit depth = 2–23 mil).

Figure 245. Photo. 0 percent chloride multi-strand specimen at the interface (pit depth = 2–36 mil).

Figure 246. Photo. 0.4 percent chloride multi-strand specimen near the void (pit depth = 2–50 mil).

Figure 247. Photo. Crevice corrosion between two stressed wires on 0.4 percent chloride concentration multi-strand specimen (mean pit depth = 4.5 mil and maximum pit depth = 8.0 mil).

Figure 248. Photo. Crevice corrosion between two stressed wires on 0.8 percent chloride concentration multi-strand specimen (mean pit depth = 4.5 mil and maximum pit depth = 6.0 mil).

For single-strand specimens, a total of 202 pit depth measurements were made on 13 wires removed from 5 12-inch segments. As summarized in table 9, measurable pits started to appear at a chloride concentration of 0.8 percent by weight of cement. For multi-strand specimens, a total of 3,426 pit depth measurements were made on 222 wires removed from 59 12-inch segments. Table 11 and table 12 provide detailed physical conditions of interface segments and in-grout segments of multi-strand specimens, respectively. The data in both tables were divided in two groups: number (percentage) of stressed and number (percentage) of unstressed segments showing superficial rust and heavy rust requiring acid cleaning. All of the unstressed segments exhibited superficial corrosion, and the acid-cleaned wires were entirely from the stressed ones.

Task 2.2: Voided Single-Strand Specimens

Figure 249 presents mean and maximum pit depth data of voided single-strand specimens. Each figure in parenthesis is the number of pits associated with a particular mean pit depth. No measureable pits were found in less than 0.8 percent chloride concentration. At higher chloride concentrations (1.0 to 2.0 percent), mean pit depth ranged between 3.6 and 6.2 mil, and maximum pit depths were between 7 and 18 mil.

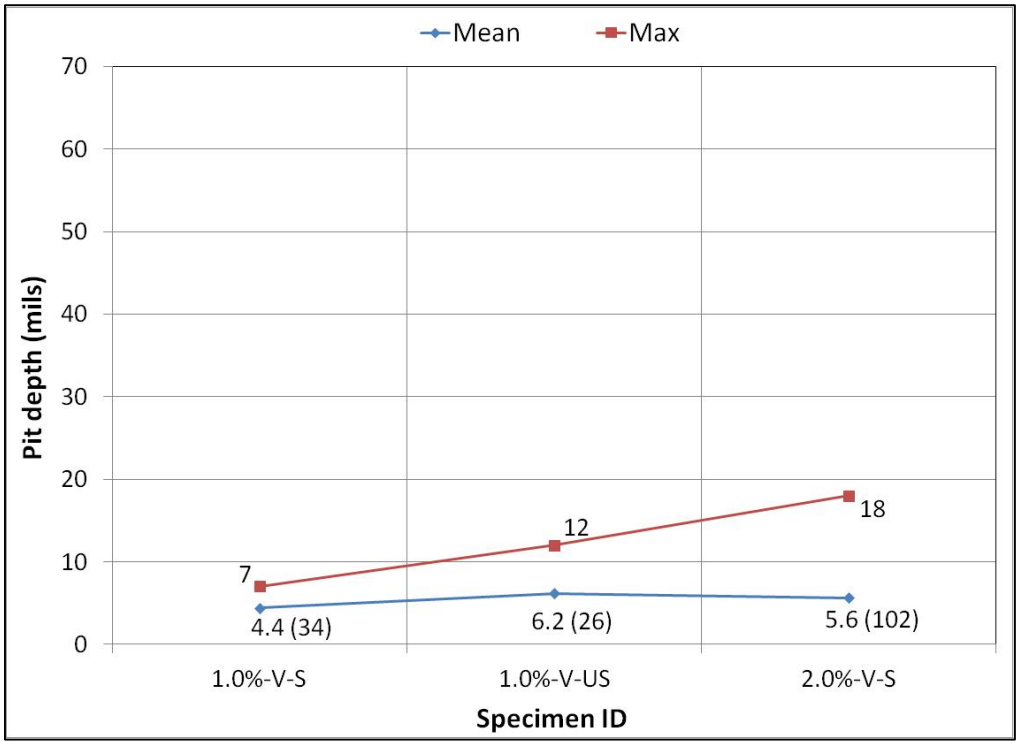

Figure 249. Graph. Mean and maximum pit depths on the voided single-strand specimens.

Task 2.3: Void/Grout Interface of Multi-Strand Specimens

Figure 250 shows fractions of stressed interface segments exhibiting superficial rust and fractions of individual wires (after untwisting strand segments) requiring acid cleaning due to heavy rust as a function of chloride concentration. Actual numbers are also listed in table 11. The data can be used to estimate severity of the strand corrosion. Reference photographs describing typical superficial rust and heavy rust are shown in figure 62 and figure 63, respectively. Corrosion appeared on some or the entire interface segments, regardless of chloride concentration, even at 0 percent chloride. As discussed previously, interface segments of 0, 0.4, and 2.0 percent chloride specimens suffered from unexpected abnormal corrosion damage due to excessive sulfate ions. If rust data of these specimens are excluded, 0.8 percent chloride is the lowest concentration to exhibit heavy corrosion products requiring acid cleaning.

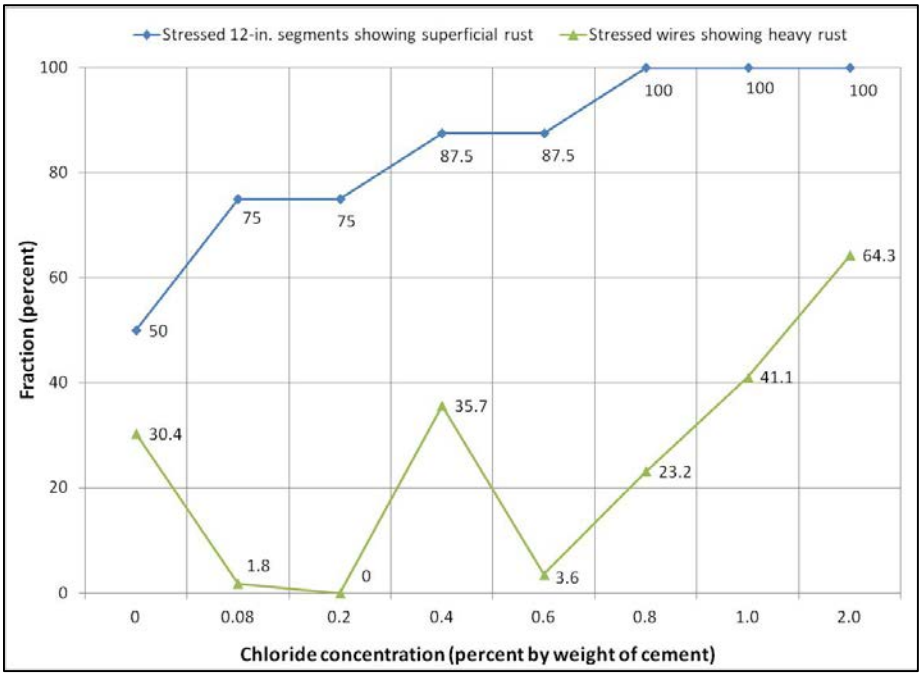

Figure 250. Graph. Condition of stressed segments at the void/grout interface of multi-strand specimens.

Figure 251 shows the number of pits measured on the interface segments. If pit data of 0 and 0.4 percent chloride specimens are ignored and the number of pits measured on 0.08 and 0.6 percent chloride specimens are considered insignificant, 0.8 percent chloride is the lowest concentration to have a meaningful number of pits. In other words, severe corrosion can be anticipated if stressed strands are exposed at the void/grout interface containing 0.8 percent chloride. Pitting corrosion tended to concentrate more on the 16- to 28-inch segments (TL and TR) compared to the 4- to 16-inch segments (BL and BR).

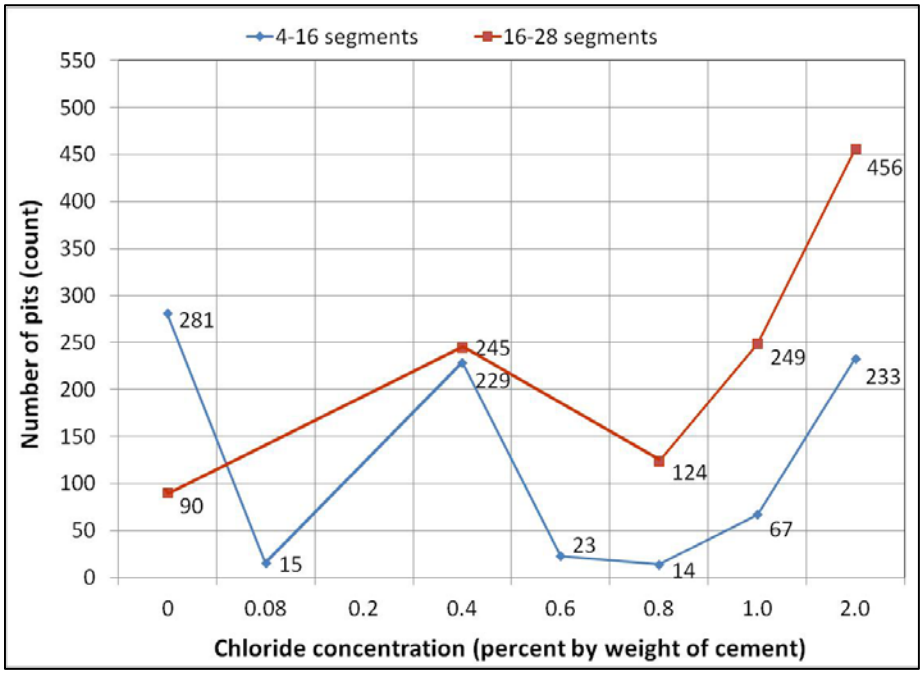

Figure 251. Graph. Number of pits on the interface segments of multi-strand specimens measured from the upper anchor plate.

Figure 252 shows mean pit depth data for the interface segments. If pit data affected by sulfate contamination are omitted, overall mean pit depth was approximately 6 mil. The largest mean pit depth was 11 mil at 2.0 percent chloride concentration.

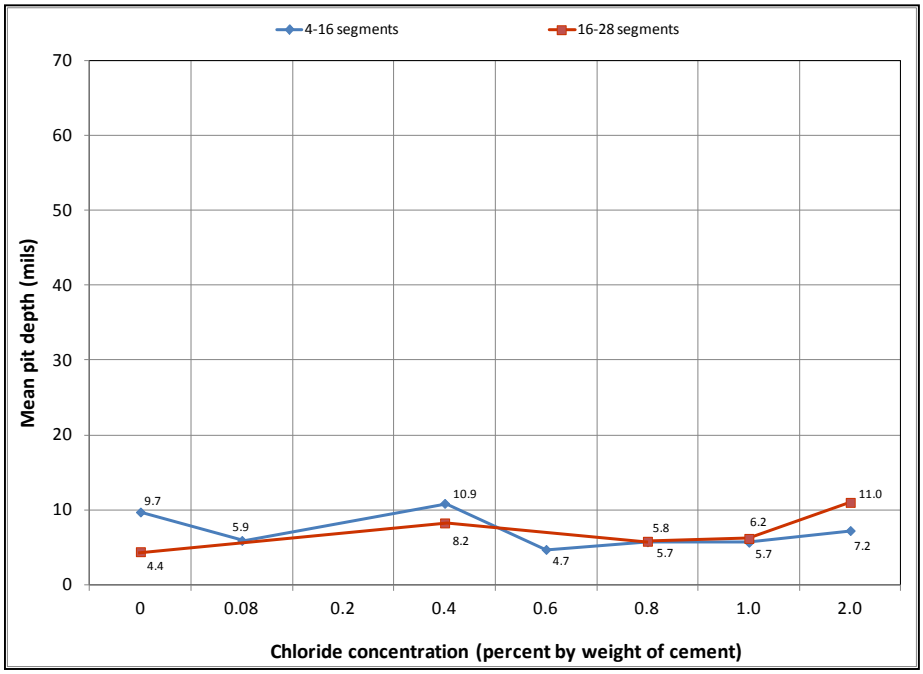

Figure 252. Graph. Mean pit depths on the interface segments of multi-strand specimens measured from the upper anchor plate.

The intensity of pitting corrosion was estimated by maximum pit depths. The results are plotted in figure 253. If excessive sulfate ions had not induced severe corrosion at the interfaces, it is reasonable to assume that maximum pit depth of 0 and 0.4 percent chloride concentrations might have been approximately 10 mil because neighboring concentrations of 0.08 and 0.6 percent chloride yielded the same number. At 0.8 and 1.0 percent chloride concentrations, maximum pit depths increased to 18 and 25 mil, respectively. The measured largest pit depth was 60 mil at 2.0 percent chloride concentration.

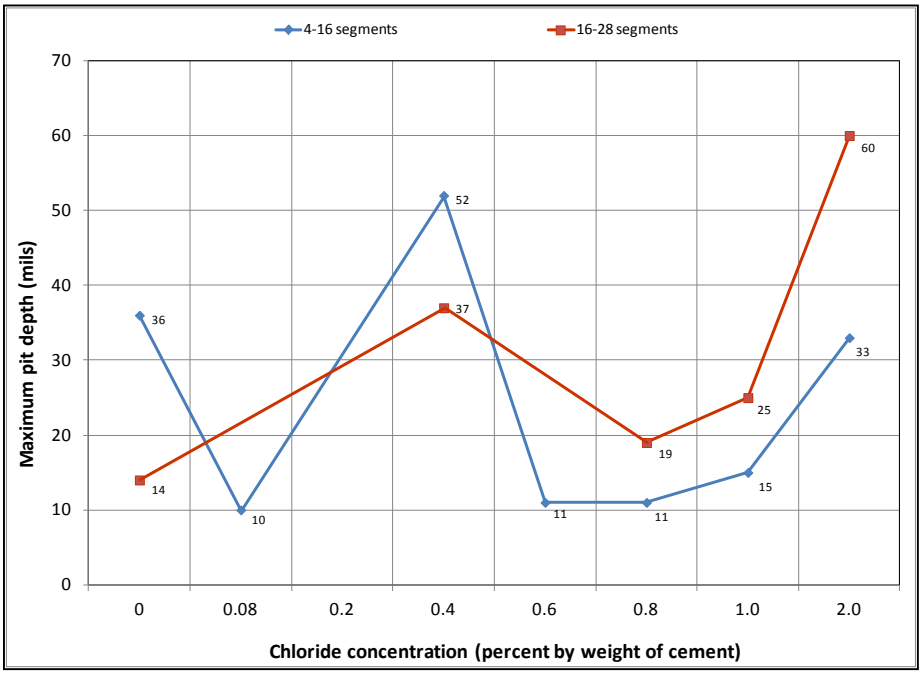

Figure 253. Graph. Maximum pit depths on the interface segments of multi-strand specimens measured from the upper anchor plate.

Task 2.2: Fully Grouted Single-Strand Specimens

Figure 254 plots mean and maximum pit depth data of fully grouted single-strand specimens. Measureable pits began to show at 0.8 percent chloride. Mean pit depth varied between 3.6 and 4.4 mil, and maximum pit depths were between 5 and 12 mil. These values are somewhat lower than those measured on the voided single-strand specimens.

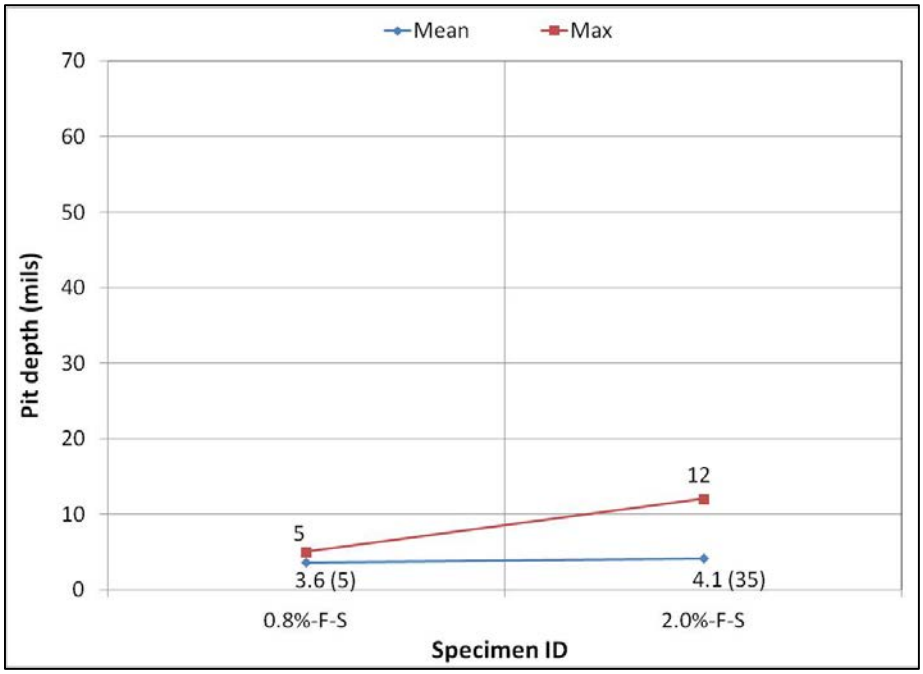

Figure 254. Graph. Mean and maximum pit depths on the fully grouted single-strand specimens.

Task 2.3: Fully Grouted Sections of Multi-Strand Specimens

Figure 255 shows fractions of stressed in-grout segments exhibiting superficial rust and fractions of individual wires (after untwisting strand segments) requiring acid cleaning due to heavy rust. Superficial rust and heavy rust started to appear when chloride concentration was 0.4 and 0.8 percent, respectively. Interface segments also exhibited heavy rust from 0.8 percent chloride concentration. With higher chloride concentrations up to 1.0 percent, more rust was observed in both rust types. Low macro-cell corrosion current density of 2.0 percent chloride specimen was responsible for its reduced number of rust spots. The stressed in-grout strands developed far less corrosion at any chloride concentration compared to the stressed interface segments. This suggests that grout might have provided some corrosion protection to the strands. Figure 256 shows the number of pits measured on the stressed segments versus their distance from the upper anchor plate. More pits were found on the segments closer to the interface and also as chloride concentration increased.

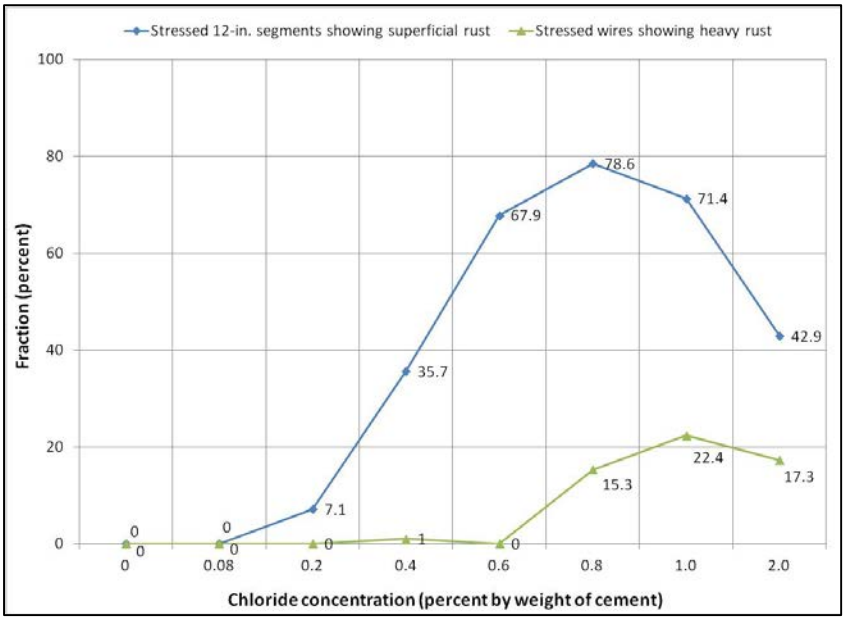

Figure 255. Graph. Physical condition of stressed in-grout segments in multi-strand specimens.

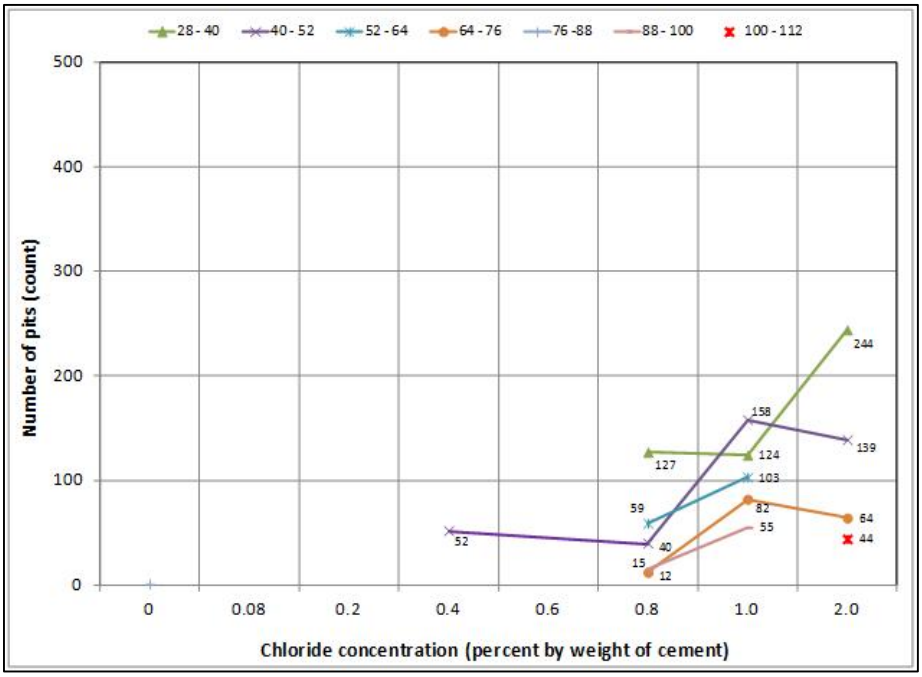

Figure 256. Graph. Number of pits observed on the stressed strands in multi-strand specimens measured from the upper anchor plate.

Figure 257 shows mean pit depth data of stressed strand segments embedded in grout by distance. Their mean pit depths varied between 3.4 and 7.4 mil when chloride concentration was 1.0 percent or less. At 2.0 percent chloride concentration, mean pit depth increased to 13 mil. Mean pit depth was not affected by distance from the upper anchor plate at any chloride concentration.

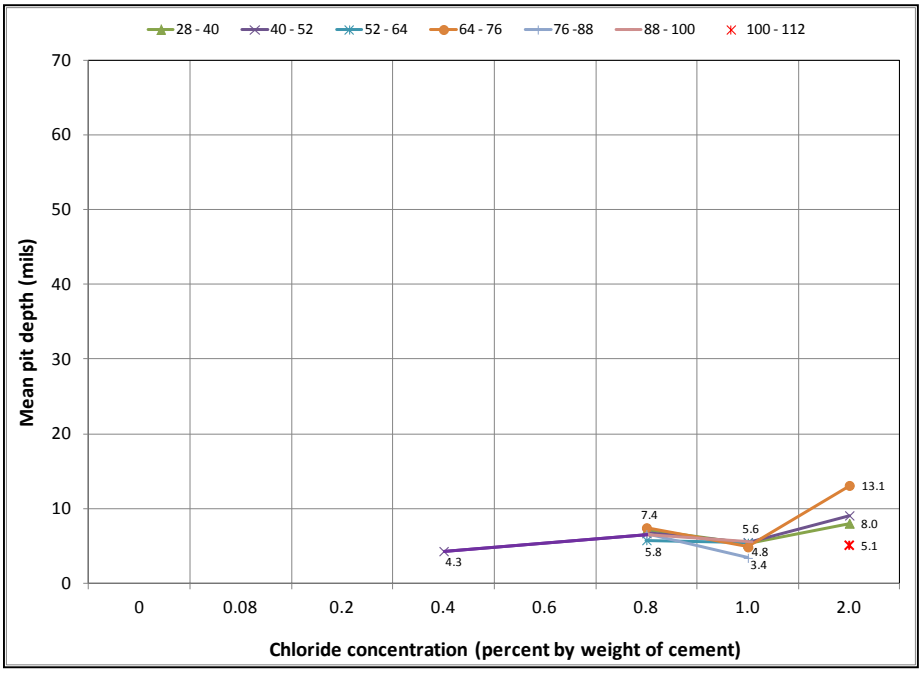

Figure 257. Graph. Mean pit depth measured on stressed strands in multi-strand specimens measured from the upper anchor plate.

Figure 258 compares the total number of pits versus chloride concentration data determined over the same in-grout length of stressed and unstressed strands. A small number of pits appeared at 0.4 percent (stressed strands) and 0.6 percent (unstressed strands), but pitting corrosion damage deeper than 2 mil (sign of corrosion propagation) was observed only on the stressed strands exposed to 0.8 percent chloride and higher concentrations. Heavy rust also developed on the stressed strands exposed to the same chloride concentration (see figure 250 and figure 255). Figure 259 shows overall mean pit depth versus chloride concentration data over the same in-grout length of stressed and unstressed strands. None of the unstressed in-grout strands exceeded the 2-mil pit depth threshold regardless of chloride concentration. Overall mean pit depth measured on the stressed in-grout strands increased from 4.3 to 9.4 mil as the chloride concentration increased from 0.4 to 2.0 percent.

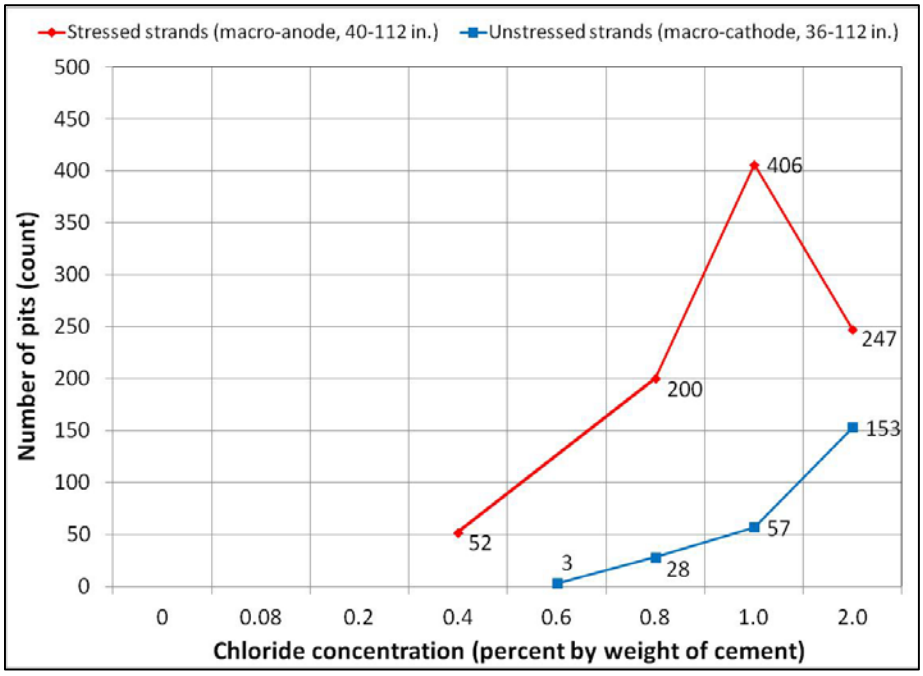

Figure 258. Graph. Number of pits observed on the in-grout strands in multi-strand specimens.

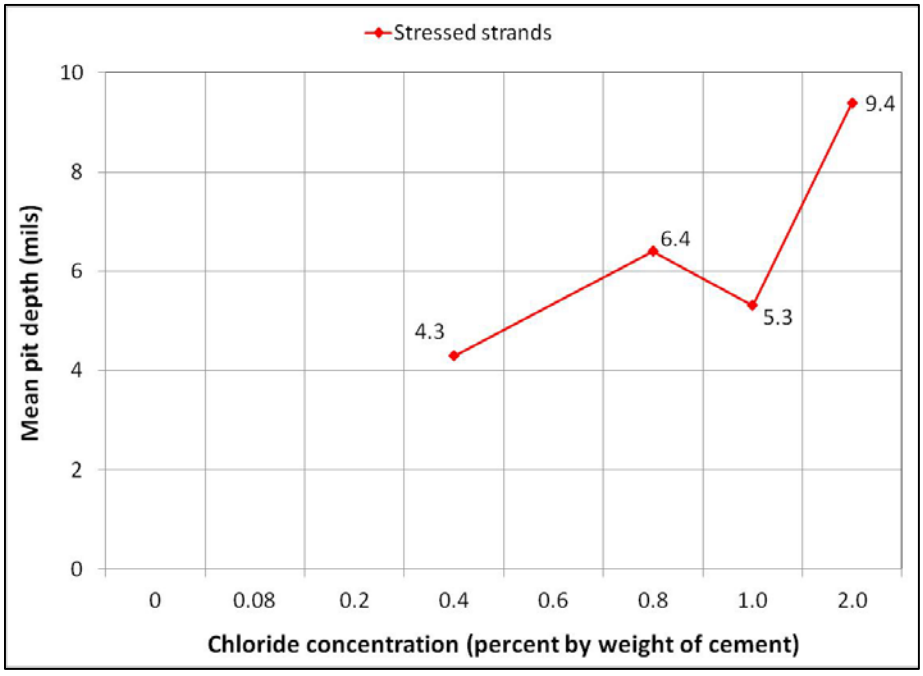

Figure 259. Graph. Mean pit depths of the in-grout stressed strands in multi-strand specimens.

As shown in figure 260, maximum pit depth tended to increase as chloride concentration increased. The measured largest pit depth was 36 mil at 2.0 percent chloride concentration. There was no strong relationship observed between distance from the upper anchor plate and maximum pit depth.

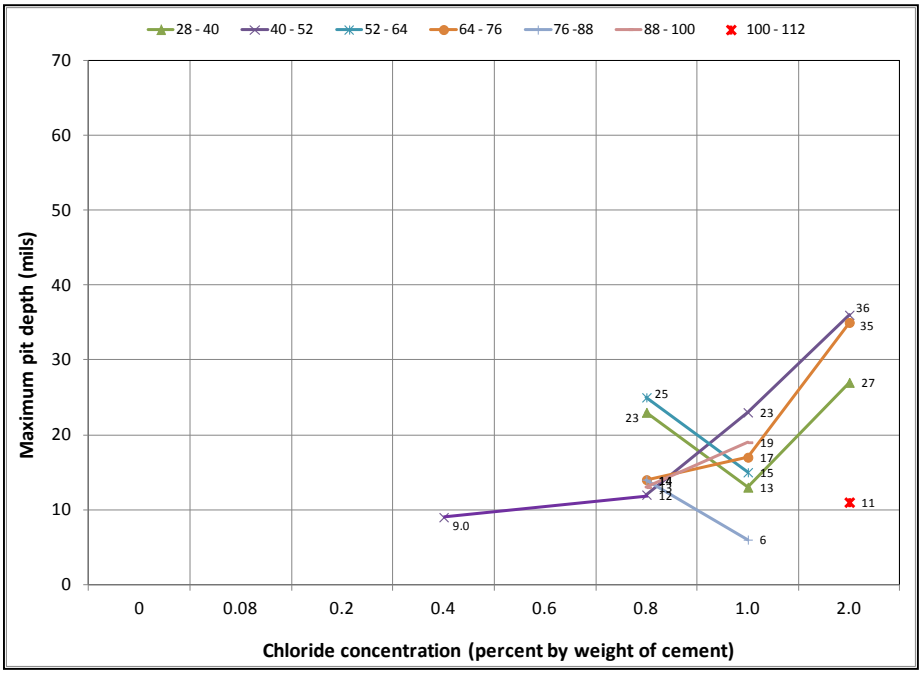

Figure 260. Graph. Maximum pit depths measured on the stressed strands in multi-strand specimens measured from the upper anchor plate.

Role of Void/Grout Interface

It is believed that premature failure of some field PT tendons was caused by a macro-cell corrosion mechanism of intensive localized corrosion in a relatively small anodic area of a PT tendon in relation to the rest of the tendon. In the present study, employment of the multi-strand specimen was intended to reproduce the worst corrosion damage by a simulated macro-cell corrosion setup in a relatively short period of time in the laboratory. The intended macro-cell corrosion was created between four stressed strands as macro-anode, especially near the void/grout interface, and five unstressed strands completely embedded in grout as macro-cathode. The majority of the electrochemical data and autopsy results of multi-strand specimens indicate that the macro-cell corrosion setup effectively facilitated accelerated corrosion of PT strands.

Figure 261 shows how macro-cell corrosion damage was influenced by distance with respect to the void/grout interface in normal grout. The stressed strands in the figure were divided into three sections: two interface segments (4–16 and 16–28 inches), a transition segment (28–40 inches), and the remaining segments (40–112 inches). Corrosion damage data of 0, 0.4, and 2.0 percent chloride concentration specimens are not included in the plot due to their excessive corrosion damage by sulfate ions.

A general trend is that more pits were found on the segments closer to the interface when chloride concentration was 0.8 and 1.0 percent. When chloride concentration was between 0.08 and 0.6 percent, no measurable pits were observed. This finding indicates that stressed strands near the interface were subjected to the most intensive corrosion if chloride concentration was 0.8 percent chloride. At this chloride concentration level, small surface area at the interface became the most anodic, probably in the presence of more oxygen and moisture in the void. The number of pits tended to decrease as a segment was getting away from the interface. It is thought that this

phenomenon was caused by weakened macro-cell corrosion current at the segments in the deeper grout upon presence of higher grout resistance from the interface.

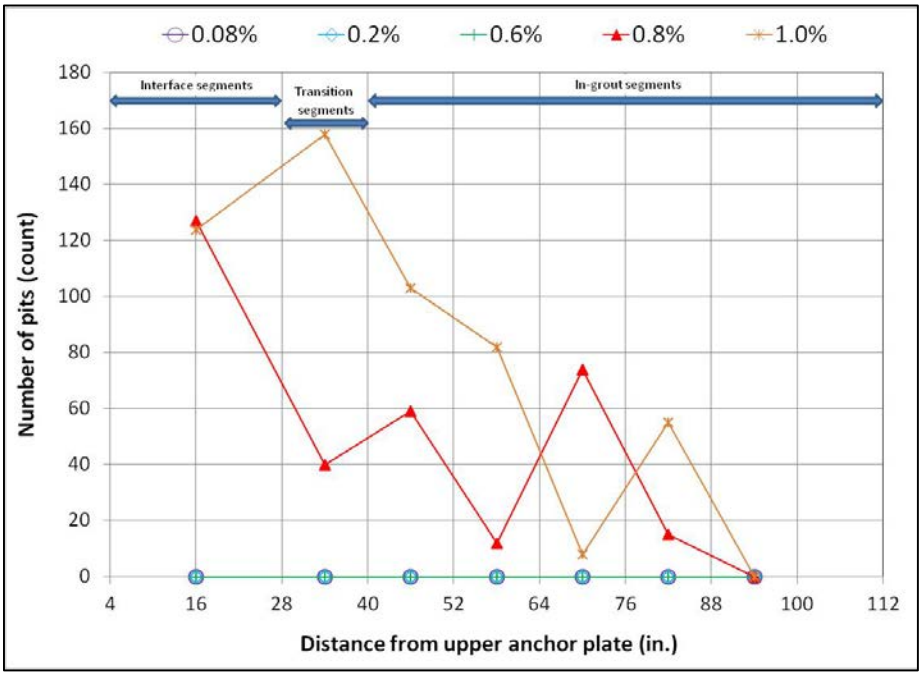

Figure 261. Graph. Number of pits measured on the stressed strands in some of the multi-strand specimens.

Figure 262 suggests that mean pit depth data did not follow the same trend. Pit depth was fairly uniform around approximately 6 mil along most of the strand length including the interface section.

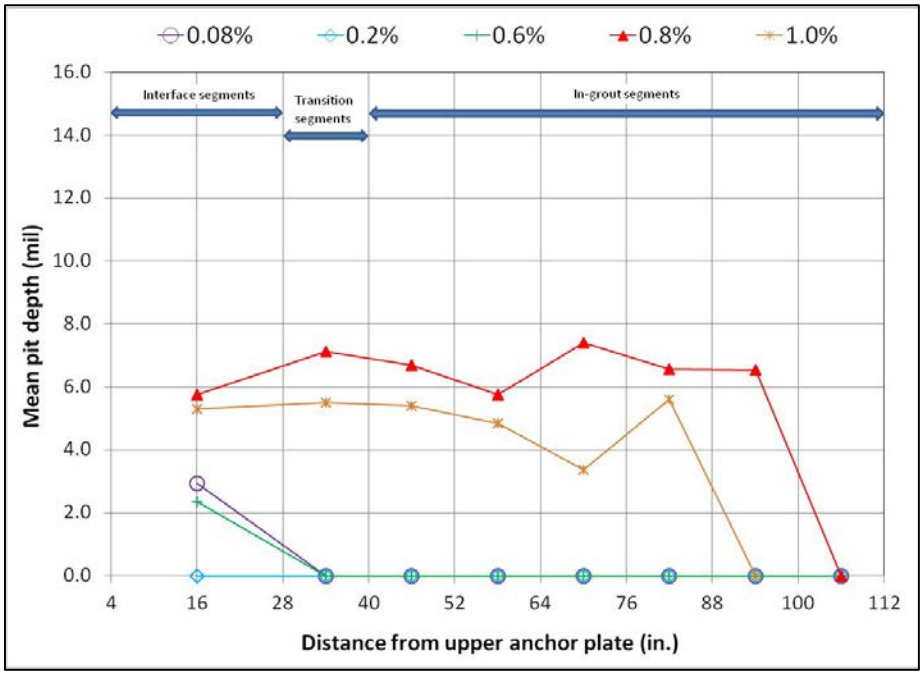

Figure 262. Graph. Mean pit depth measured on the stressed strands in some of the multi-strand specimens.

SUMMARY OF MAJOR FINDINGS

The electrochemical testing of center wires conducted under task 2.1 revealed that the corrosion rate of center wires in pH 13.6 solutions was less than 0.05 mil/year at chloride concentrations up to 0.6 percent and increased at higher chloride concentrations. For the specimens tested in pH 9.0 solutions containing 0.04 percent and higher chloride concentrations, typical active corrosion behavior was observed: corrosion potentials became more negative and corrosion rates increased. The electrochemical testing results suggest that the PT strand can tolerate chloride contamination without significant corrosion up to 0.6 percent by weight of cement in carbonation-free (high pH) grout, whereas as low as 0.04 percent chloride by weight of cement can initiate active corrosion in the carbonated (low pH) grout. This is below the AASHTO specified chloride limit of 0.08 percent by weight of cement. Once corrosion starts in the low pH environment, level of corrosion damage will depend on chloride concentration.

The apparent grout resistivity of single-strand specimens and grout resistance of multi-strand specimens were sensitive to temperature. High grout resistivity/resistance was measured during the F & D cycles, and low resistivity/resistance was measured during the H & H cycles. Chloride concentration did not affect the apparent grout resistivity/resistance values.

For single-strand specimens (task 2.2), chloride concentration of 0.4 percent by weight of cement was the lowest concentration to make the strands more prone to corrosion in most conditions. Mean corrosion potential became gradually negative starting from 0.4 percent chloride in initial ambient, ambient, and hot and H & H conditions. Mean corrosion rate became progressively higher starting from 0.4 percent chloride, and a dependence of corrosion rate on temperature was observed—corrosion rate increased during the H & H cycles, and intermediate corrosion rate was observed in the ambient condition. In F & D cycles, corrosion of all specimens decreased to a negligible state

regardless of chloride concentration. But, absolute values of the measured corrosion rates were very low due to small corroding areas compared to conventional corrosion rate criteria for ordinary reinforcing steel. There were no definite trends observed in single-strand specimens regarding stress level and presence of void, although limited data suggest that the stressed strands exposed to water in the grout void may be more susceptible to corrosion than the unstressed ones if acid-soluble chloride concentration is higher than 0.08 percent by weight of cement and the risk of corrosion is elevated with increased chloride concentration. All control specimens experienced steadily decreasing corrosion rates as their corrosion potential data also indicated the passive behavior.

An autopsy of single-strand specimens revealed that rust began to appear when chloride concentration was 0.4 percent. However, measurable pits were observed if chloride concentration was 0.8 percent. As chloride concentration increased, the severity of the corrosion got worse, particularly for the stressed specimens with void. However, the same observation was not indicated by their corrosion rate data. Mean pit depths ranged between 3.6 and 6.2 mil. A combination of a void, recharged water, and elevated chloride concentration can be detrimental, evidenced by markedly higher number of pits found on the 2.0 percent chloride stressed specimen with void.

For multi-strand specimens (task 2.3), chloride concentration was a more influential parameter for corrosion potential than exposure condition. As the macro-cell corrosion setup intended, stressed strands exhibited more negative corrosion potentials than unstressed ones, making the stressed strands anodic to the unstressed ones at any chloride concentration. It is unclear if presence of stress or localized corrosion at the void/grout interface or both made the entire stressed strands active. When chloride concentration increased to 0.4 percent, mean corrosion potentials of the stressed strands fell into the 90 percent corrosion probability. For unstressed strands, the same condition occurred only after chloride concentration reached 2.0 percent. Overall mean macro-cell corrosion current density also began to increase at 0.4 percent chloride. At any chloride concentration, the H & H and F & D cycles produced the highest and the lowest mean macro-cell corrosion current densities, respectively. Water recharging did not influence the mean corrosion potentials and mean macro-cell current densities significantly.

Autopsy of multi-strand specimens revealed that, in general, stressed segments started to show superficial rust at 0.4 percent chloride concentration, and heavy rust required acid cleaning at 0.8 percent chloride concentration. This observation could be made with both of the interface segments and in-grout segments. Mean pit depths measured on the stressed in-grout strands increased from 4.3 to 9.4 mil if chloride concentration increased from 0.4 to 2.0 percent. For the interface segments, mean pit depth was approximately 6 mil when chloride concentration was less than 1.0 percent. At 2.0 percent chloride concentration, mean pit depth increased to 11 mil. The largest measured pit depths were 60 and 36 mil for the interface segments and in-grout segments, respectively. For unstressed strands, superficial rust began to show up at 0.6 percent chloride concentration, and none of the pits exceeded 2 mil regardless of chloride concentration.

A general trend observed from the multi-strand specimens with normal grout at the interface is that more pits were found on the segments closer to the interface when chloride concentration was 0.8 and 1.0 percent. When chloride concentration was between 0.08 and 0.6 percent, no measurable pits were found at all. This finding suggests that stressed strands near the interface were subjected to the most intensive macro-cell corrosion if chloride concentration was 0.8 percent chloride. At this level of chloride, small surface area of the interface became the most anodic in the presence of abundant

dissolved oxygen and moisture in the void. The number of pits tended to decrease as a segment was getting away from the interface. It is thought that this phenomenon was related to weakened macro-cell corrosion current in the deeper grout. Mean pit depth data did not follow the same trend in that it was fairly uniform in the neighborhood of 6 mil along the most part of the stressed strand length, including the interface section.

CHAPTER 5. CHLORIDE THRESHOLDS

Chloride threshold is defined as the minimum chloride concentration required to induce corrosion. By this definition, the lowest chloride concentration creating signs of corrosion seems to be the appropriate chloride threshold. Because exact amount of admixed chloride concentrations were known in this study, corrosion performance of stressed PT strands exposed to seven different chloride concentrations and one chloride-free mix was characterized by their electrochemical data collected through 6-month accelerated corrosion testing and subsequent autopsy results. The other chloride threshold for corrosion propagation was also sought by determining the lowest chloride concentration needed to produce measurable pits. Table 13 lists the lowest acid-soluble chloride concentrations experimentally determined for corrosion initiation and corrosion propagation.

Table 13. Summary of the lowest chloride concentrations observed in the present study.

	Grout with Void		Fully Grouted	
Criteria	**Specimen Type**	**Lowest Chloride Concentration (Percent by Weight of Cement)**	**Specimen Type**	**Lowest Chloride Concentration (Percent by Weight of Cement)**
Corrosion initiation	Single-strand specimens	0.4	Single-strand specimens	0.6
Corrosion propagation	Multi-strand specimens contaminated with excessive sulfate ions	0	Multi-strand specimens	0.4
	Single- and multi-strand specimens	0.8	Single- and multi-strand specimens	0.8

Finally, two chloride threshold values were selected among the numbers in table 13 for the PT strands protected by normal grout (see table 14). The first threshold is 0.4 percent by weight of cement including mixing water ($[Cl^-]_{(cement+water)}$), which is the lowest amount to initiate corrosion of strands fully encased in normal grout. At this threshold, a small number of pits can begin to form on the strands in association with corrosion initiation process, but the rate of corrosion should be low. It is a conservative number, and there is still sufficient time to act against potential corrosion problems. Therefore, it can serve as the lower limit in assessing longer-term corrosion risk of PT bridges. The second critical chloride threshold is determined in association with corrosion propagation. At this threshold, corrosion starts to intensify in terms of number of pits and pit depth. Test results obtained in this study suggest that 0.8 percent $[Cl^-]_{(cement+water)}$ seems to be the critical threshold, which can be considered the upper limit in corrosion risk assessment. Once chloride concentration exceeds it, it is possible that significant corrosion damage can occur rapidly, and structural integrity of the PT bridges will be compromised. However, the actual rate of corrosion is influenced by many other factors set by individual bridges.

Table 14. Suggested chloride threshold values for normal grout.

Classification	$[Cl-]_{(cement+water)}$
Chloride threshold for corrosion initiation	0.4 percent
Critical chloride threshold for corrosion propagation	0.8 percent

It should be emphasized that these values are applicable to normal grout conditions only. They may not be adequate in other conditions such as segregated grout, duct cracks, grout voids filled with excessive water with or without chloride ions, and free sulfate ions in contact with the strands. In these circumstances, corrosion can start at different chloride concentrations, most likely below the suggested threshold values.

As shown in table 8, there are three units of chloride concentration to determine whether hardened grout powder samples taken from a PT bridge contain acid-chloride concentrations more than the chloride thresholds. When performing acid-soluble chloride titration with the field powder samples, the results are reported by $[Cl^-]_{sample}$. For the grout product used in this study, they represent approximately 50 percent of actual chloride content included in the grout powder samples. Therefore, 50 percent of the established chloride thresholds should be used—0.2 percent for corrosion initiation and 0.4 percent for corrosion propagation. If construction records of detailed grout mix proportions are available, the $[Cl^-]_{sample}$ can be converted to those expressed by $[Cl^-]_{(cement+water)}$ using a correction factor that accounts for weight of cement and weight of mixing water in a particular grout product. The converted concentrations in the grout samples indicated total (100 percent) acid-soluble chloride concentrations present. Therefore, it is easy compare the analysis results against the chloride threshold values listed in table 14. If information about precise weight of cement is known but weight of mixing water is not, a concentration unit of $[Cl^-]_{cement}$ should be used with another correction factor. For the same grout product, this conversion method yields about 75 percent of the acid-soluble chloride concentrations resided in the grout samples. Therefore, 75 percent of the suggested chloride thresholds should be used—0.3 percent for corrosion initiation and 0.6 percent for corrosion propagation. Table 15 summarizes the adjusted threshold values for three different concentration units.

Table 15. Adjusted chloride threshold values to be used for field grout powder samples.

Classification	$[Cl^-]_{(cement+water)}$	$[Cl^-]_{cement}$	Fraction of $[Cl^-]_{(cement+water)}$	$[Cl^-]_{sample}$	Fraction of $[Cl^-]_{(cement+water)}$
Corrosion initiation	0.4 percent	0.3 percent	0.75 percent	0.2 percent	0.5 percent
Corrosion propagation	0.8 percent	0.6 percent	0.75 percent	0.4 percent	0.5 percent

CHAPTER 6. MISCELLANEOUS WORK

CORROSION RISK ASSESSMENT

It has been shown that PT corrosion can initiate at any chloride concentration depending on grout condition and many other external and environmental conditions pertaining to particular sets of PT tendons. In high-quality normal grout without any other deficiencies, the severity of pitting corrosion induced by chloride ions begins to increase significantly when $[Cl^-]_{(cement+water)}$ is 0.8 percent or higher. In performing the corrosion risk assessment of field PT bridges, total (acid-soluble) chloride concentration in grout powder samples must be determined first through a statistically sound grout powder sampling methodology. Once distribution of acid-soluble chloride contents in the bridge is determined, the corrosion risk assessment can be performed using the pre-determined risk criteria. As an example, table 16 lists three corrosion risk levels and maintenance strategies for the affected PT bridges containing various levels of chloride contamination.

Table 16. Example of corrosion risk management plan with the suggested chloride threshold values.

Risk Level Classified by Different Chloride Threshold Values	If Weight of Cement and Mixing Water are Known	If Cement Weight is Known and Mixing Water Weight is Uncertain	If Weight of Cement and Mixing Water are not Known	Recommended Actions
	Matching Corrected Chloride Threshold Values for Different Concentration Units			
	$[Cl^-]_{(cement+water)}$	$[Cl^-]_{cement}$	$[Cl^-]_{sample}$	
Low	< 0.4 percent	< 0.3 percent	< 0.2 percent	Routine biennial bridge inspection
Intermediate	0.4–0.8 percent	0.3–0.6 percent	0.2–0.4 percent	Routine biennial bridge inspection; develop a longer-term maintenance plan
High	> 0.8 percent	> 0.6 percent	> 0.4 percent	Conduct immediate in-depth inspection; more frequent inspections

The classification of risk levels and proposed actions for bridge inspection and maintenance are discussed below based on the chloride threshold values in terms of $[Cl^-]_{(cement+water)}$. The same approach can be adopted for the other sets of chloride threshold values listed in table 15. Depending on situation of each bridge, any of these categories may be modified for corrosion risk assessment.

The PT bridges may be classified as low-risk bridges if the mean $[Cl^-]_{(cement+water)}$ is less than 0.4 percent. At this chloride level, the PT tendons are likely to maintain corrosion-free condition; therefore, regular biennial bridge inspection is sufficient.

The intermediate risk group bridges contain mean $[Cl^-]_{(cement+water)}$ between 0.4 and 0.8 percent. Even though rate of corrosion in this group may be slow enough not to cause an immediate concern,

they may progress into the high-risk group if PT seal systems are breached. Therefore, along with routine biennial inspection, development of an appropriate longer-term maintenance plan is recommended for bridges in this group due to their unpredictable corrosion behaviors. Specifically, all of the potentially problematic areas should be identified in the maintenance plan and subsequently inspected in detail when time and resources are available.

High-risk bridges refer to ones containing mean $[Cl^-]_{(cement+water)}$ higher than 0.8 percent. They require an immediate initial indepth inspection and subsequent inspections at closer intervals. It is safe to assume that these bridges may well undergo intensive pitting corrosion. This assumption is particularly true for bridges exposed to warm weather and those already having long post-construction service life. Every tendon deficiency found in a high-risk bridge needs to be addressed immediately or kept on a close watch until appropriate repair measures are developed.

The important issue here is how to determine statistically sound mean chloride concentrations for the whole bridge or various sections depending bridge characteristics. A separate small study is recommended to develop a statistically sound sampling methodology for sample size and its distribution, confidence interval, and acceptable data variation indicated by standard deviation, coefficient of variance, etc. The goal is to make sure that mean chloride concentrations are truly representative values for the bridge or sections of the bridge without unacceptable deviations. Otherwise, corrosion risk may be elevated, as there can be some outliers that are undetected through the improper statistical analyses. The outcomes of the study can be incorporated into the existing grout sampling guideline.[20] In addition to level of chloride contamination, annual temperature variation needs to be considered as part of the corrosion risk assessment since corrosion rate is heavily influenced by temperature. Longer duration of warm weather promotes more intense corrosion, as seen by the data obtained in this study.

The preceding section discusses corrosion risk of the PT bridges under the assumption that they are surrounded by reasonably good quality grout. As some test results indicated in this study, however, chloride threshold values for poor-quality grout having segregation and voids can be meaningless, as corrosion can initiate without chloride ions under these conditions. It is particularly alarming to learn that excessive corrosion damage can occur at much higher rates if the segregated grout contains elevated water-soluble free sulfate ions.

It is critical to assess condition of the strands and thoroughly and accurately locate grout defects. As the current state of inspection practices for PT bridges are labor intensive partly due to limited inspection tools and techniques, it is highly desirable to develop new technologies or improve the existing ones. While dealing with chloride contaminated grout issues, there should be more effort on a national level to develop 100 percent reliable non-destructive inspection technologies to diagnose corrosion damage in the tendons and identify grout defect areas.

SERVICE LIFE PREDICTION MODEL

This section offers an example of service life prediction modeling with a very simplified approach. It is hoped that more sophisticated modeling software will be developed in the near future to analyze various field conditions and provide accurate and reliable predictions.

A stressed PT strand will fail by corrosion when stress in the remaining cross-sectional area of the strand reaches the 270 ksi GUTS under a constant tensile load. Figure 263 shows an example of corrosion damage prediction model outputs for a corroding strand at different penetration rates. The following assumptions were made for the modeling:

- Annual loss of cross-sectional area of a wire is the square of annual penetration rate expressed by mils per year. For example, if corrosion penetration rate is 6 mil/year, annual section loss is 0.000036 inch^2 = 0.006 inch^2.
- Annual penetration rate is constant (i.e., no change over time).
- Fixed number of wires corrode simultaneously at the same rate.
- Structural behavior of stressed strands is independent of the number of strands.
- Temperature effect is not considered.
- The tensile stress in the strand is 60 percent GUTS, and it remains the same over time.

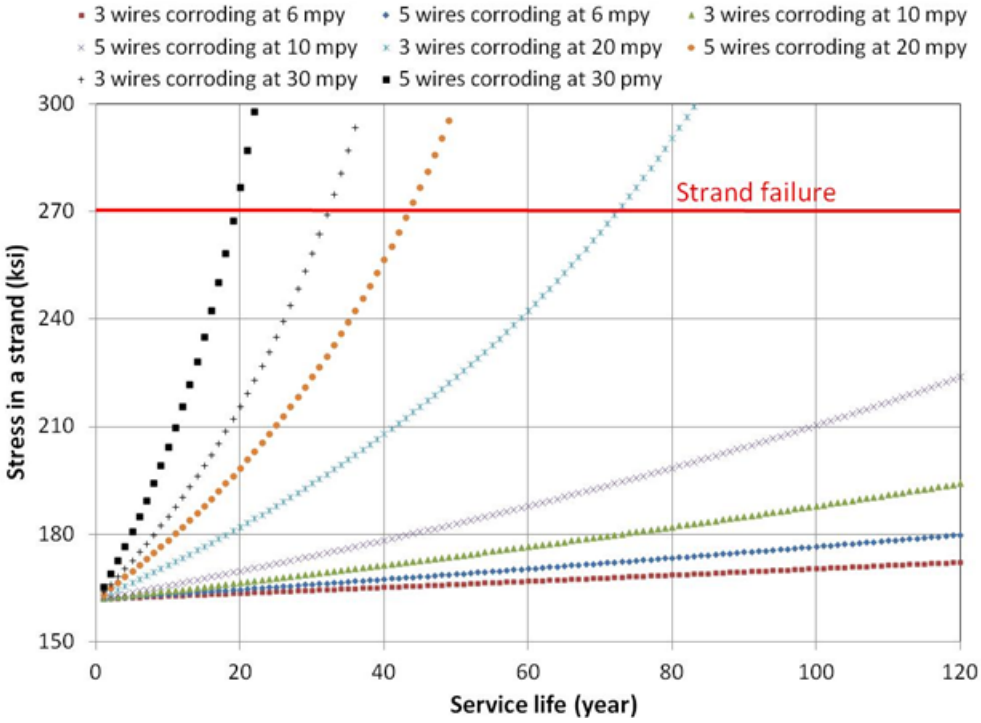

Figure 263. Graph. Example of a time-to-failure plot for a corroding strand at different penetration rates.

These assumptions may be unrealistic in the real world, but the model outputs can be informative because they illustrate the effects of cross section loss and penetration rates on structural integrity. The penetration rates used in the example are representative pit depths observed in the autopsied strands in the present study. If corrosion intensifies by rapidly losing cross-sectional area, the rate of stress buildup in the strand is no longer linear or linear-like, and strand failure occurs

prematurely at higher rates. The test results indicate that corrosion damage of stressed strands increased significantly if total chloride concentration exceeded the critical chloride threshold of 0.8 percent by weight of cement. It is critical to determine present chloride concentrations in the affected bridges as soon as possible and take appropriate actions based on level of chloride contamination.

CHAPTER 7. CONCLUSIONS

Based on the test results obtained from the 6-month accelerated corrosion laboratory study and subsequent data analyses, the following conclusions can be made:

- There are two chloride threshold values determined for PT strands. The first threshold is 0.4 percent $[Cl^-]_{(cement+water)}$ which is the lowest concentration to initiate corrosion of strands fully encased in normal grout. At this threshold, a small number of pits start to form on the strands in association with corrosion initiation process. The second "critical" chloride threshold of 0.8 percent $[Cl^-]_{(cement+water)}$ is determined in association with corrosion propagation. At this threshold, corrosion starts to intensify in term of number of pits and pit depth.

- If mean acid-soluble chloride concentration in the grout powder samples from a PT bridge is determined to be less than 0.4 percent $[Cl^-]_{(cement+water)}$, this bridge belongs to the low risk group and regular biennial inspection is sufficient. If its mean acid-soluble chloride concentration is higher than 0.8 percent $[Cl^-]_{(cement+water)}$, it is considered a high risk bridge that should require an immediate in-depth inspection and subsequent routine inspections at closer intervals. For the PT bridges containing mean acid-soluble chloride concentrations between these two sets of threshold values, they should be included in the intermediate risk bridge group as there is a chance that they may progress into the high risk group.

APPENDIX A. EXAMPLES OF CORROSION PROBLEMS CAUSED BY INSUFFICIENT GROUT COVER

This appendix contains examples of tendon corrosion problems caused by insufficient grout cover that were observed in three PT bridges in service. Figure 264 shows a failed externa PT tendon of the Verina-Enon bridge in Virginia. Little grout cover is visible between the 6 and 12 o'clock orientation.

Figure 264. Photo. Failed external PT tendon of Verina-Enon bridge in Virginia.

Figure 265. Photo. Other matching end of the retrieved tendon sample shown in figure 264.

Figure 266 shows a corroding PT tendon of the Verina-Enon bridge in Virginia. Corrosion started in some areas with no grout cover near a deviation block that was exposed to stagnant water.

Figure 266. Photo. Corroding PT tendon of Verina-Enon bridge in Virginia.

Figure 267 shows an external PT tendon of the Verina-Enon bridge in Virginia. Little or no grout cover is visible along the free length of the tendon, but no corrosion was observed.

Figure 267. Photo. External PT tendon of Verina-Enon bridge in Virginia.

Figure 268 shows an external PT tendon of the Mid-Bay bridge in Florida. No grout cover was discovered.

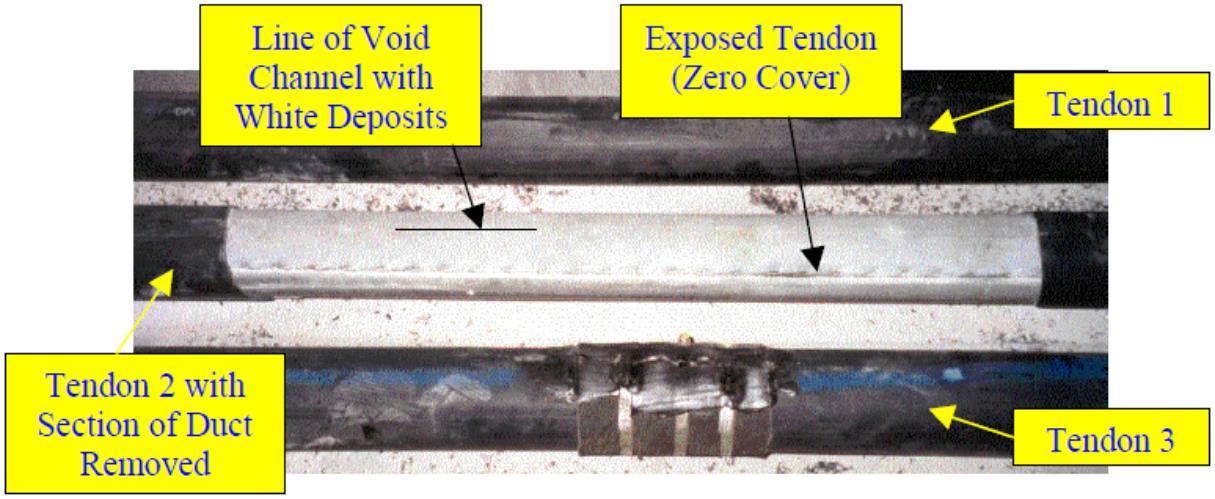

Figure 268. Photo. External PT tendon of Mid-Bay bridge in Florida.[21]

Figure 269 shows an external PT tendon of the Ringling Causeway bridge in Florida. Significant corrosion was observed in the areas with no grout cover in contact with segregated thin grout cover.

Figure 269. Photo. External PT tendon of Ringling Causeway bridge in Florida.[(4)]

REFERENCES

1. Corven Engineering Inc. (2004). *Post-Tensioning Tendon Installation and Grouting Manual*, Federal Highway Administration, Washington, DC.

2. Figg Bridge Engineers, Inc. (2010). *I-295 Verina-Enon Bridge Tendon Replacement for the Virginia Department of Transportation*, Final Report, Exton, PA.

3. Lee, S-K. (2012). *Literature Review of Chloride Threshold Values for Grouted Post-Tensioned Tendons*, Report No. FHWA-HRT-12-067, Federal Highway Administration, Washington, DC.

4. Lau, K., Lasa, I., and Paredes, M. (2013). *Corrosion Failure of Post-Tensioned Tendons in Presence of Deficient Grout*, Paper No. 2600, Corrosion/2013, National Association of Corrosion Engineers International, Florida Department of Transportation, Tallahassee, FL.

5. Merrill, B.D. (2010). *Memorandum—Grout Testing and Analysis of Carbon Plant Road over IH 37*, Texas Department of Transportation, Austin, TX.

6. Federal Highway Administration. (2011). *Elevated Chloride Levels in SikaGrout® 300 PT Cementitious Grout*, U.S. Department of Transportation, Washington, DC. Obtained from: https://www.fhwa.dot.gov/bridge/111123.cfm.

7. American Concrete Institute. (2011). *Building Code Requirements for Structural Concrete and Commentary*, ACI 318M-11, Farmington Hills, MI.

8. American Concrete Institute. (2008). *Guide to Durable Concrete*, Reported by ACI Committee 201 (ACI 201.2R-08), Farmington Hills, MI.

9. American Concrete Institute. (2010). *Protection of Metals in Concrete Against Corrosion*, Reported by ACI Committee 222 (ACI 222R-01), Farmington Hills, MI.

10. American Association of State Highway and Transportation Officials. (2010). *LRFD Bridge Construction Specifications*, 3d Edition, AASHTO, Washington, DC.

11. Florida Department of Transportation. (2010). *Standard Specifications for Road and Bridge Construction: Section 934 Non-Shrink Grout*, Florida Department of Transportation, Tallahassee, FL.

12. Whiting, D.A. (1997). *Origins of Chloride Limits for Reinforced Concrete*, PCA R&D Serial No. 2153, Page 3, Portland Cement Association, Washington, DC.

13. Powers, R.G., Sagues, A.A., and Virmani, Y.P. (2002). "Corrosion of Post-Tensioned Tendons in Florida Bridges," *Technical Memorandum of Public Works Research Institute*, No. 3843, 579–594.

14. Cui, F. and Sagues, A.A. (2003). *Corrosion Performance of Stainless Steel Clad Rebar in Simulated Pore Water and Concrete*, Paper No. 03310, Corrosion/2003, National Association of Corrosion Engineers International, Houston, TX.

15. AASHTO T 260-97. (2011). *Standard Method of Test for Sampling and Testing for Chloride Ion in Concrete and Concrete Raw Materials*, American Association of State and Highway Transportation Officials, Washington, DC.

16. ASTM C1218/C1218M-99. (2008). "Standard Test Method for Water-Soluble Chloride in Mortar and Concrete," *Book of Standards Volume 04.02*, ASTM International, West Conshohocken, PA.

17. ASTM C876-09. (2009). "Standard Test Method for Corrosion Potentials of Uncoated Reinforcing Steel in Concrete," *Book of Standards Volume 03.02*, ASTM International, West Conshohocken, PA.

18. Wang, H., Sagues, A.A., and Powers, R. (2005). *Corrosion of the Strand-Anchorage System in Post-Tensioned Grouted Assemblies*, Corrosion/2005 Conference Paper No. 05266, National Association of Corrosion Engineers International, Houston, TX.

19. ASTM G1-03. (2011). "Standard Practice for Preparing, Cleaning, and Evaluating Corrosion Test Specimens," *Book of Standards Volume 03.02*, ASTM International, West Conshohocken, PA.

20. Theryo, T.S., Hartt, W.H., and Paczkowski, P. (2013). *Guidelines for Sampling, Assessing, and Restoring Defective Grout in Prestressed Concrete Bridge Post-Tensioning Ducts*, Report No. FHWA-HRT-13-028, Federal Highway Administration, Washington, DC.

21. Hartt, W.H. and Venugopalan, S. (2002). *Corrosion Evaluation of Post-Tensioned Tendons on the Mid Bay Bridge in Destin, Florida*, Final Report for FDOT, Tallahassee, FL.

HRDI-60/05-14(600)E